THESIS FOR THE DEGREE OF LICENTIATE OF ENGINEERING

BEV Powertrain Component Sizing With Respect to Performance, Energy Consumption and Driving Patterns

EMMA ARFA GRUNDITZ

Department of Energy and Environment
Division of Electric Power Engineering
CHALMERS UNIVERSITY OF TECHNOLOGY
Göteborg, Sweden 2014

BEV Powertrain Component Sizing With Respect to Performance, Energy Consumption and Driving Patterns
EMMA ARFA GRUNDITZ

Licentiante Thesis at the Graduate School in Energy and Environment

Department of Energy and Environment
Division of Electric Power Engineering
Chalmers University of Technology
SE–412 96 Göteborg
Sweden
Telephone +46 (0)31–772 1000

Chalmers Bibliotek, Reproservice
Göteborg, Sweden 2014

To my sweet family . . .

BEV Powertrain Component Sizing With Respect to Performance, Energy Consumption and Driving Patterns

EMMA ARFA GRUNDITZ
Department of Energy and Environment
Chalmers University of Technology

Abstract

In this thesis, various drive cycles, legislative, official real-world and measured within the frame of the project, have been studied and characterized in terms of speed and acceleration cycle parameters, as well as acceleration and speed distribution. The objective was to assess typical vehicle usage on different road types, but also to study the implication on vehicle energy consumption due to the drive cycle's characteristics. For this evaluation, three reference vehicles were designed after different set performance requirements, with data on existing BEVs as a frame of reference. An available traction motor, power electronic module and battery cell were utilized, where the motor was scaled by active length. Finally, the consequence of downsizing the electric drive system in terms of energy consumption and performance was also studied.

Through comparison between legislative together with official real-world cycles and measured drive cycles, it was found that even though the measured cycles reach higher peak acceleration levels for a certain speed level, they still spend only slightly more time at higher levels of acceleration compared to the official cycles, at least on average over a group of similar cycles. During the powertrain sizing regarding torque and power, it turned out that the acceleration requirement was dominating over other requirements such as top speed, and grade levels. The analysis shows that for two cycles with similar speed parameters such as maximum and average speed and time share at low speed, but where the speed time traces are very different with many more speed fluctuations in one cycle compared to the other, in combination with generally higher acceleration levels, the increase in net battery energy consumption per distance may be as high as $28\,\%$ for the cycle with more speed fluctuations. By down-scaling the electric drive system of the City car by $40\,\%$, the net battery energy per driven distance for low speed cycles increased by about $3 - 6\,\%$, while three of the cycles could not be fulfilled due to limited acceleration capability.

Index Terms: Battery Electric Vehicle, sizing, energy consumption.

Acknowledgements

The financial support through Chalmers Energy Initiative (CEI) is gratefully appreciated.

My greatest appreciation is given to the initiator of this project, likewise the main supervisor and examiner, Torbjörn Thiringer, whose continuous support and tremendous commitment was an important base during the execution of this work. I would also like to thank my co-supervisors; Mikael Alatalo for sharing his knowledge in many interesting discussions, and Sonja Lundmark for her help during the project and with the finalizing of this thesis.

Additionally, I would like to thank all my colleagues at the division of Electric Power Engineering, for contributing to a very pleasant working environment. Specifically, I would also like to thank my room-mates; Christian Dubar, Ali Rabiei and Andreas Andersson for the support and for the humor and music they share.

Finally, I give my warmest thanks to my family, whose support is the most essential.

Emma Arfa Grunditz
Göteborg, Sweden
June, 2014

Contents

Chapter 1

Introduction

1.1 Background

Today, a large part of the major automotive manufacturers in the world have developed their own battery electric vehicle (BEV) model, which they offer to passenger car customers. Therefore, many different models now exist on the market, with various performance capabilities, but also different energy efficiency.

The main benefits with BEVs over combustion engine vehicles are related to environmental issues such as; zero tailpipe emissions and the nonexistent oil dependency during the use phase. Yet, there is an ongoing research around the world on how to improve the relatively limited driving range of the BEVs compared to combustion engine vehicles, without a major cost increase.

In this light, it becomes important to investigate the effect on energy efficiency as well as performance that different design choices have, both when it comes to design of the different components in the powertrain, but also regarding the design of the drive system as a whole. Another interesting research aspect is to investigate the possibility to design the drive system according to a specific type of usage, and then to assess the consequence on energy efficiency.

1.2 Previous work

In order to evaluate tailpipe emissions and fuel consumption of conventional combustion vehicles, various drive cycles have been developed over the last few decades. Numerous studies have been conducted that relate different types of cycles and their speed and acceleration characteristics, to the resulting levels of fuel consumption [1], [2], [3] and [4]. However, the influence of speed and acceleration measures on the energy consumption of a BEV is missing. Moreover the time resolution of the available cycles is often relatively low, which may have influence on the type of information that is possible to extract. Accordingly,

there is a need for having access to more high frequency gathered cycles.

A valuable contribution is done in [5] which gives a more detailed description of different performance targets. A developed electric machine design tool is then utilized in order to gain suitable geometrical parameters of a machine that is modeled. The efficiency map is compared to the machine of Toyota Prius II, showing a reasonable coherence. The machine size and transmission ratios are then optimized for three different official cycles. Especially regarding the design of the electric machine there are several interesting contributions, for instance [6] and [7]. Unfortunately in these optimizations, the loss consequence of a subsequently scaled inverter is not accounted for at the same time, and in the second article also battery losses are excluded from the study.

When it comes to electric powertrain design using performance targets and drive cycles, there are also a number of interesting articles, for instance [8] and [9]. Although these references contain a lot of useful information, they are often limited to some single case, an arbitrary vehicle, a few drive cycles, and sometimes with missing component data, which makes reproducibility difficult. Furthermore, much related work is done with relevant methods used, usually applied to hybrid electric vehicles, e.g. in [10], where component sizes of a plug in hybrid electric vehicle are optimized based on cost parameters, while also considering drive cycles and performance targets. Also in [11] and [12], vehicle simulation over drive cycles, and performance targets for hybrid electric vehicle design are discussed.

1.3 Purpose of the thesis and contributions

The purpose of this thesis is to investigate and quantify the relation between vehicle performance, component size, and energy consumption, while accounting for a large number of drive cycles as well as vehicles designed based on an extensive number of existing BEVs. Moreover, a target was to account for the performance requirements in an adequate way, which brought a need to collect high frequency drive cycles where also the acceleration was determined using an accelerometer in addition to just deriving it from a GPS speed signal. Finally, an aim was to check the needed drive train sizing in order to fulfill various drive cycles.

The main contributions are:

- Sorting and parameterized characterization of official drive cycles, put in relation with own measured cycles
- BEV powertrain component sizing after three differently put performance requirements, with various existing BEVs as a frame of reference
- Quantification of the consequence in energy consumption per distance for different cycles, while the electric drive system size is varied

Chapter 2

BEV dynamics and powertrain component modeling

This chapter deals with basic concepts and what is considered to be necessary information for taking part of the rest of the report.

2.1 Battery Electric Vehicle (BEV) powertrain

The powertrain of a Battery Electric Vehicle (BEV) consists of an electric drive system with a battery serving as an energy buffer. Usually there is only one electric machine, typically of three phase AC type, connected to the wheel shaft via a gearbox and a differential. However some applications may utilize several electric machines, e.g. hub wheel motors. The energy is stored chemically in a battery, which is electrically connected to the machine via a DC/AC power electronic converter accompanied by a control system. The control system controls the frequency and magnitude of the three phase voltage supplied to the electric machine, depending on the driver's present request, communicated via the acceleration and/or brake pedal.

In vehicle applications, it is usually desirable to keep the physical volume of the electric machine down. This can be done by designing it for higher speed levels. A reasonable compromise is a maximum speed between $12\,000$ to $16\,000\,rpm$ [13], since it serves as a good compromise between volume and performance. Still, during normal on road driving the speed range of a vehicle may vary between zero to about $130\ km/h$ or even higher at times. This means that the wheels will spin up to around $1200\,rpm$ or higher. Therefore a reduction gear ratio towards the wheels, is inherently needed. Additionally, in order to give the left and right traction wheels a chance to spin at slightly different speeds during turning, there is also a need for a differential to be connected between the wheels. Sometimes the differential often also includes a final gear ratio. A typical BEV drive system, which is also the type of system studied in this theses, is depicted in Figure 2.1.

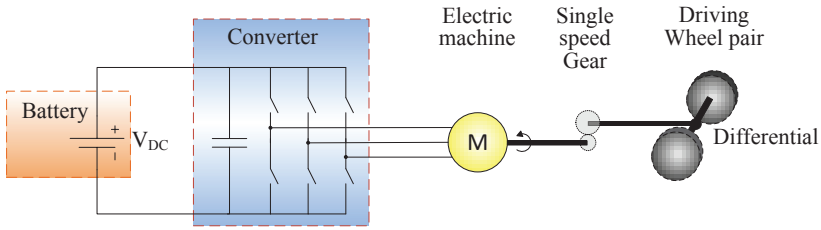

Figure 2.1 Simple schematic sketch of a BEV powertrain.

2.2 Vehicle dynamics

Vehicle dynamics aim to describe how a vehicle moves on a road surface while it is under the influence of forces between the tire and the road, as well as aerodynamics and gravity.

During the powertrain design phase, basic knowledge in vehicle dynamics is essential, since it reveals what loads and load levels that the powertrain needs to cope with during driving. The understanding of vehicle dynamics is equally important while evaluating the powertrain's impact on the vehicle's performance (usually assessed through simulations), whether it may be time to accelerate, or average energy consumption per driven distance.

As with modeling of any object, a rolling vehicle can be modeled with various levels of detail depending on what main phenomena that is targeted to be studied. For the type of dynamical studies in this thesis, where powertrain load levels and energy consumption will be analyzed, it is reasonable to assume that the vehicle body is rigid, hence it can be modeled as a lumped mass at the vehicle's center of gravity [14]. Furthermore, only dynamics in one direction, i.e. the longitudinal forward direction, is of interest while under the assumption that vehicle stability is not under any circumstances violated.

According to Newton's second law of mechanics, the dynamical movement of a vehicle in one coordinate axis is entirely determined by the sum of all the forces acting on it in that same axis of direction, as described in the translational form

$$m\,a = m\,\frac{d}{dt}\,v(t) = F_{tractive}(t) - F_{resistive}(t) \tag{2.1}$$

where $m\ (kg)$ is the equivalent mass to be accelerated including possible rotating inertias in the powertrain, $a\ (m/s^2)$ and $\frac{d}{dt}v(t)$ is the time rate of change of vehicle speed $v(t)\ (m/s)$, i.e. acceleration $a\ (m/s^2)$, $F_{tractive}(t)\ (Nm)$ is the sum of all the tractive forces acting to increase the vehicle speed and $F_{resistive}(t)$ is the sum of the resistive forces acting to decrease the speed.

The main tractive force is the one exerted from the powertrain via the gear, differential and the wheel shaft to the contact area between the wheels and the road. During downhill driving gravity may also serve as a major tractive force, however during uphill driving it may instead be a large resistive force. Other major resistive forces are aerodynamic drag

and rolling resistance, as well as regenerative braking using the electric power train and braking using conventional friction brakes.

To conclude, a vehicle will accelerate when the sum of the tractive forces is larger than the sum of the resistive forces, and thus will decelerate when the opposite applies. To keep a constant speed, the net resistive force must be exactly matched by the net tractive force.

2.2.1 Aerodynamic drag

The aerodynamic drag that any vehicle unavoidably is exposed to during driving, springs from the flow of air around and through the vehicle also often referred to as external and internal flows respectively.

The **external** drag is caused by two main phenomena; *pressure drag* and *skin friction*. The skin friction is caused by the viscous friction between the air and the surface of the moving car, both over and under. The friction is also one of the reasons that air is pushed in front of a moving vehicle, causing an increase in air pressure, while at the same time leaving a wake in the rear with lower air pressure. This pressure difference causes the pressure drag. Due to the typical shape of most car bodies, the pressure drag dominates over the skin drag [15].

The **internal** sources of drag are due to the fact that, vehicle manufacturers have learned to, via inlets in the front, utilize the air flow, e.g. to cool the engine, but also for heating, air conditioning and ventilation of the passenger compartment [15]. Still the external sources are the main contributors to the total drag.

Due to the complex shape of automobiles, along with the even more complex nature of fluid dynamics, accurate reliable analytical models of aerodynamical drag are very difficult to develop, even with advanced CFD softwares at hand. A compromise often used to model the aerodynamical drag force, F_a, is the partly empirical model, partly based on the expression of dynamical pressure, which is showing a strong dependance on the square of the vehicle speed as

$$F_a = \frac{1}{2}\,\rho_a\,C_d\,A_f\,(v_{car} - v_{wind})^2 \tag{2.2}$$

where ρ_a (kg/m^3) is the air density, C_d is the aerodynamic drag coefficient, $A_f\,(m^2)$ is the effective cross sectional area of the vehicle, $v_{car}\,(m/s)$ is the vehicle speed and $v_{wind}\,(m/s)$ is the component of wind speed moving in the direction of the vehicle [14].

The aerodynamical drag thus increases with head **wind** speeds; at head wind speeds of $10\,m/s$ the added drag is equal to a vehicle driving $36\,km/h$ in no wind, and $25\,m/s$ is equal to a vehicle speed of $90\,km/h$. However, the direction of the wind that hits the vehicle is rather random, and non-head winds increase not only the vehicle's effective cross sectional area, but also the aerodynamic drag coefficient by around 5 to $10\,\%$ for passenger cars, in common wind conditions, (slightly more for family sedans and slightly less for sports cars), according to [14].

Air density varies depending on temperature, humidity and pressure, where the later indicates an altitude dependance. For comparative studies, often the density value of $1.225\,(kg/m^3)$

is used, which represents standardized conditions such as dry air at $15\,^{\circ}\mathrm{C}$ at standard atmospheric pressure ($1013.25\,Pa$) i.e. at sea level [14]. For temperatures between -30 to $50\,^{\circ}\mathrm{C}$ the density of dry air may be 80 to $110\,\%$ of the standard air density, while an increase in altitude of about $300\,m$ above sea level leads to a decrease in the dry air density of about $3\,\%$ relative to the standard air density [16].

The effective cross sectional **area** of the vehicle varies depending on the vehicle size and shape. According to [17], the area is to a large part determined by what is considered to be a comfortable seating position, and states that for a sedan with two seating rows, the area can be as small as $1.95\,m^2$, while for a 4-5 seat car the area could be around $1.75,\,m^2$. For auto manufacturers, the value of a certain car model's area can be found through detailed drawings or perhaps wind tunnel tests, yet the resulting value is not always communicated in official vehicle specifications. Therefore external parties are often forced to make rough estimations which relate the area to the product of a vehicle's height and width or track width. Various such estimations can be found in literature; $79-84$ % in [18], 81 % in [15] and 90 % of the product of track width and height in [19].

In [15] by Hucho from 1998, typical areas for different car classes are stated as can be seen in Table 2.1. In [18] p. 226 from Wong, sample values of 5 commercial passenger car areas and C_d values are published for different car sizes, see Table 2.1, while the stated source is a publication of Hucho from 1990. These two sources show a good coherence, apart from possible differences in terminology. It should be noted though, that the difference between the largest and smallest area within each category in [18], may be as large as 0.1 to $0.26\,m^2$. The large difference shows that this is a quite rough generalization, which should not blindly be trusted.

Table 2.1 Typical frontal areas depending on car size.

	Hucho 1998, [15]	Hucho 1990, through Wong 2008, [18]	max(A)-min(A) [18]
Mini:	1.8	1.76	0.11
Lower Medium:	-	1.84	0.15
Medium:	1.9	1.87	0.03
Upper medium:	2.0	2.02	0.26
Full size:	2.1	-	
Luxury:	-	2.06	0.24
Sports:	-	1.81	0.10

The **drag coefficient**, C_d is a dimensionless parameter that represents all the drag effects that are active on the vehicle, i.e. both external and internal, still to acquire an accurate estimate, it has to be measured. Thus automotive manufacturers measure the total drag force, F_a in wind tunnels or coast down tests, as well as the cross sectional area, air density and vehicle speed. Then, the drag coefficient can be found via (2.2). In comparison to area, this parameter is often made official and communicated in car model specifications. Typically the C_d value is in the range 0.25-0.35 in today's passenger cars [18], yet it may vary between 0.15 for a more streamlined shape up to 0.5 or higher for open convertibles, off-road vehicles or other rough shaped vehicles. Furthermore, the C_d value will change if the airflow around

and through the vehicle is altered during driving, for instance an open side window may increase the C_d value by about $5\,\%$ [18]. During the last few decades the general trend has been decreasing C_d values on new passenger cars [15], much due to the increased interest in fuel efficiency and emissions. In order not to compromise too much on the design and compartment comfort for the passengers, most work on aerodynamical drag reduction is likely to be focused on the C_d value [15] rather than on the area.

2.2.2 Rolling resistance

Rolling resistance is caused by a number of different phenomena taking place in and around the car tires during rolling. One of the major effects is that the repeated deflection of the tire causes a hysteresis within the tire material, which gives rise to an internal force resisting the motion [18]. Still, according to [14] p. 110 rolling resistance depends on more than seven different phenomena, which makes estimation of rolling resistance through analytical modeling very difficult. Therefore, the rolling resistance force, F_r acting on a vehicle in the longitudinal direction, is usually expressed as the effective normal load of the vehicle multiplied by the dimensionless rolling resistance coefficient, C_r as

$$F_r = C_r\, m\, g\, cos(\alpha) \tag{2.3}$$

where $m\,(kg)$ is the vehicle mass, $g\,(m/s^2)$ is the gravity constant, $\alpha\,(rad)$ is the road inclination angle. Often the $cos(\alpha)$ term is neglected since even a large grade such as $10\,\%$ ($\alpha \approx 0.1\ rad$), means that $cos(\alpha) \approx 0.995$ i.e. an error of less than $0.5\,\%$ of the rolling resistance force.

Empirical studies show that the C_r value depends on factors such as; tire material and design, but also tire working conditions such as inflation pressure (C_r decrease with increasing pressure), tire temperature (C_r decrease with increasing temperature), road surface (structure, wet or dry) and speed (C_r increase with increasing speed) [18].

For low speed levels, C_r increases only slightly with speed, while for at higher speed levels, C_r increases with almost the square of the speed [14]. At even higher speed levels a standing wave appears in the tire which greatly increases the energy loss and temperature rise in the tire, and which may eventually lead to tire failure [18], [14].

The rolling resistance coefficient's dependency on speed also varies with tire temperature, where higher temperature causes a weaker speed dependency [18]. During operation, it may take over 30 minutes of driving at a constant speed level, before the tire temperature reaches its steady-state value [20]. Then the rolling resistance coefficient may be somewhat smaller compared to the initial value at the same speed level. For tires found to have a relatively small positive speed dependency by non thermal steady-state measurements; a measurement made after reaching thermal steady-state may even show a small negative speed dependency of the rolling resistance coefficient, according to [20].

Various published speed dependencies of C_r can be seen in Figure 2.2, where some of the information represent data found in *Bosch Automotive Handbook* [19] and Guzzella's

Vehicle Propulsion Systems [21], both of which are here assumed to be based on measurements of typical available tires. The notations from Bosch stand for design speed limits of the tires; $180km/h$ for S, $190\,km/h$ for T, $210\,km/h$ for H, $240\,km/h$ for V, $270\,km/h$ for W, above $240\,km/h$ for Z, and finally the ECO tires are low rolling resistance tires that come in various speed ranges. In addition, Figure 2.2 shows three often referred to analytical estimations; one linear found in [22] (Ehsani), one that is weakly dependant on the square of the speed found in [18] (Wong), and one strongly depending on the square of the speed found in [14] (Gillespie). From the comparison in the figure, it is clear that the analytical expressions deviate quite a lot from the typical tire data. It can also be seen that C_r is slightly larger for tires of higher speed rating, and that the increase of C_r with speed is somewhat smaller compared to tires of the lower speed ratings.

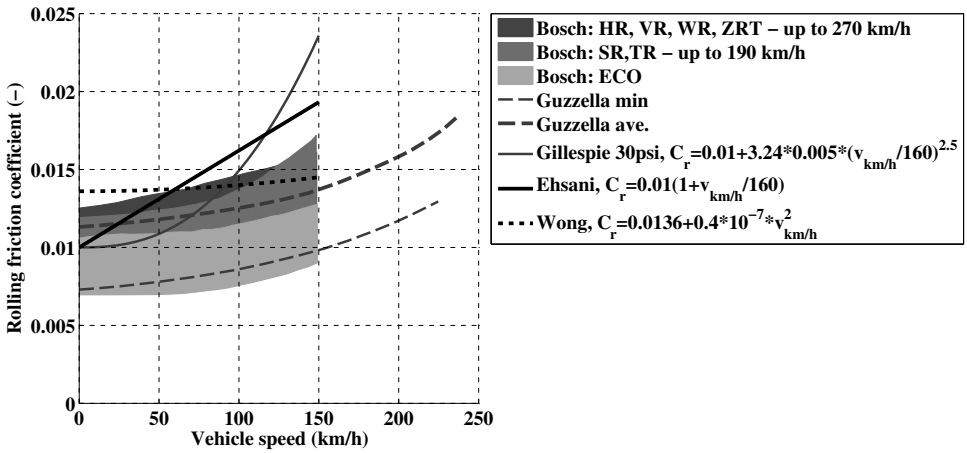

Figure 2.2 Rolling resistance coefficient as a function of speed from different literature sources; [19], [18], [14], [22] and [21].

During estimations of vehicle performance or fuel economy, C_r is often assumed to be constant, with typical values around 0.011 to 0.015 for radial types representing passenger car tires on dry concrete or asphalt [19], [13] and [14]. Due to increased environmental concerns in recent years, low rolling resistance tires are now also available, thus C_r values as low as 0.007 to 0.009 may also be used [13]. In addition, according to [23] most tires sold in the USA have measured C_r values between 0.007 to 0.014. Furthermore, [23] states that there are few sources with published data on rolling resistance coefficients of presently common passenger car tires, nevertheless a review of published data is provided, covering some of the main tire manufacturer's most sold models. The format of the data is; rolling resistance coefficients of new tires, measured under standardized circumstances, according to the SAE J1269 or J2452. The first standard measures the tire's C_r at a speed of $80\,km/h$, but after the tire has reached thermal steady state. The second standard measures C_r during a $180\,s$ stepwise coast down test from $115\,km/h$ to $15\,km/h$, but only after the tire initially

has reached thermal steady-state at $80\,km/h$. Most of the data presented in [23], adhere to the first standard (J1269). Even data deduced with the second standard (J2452) are presented as average values. According to [23], based on tire manufacturer data of new tires from 2005, the average C_r of low speed tires (up to $180\,-\,190\,km/h$) is 0.0098, for high speed tires (up to $210\,-\,240\,km/h$) it is 0.0101, while for very high speed tires (above $240\,km/h$) it is 0.0113.

2.2.3 Grading force

In case of a road grade (or inclination), the vehicle's dynamics will be affected by the component of the gravitational force F_g that is parallel with the road as

$$F_g = m\,g\,sin(\alpha) \tag{2.4}$$

where $\alpha\,(rad/s)$ is the angle between the level road and the horisontal plane as in

$$\alpha = arctan(\frac{rise}{run}) \;=\; arctan(\frac{\%grade}{100}) \tag{2.5}$$

where *rise* is the vertical rise and *run* is the horisontal distance. Road slope is often expressed in terms of % *grade*, hence this terminology will be used throughout the thesis.

Since the vehicle may be traveling uphill or downhill this force may either be resisting or contributing to the net tractive force on the vehicle, i.e. it will either be positive or negative.

From an energy perspective, driving on a non level road will cause buffering and draining of potential energy in the vehicle. However, since passenger cars are usually displaced only temporarily over a day or so, from it's starting position (e.g. at home), whatever the route traveled the potential energy when coming back remains the same. As with deceleration, a BEV is normally able to recuperate some of the energy from going downhill.

Grade and acceleration force comparison

Both acceleration force and grading force are products of vehicle mass, thus it follows that for any vehicle, a certain acceleration level causes the same wheel force as a certain road grade level. Typical acceleration and grade levels which have equivalent wheel force, can be seen in Table 2.2.

Table 2.2 Equivalent force for certain acceleration and grade levels.

a (m/s^2)	1	2	3	4	5	6
Grade $(\%)$	10.3	20.8	32.1	44.7	59.2	77.3
Grade $(\%)$	5	10	15	20	25	30
a (m/s^2)	0.49	0.98	1.46	1.92	2.38	2.82

2.2.4 Wheel force

The tractive force, F_{wheel} that has to come to the wheels from the powertrain in order to sustain a certain speed level, road grade and acceleration can be found as in

$$F_{wheel}(t) = F_{acc}(t) + F_a(t) + F_r(t) + F_g(t) \tag{2.6}$$

where $F_{acc}\,(Nm)$ is the force required to accelerate the vehicle mass at a certain magnitude of acceleration ($F_{acc} = m\,a$), see (2.1).

A positive value of F_{wheel} then strives to accelerate the vehicle, while a negative value can represent either a regenerative braking force from an electric motor or friction braking. Finally, if $F_{wheel}(t) = 0$ and the friction brake is disengaged, the vehicle is said to be coasting, that is only F_a, F_r and possibly F_g are acting on the vehicle.

The maximum tractive force on the driving wheels can be limited by either the powertrain's maximum force capability or the maximum adhesive capability between tire and ground that is possible to be applied on the wheel without loosing the grip of the road, i.e. starting to spin or slide [14] p. 35. The later is limited by the current normal force on the driving wheels, F_N and the coefficient of friction between the tire and the road, μ [13] as

$$F_{wheel,max} = \mu\,F_N \tag{2.7}$$

The normal load on the driving wheels or wheel pair is affected by the weight distribution in the car, hence it varies from car to car, and even from occasion to occasion for the same car since the loading may vary, and finally by the change in weight distribution during an acceleration or deceleration, [14] and [13].

The friction coefficient depends nonlinearly on the longitudinal tire slip, which is caused by deformation of the tire during acceleration and decelerations [13]. The slip is defined as

$$slip = (1 - \frac{v_{car}}{\omega\,r})100\ (\%) \tag{2.8}$$

and it leads to a non unity relation between the car speed, $v_{car}\,(m/s)$ and the product of wheel speed $\omega\,(rad/s)$ and wheel radius $r\,(m)$, which would otherwise be valid.

Starting from zero slip and friction, the friction coefficient increases with increasing slip, up to slip values of about 15 to $20\,\%$ where the coefficient peaks at values around 0.8 to 1, depending on type of tire and road condition, [13] and [22]. At even higher slip values, the friction coefficient decreases, but at a lower rate than before. Moreover, high slip values means that the wheels, hence also the electric machine will spin faster than calculated directly from the vehicle speed while ignoring the tire slip.

2.2.5 Wheel power and energy

The instantaneous tractive power, P_{wheel} that has to come to the wheels from the powertrain in order to sustain a certain speed level, road grade and acceleration is determined by the tractive force and the vehicle speed as

$$P_{wheel}(t) = F_{wheel}(t)\, v_{car}(t) \tag{2.9}$$

The total consumed energy at the wheel can be found from the time integral of the power as

$$E_{wheel}(t) = \int P_{wheel}(t)\, dt \tag{2.10}$$

During regenerative braking while F_{wheel} is negative also P_{wheel} will be negative, hence the total consumed energy over time will be reduced.

2.3 Permanent Magnet Synchronous Machine (PMSM)

A PMSM consist of a rotor with permanent magnets and a wound stator which is energized by an external AC voltage source, typically of three phase type. The stator core and the rotor is made of laminated steel plates that serve as conduction paths for the magnetic flux.

2.3.1 Equivalent electric circuit model

An often used representation is the circuit equivalent dynamic *dq*-model of a PMSM which can be seen in Figure 2.3, where *dq* implies the rotor frame of reference, or synchronous coordinates. The *direct* or *d*-axis physically represent a radial axis crossing the centerline of the magnets, i.e. directed in the direction of the magnetic flux from a magnet, while the *quadrature* or *q*-axis represent an axis crossing in between two magnets, (i.e. two magnetic poles), and that is 90 electrical degrees ahead of the *d*-axis.

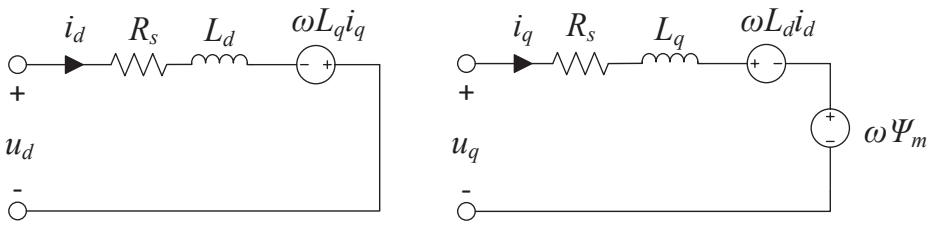

Figure 2.3 Circuit equivalent model of a PMSM.

The dynamic *d*- and *q*-axis stator voltage equations as functions of the *d*- and *q*-axis stator currents (i_d and i_q) are;

$$u_d = L_d \frac{di_d}{dt} + R_s i_d - w_r L_q i_q \tag{2.11}$$

$$u_q = L_q \frac{di_q}{dt} + R_s i_q + w_r L_d i_d + w_r \Psi_m \tag{2.12}$$

where R_s is the stator winding resistance, w_r is the electrical angular speed ($w_r = n_p w_m$ where w_m is the rotor angular speed and n_p is the number of pole pairs), L_d and L_q are the *d*- and *q*-axis winding inductances, and Ψ_m is the permanent magnet flux linkage.

When considering electrical steady state, the di/dt-terms may be omitted.

2.3.2 Mechanical output

For salient machines the produced electromechanical torque can be expressed as

$$T_e = \frac{3n_p}{2K^2}(\Psi_d i_q - \Psi_q i_d) = \frac{3n_p}{2K^2}(\Psi_m i_q + (L_d - L_q)\, i_d\, i_q) \tag{2.13}$$

where Ψ_d and Ψ_q are flux linkage in the *d*- and *q*-axis, Ψ_m is the magnet flux linkage, and K is the scaling constant for transformation between three phase to two phase space vectors. For amplitude invariant scaling, K should be set to unity.

The stator inductance relates a change in current with a change in flux linkage (as $\Psi = L\, i$), and for low current levels (i.e. low torque levels) the relation is close to linear, but at higher current levels the iron becomes magnetically saturated, thus an equally large increase in current will then only cause a minor increase in the flux linkage (i.e. only a minor increase of the torque). In order for this effect to be represented in the circuit diagram, both the *d*- and the *q*-axis inductance could be modeled as functions of current. The saturation also limits the magnet flux linkage, hence it could also be modeled as a function of current.

The part of the *electromagnetic torque* production that is caused by the *d*-axis current is called *reluctance torque*. In salient machines, often L_d is smaller than L_q, due to a higher reluctance of magnetic material compared to iron. Thus, to be able to produce a positive reluctance torque, the *d*-axis current must be negative.

Ideally the mechanical output of an electric motor, in terms of torque and power as a function of speed, can be divided into two main areas of operation; the *constant torque* region and the *constant power* region. In the constant torque region starting from zero speed, the machine is capable of producing its maximum torque given that it can be fed by the same level of maximum current. As the speed increases, so does the induced voltage, hence the applied voltage must also increase, until the maximum voltage limit is hit. At this point the machine is operating at its maximum power limit. The speed level where this occurs is referred to as *base speed*. To be able to reach still higher speeds, the effect of the induced voltage must be decreased. This is done by reducing the flux-linkage in the *d*-axis, by utilizing the *d*-axis current. Therefore, the same level of maximum torque can no longer be provided. Instead the torque becomes inversely proportional to the speed. The power, however is ideally kept constant up to the top speed of the motor, hence the name constant power region.

For a certain machine, the maximum transient low speed torque is often limited by the maximum converter current, which in turns is set by thermal limitations. The base speed depends on the maximum available voltage from the voltage source. Naturally both the current and voltage will affect the maximum available power.

2.3.3 PMSM power losses

The two largest losses in a PMSM are the resistive losses in the copper windings in the stator, and the iron losses mainly in the stator core, where the copper losses are usually the larger of the two [24]. Other causes of power loss are the mechanical; windage and friction.

Copper losses:

Copper losses depend on the number of phases, the stator winding phase resistance, R_s, and the square of the *RMS* phase current, $I_{s,RMS}$. In the *dq*-reference frame it can be expressed as

$$P_{cu} = \frac{3}{2} R_s {I_{s,RMS}}^2 = \frac{3}{2} R_s ({i_d}^2 + {i_q}^2) \tag{2.14}$$

The stator resistance increases with temperature, such that for every $25\,^{\circ}\mathrm{C}$ increase in wire temperature, the resistance increases by about $10\,\%$. This means that, for the same magnitude of current, the copper losses will increase by the same factor.

Another factor that may increase the resistance during operation is the frequency of the supply voltage, through the so called **skin effect** or by the **proximity effect**. These effects are however fairly small.

Iron (core) losses:

Iron losses or core losses depend mainly on two phenomena; magnetic hysteresis and induced eddy currents. The mean losses can be described as

$$P_{fe} = k_h f_r {B_{pk}}^n + k_e {f_r}^2 {B_{pk}}^2 \tag{2.15}$$

where

k_h	a hysteresis parameter
f_r	frequency of the supply voltage
B_{pk}	the peak flux density in the B-H hysteresis curve
n	depends on steel material, (typically 1.6-2.2), B_{pk} and f_r
k_e	an eddy current parameter

The core losses are generally very difficult to estimate correctly. Even with advanced FEM softwares the error may be quite large. One of the complexities is that, induced voltages in machines which are fed by switched inverters contain harmonics beside the base frequency, hence the flux linkage will also contain harmonics that causes excess core losses. Both the characteristics of the harmonics and their effect in the material are difficult to predict correctly.

The rotor losses are usually rather small in PMSM machines, and mainly caused by eddy current losses in the iron core and the magnets, which can be reduced by certain design choices such as thinner laminations, core material with higher resistivity and by segmentation of the magnets.

2.3.4 PMSM control

As stated above, the PMSM losses depend on the operating conditions, i.e. the current and the voltage frequency. Moreover, the operating conditions depend on the control method used, since any given torque and speed operating point, can be realized with a range of combinations of *d*- and *q*-axis currents. One control strategy that is rather simple to implement in theoretical calculations, is the so called Maximum Torque Per Ampere (MTPA) method, where the angle ϕ between the *d*- and *q*-axis currents is found such that the highest torque for a certain magnitude of current, I_s, is produced (where $I_d = I_s\, sin(\phi)$ and $I_q = I_s\, cos(\phi)$). This method thus also minimizes the copper losses. The MTPA angel can be found as

$$sin(\phi) = -\frac{\Psi_m}{4(L_d - L_q)I_s} - \sqrt{\Big(\frac{\Psi_m}{4(L_d - L_q)I_s}\Big)^2 + \frac{1}{2}} \tag{2.16}$$

where I_s is the stator current magnitude [25]. The MTPA strategy is valid until the voltage limit is hit, after which another strategy has to be implemented, e.g. Maximum Torque Per Voltage.

2.3.5 PMSM steady state modeling with regard to core losses

Since core losses are rather difficult to estimate with a high level of accuracy, an alternative method may be to introduce a core loss resistance, R_c as was done in [25] and [26], see Figure 2.4.

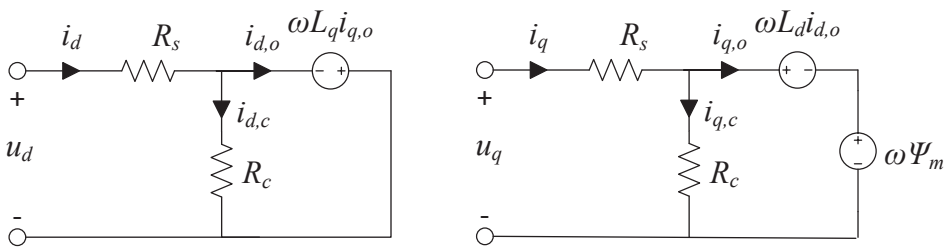

Figure 2.4 Model of a PMSM, taking no load losses into account.

Then the stator voltage equations becomes

$$u_d = R_s i_d - w_r L_q i_{q,o} \tag{2.17}$$

$$u_q = R_s i_q + w_r L_d i_{d,o} + w_r \Psi_m \tag{2.18}$$

The electromechanical torque can be expressed as

$$T_e = \frac{3n_p}{2}(\Psi_m i_{q,o} - (L_d - L_q) i_{d,o} i_{q,o}) \tag{2.19}$$

2.4 DC-AC Converter loss modeling

A DC-AC converter typically utilizes power electronic switching devices in order to convert between the battery DC voltage and the three phase AC voltage which is demanded by the electric machine. In automotive application each switch normally consist of one or a few paralleled IGBT chips in parallel with one or a few diode chips, depending on current rating.

During operation, the main losses in the converter are due to *conduction* and *switchings* both in the transistor and the diode. The losses can be modeled as in [27] where an ideal sinusoidal Pulse Width Modulated (PWM) three phase voltage is assumed. Losses dissipated in the driver and snubber circuits, as well as due to capacitive and inductive parasitics, are assumed negligible. For the IGBTs, on-state, turn-on and turn-off losses are considered, while the reverse blocking losses are assumed negligible. Similarly for the diodes, on-state and turn-on losses are considered, however the turn-on losses are also neglected, due to an assumed fast diode turn-on process.

According to [27] the average on-state losses in the IGBTs in one switch can be estimated according to

$$P_{cond.\,IGBT} = \Big(\frac{1}{2\pi} + \frac{m\,cos\,\varphi}{8}\Big) V_{CE0}\,\hat{I}_s + \Big(\frac{1}{8} + \frac{m\,cos\,\varphi}{3\pi}\Big) R_{CE}\,\hat{I}_s{}^2 \tag{2.20}$$

and the average (per switching period) turn-on and turn-off switching losses as

$$P_{sw.\,IGBT} = f_{sw}\,E_{(on+off)}\,\frac{1}{\pi}\,\frac{\hat{I_s}}{I_{ref}}\,\Big(\frac{V_{DC}}{V_{ref}}\Big)^{K_v} \tag{2.21}$$

where the following parameters are component dependent (most are extractable from the semiconductor component data sheet)

V_{CE0}	IGBT threshold voltage of the on-state characteristics, temperature dependent
R_{CE}	IGBT on-state resistance, temperature dependent
E_{on+off}	Energy dissipated during turn-on and turn-off
I_{ref}	Reference current, to which switching losses in data sheet correlate
V_{ref}	Reference DC voltage, to which switching losses in data sheet correlate
K_v	Parameter describing voltage dependency of switching losses, typically 1.3 to 1.4

while the others are operation dependent

m	PWM modulation index
φ	phase angle between voltage and current
$\hat{I}_s$	Amplitude of AC phase current
f_{sw}	switching frequency
V_{DC}	DC voltage level

The average diode on-state losses can be estimated as

$$P_{cond.\,diode} = \Big(\frac{1}{2\pi} - \frac{m\,cos\,\varphi}{8}\Big) V_{F0}\,\hat{I}_s + \Big(\frac{1}{8} - \frac{m\,cos\,\varphi}{3\pi}\Big) R_F\,\hat{I}_s{}^2 \tag{2.22}$$

and the average turn-off losses as

$$P_{sw.\,diode} = f_{sw}\,E_{rr}\,\Big(\frac{1}{\pi}\,\frac{\hat{I}_s}{I_{ref}}\Big)^{K_i}\,\Big(\frac{V_{DC}}{V_{ref}}\Big)^{K_v} \tag{2.23}$$

where

V_{F0}	diode threshold voltage of the on-state characteristics, temperature dependent
R_F	diode on-state resistance, temperature dependent
E_{rr}	Energy dissipated during turn-off (due to the reverse recovery process)
K_i	Parameter describing current dependency of switching losses, typically 0.6
K_v	Parameter describing voltage dependency of switching losses, typically 0.6

Due to symmetry in operation, it is enough to model the losses in a single switch, and to attribute the same power loss in the other switches in order to find the total converter losses.

According to [28], by utilizing the so called *third harmonic injection* operation of the converter, the output amplitude of the AC phase voltage, $\hat{U}_{ph}$, ideally depends on the present DC voltage, V_{DC}, and the controlled PWM modulation index, m_a as

$$\hat{U}_{ph} = m_a\,\frac{V_{DC}}{\sqrt{3}} \tag{2.24}$$

In order to maintain controllability of the current, [28] recommends a maximum m_a of 0.9, which then sets the limit of the possible output AC voltage relative to the DC voltage.

IGBT converter modules are typically designed to withstand specific voltage levels of around $600\,V$, $1200\,V$ etc. Then at each voltage level, a number of slightly different modules are normally available, with various current ratings, such as $200\,A$, $400\,A$ etc. Since the losses to a large part depend on the magnitude of current, the current ratings implies how large temperature rise due to losses, that the cooling system is able to handle without risking overheating of the transistor or diode chips.

2.5 Battery modeling

A very simple equivalent circuit model of an electrochemical battery can be seen in Figure 2.5, where V_{OC} represent an ideal no load battery voltage, R_{dis} and R_{ch} represent the

internal resistances during discharge and charge of the battery by the current I_b, leading to a load dependent terminal voltage V_t, [29], [21] and [22].

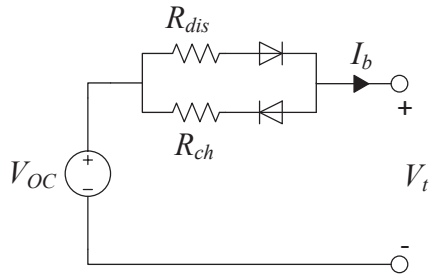

Figure 2.5 Simple battery model, with separate internal resistance for discharge and charge, with ideal symbolic diodes.

The terminal voltage equation is thus

$$V_t = V_{OC} - R_{dis}\, I_b \tag{2.25}$$

The charge content in the battery is often described by the term *state-of-charge* (SOC) which changes with battery current as

$$SOC(t) = SOC_{init} - \frac{\int_{t_0}^{t} I_b\,(\tau)\, d\tau}{Q_{tot}} \tag{2.26}$$

where SOC_{init} is the initial SOC level, Q_{tot} (Ah) is the total charge capacity of the battery.

In order to make the model in Figure 2.5 a bit more advanced the no load voltage can be modeled as a function of the battery's state of charge. During operation the battery energy content is drained which leads to a decrease in the no load voltage, down to a certain point at a very low SOC level where the no load voltage suddenly drops very rapidly.

The main power losses in the battery are due to the internal resistance and can be modeled as RI^2 conduction losses.

Normally a lithium ion battery cell has a maximum and minimum allowed terminal voltage level, and a maximum and minimum allowed current, or *C-rate*, where a discharge rate of 1C means that the current is such that the battery will be discharged in one hour. According to [30] the test to determine a battery's energy content is usually done for a constant current discharge at a $C/3$ discharge rate.

With the battery model as in Figure 2.5, the maximum power that can be transferred to the load is $P_{max,theoretic} = \frac{1}{4}\frac{{V_{OC}}^2}{R_{dis}}$, however according to [30], for practical reasons the limit is rather set as

$$P_{max,theoretic} = \frac{2}{9}\frac{{V_{OC}}^2}{R_{dis}} \tag{2.27}$$

The output power may also be limited by either a minimum voltage as

$$P_{max,V_{min}} = V_{min}\,\frac{V_{OC} - V_{min}}{R_{dis}} \tag{2.28}$$

or by a maximum current limit, which may be due to lifetime or thermal issues, as

$$P_{max,I_{max}} = I_{max}(V_{OC} + R_{dis}\,I_{max}) \tag{2.29}$$

Both the no load voltage and internal resistances vary depending on SOC level and battery temperature.

According to [29], a more dynamical representation of the terminal voltage is achieved with one or more RC-links in the model, where the main capacitive effects within the battery are also represented.

2.6 Transmission

Automotive gearbox losses generally depend on various operating conditions, where the main factors are; speed, load level and temperature, resulting in typical vehicle gearbox efficiencies of $95 - 97\,\%$ [21]. According to [31] the losses spring from phenomena that are both load independent (spring losses; oil churning and air windage) and load dependent (mechanical losses; rolling and sliding), where sliding losses may be the dominating contributor. The load independent losses cannot easily be modeled accurately with general analytical expressions. Instead experimental results are required in order to develop empirical loss models whose validity naturally will be rather limited. A number of these types of models have been suggested by various researchers. For the load dependent losses, physical expressions can be utilized in the loss modeling, however accurate parameter estimation can still be difficult.

In a BEV the transmission is typically of single-speed spur gear type, which according to [32] and [33] can be assumed to have an efficiency of 95%, in energy consumption assessments.

2.7 Auxiliary loads

During normal vehicle operation, not only the propulsion will drain the battery of energy, but also a number of secondary loads, which are often fed by a low voltage circuit. These loads may be air-conditioner, radiator fan, pumps, wipers, windows, lights, radio as well as various control systems in the vehicle [34]. Apart from an overall increased energy consumption, these types of loads may also demand relatively high peak power levels from the battery, e.g. $1.5\,kW$ for compact cars and $2.8\,kW$ for a mid-size car, according to [13]. Furthermore, according to [13], an electrical air conditioning system is designed for a peak power of $6.5\,kW$ and a continuous power of $4\,kW$.

Chapter 3

Road type driving patterns, road grade and daily driven distances

For a successful vehicle design, as with design of any product, knowledge of the use phase is essential. Vehicles are used in various environments, by different types of drivers and for numerous purposes. Each of these circumstances put their specific capability requirements on the vehicle, in terms of static and dynamic road load levels.

Through the years much research has been conducted, especially in Europe and the US, aiming to identify typical *driving patterns* on different *road types*. The main reason has then been to assess in which way, and to what degree, vehicle pollutant emissions and fuel consumption are effected by different driving patterns and situations.

This chapter attempts to identify typical levels of **speed**, **acceleration** and **road grade** attributed to different road types, such as urban (or city) driving and high speed motorway driving, for the purpose of finding suitable powertrain design criteria regarding torque speed and power. Additionally, typical daily driving distances will be investigated, since range is an important design factor for a BEV.

3.1 Driving patterns

Normal on-road driving is thus affected by many different factors such as; driver behavior, weather conditions, street type, traffic conditions, journey type as well as vehicle type and specifications [1]. This makes it a quite challenging task to identify and to specify typical driving characteristics.

Many studies have been done under the sponsorships of American and European national emission regulatory organizations, such as the US Environmental Protection Agency (EPA), the California Air Resources Board (CARB) and the United Nations Economic Commission for Europe (UN/ECE). The purpose has then been to develop test procedures which describe repeatable standardized laboratory tests on light duty vehicles, i.e. passenger cars,

as a part of the type approval procedure. Then legally regulated emissions as well as fuel economy/efficiency are measured while the vehicle is driven according to a prerecorded speed over time; a so called *drive cycle*. In order to make sure that the legally set emission targets are not exceeded in typical real-world traffic, it is highly desired that the laboratory test fallout is fairly close to that. Another important outcome of the test is that they represent a fair estimation of fuel economy/efficiency for customers.

However as recognized by EPA most test drive cycles were developed a few decades ago, and both legal speed limits and vehicle power specifications thus performance have increased since, [2], the later which has also been noted in Sweden by [35]. It was to account for this that EPA updated the fuel economy test procedure in 2008 to also include two more aggressive cycles.

In recent years, several extensive studies have been conducted all around the world, targeting investigation and identification of typical driving patterns and their effect on fuel consumption and emissions. As a fact, apart from the added cycles, EPA has also considered such studies in order to find other causes of fuel consumption during real-world driving, such as fuel energy density, wind, tire pressure and road roughness [2]. But instead of expanding the test procedure, EPA has developed an intricate formula where the city and highway fuel economy label data are calculated based on certain weighting factors on sections of each test cycle.

So far, the test procedures in Europe are the same since the year 2000. Yet several large projects have been conducted, where driving data has been collected using instrumented vehicles, and corresponding drive cycles have been developed. The most known studies are the INRETS, HYZEM, ARTEMIS and the latest is the WLTC.

Due to the large interest in gathering information of local driving patterns, a wide range of real-world cycles have been developed to capture the specific circumstances of driving on a certain type of road, in a particular city, or region of the world. Cycles of this type can be found from regions such as; (Pune) India, China, Hong Kong, Tehran Iran, (Melbourne, Perth) Australia, Manila Filipines, Edingburgh UK, Latvia, Athens Greece and Vietnam.

In the Chalmers initiated, *The Swedish Car Movement Data Project*, 714 cars have been instrumented during the years 2010-2012, in the south west of Sweden and the data is gathered in a data base [36]. As a researcher, access to the data base can be granted, however it has not been used within the scope of this project.

Instead, in this project sample in-house-measurements have been conducted, mostly covering the area in and around Göteborg, but also longer highway sections, e.g. between Göteborg and Jönköping and Torslanda-Stenungsund. Data regarding speed and acceleration has been measured with a GPS and an accelerometer, see Appendix B.

3.1.1 Legislative cycles

During the standardized tests, the vehicle is driven on a chassis dynamometer with the driving wheel pair on a roller, attempting to, within specified limits, follow the time series speed trace of a specified drive cycle. The vehicle's rolling resistance and air drag is estimated

and added as an extra load on the roller. Traditionally, there are separate test procedures for measuring pollutant emissions like (CO, HC, NOx, and PM) compared to measuring CO_2 emissions together with fuel economy/consumption. The differences in procedures may be; the used drive cycle/-s, or at which ambient temperature the test is run. European and Japanese test procedures include only one specified drive cycle (NEDC) and (JC08) for both test procedures including BEVs, while the US test procedures utilize five dissimilar drive cycles, each aiming to represent various types of driving on different road types.

Here follows a short review of the history of the development of the legislative drive cycles in the US, Europe and Japan.

3.1.1.1 Test drive cycles in the US

Vehicle driving patterns and emissions were studied in Los Angeles, USA, in the 1950s, due to the strong suspicion that the city's smog was to a large part caused by motor vehicles. In the end of the 1950s one of the first test cycles was developed. Input data was collected by driving with seven different cars on different types of roads around Los Angeles, and recording the amount of time spent in certain bins of engine speed and manifold pressure, as well as time spent to accelerate between the speed levels. The resulting cycle was a so called *modal drive cycle* with sixteen modes of constant speed and acceleration, where the relative duration of each mode served as a reflection of the measurements. The top speed was $80\,km/h$ and the maximum acceleration was $1.34\,m/s^2$ [37]. But it wasn't until about a decade later, in 1966, that a shortened version of it, a seven-mode cycle, (same top speed but lower maximum acceleration $0.8\,m/s^2$ representing 24 hours average conditions) was adopted in Californians first test procedure to measure vehicle emissions (HC and CO) and fuel economy in a standardized manner [38], [37]. In 1968 the procedure was adopted in the rest of the USA [37].

However already in 1969 the work continued towards an updated test cycle which could better represent typical morning traveling in Los Angeles, and more measurements were done. Finally the new cycle was taken from direct speed measurements from a vehicle driving on a specific route (the LA-4 route) around Los Angeles, as the one out of six runs which was closest to the average [37]. The cycle distance was then shortened to represent the typical driving distance in Los Angeles at the time, $12\,km$ [37]. The maximum acceleration and deceleration rate of the cycle was limited to $1.48\,m/s^2$ ($3.3\,mph/s$), due to a limited measuring range of the lab chassis dynamometer [37], [38]. The cycle was called the Urban Dynamometer Driving Schedule (**UDDS**), but it is also known as the LA4-S4 cycle or **FTP-72**, and was adopted as a new test cycle in the US in 1972 [38]. Test runs in labs measuring HC, CO and CO2 showed a very good correspondence with the real route emissions. In 1975 the cycle was somewhat modified such that the initial cycle was followed by a 10 min long stand still (soak), after which the initial 505 seconds were repeated, thus forming the **FTP-75** cycle, which is still used today to represent urban/city driving.

As EPA started publishing fuel economy data of new cars, using the city cycle FTP in the 1970s, the interest rose in similar data also for highway driving, [38]. Therefore, EPA started

a "chase car" measurement series and drove over $1\,690\,km$ on non-urban roads in the area of Michigan, Ohio and Indiana, where the maximum speed limit was $88.5\,km/h$ ($55\,mph$), as in most of the USA at the time. The collected data was analyzed and resulted in the Highway Fuel Economy Test cycle (**HWFET**). Also in this cycle, acceleration and deceleration rates were limited to $1.48\,m/s^2$, due to belt slippage during chassis dynamometer tests, however these modifications are considered to have only minor influence since they were limited to the fist ten and last twenty seconds of the cycle [37].

According to a study by CARB in 1990, large accelerations could have dramatic effects on emission levels, still these events were missing in the FTP cycle [39]. As EPA found a lack of data on the occurrence frequency of such accelerations during normal driving, they initiated a new study. Hence in 1992 EPA together with CARB and two manufacturer organizations[1] conducted a vast real-world-driving study based on 100-150 instrumented vehicles in each of the three cities; Baltimore, Spokane and Atlanta [39]. Data was also recorded using the "chase car" method on routes in Baltimore, Spokane and Los Angeles [39]. The recorded driving data showed that during almost $13\,\%$ of the time, the vehicle was experiencing higher speed and acceleration levels than what was represented in the FTP cycle [39]. Based on the measured data from Baltimore together with the collected data from Los Angeles, Sierra Research which was contracted by EPA, divided the time traces into micro-trips, i.e. cutting the cycle at each stand still. A software was then developed which sampled different micro-trips together to form a drive cycle, according to certain cycle targets. In this way thousands of cycles were created. Finally those few with the best match to targeted speed-acceleration-distribution were chosen to be continued with [39]. One of the most famous ones is the **REP05** which represents aggressive highway driving where about $70\,\%$ of the time is spend at higher speed and acceleration levels compared to the FTP cycle [39]. Other known cycles are the **ARB02** and **LA92** or Unified Cycle (**UC**).

Later in the mid 1990s, the EPA emission test procedure was updated, the so called Supplemental Federal Test Procedure (SFTP), now including two new cycles which represents more aggressive driving and rapid speed fluctuations. One of them was the **SC03**, which is a low speed cycle, but contains rapid speed fluctuations. The other one was the **US06** cycle, which is developed as a shortened combination of the REP05 and the ARB02 cycles, representing high speed and acceleration levels.

Today EPA's test procedure for emissions comprise of the FTP-75, SC03, UDDS (FTP-72), US06 and the LA92 cycles, regulated under $Tier1-3$. For fuel economy and CO_2 emission labeling (regulated since 2012 on a fleet average basis), the FTP and HWFET were the only cycles used until vehicle model year 2008, when also the US06, SC03 (run at $35\,^{\circ}\mathrm{C}$) and a cold version of the FTP ($-6.7\,^{\circ}\mathrm{C}$, instead of $23.9\,^{\circ}\mathrm{C}$ as for HWFET and hot FTP) were added.

When it comes to driving range and fuel economy of BEVs, either the FTP and HWFET cycles can be used, or the five cycles used for conventional vehicle fuel economy can be used, until EPA's rules are updated for BEVs [40].

[1] The American Automobile Manufacturers Association (AAMA) and the Association of International Automobile Manufacturers (AIAM)

Another cycle which has been developed by the EPA, is the New York City Cycle (**NYCC**), which represents congested traffic in a large city. Even though it is not utilized in any regulatory test procedure, it can be seen in many published articles regarding Hybrid (HEV) and Plug-In Hybrid Electric Vehicles (PHEV).

3.1.1.2 Test drive cycles in Europe

Smog was also an increasing problem in larger cities in Europe during the 1950s and 1960s, especially in London. According to [37], a modal cycle was developed in the mid 1960s, which was based on measurements in Paris of engine speed, pressure, brake pedal activity and selected gear position, (very much like the work previously done in Los Angeles),i.e. with modes of constant speed and accelerations. Furthermore, according to [37], this cycle was then modified into the first **ECE 15** cycle (15 modes), based on additional measured driving patterns in ten European cities. The cycle was adopted in the European Community's first vehicle emission regulation in 1970 (directive 70/220/EEC) as a part of a vehicle's type approval, with limits on gaseous pollutants depending on the vehicle weight [41].

In 1990 EU test procedures, the **EUDC** part was added after four ECE-15 cycle repetitions, aiming to also represent more aggressive and high speed driving. This combination formed a cycle called ECE+EUDC, or MVEG-A, which was also initiated by a $40\,s$ period of engine idling [42]. From the year 2000, the idling period was removed, thus it became an engine cold start cycle, called New European Driving Cycle (**NEDC**), or MVEG-B [42].

Today the NEDC cycle is utilized in test procedures of both pollutant emissions (regulated in $Euro1-6$) and or testing fuel consumption and CO_2 emissions. The later is regulated since 2012. NEDC is also utilized when determining the driving range and energy consumption of BEVs. The temperature during the test may be between between $20-30\,^{\circ}\mathrm{C}$.

3.1.1.3 Test drive cycles in Japan

Also in Japan a modal cycle was developed 1969. It was replaced 1973 by an early version of the 10-mode cycle simulating driving in Tokyo with max speed of $40\,km/h$ used in emission certifications, and 1975 an 11-mode was developed simulating suburban driving with a top speed of $60\,km/h$ [37] however this part was not added to the test procedure. Not until 1991 was a high speed mode added to the Japanese test; the 15-mode cycle, still with a moderate top speed of $70\,km/h$ [43]. During recent years, from 2008 to 2011 the latest and current test cycle was introduced in the regulations; the **JC08** cycle, which is a step away from the earlier modal cycles, yet still representing congested city driving with the relatively low top speed of $80\,km/h$ [42]. As in Europe, the same cycle is used for measuring both pollutant emissions as well as fuel economy and CO_2 emissions.

3.1.1.4 Test drive cycles in the world

Since the 1970s many more countries around the world have adopted emission regulations (for light duty vehicle emissions of CO, HC, NOx and PM in gram per driven km) and

related test procedures, often based on either the US *Tier* or European *Euro* [43] and [42]. Today Australia[1], half of south America and most of Asia[2], including China and India, but except Japan, have adopted the European regulations, while North America and about half of south America have adopted the US emission regulations [19].

3.1.2 Non-legislative cycles

Many of the non-legislative cycles are not easily accessible for external parties, while it can be assumed that the majority of the automotive industry has gained access in order to develop their final products.

This work is based on cycles from Artemis, WLTC as well as own in-house measurements in the area around Göteborg.

3.1.2.1 Artemis

The Artemis project involved 40 European research laboratories and was founded by the European Commission, to develop new European methods, tools, models and databases for accurate estimation of pollutant emissions from transport [44]. Within the project, a set of real world driving cycles for passenger cars were developed, categorized as *urban*, *rural* and *motorway*, each with sub-cycles representing various driving conditions such as traffic density.

The Artemis cycles are based on data from 77 instrumented vehicles in France, UK, Germany and Greece collected in 1990s in the previous research projects *DRIVE-MODEM* and *HyZem*, each in which a number of cycles were also developed (in the categories; urban, congested urban, road and motorway) [44].

The Artemis Urban cycle has sub-cycles of congested, dense and free flow traffic, where the speed level differs between about $10 - 60\,km/h$ as well as the number of and duration of stops. The Rural cycle has sections of steady and unsteady speeds at rural secondary to main roads at speed levels around $50 - 100\,km/h$. Finally the Motorway cycle also has sub-cycles of steady and unsteady speed at speed levels between about $90 - 150\,km/h$ [44].

3.1.2.2 WLTC

Since 2008, the United Nations Economic Commission for Europe (UN-ECE) are presently working on finalizing a proposal for a new Worldwide harmonized Light duty driving Test Cycle (WLTC), which can be used for type approval fuel consumption and emission tests. The cycle is aimed to represent typical driving on a global scale. Vehicle data has been collected from instrumented vehicles in USA, Japan, India, Korea and the European countries Belgium, Germany, Spain, France, Italy, Poland, Slovenia, Switzerland, United Kingdom

[1] Australian emission regulations are based on European regulations but with some additional selected parts from US and Japanese standards [42].

[2] In South Korea the diesel engine vehicles are under European regulation while the gasoline engine vehicles are under US regulations [42].

and Sweden. The logged data has then been chopped into micro trips which in turn have been categorized for further analysis [45].

Three classes of drive cycles have been developed, where Class 1 is to be used by vehicles with power-to-mass ratio of $\leq 22\,W/kg$, Class 2 by vehicles with power to mass ratios > 22 and $\leq 34\,W/kg$, and finally Class 3 by vehicles with ratios $> 34\,W/kg$ [45]. Each class consist of 2 to 4 cycles called; Low, Middle, High, ExtraHigh, regarding speed levels. They have different characteristics such as speed and acceleration levels, and cover scenarios like congestion or free flow traffic.

3.1.2.3 Electric Power Engineering, Chalmers

At the beginning of this work, there was a lack of awareness of and access to real-world cycles, except those used as test cycles. Another important aspect was the desire to attain vehicle operation information at a higher time resolution than what is typically available from the official test cycles, which are mainly second based. Therefore a measurement system was purchased and a few different cars were instrumented during typical driving in the area of Göteborg. The measurement system consists of a $5\,Hz$ GPS receiver and a $20\,Hz$ 3D acceleratorer, thus giving a higher time resolution than what can be found in most official real-world cycles. Apart from vehicle speed and acceleration, also the road grade has been estimated with this system, while this is often omitted in official real-world cycles. See Appendix B for a more detailed description of the measurement system, as well as filtering of measured data.

The selected data represent collected logs mostly in the area of Göteborg, by a limited set of; car models, drivers, and routes. Some routes represent typical home-to-work routes, others only typical driving in the city or on the highway.

3.1.3 Driving pattern characterization parameters

Research on the topic of driving patterns have traditionally been focused on identifying specific events during driving that may have an effect on fuel consumption and emissions, as well as on quantifying this effect through empirical field studies with instrumented vehicles. In several such studies, it has been found that high acceleration levels in general, and in combination with high speed in particular, have a major effect on both emissions and fuel consumption, even though the frequency of occurrence of these events is rather small i.e. only a few percent of the total driving time, [3] and [4]. Still these findings belong to conventional vehicles with internal combustion engines, it is likely that similar measures will also have an important impact on electrically powered vehicles. Power demanding measures are especially interesting in this study since the maximum demanded powertrain power is sought.

The analysis is often based on a set of calculated parameters related to time, speed and acceleration. According to [3], the parameters can be divided into; **level parameters** such as *max., average and standard deviation of speed and acceleration*, **distribution measures**

like *relative time spent in bins of speed and acceleration*, and by **oscillatory measures** considering for example *changes of speed levels per distance or time*. It is not evident, which parameters that are relevant when considering the power demand and energy consumption of a BEV, however 15 parameters have been chosen to be used for all of the discussed drive cycles in this thesis. As level parameters; total time, driven distance, maximum speed, average speed, average running speed (i.e. without stops) and standard deviation of speed, have been used as well as maximum, average, and standard deviation of positive and negative acceleration. As distribution measures; relative time spent standing still, and in certain speed levels have been used, as well as relative time spent during positive and negative acceleration, and within certain acceleration level intervals. Finally an oscillatory measure is also used; Relative Positive Acceleration (RPA), defined as

$$RPA = \frac{\int speed(t)\ positive\,acceleration(t)\ dt}{\int speed(t)\,dt = total\,driven\,distance}. \tag{3.1}$$

RPA is an indicator of accelerations which demand high power, since a large acceleration may demand a high torque but not necessarily a high power, unless it is combined with a high speed [3] [1].

3.2 Road type specification based on speed levels

The speed levels experienced by vehicles are of great interest for finding necessary top speed of the vehicles. It is also interesting to know what speed levels that typically occur on which road type.

3.2.1 Legal speed limits

Vehicles are driven on roads which are subjected to national legally regulated speed limits, which depend on the surrounding area or type of road. There are different types of roads with various and overlapping associated speed limits which induce a relatively high level of ambiguity and makes generalizations difficult, however attempts of general categorizations have been made in the found references; *inside* and *outside built up areas* and *motorways*. Typically, road types within built up areas have speed limits around $30 - 70\,km/h$, outside built up areas $70-110km/h$, and on the fastest motorways $110-130\,km/h$ [46], [47], [48]. Additionally, a few countries in the world have motorway sections with speed limits of $140km/h$; higher quality highways in Bulgaria, Poland and the United Arab Enirates [46]. Some motorway sections in Italy may even have speed limits of $150\,km/h$. The Auto-bahn in Germany is known to have no speed limits at all, however nowadays, over half of the German auto-bahn's have speed limits up to $120\,km/h$, while the rest have recommended speed limits of $130\,km/h$. On the contrary, in Norway and Japan the speed limit on motorways is not more than $100\,km/h$ [46].

3.2.2 Road type speed levels for test cycles/Previous studies

The US EPA has chosen to divide their fuel consumption cycles in two categories; city or highway, where driving below $72\,km/h$ ($45\,mph$) is considered to be typical for city driving, while the rest is considered to be Highway driving [2].

In the ARTEMIS project, there were three road type categories, which were defined partly by average speed; Urban (average speed below $40\,km/h$), Rural (average speed between $40 - 90\,km/h$) and Motorway (average speed above $90\,km/h$), [44]. The Urban cycle has sections of congested, dense and free flow traffic, where the the speed level differs between about $10 - 60\,km/h$ as well as the number of and duration of stops. The Rural cycle has sections of steady and unsteady speeds at rural secondary to main roads at speed levels around $50 - 100\,km/h$. Finally the Motorway cycle also has sections of steady and unsteady speed at speed levels between about $90 - 150\,km/h$.

In the preparation work with the Worldwide harmonized Light duty driving Test Cycle (WLTC) by the United Nations Economic Commission for Europe (UN-ECE), road types were defined as; Urban $\leq 50\,km/h$, Rural $50 - 80\,km/h$, and Motorway had no specified speed limit, [49]. However, during the continuation of the work, these three road type categories were abandoned, partly due to too large deviations in road type speed limits between the different regions in the world [45], but also due to found differences in speed frequency distributions between instrumented vehicles in the different regions. For the Urban category the speed distributions between sample regions showed a fair coherence, however for the Rural category a discrepancy could be seen where Korean and Japanese data indicated lower speed levels than sample European countries. For the Motorway data this discrepancy was even larger. Thus, instead four speed classes were defined; *low* $< 60km/h$, *median* $< 80\,km/h$, *high* $< 110\,km/h$ and *extra high* $> 110\,km/h$ [45]. The chosen combination of speed levels were decided after a comparative study between different combinations and their correlation with various driving pattern parameters such as average speed, speed acceleration distribution and vehicle speed frequency distribution, [50].

3.2.3 Chosen road type categorizations

In this thesis, all used cycles have been assigned to either of the three road type categories; *Urban*, *Rural* or *Highway*, mainly based on share of time spent at speed levels up to $60\,km/h$, between $60 - 90\,km/h$, and above $90\,km/h$, respectively, as can be seen in Table 3.1. With this general rule, many cycles could be categorized both as Urban and Rural, due to the ambiguous data. However, for cycles that were categorized as Urban, the time share at speed levels above $90\,km/h$ was nil or only a few percent, otherwise they were categorized as Rural.

As already stated, the purpose of this categorization is to find typical driving characteristics for the chosen road types, therefore the majority of the time spent at certain speed levels is dominating the categorization.

Table 3.1 General categorization of cycles based on time share at speed levels.

	$60 - 90\,km/h$	$> 90\,km/h$
Urban:	$< 20\,\%$ of the time	$\approx 0\,\%$ of the time
Rural:	$> 20\,\%$ of the time	$< 20\,\%$ of the time
Highway:	-	$> 20\,\%$ of the time

3.2.4 Urban

The time series of speed and acceleration for the Urban Test cycles can be seen in Figure 3.1, and for the Logged Urban cycles in Figure 3.2. Three logged urban cycles were excluded from the figure, since two of them represent already displayed routes, and one was similar to the others.

Cycle data regarding time duration, driven distance and speed levels can be seen in Table 3.2, for both Test cycles and Logged cycles. In order to account for non zero measured speed from the GPS, the average running speed as well as the time share standing are based on speed levels at $3\,km/h$ and below, for all cycles, i.e. including the test cycles.

Regarding the time shares within certain speed intervals, the selected logs match the test cycles quite well. The main difference is a longer mean time share standing for the test cycles ($27\,\%$ compared to $17\,\%$), and thus a shorter time share at low speed, compared to the logs. Most certainly some of the test cycles represent more dense traffic conditions than what was experienced in the Logged cycles.

For the test cycles, the maximum speed varies between $45\,km/h$ for the NYCC cycle to $91\,km/h$ for the FTP cycles, while the difference is smaller for the logged cycles; 49 for the V774 120312 log to $78\,km/h$ for the Prius 120403 log. Still, the logged cycles have a somewhat higher mean average speed value compared to the test cycles, while the average running speed is rather similar. The spread in speed levels seen by the speed standard deviation is a bit larger for the test cycles, especially for those with the highest top speed.

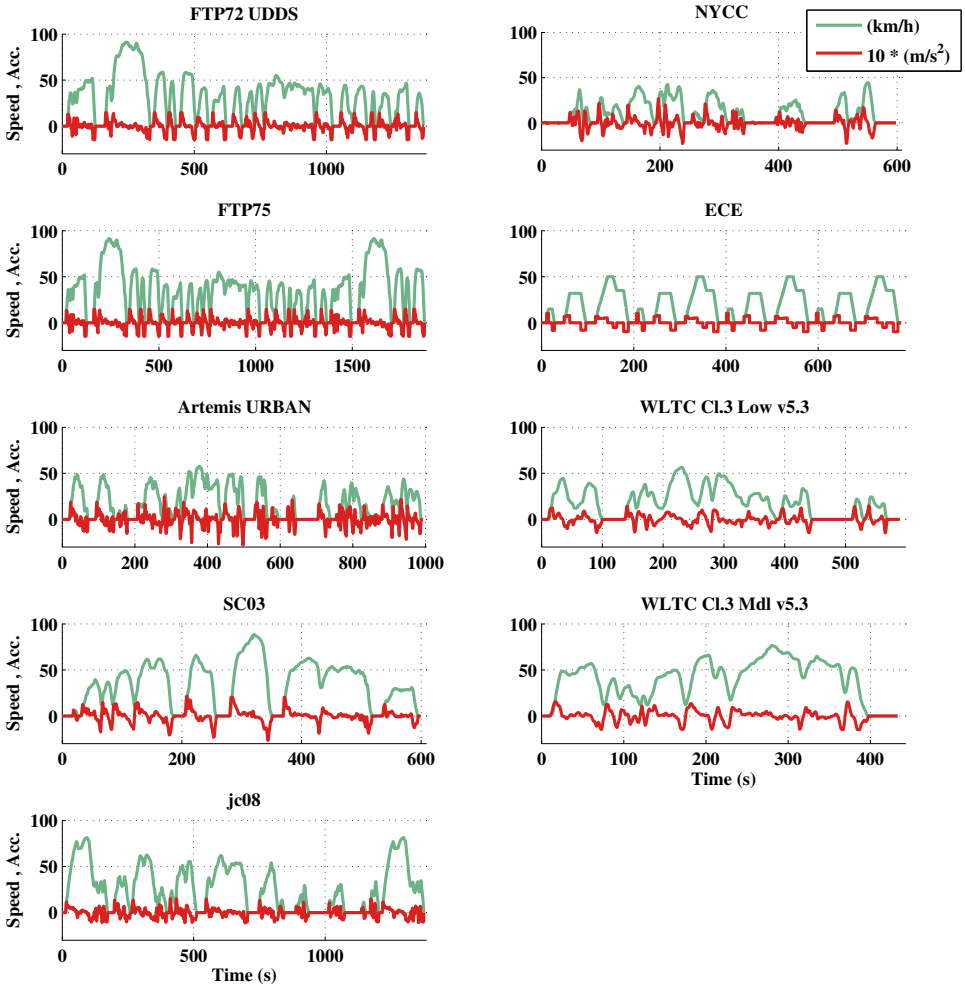

Figure 3.1 Acceleration and speed over time for Urban test cycles, [51], [42], [52] and [53].

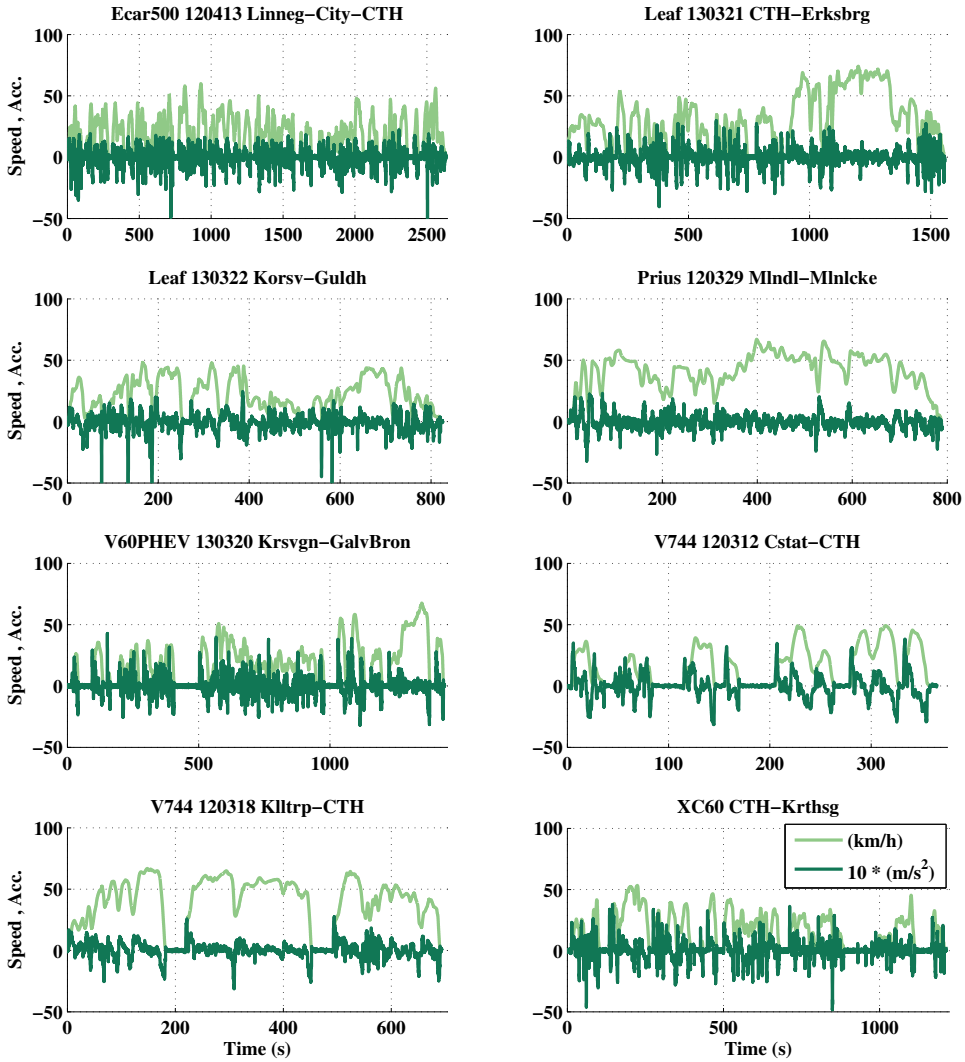

Figure 3.2 Acceleration and speed over time for Logged Urban cycles.

Table 3.2 Cycle data for Urban Test cycles, and Logged Urban cycles.

Urban Test Cycles	Cycle duration (s)	Driven distance (m)	Max. speed (km/h)	Average speed (km/h)	Average running speed (km/h)	Std. speed (km/h)	Time share standing (%)	Time share <60 km/h (%)	Time share 60-90 km/h (%)	Time share > 90 km/h (%)
Artemis URBAN	993	4 870	58	18	25	17	33	66	0	0
ECE	780	4 058	50	19	27	17	34	66	0	0
NYCC	598	1 898	45	11	18	13	44	56	0	0
WLTC Cl.3 Low	589	3 095	57	19	25	16	28	72	0	0
FTP72 UDDS	1 369	11 990	91	32	39	24	21	71	7	1
FTP75	1 874	17 769	91	34	42	26	21	67	11	2
SC03	599	5 761	88	35	43	25	21	65	14	0
jc08	1 376	10 317	82	27	37	24	28	60	12	0
WLTC Cl.3Mdl v5.3	433	4 756	77	40	44	22	12	70	18	0
MEAN	**957**	**7 168**	**71**	**26**	**33**	**20**	**27**	**66**	**7**	**0**

Logged Urban Cycles	Cycle duration (s)	Driven distance (m)	Max. speed (km/h)	Average speed (km/h)	Average running speed (km/h)	Std. speed (km/h)	Time share standing (%)	Time share <60 km/h (%)	Time share 60-90 km/h (%)	Time share > 90 km/h (%)
Ecar500 120413 Linneg-City-CTH	2 633	12 927	60	18	24	15	28	72	0	0
Leaf 130321 CTH-Erksbrg	1 558	13 130	74	30	35	21	14	71	14	0
Leaf 130322 Korsv-Guldh	826	4 959	48	22	24	13	10	90	0	0
Prius 120329 Mlndl-Mlnlcke	790	9 098	67	41	42	14	2	94	4	0
Prius 120329 Mlnlcke-Mlndl	866	9 773	75	41	44	20	8	76	16	0
Prius 120403 Mlnlcke-CTH	1 036	11 585	78	40	43	20	7	73	20	0
V60PHEV 130320 Krsvgn-GalvBron	1 437	7 454	68	19	26	17	29	69	2	0
V744 120312 Cstat-CTH	365	1 608	49	16	25	16	37	63	0	0
V744 120318 Klltrp-CTH	694	7 762	67	40	46	20	13	75	12	0
V744 120327 CTH-Klltrp	806	7 932	64	35	39	18	9	83	8	0
XC60 CTH-Krthsg	1 213	5 246	53	16	23	14	33	67	0	0
MEAN	**1 111**	**8 316**	**64**	**29**	**34**	**17**	**17**	**76**	**7**	**0**

3.2.5 Rural

The time series of speed and acceleration for the Rural Test cycles can be seen in Figure 3.3, and for the Logged Rural cycles in Figure 3.4. One logged cycle was excluded from the figure, since the same route was already displayed in the opposite direction. However the graphs show the same route at three different occasions, which illustrates the deviation between different runs on the same route.

Cycle data for both Logged Rural and Rural Test cycles can be seen in Table 3.3. Also in this case the mean time share standing is larger for the test cycles compared to the logs ($13\,\%$ respective $9\,\%$). Then the time share on medium to high speed levels are somewhat higher for the test cycles compared to the logs. This is also reflected in the maximum speed levels which are larger for the test cycles. In the same time, the mean average speed as well as the average running speed are very similar between the test and logged cycles. The UCLA has the lowest average speed of only $39\,km/h$, while the EUDC has the highest at $63\,km/h$, followed by the Artemis Rural and WLTC High. It is also EUDC and NEDC that have the highest maximum speed levels. For the logs there are four cycles with maximum speed levels around 100 to $110\,km/h$. It can be seen that a high maximum speed is not necessarily linked with a high average speed, instead cycles with lower max. speed may have similar level of average speed.

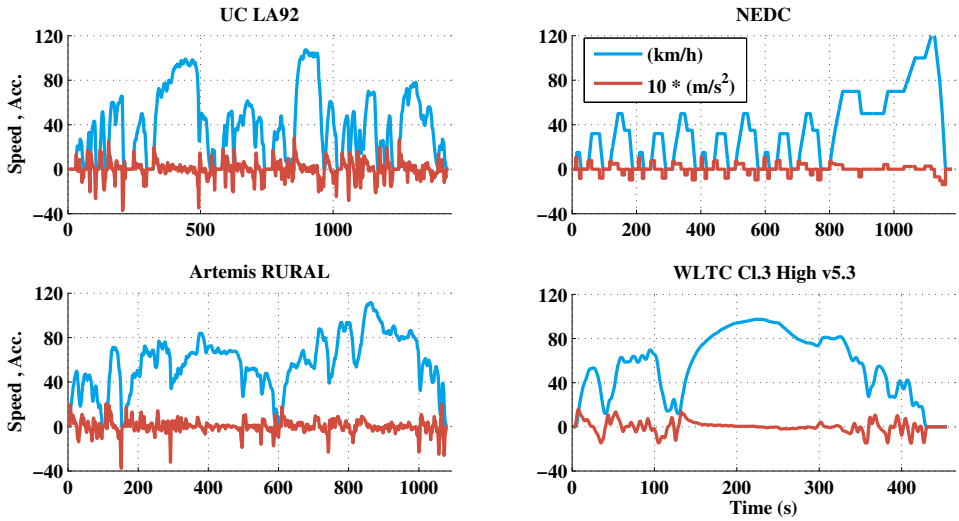

Figure 3.3 Acceleration and speed over time for Rural test cycles, [51], [42], [52] and [53].

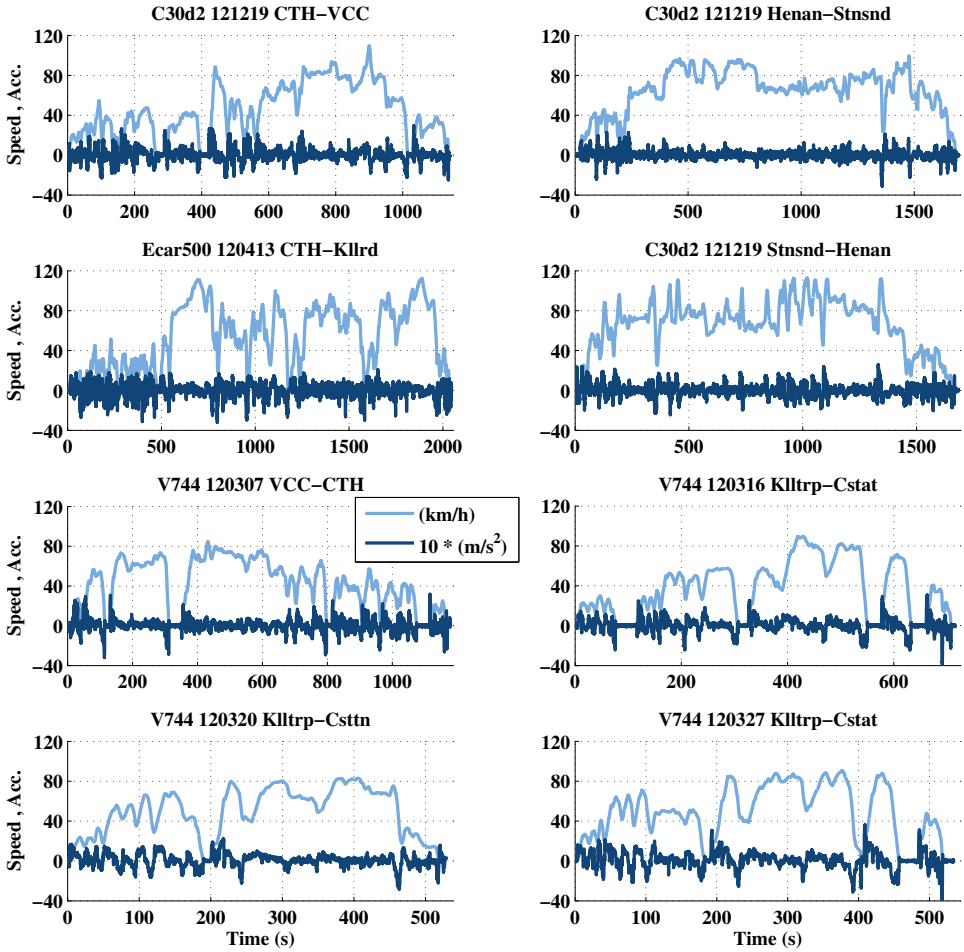

Figure 3.4 Acceleration and speed over time for Logged Rural cycles.

Table 3.3 Cycle data for Rural Test cycles, and Logged Rural cycles.

Rural Test Cycles	Cycle duration (s)	Driven distance (m)	Max. speed (km/h)	Average speed (km/h)	Average running speed (km/h)	Std. speed (km/h)	Time share standing (%)	Time share <60 km/h (%)	Time share 60-90 km/h (%)	Time share > 90 km/h (%)
UC LA92	1 435	15 706	108	39	47	32	19	56	14	11
EUDC	400	6 955	120	63	70	31	10	31	37	21
NEDC	1 180	11 013	120	34	44	31	26	55	13	7
Artemis RURAL	1 082	17 272	112	57	59	25	4	47	42	7
WLTC Cl.3 High v5.3	455	7 162	97	57	61	29	7	42	36	15
MEAN	**910**	**11 622**	**111**	**50**	**56**	**30**	**13**	**46**	**28**	**12**

Logged Rural Cycles	Cycle duration (s)	Driven distance (m)	Max. speed (km/h)	Average speed (km/h)	Average running speed (km/h)	Std. speed (km/h)	Time share standing (%)	Time share <50 km/h (%)	Time share 50-90 km/h (%)	Time share > 90 km/h (%)
C30d2 121219 CTH-VCC	1 141	14 349	110	45	49	26	8	60	29	3
C30d2 121219 Henan Stnsnd	1 696	30 541	100	65	66	22	2	26	60	12
C30d2 121219 VCC-CTH	1 340	13 726	84	37	41	25	10	64	26	0
Ecar500 120413 CTH-Kllrd	2 046	30 557	112	54	58	32	7	45	36	12
C30d2 121219 Stnsnd Henan	1 684	30 879	113	66	68	26	3	27	55	15
V744 120307 VCC-CTH	1 178	13 899	85	42	49	25	13	55	32	0
V744 120316 Klltrp-Csttn	716	7 574	90	38	47	27	19	59	22	0
V744 120320 Klltrp-Csttn	529	7 191	83	49	51	24	4	52	44	0
V744 120327 Klltrp-Cstat	534	7 164	91	48	55	28	12	51	37	0
MEAN	**1 207**	**17 320**	**96**	**49**	**54**	**26**	**9**	**49**	**38**	**5**

3.2.6 Highway

The time series of speed and acceleration for the Highway Test cycles can be seen in Figure 3.5, and for the Logged Highway cycles in Figure 3.6. Cycle data regarding time duration, driven distance and speed levels can be seen in Table 3.4, for both Logged and Test cycles.

Here it can be seen that the time share standing is only a few percent for both test and logged cycles, while the time shares at high speed are in general higher for the test cycles ($58\,\%$) compared to the logged ($41\,\%$). The max. speed levels are higher for the test cycles with one exception; the HWFET cycle. Consequently, also the average speed levels are higher for the test cycles, with the Artemis cycles at the highest levels. The highest average speed is logged for the V70 120515 cycle, followed by the C30d2 121219 Vcc-Stnsnd log.

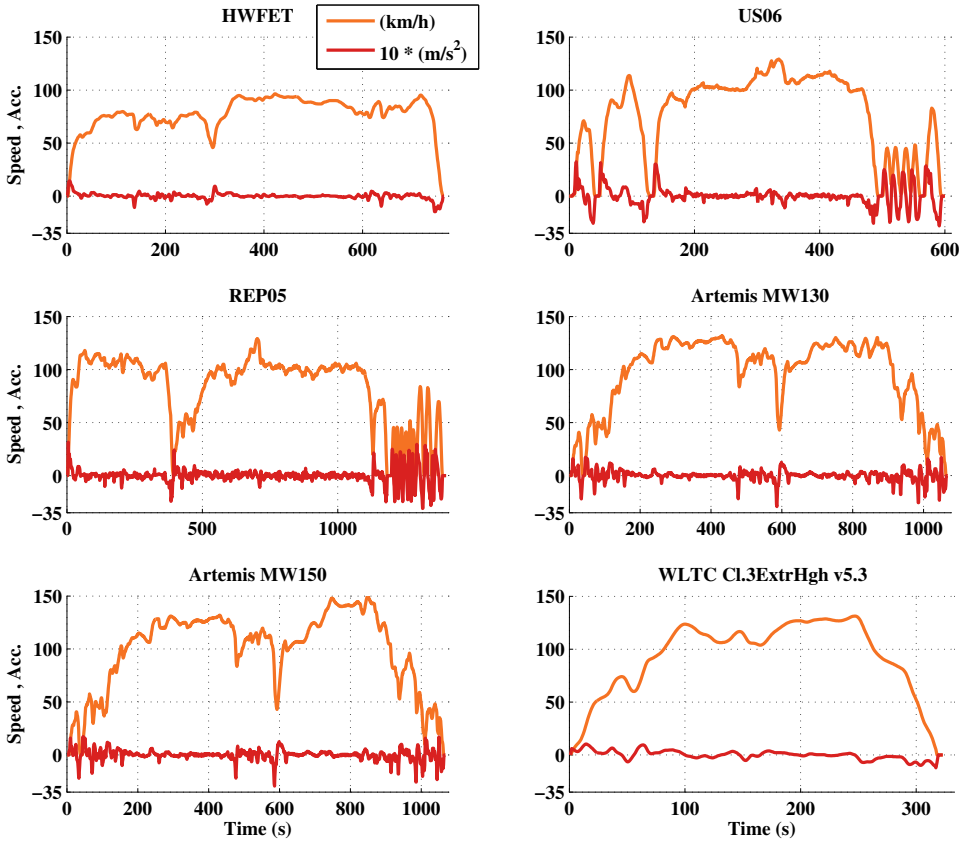

Figure 3.5 Acceleration and speed over time for Highway cycles, [51], [42] and [53].

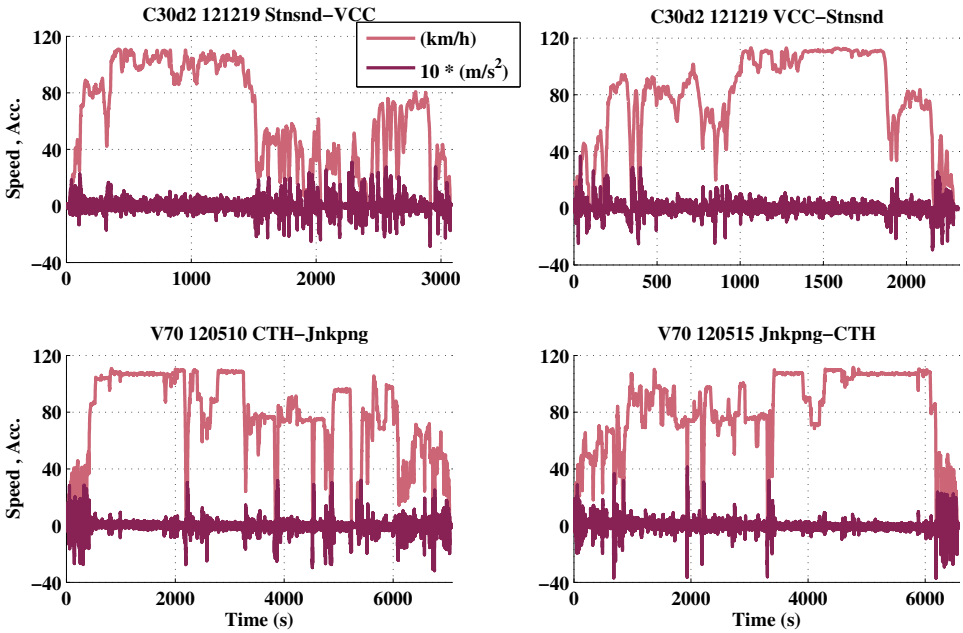

Figure 3.6 Acceleration and speed over time for Logged Highway cycles.

Table 3.4 Cycle data for Highway test cycles, and logged Highway cycles.

Highway Test Cycles	Cycle duration (s)	Driven distance (m)	Max. speed (km/h)	Average speed (km/h)	Average running speed (km/h)	Std. speed (km/h)	Time share standing (%)	Time share <60 km/h (%)	Time share 60-90 km/h (%)	Time share > 90 km/h (%)
HWFET	765	16 507	96	78	78	16	1	10	66	23
US06	600	12 888	129	77	83	40	9	20	15	56
REP05	1 400	32 253	129	83	86	32	4	19	13	65
Artemis MW130	1 068	28 736	132	97	98	35	2	18	10	70
Artemis MW150	1 068	29 545	150	100	101	38	2	18	10	70
WLTC Cl.3ExtrHgh v5.3	323	8 254	131	92	94	36	2	17	18	63
MEAN	**871**	**21 364**	**128**	**88**	**90**	**33**	**3**	**17**	**22**	**58**

Logged Highway Cycles	Cycle duration (s)	Driven distance (m)	Max. speed (km/h)	Average speed (km/h)	Average running speed (km/h)	Std. speed (km/h)	Time share standing (%)	Time share <60 km/h (%)	Time share 60-90 km/h (%)	Time share > 90 km/h (%)
C30d2 121219 Stnsnd-VCC	3 080	54 194	111	63	69	36	9	36	21	34
C30d2 121219 VCC-Stnsnd	2 309	50 426	113	79	81	32	3	21	32	44
V70 120510 CTH-Jnkpng	7 075	149 402	111	76	79	31	4	20	36	40
V70 120515 Jnkpng-CTH	6 576	149 413	112	82	83	27	2	16	36	46
MEAN	**4 760**	**100 859**	**112**	**75**	**78**	**32**	**5**	**23**	**31**	**41**

3.3 Acceleration distributions

Since the peak force and power on the wheels often is due to the vehicle's acceleration, it is vital to study what levels of acceleration that are to be expected to occur during normal driving in the different three road types.

In this section acceleration levels will be studied as a function of speed and time. Logged real-world cycles will be compared with official test cycles.

For official test cycles the speed time series is given, usually as one value per second. Acceleration has been calculated while considering one time step forward and one backward as

$$a(k) = \frac{dv}{dt} = \frac{v(k+1) - v(k-1)}{t(k+1) - t(k-1)}, \tag{3.2}$$

since it is proven to minimize the estimation error, compared to only considering one time step in the forward or backward direction (Euler forward or Euler backward).

3.3.1 Urban

Cycle data regarding acceleration levels can be seen in Table 3.5, for Urban Logged and Test cycles.

It can be seen that the time share of positive and negative acceleration are similar for both the test and logged cycles, where they are shorter for the test cycles due to the longer time share standing. Regarding the time shares at certain acceleration levels, the mean values are very similar for the test and the logged cycles.

The main difference between test cycles and the logged cycles are the much larger maximum acceleration levels seen in the logs, both positive and negative. Amongst the test cycles, it is the NYCC and Artemis Urban that have the highest levels of peak acceleration, at $2.7\,m/s^2$ and $2.4\,m/s^2$ respectively, while many of the logs have maximum values over $3\,m/s^2$. Still the average positive and negative acceleration levels are similar for all cycles, while the standard deviations are slightly higher for the logs. Another interesting point is that ECE has the lowest maximum acceleration level between the test cycles, yet in the same time it has the highest average acceleration, both positive and negative.

Finally the mean RPA values are similar for the test and logged cycles. Many test cycles have RPA values around 0.17 to $0.20\,m/s^2$. However two cycles stand out; Artemis Urban and NYCC, with RPA values of 0.30 and 0.29 respectively. The spread in RPA values seem to be larger for the logged cycles. The largest values are seen for the V744 120312 (0.37) and XC60 $.0.32\,m/s^2$.

Table 3.5 Acceleration cycle data for Urban test and Logged cycles.

Urban Test Cycles	Max. pos. acc. (m/s^2)	Max. neg. acc (m/s^2)	Average pos. acc. (m/s^2)	Average neg. acc. (m/s^2)	Std. pos. acc. (m/s^2)	Std. neg. acc. (m/s^2)	RPA (m/s^2)	Time share pos. acc. (%)	Time share neg. acc. (%)	Time share a<1 m/s^2 (%)	Time share 1<a<2 m/s^2 (%)	Time share 2<a<3 m/s^2 (%)	Time share a>3 m/s^2 (%)
Artemis URBAN	2.4	-2.8	0.6	-0.7	0.5	0.6	0.30	38	35	92	8	0	0
ECE	1.0	-0.9	0.7	-0.7	0.2	0.2	0.14	19	19	98	2	0	0
NYCC	2.7	-2.3	0.6	-0.5	0.5	0.5	0.29	34	35	94	5	1	0
WLTC Cl.3 Low	1.5	-1.5	0.5	-0.4	0.4	0.3	0.20	35	40	96	4	0	0
FTP72 UDDS	1.5	-1.5	0.5	-0.5	0.4	0.5	0.17	41	37	94	6	0	0
FTP75	1.5	-1.5	0.5	-0.5	0.4	0.5	0.17	40	37	93	7	0	0
SC03	2.2	-2.7	0.5	-0.6	0.5	0.6	0.20	43	37	94	5	1	0
jc08	1.5	-1.1	0.4	-0.5	0.3	0.3	0.17	39	34	97	3	0	0
WLTC Cl.3Mdl v5.3	1.6	-1.5	0.4	-0.5	0.4	0.5	0.20	49	39	94	5	0	0
MEAN	**1.8**	**-1.7**	**0.5**	**-0.6**	**0.4**	**0.4**	**0.21**	**38**	**35**	**95**	**5**	**0**	**0**

Logged Urban Cycles	Max. pos. acc. (m/s^2)	Max. neg. acc (m/s^2)	Average pos. acc. (m/s^2)	Average neg. acc. (m/s^2)	Std. pos. acc. (m/s^2)	Std. neg. acc. (m/s^2)	RPA (m/s^2)	Time share pos. acc. (%)	Time share neg. acc. (%)	Time share a<1 m/s^2 (%)	Time share 1<a<2 m/s^2 (%)	Time share 2<a<3 m/s^2 (%)	Time share a>3 m/s^2 (%)
Ecar500 120413 Linneg-City-CTH	2.2	-5.2	0.5	-0.5	0.4	0.6	0.26	50	50	93	7	0	0
Leaf 130321 CTH-Erksbrg	3.0	-4.0	0.5	-0.5	0.6	0.6	0.24	50	50	92	7	1	0
Leaf 130322 Korsv-Guldh	2.5	-8.5	0.5	-0.6	0.4	0.7	0.21	45	55	94	6	0	0
Prius 120329 Mlndl-Mlnlcke	2.3	-3.2	0.4	-0.4	0.4	0.4	0.17	42	58	95	5	0	0
Prius 120329 Mlnlcke-Mlndl	3.4	-4.1	0.5	-0.5	0.6	0.6	0.22	49	51	91	8	1	0
Prius 120403 Mlnlcke-CTH	3.1	-2.7	0.4	-0.4	0.5	0.5	0.19	48	52	93	7	1	0
V60PHEV 130320 Krsvgn-GalvBron	4.3	-3.2	0.5	-0.5	0.6	0.5	0.27	47	53	93	5	1	0
V744 120312 Cstat-CTH	3.8	-3.2	0.6	-0.6	0.7	0.7	0.37	48	52	88	9	2	1
V744 120318 Klltrp-CTH	2.8	-3.1	0.4	-0.4	0.4	0.6	0.21	55	45	96	4	0	0
V744 120327 CTH-Klltrp	3.0	-2.7	0.4	-0.4	0.4	0.5	0.21	54	46	95	4	1	0
XC60 CTH-Krthsg	3.8	-4.8	0.5	-0.5	0.6	0.6	0.32	52	48	92	6	2	0
MEAN	**3.1**	**-4.1**	**0.5**	**-0.5**	**0.5**	**0.6**	**0.24**	**49**	**51**	**93**	**6**	**1**	**0**

The maximum acceleration as well as second based operating points, for the Test cycles can be seen in Figure 3.7 and for the Logged cycles in Figure 3.8. As can be seen, the largest acceleration levels are experienced at the lower speed levels.

For the test cycles; at speed levels up to around $40\,km/h$ Artemis Urban, NYCC and SC03 have the highest levels of positive and negative acceleration at $1.7 - 2.5\,m/s^2$ and -2.3 to $-2.8\,m/s^2$. At higher speeds it is SC03, FTP75 and WLTC Middle that have the highest positive acceleration levels, although strongly descending with increasing speed. At about $50\,km/h$ the peak acceleration levels are around $0.4 - 1.4\,m/s^2$, while at about $80\,km/h$ they are around $0.2 - 0.5\,m/s^2$.

As already noted from the cycle parameter data, the peak acceleration levels of the logged cycles are higher compared to the test cycles, also when considering the different speed levels. For the logged cycles, at about $50\,km/h$ the peak acceleration levels are around $1 - 2.5\,m/s^2$, while at about $80\,km/h$ the cycles have already reached their top speed.

In order to compare the distribution of acceleration over the speed range, between Urban test cycles and Logged Urban cycles, the relative time spent in bins of $0.5\,m/s^2$ and $5\,km/h$ is depicted in Figure 3.9 and 3.10, along with the highest reached acceleration level at each speed. When creating the plots, to each speed and acceleration operating point a gaussian noise was added, which was later compensated for in the final result. The benefit is smoother contour lines, however a small error is also introduced, it can be regarded as negligible. Hence the contour lines outside of the maximum acceleration graph should be disregarded. The method is further illustrated in Appendix C.

As was also indicated by the standard deviations, the logged cycles spend a somewhat

larger share at slightly larger acceleration levels, compared to the test cycles. This can be seen by comparing the acceleration levels for the same time share contour line.

The figures show that for the test cycles, most of the time is spent around zero speed at very low levels of accelerations (less than $1\,m/s^2$), due to frequent stops. For the logged cycles, most time is spent at speed levels around 5 to $10\,km/h$, but also within $1\,m/s^2$. Furthermore, the test cycles spend a somewhat larger time share at higher speed levels compared to the logged cycles.

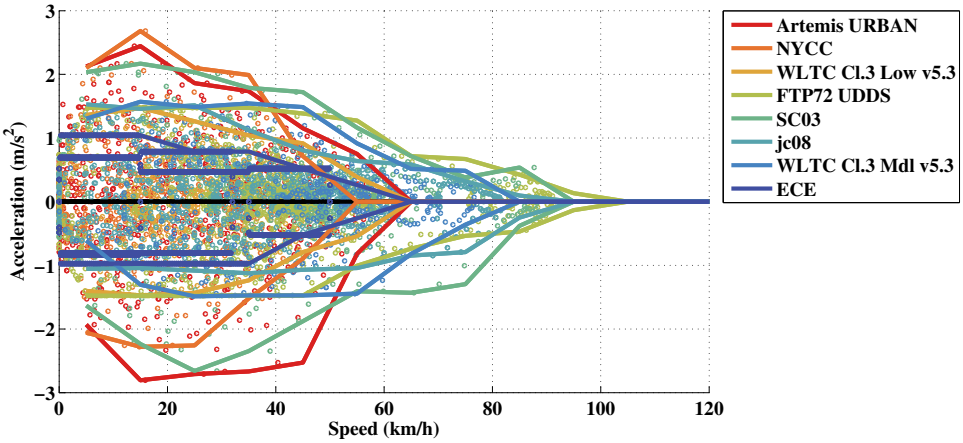

Figure 3.7 Maximum acceleration over speed along second with operation points per second, for Urban Test cycles.

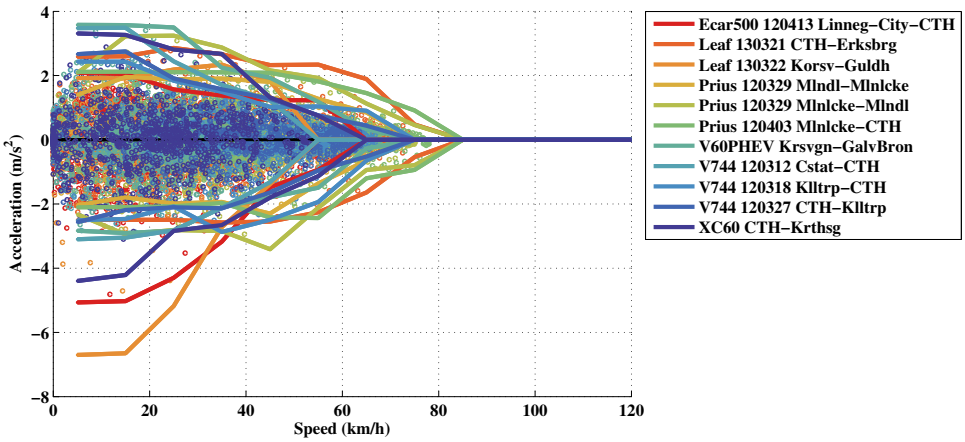

Figure 3.8 Maximum acceleration over speed along second with operation points per second, for Logged Urban cycles.

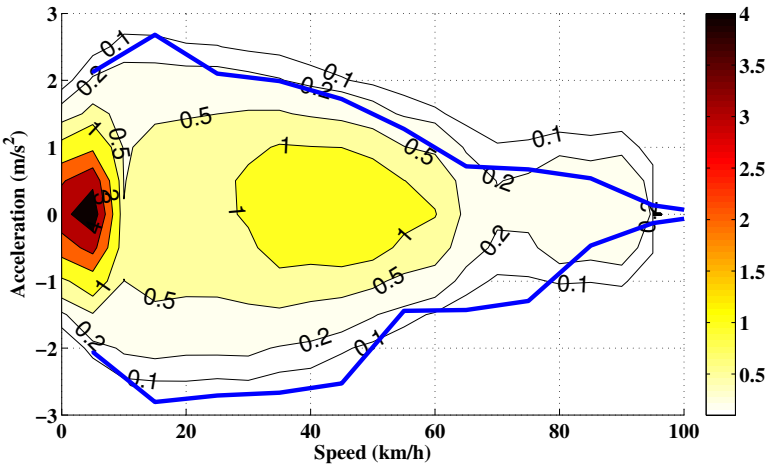

Figure 3.9 Share of total time $(\%)$ of operation in acceleration bins of $0.5\ m/s^2$ and speed bins of 5 km/h, with added noise, for all Urban Test cycles.

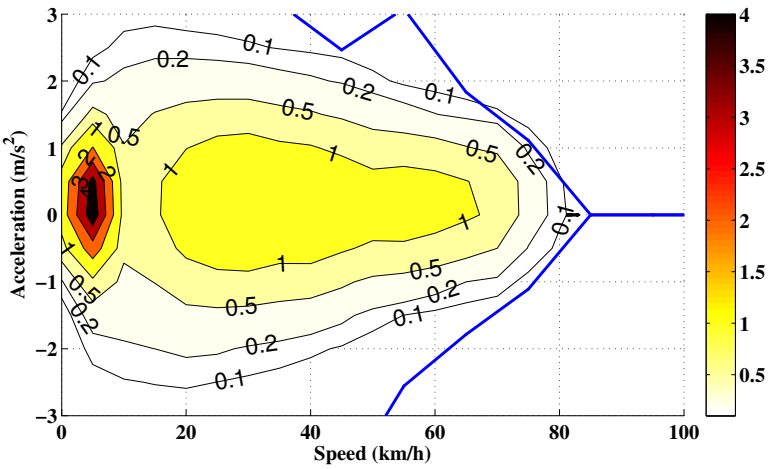

Figure 3.10 Share of total time $(\%)$ of operation in acceleration bins of $0.5\ m/s^2$ and speed bins of 5 km/h, with added noise, for all Logged Urban cycles.

3.3.2 Rural

Cycle data regarding acceleration levels can be seen in Table 3.6, for Rural Logged and Test cycles.

Also for the Rural cycles, the logs show higher peak acceleration levels and standard deviations compared to the test cycles, while the average values are similar. The test cycles have a slightly larger time share below $1\ m/s^2$, while the logs have slightly a higher time

share for acceleration levels between 1 to 2 m/s^2. Furthermore, high RPA values are more frequent amongst the logs.

For the test cycles it is the UC (LA92) cycle that has the highest peak acceleration both positive and negative, as well as the highest RPA value. On the contrary, EUDC and NEDC have the lowest peak acceleration levels and the lowest RPA value.

Amongst the logs, two cycles have similar peak acceleration levels; C30d2 121219 VCC-CTH and V744 120327 Klltrp-Cstat, however the later have a slightly higher average acceleration, and a much larger RPA value (0.34 compared to 0.19 m/s^2).

Table 3.6 Acceleration cycle data for Rural test and Logged cycles.

Rural Test Cycles	Max. pos. acc. (m/s^2)	Max. neg. acc (m/s^2)	Average pos. acc. (m/s^2)	Average neg. acc. (m/s^2)	Std. pos. acc. (m/s^2)	Std. neg. acc. (m/s^2)	RPA (m/s^2)	Time share pos. acc. (%)	Time share neg. acc. (%)	Time share a<1 m/s^2 (%)	Time share 1<a<2 m/s^2 (%)	Time share 2<a<3 m/s^2 (%)	Time share a>3 m/s^2 (%)
UC LA92	3.1	-3.9	0.7	-0.7	0.5	0.7	0.24	38	34	91	9	1	0
EUDC	0.8	-1.4	0.4	-0.9	0.2	0.3	0.09	26	11	100	0	0	0
NEDC	1.0	-1.4	0.6	-0.8	0.3	0.2	0.11	21	16	99	1	0	0
Artemis RURAL	2.4	-4.1	0.5	-0.5	0.4	0.6	0.18	41	40	96	3	0	0
WLTC Cl.3 High v5.3	1.7	-1.5	0.4	-0.4	0.4	0.4	0.14	47	41	96	4	0	0
MEAN	**1.8**	**-2.5**	**0.5**	**-0.7**	**0.3**	**0.4**	**0.15**	**35**	**28**	**96**	**4**	**0**	**0**

Logged Rural Cycles	Max. pos. acc. (m/s^2)	Max. neg. acc (m/s^2)	Average pos. acc. (m/s^2)	Average neg. acc. (m/s^2)	Std. pos. acc. (m/s^2)	Std. neg. acc. (m/s^2)	RPA (m/s^2)	Time share pos. acc. (%)	Time share neg. acc. (%)	Time share a<1 m/s^2 (%)	Time share 1<a<2 m/s^2 (%)	Time share 2<a<3 m/s^2 (%)	Time share a>3 m/s^2 (%)
C30d2 121219 CTH-VCC	2.9	-2.5	0.5	-0.5	0.5	0.5	0.24	53	47	93	6	1	0
C30d2 121219 Henan Stnsnd	2.3	-3.1	0.3	-0.3	0.3	0.3	0.13	48	52	97	3	0	0
C30d2 121219 VCC-CTH	3.6	-2.8	0.5	-0.4	0.5	0.4	0.19	44	56	93	6	1	0
Ecar500 120413 CTH-Kllrd	2.1	-3.2	0.5	-0.5	0.4	0.5	0.23	56	44	93	7	0	0
C30d2 121219 Stnsnd Henan	2.6	-2.4	0.5	-0.4	0.5	0.4	0.24	48	52	93	7	0	0
V744 120307 VCC-CTH	3.2	-3.2	0.4	-0.4	0.4	0.5	0.20	53	47	95	5	1	0
V744 120316 Klltrp-Csttn	3.1	-4.2	0.5	-0.5	0.5	0.6	0.25	54	46	93	7	1	0
V744 120320 Klltrp-Csttn	2.2	-2.9	0.5	-0.5	0.4	0.5	0.25	57	43	93	7	0	0
V744 120327 Klltrp-Cstat	3.6	-4.3	0.6	-0.6	0.6	0.7	0.34	56	44	87	12	1	0
MEAN	**2.8**	**-3.2**	**0.5**	**-0.5**	**0.5**	**0.5**	**0.23**	**52**	**48**	**93**	**7**	**1**	**0**

The maximum acceleration as well as second based operating points, for the Test cycles can be seen in Figure 3.11 and for the Logged cycles in Figure 3.12.

In Figure 3.11 it is clearly seen that the two cycles UC LA92 and Artemis Rural differs quite a bit from the others since the levels of acceleration are larger over the whole speed range, and even more so for negative accelerations. Also when comparing with the Urban test cycles, these two cycles stand out. For the logged cycles it can be seen in Figure 3.12 that the highest peak accelerations only occur at very low speed levels (below 20 km/h). Around 40 km/h most cycles have peak accelerations between 1.5 to 2.5 m/s^2, while for higher speed levels the difference between the cycles increase.

At about 50 km/h the peak acceleration levels are around $1 - 2.5\,m/s^2$ for the logs and 0.5 to 1.5 m/s^2 for the test cycles, while at about 80 km/h they are $0.5 - 2\,m/s^2$ for the logs and 0.3 to 1 m/s^2 for the test cycles.

As for the Urban cycles, the relative time spent in acceleration bins of 0.5 m/s^2 and 5 km/h is depicted in Figure 3.13 and 3.14, along with the highest reached acceleration level at each speed.

Also for the Rural cycles, the logged cycles spend slightly more time at somewhat higher acceleration levels over the whole speed range. I can also be seen that apart from the time spent at stand still and very low speed, also much of the time is spent around $40\,km/h$ for both test and logged cycles, $55\,km/h$ for the test cycles, and finally around $70\,km/h$ for both test and logged cycles.

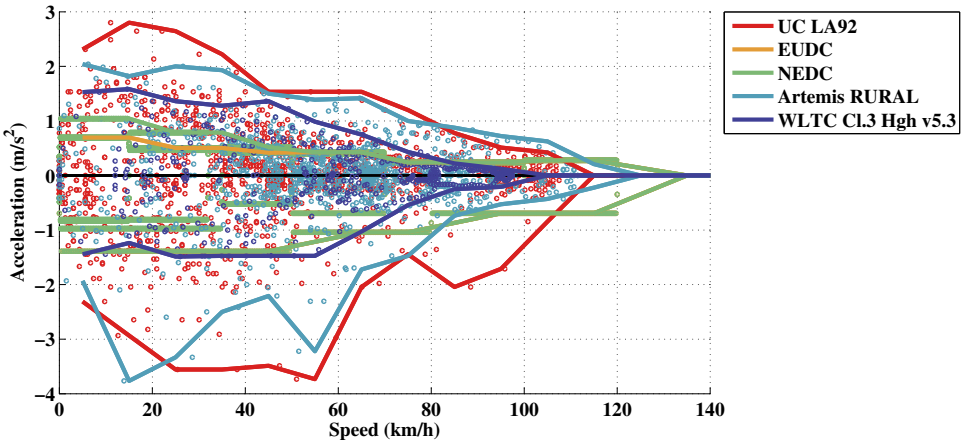

Figure 3.11 Maximum acceleration over speed along second with operation points per second, for Rural Test cycles.

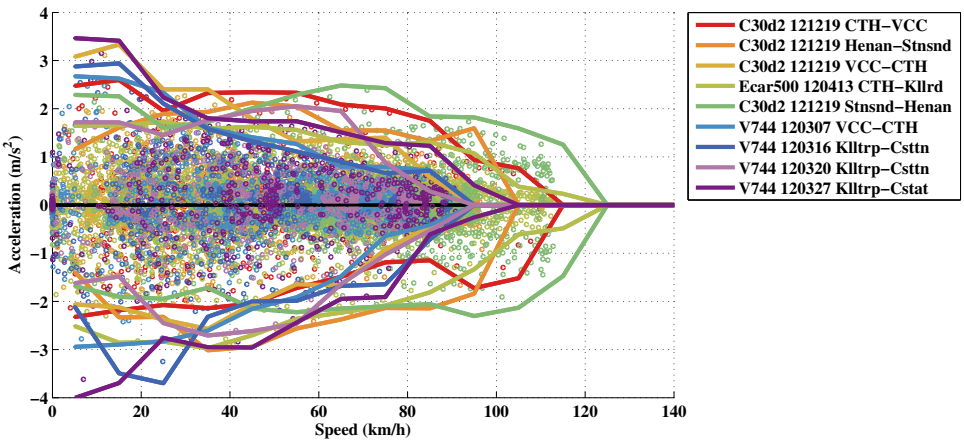

Figure 3.12 Maximum acceleration over speed along second with operation points per second, for Logged Rural cycles.

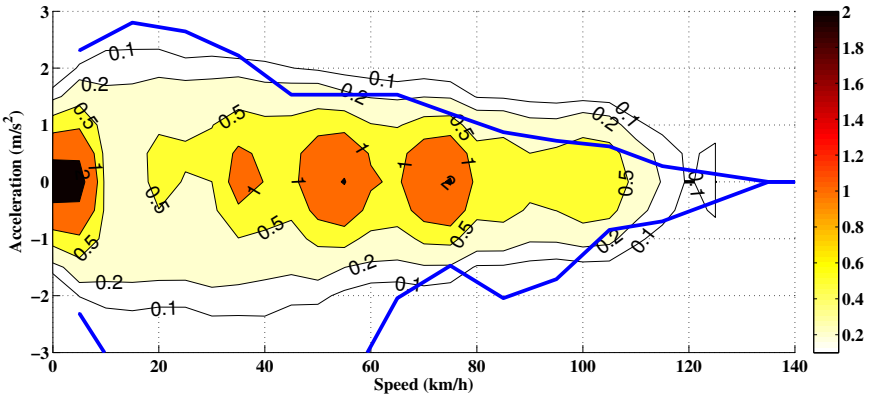

Figure 3.13 Share of total time $(\%)$ of operation in acceleration bins of $0.5\ m/s^2$ and speed bins of 5 km/h, with added noise, for all Rural Test cycles.

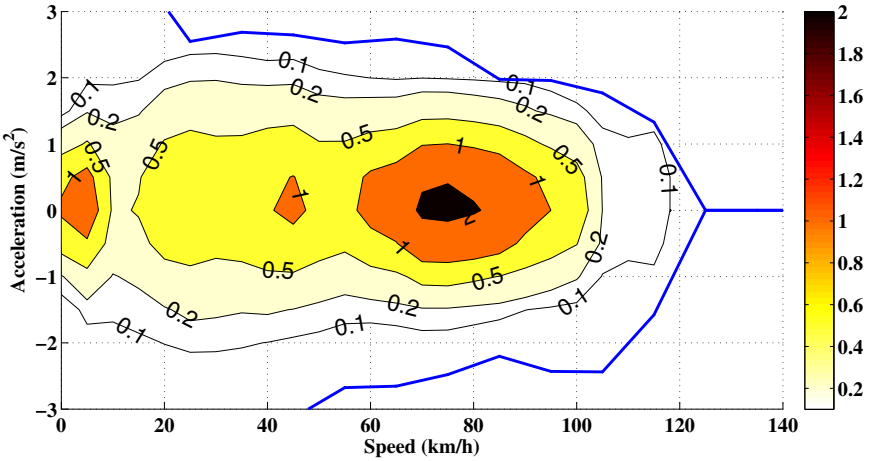

Figure 3.14 Share of total time $(\%)$ of operation in acceleration bins of $0.5\ m/s^2$ and speed bins of 5 km/h, with added noise, for Logged Rural cycles.

3.3.3 Highway driving

Cycle data regarding acceleration levels can be seen in Table 3.7, for Highway Logged and Test cycles.

As for the Urban and Rural cycles, the peak accelerations of the logged Highway cycles are higher compared to the test cycles, while the average, standard deviations and the time shares at different acceleration levels are similar. In this case the test cycles have higher RPA values.

Amongst the test cycles, the US06 and REP05 have the highest peak acceleration levels, however the average and standard deviation of acceleration as well as the RPA value is higher for US06.

The acceleration parameters of the logged cycles are rather similar to one another.

Table 3.7 Acceleration cycle data for Highway test and Logged cycles.

Highway Test Cycles	Max. pos. acc. (m/s^2)	Max. neg. acc (m/s^2)	Average pos. acc. (m/s^2)	Average neg. acc. (m/s^2)	Std. pos. acc. (m/s^2)	Std. neg. acc. (m/s^2)	RPA (m/s^2)	Time share pos. acc. (%)	Time share neg. acc. (%)	Time share a<1 m/s^2 (%)	Time share 1<a<2 m/s^2 (%)	Time share 2<a<3 m/s^2 (%)	Time share a>3 m/s^2 (%)
HWFET	1.4	-1.5	0.2	-0.2	0.2	0.3	0.07	47	42	99	1	0	0
US06	3.2	-2.8	0.7	-0.7	0.8	0.7	0.19	45	44	90	5	5	1
REP05	3.2	-3.1	0.4	-0.5	0.6	0.6	0.14	52	45	94	4	2	0
Artemis MW130	1.7	-2.9	0.3	-0.4	0.3	0.5	0.12	48	37	97	3	0	0
Artemis MW150	1.7	-2.9	0.3	-0.4	0.3	0.5	0.12	47	37	97	3	0	0
WLTC Cl.3ExtrHgh v5.3	1.0	-1.2	0.3	-0.3	0.2	0.3	0.12	51	46	99	1	0	0
MEAN	**2.1**	**-2.4**	**0.4**	**-0.4**	**0.4**	**0.5**	**0.13**	**48**	**42**	**96**	**3**	**1**	**0**

Logged Highway Cycles	Max. pos. acc. (m/s^2)	Max. neg. acc (m/s^2)	Average pos. acc. (m/s^2)	Average neg. acc. (m/s^2)	Std. pos. acc. (m/s^2)	Std. neg. acc. (m/s^2)	RPA (m/s^2)	Time share pos. acc. (%)	Time share neg. acc. (%)	Time share a<1 m/s^2 (%)	Time share 1<a<2 m/s^2 (%)	Time share 2<a<3 m/s^2 (%)	Time share a>3 m/s^2 (%)
C30d2 121219 Stnsnd-VCC	3.1	-2.9	0.4	-0.3	0.4	0.4	0.14	48	52	96	4	0	0
C30d2 121219 VCC-Stnsnd	3.7	-2.9	0.3	-0.3	0.4	0.4	0.13	49	51	96	3	1	0
V70 120510 CTH-Jnkpng	3.2	-3.2	0.2	-0.2	0.3	0.4	0.09	51	49	98	2	0	0
V70 120515 Jnkpng-CTH	4.1	-3.7	0.3	-0.2	0.4	0.3	0.09	46	54	98	2	0	0
MEAN	**3.5**	**-3.2**	**0.3**	**-0.3**	**0.4**	**0.4**	**0.11**	**49**	**52**	**97**	**3**	**0**	**0**

The maximum acceleration as well as second based operating points, for the Test cycles can be seen in Figure 3.15 and for the Logged cycles in Figure 3.16.

As could be noted in the cycle parameters, the US06 and REP05 cycles have higher levels of acceleration over the speed interval than the other test cycles, with many operating points above $2\,m/s^2$ up to a speed level of $60\,km/h$. Next to US06 and REP05, the Artemis Motorway cycles have the highest acceleration levels over the speed range, and a particulary strong braking acceleration at high speed (about 2 to $3\,m/s^2$).

As can be seen in Figure 3.16, the peak acceleration over the speed range of the logged Highway cycles are close to one another, but also fairly close to those of the US06 and REP05.

The relative time spent in bins of $0.5\,m/s^2$ and $5\,km/h$ is depicted in Figure 3.17 and 3.18, along with the highest reached acceleration level at each speed.

When comparing the distribution of logged cycles with the test cycles, the differences in time spent at various acceleration levels over the speed range is rather small. The main difference that can be seen is the relatively larger time spent at higher speed levels in the test cycles compared to the logged cycles. It can be seen that in the test cycles most time is spent at speed levels close to 80 to $130\,km/h$ ($110\,km/h$ in particular), while for the logged cycles most time is spent at $50\,km/h$ and between 70 to $120\,km/h$.

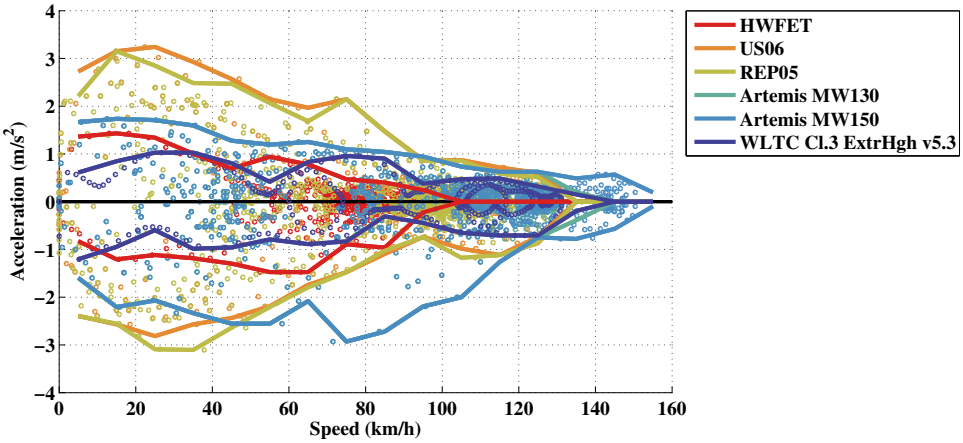

Figure 3.15 Maximum acceleration over speed along second with operation points per second, for Highway Test cycles.

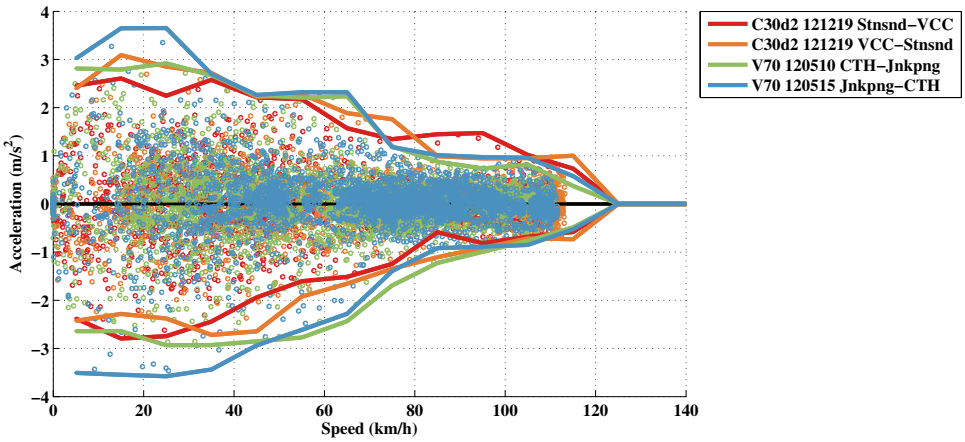

Figure 3.16 Maximum acceleration over speed along second with operation points per second, for Logged Highway cycles.

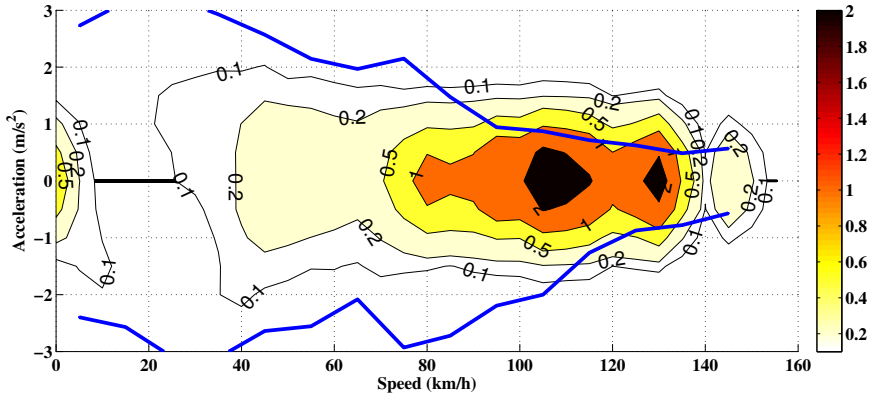

Figure 3.17 Share of total time $(\%)$ of operation in acceleration bins of $0.5\ m/s^2$ and speed bins of 5 km/h, with added noise, for all Highway Test cycles.

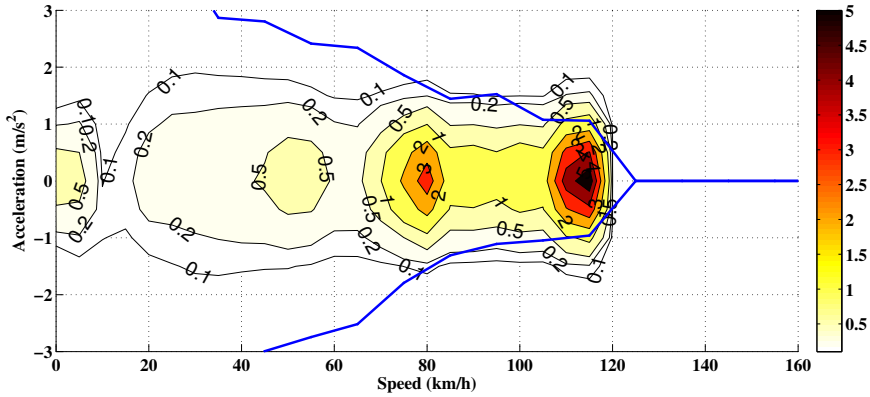

Figure 3.18 Share of total time $(\%)$ of operation in acceleration bins of $0.5\ m/s^2$ and speed bins of 5 km/h, with added noise, for Logged Highway cycles.

3.4 Road grade levels

As with speed and acceleration, common levels of road grade are of great interest when seeking typical vehicle load levels.

The Swedish office of traffic (Trafikverket) has specified recommended maximum road grade levels for new roads to $6\ \%$, and for improved roads to $8\ \%$, in their guidelines for how roads are to be designed [54].

Similarly, according to [55] the National System of Interstate and Defence Highways in the US are designed after guidelines that state a recommended maximum grade level depending on the road's speed limit. For speeds up to $90\ km/h$, maximum grade levels of

$5\,\%$ are recommended, while it is $6\,\%$ for mountainous areas. At higher speed levels the recommended max grade is $4\,\%$. According to [14] p. 13, grade levels on US primary and secondary roads may reach 10 to 12%.

Trafikverket also provide a searchable database called PMSV3 [56], that contains measured road data covering different roads in Sweden, which are gathered from several occasions over the last decades via a special measurement van. Amongst other data, road grade, road speed limit and speed of measurement vehicle have been recorded. It is possible to make combined searches in the data base on one or more parameters. A search on speed limit of at least 110 km/h and grades of at least 6% but maximum 12%, results in three hits, i.e. three different highways in Sweden has sections of grade 6% or larger. One is on E6 Bohuslän between Munkedal and Tanum, one in Dalarna between Borlänge and Falun, and one in Skåne south of Skottorp across Hallandsåsen with grades of $6 - 7\%$ over a distance of $1.8\ km$. Another steep slope with a grade of about 7 %, is west of Jönköping on road 40 along a section of about 1 km at a speed limit of 90 km/h. Further searches leads to about a 170 hits on sections with speed limits of $100\,km/h$ and grades of at least 6% but maximum 12%, and $1\,330$ hits on sections with speed limits of $90\,km/h$ and grades of at least $6\,\%$ but maximum $12\,\%$, for $70\,km/h$ the number of hits is $31\,638$, and for $50\,km/h$ it is 5905. These numbers are however not to be blindly trusted, since some of the later measurements are not coherent with the previous ones and thus indicates much larger grades than previously.

At low speed levels, e.g. in cities or on drive ways the road grade can be even larger, perhaps up to and above $30\,\%$ as indicated by [57] for several streets is San Francisco in the US.

3.4.1 Measured road grades

Road grade levels have also been estimated from the logged data, see histogram representation in Figure 3.19. A fair accuracy of the estimation proved to be rather difficult with the used measurement system at hand, especially at low speed levels. Nevertheless, the resulting data corresponds rather well to expected values with respect to the information in the previous section.

Analysis showed only a small dependence on speed, i.e. that higher grade levels are relatively less common for the Highway cycles.

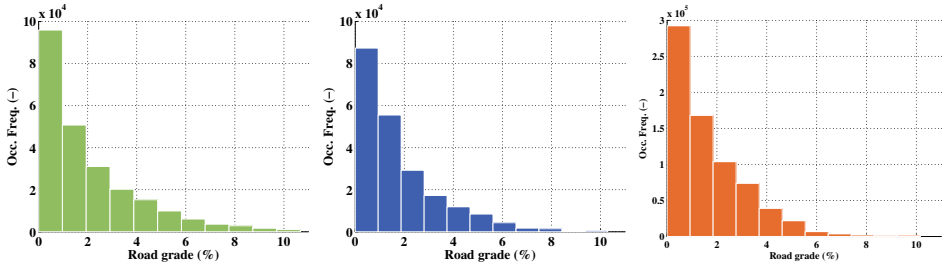

(a) Urban. (b) Rural. (c) Highway.

Figure 3.19 Road grade histogram of all Logged Urban, Rural and Highway cycles.

Figure 3.20 presents the difference in altitude between the end and start of the Logged cycles, as well as the difference between maximum and minimum reached altitudes. For a cycle with a large positive difference between the end and the start altitude, a significant part of the energy that is consumed during driving is due to the increases in potential energy. For those cycles that adhere to the same driving route and are driven in opposite directions, it can be seen that the difference between end and start altitude is similar but with opposite signs. Thus, the total energy consumption may be different for the two cycles.

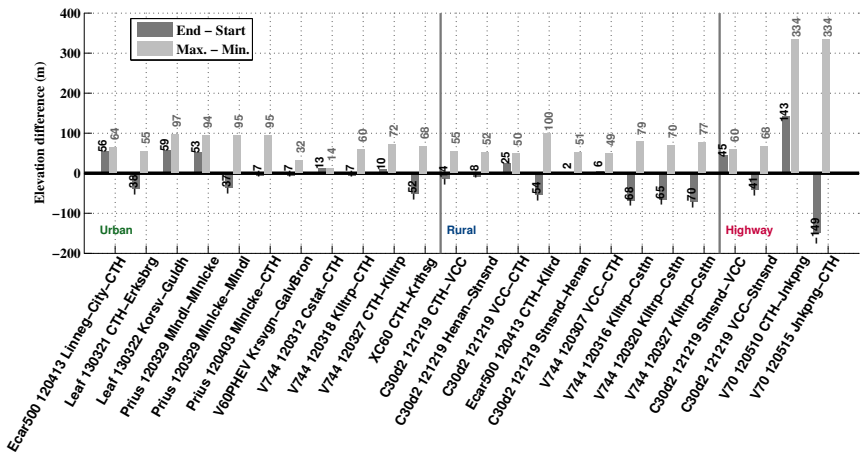

Figure 3.20 The net altitude difference between the cycle end and start points, as well as the difference between maximum and minimum altitude that is experienced during the Logged cycles.

3.5 Average Daily Driving/Traveling Distance

In order to find suitable driving ranges for electric cars it is essential to gain knowledge of how far drivers usually travel. By assuming that the only definite time to charge is over

night, one can consider information regarding traveled distances per day.

Many countries around the world try through surveys, to map typical mobility habits of people traveling by different commodities. In these surveys respondents are asked to keep a traveling or driving journal usually for a single specified day, thus regarded to be typical, or in the case of some studies for a number of consecutive days. The main drawbacks with these kinds of studies (when it comes to estimating necessary EV driving range) are that the results are strictly related to mobility of persons, who may use different vehicles during the same day, but also that the quality of the results highly depend on the estimates done by the respondents as stated in [36]. More preferably, single vehicles are tracked and studied during a much longer period, e.g. The Swedish Car Movement Data Project or an American study in the Atlanta region [58].

The type of information gained may be average daily commuting distances, average daily driving over a whole population studied. It may also be a cumulative distribution of share of daily distances that at least has been covered.

According to National Household Travel Survey in the US(NHTS) [59], the average commuting distance by private vehicles in US was $19.5\ km$, and the average driven distance per driver in 2001 and 2009 respectively were 55 and 49 km on a weekday and 46 and 40 km on a Saturday or Sunday.

According to the latest major National Travel Survey in Sweden, the average driven distance per day with private car in 2005/2006 range between 20 to 36 km depending on region, with a national average of 30 km [60]. However according to another report from the same period (Körsträckor 2006) which is based on data from vehicle trip meter (checked during yearly car check up at Bilprovningen), the average total driven distance per vehicle during 2006 was 14 390 km, which gives an average daily driving distance of about 39 km [61].

A survey in Europe finds that the average driven distance in six European countries (France, Germany, Italy, Poland, Spain and UK) vary between 40 km (UK) to 80 km (Poland) per day, and shows no important difference between the days in a week [62].

Various sources have been found that present the needed type of data, [63], [64], [65], [66], [67], [68], [69] and [58]. However the results differ between countries, and studies, and even between the same studies depending on how the answers are chosen to be analyzed, which makes general conclusions difficult to make, see Figure 3.21. For more details on the different studies, see the related references mentioned here.

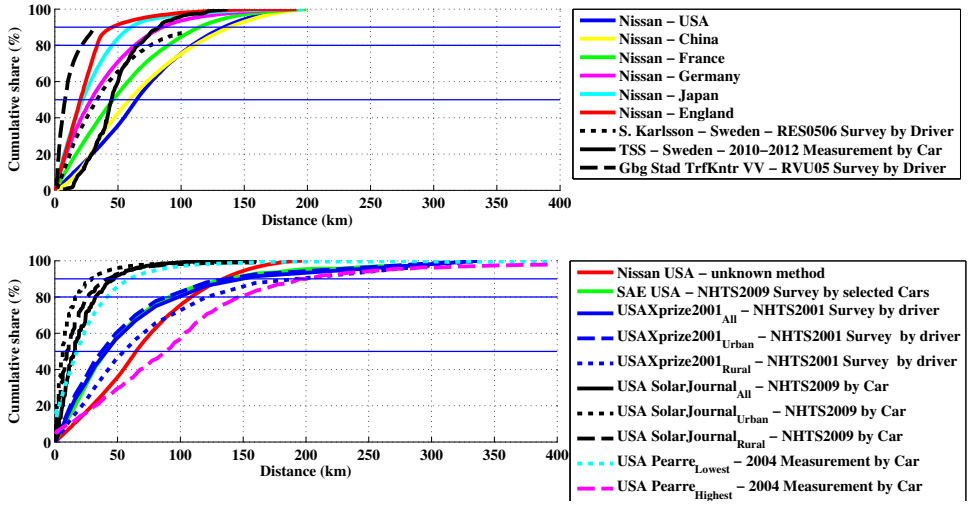

Figure 3.21 Daily driving distances in various countries, for either drivers or cars, extracted by different methods.

According to [63], $90\,\%$ of the people in European countries drive less than about $120\,km$ per day on an average, while $90\,\%$ of the people in USA drive less than $135\,km$ per day. It is also seen that Japan seem to have similar driving patterns as EU and that China seem to have similar driving patterns as US.

As can be seen the information regarding Sweden differs a bit between the different sources, perhaps this is due to different methods used, see [64], [65] and [66]. Based on results from The Swedish Car Movement Data Project which cover cars in the south west of Sweden, $90\,\%$ of the cars travel less than about $70\,km$ per day on average.

In the US the spread between different published data is relatively large. As a summery of all presented graphs, $50\,\%$ of the average daily driving distances are shorter than 6 to $89\,km$, and $80\,\%$ of them are shorter than $16\,148\,km$. One study indicate that larger distances are covered during rural driving compared to urban driving, [69].

Chapter 4

Performance requirements and wheel load analysis of studied vehicle concepts

Vehicle performance can be summarized in single quantitative measures such as; top speed, minimum time to accelerate from $0 - 100\,km/h$, and specifically for BEVs, driving range.

The work in this thesis is concentrated to three concept light duty BEVs, i.e. passenger cars, each with their own targeted qualitative specification which can be seen in Table 4.1. Apart from the qualitative targets, all vehicles should be able to manage highway driving in most countries around the world.

In this section the stated qualitative targets will be further specified into quantitative performance requirements for each of the concept cars, with collected data on 28 existing light duty BEV models as a frame of reference.

Table 4.1 Qualitative design targets for the three concept BEVs.

	Seats	**Size**	**Speed and acceleration**	**Range**
City:	4-5	Small	Medium	Medium
Highway:	5	Medium	High	Long
Sport:	2	Small	Very high	Very long

4.1 Performance requirements based on data of selected existing BEVs

The performance requirements of the three concept vehicles are mainly based on data found on existing BEVs, and in some cases also on information in Chapter 3. Car data that is relevant for this chapter is; curb weight, height and width in order to estimate effective

vehicle area, drag coefficient C_d, top speed, time to accelerate, certified driving range as well as energy consumption per driven distance.

Data on the existing light duty BEV models (including concepts) has been gathered mainly from manufacturer web sites, mostly American and Swedish but also British and German. In case of data gaps from manufacturers, data has also been collected from sources such as automobile magazines, online test reports and Wikipedia. The full list of vehicle models along with the collected data and their sources, can be seen in Appendix A.

For some of the data there exists a level of uncertainty on the correctness and reliability, since it is not specified in a standardized way, and many sources do not declare under which conditions the data is valid.

Firstly, the definition of curb weight is not consistent between countries and regions, where American sources often do not include neither the mass of a driver nor cargo, whilst European sources might do. The curb weight may also differ depending on initial amount of fuel and level of equipment that a base car is set up with.

Secondly, the cross sectional area is very seldom stated, thus it has to be estimated, e.g. by a method such as the ones suggested in Chapter 2, i.e. as a weighted product of vehicle height and width.

Lastly, the vehicle driving range given is usually specified as the certified range gained by driving according to either American EPA cycles or the European NEDC cycle, however in some sources this is not declared. Furthermore, in some sources manufacturers advertise their vehicles with only general driving range figures meant to represent real-world driving. The same issue is also valid for energy consumption per distance.

For further ease of benchmarking, the existing vehicles have been categorized into vehicle classes based on size and/or utility into; small cars, medium-large cars and sport cars. The following 12 models are considered to be included in the small car category; BMW i3, Chevrolet Spark EV, eCar 500 EV, Fiat 500e, Mercedes Smart fortwo, Mini Mini E, Mitsubishi i.MiEV, Peugeot iOn, Reault Zoe, Scion iQ EV and Volkswagen e-Up!. The 12 medium-large car models are; BMW Active E, CODA Automotive CODA, Ford Focus EV, Honda FIT, Nissan Leaf, Renault Fluence Z.E., Volkswagen e-Golf, Volvo C30 and four Tesla Model S models; 40kWh, 60kWh, 85kWh and Performance (85kWh). Finally, the 4 sport car models are; Lightning Lightning GT, Mercedes-Benz SLS AMG Electric Drive, Rimac Concept_One and Tesla Roadster.

4.1.1 Speed and acceleration performance

All three concept vehicles should be able to handle highway driving in most countries, which is typically between $110 - 130\,km/h$, as stated in Chapter 3. Only a few countries have speed limits above this, where the highest limit is $150\,km/h$.

Data on top speed has been found for all of the selected existing BEV models, which shows a rather wide variety. However the majority (20) of the cars have top speeds around $150\,km/h$ or lower; three at $125 - 126\,km/h$, five at $130\,km/h$, six at $135 - 137\,km/h$, four at $145\,km/h$ and two at $150 - 152\,km/h$. The top speed of the small cars ranges from

$126 - 152\,km/h$, while it is $125 - 210\,km/h$ for the medium-large cars, or $125 - 145\,km/h$ when excluding the Model S models. The top speed of the sport cars varies between $200 - 300\,km/h$.

Based on the data found, the top speed of the **City car** is settled to $135\,km/h$ on a flat road in order to manage highway driving in most countries with a small margin included. This speed is somewhat higher compared to the lowest speed models, yet it is not as high as for the fastest small cars. The top speed of the **Highway car** is set to $150\,km/h$ to handle highway driving in all countries. This speed level matches the fastest small size BEVs. The top speed of the **Sport car** is chosen to be $210\,km/h$ on a flat road, which matches two of the existing sport cars, but not the fastest ones.

The top speed and acceleration time of the three concept vehicles along with specified data of the existing BEVs can be seen in Figure 4.1.

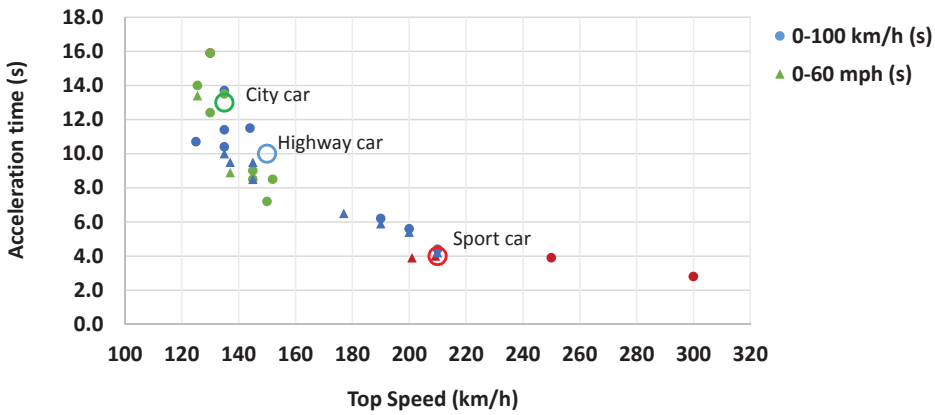

Figure 4.1 Top speed vs. acceleration for the three concept BEVs (circles), as well as for the existing BEVs (filled circles $0 - 100\,km/h$ and triangles $0 - 60\,mph$), where small cars are green, medium to large cars are blue and sport cars are red.

Acceleration performance is usually stated as the minimum time to accelerate from $0 - 100\,km/h$ or $0 - 60\,mph$ (which corresponds to $0 - 96.5\,km/h$), i.e. while using the maximum power from the powertrain. This type of data has been found for 26 of the existing BEVs.

In the found data it can be noted that those models with the highest top speed levels, are also those with the shortest time to accelerate. For the sport cars the time is around $4\,s$, with one exception at $2.8\,s$. For the small cars, the spread in acceleration time is relatively large; with four models around $7 - 9\,s$ and the 7 rest around $12 - 16\,s$. The medium-large cars have acceleration times between $4 - 14\,s$, or $9 - 14\,s$ when excluding the high performing Model S models. It can be noted that despite their larger volume, the Model S cars have

similar speed and acceleration performance as for some of the sport cars.

For the three concept vehicles, only the time to accelerate from $0 - 100\,km/h$ is specified. For the **City car**, the time is decided to be maximum $13\,s$, which corresponds to a medium performance small car. For the **Highway car**, it is decided to be $10\,s$, which is also somewhat of a medium value for the category. Finally the chosen $0 - 100km/h$ acceleration time for the **Sport car** is set to $4\,s$, in order to match the sport cars with the highest performance.

4.1.2 Gradability

A vehicle's *gradability* is the maximum grade that a vehicle can climb at a certain speed while using the maximum power from the powertrain. Data on gradability for the concept vehicles is not based on typical values from existing BEVs, since this type of data could not be found.

There are however a few sources that present general gradability design goals, such as [70], in which a set of minimum gradability requirements are defined (among others), in order for a BEV to be considered to be comparable in the so called *EV America* evaluation project, sponsored by the US Department of Energy. According to the goals, the BEVs should be able to start in a $25\,\%$ uphill grade, drive in a speed of $88.5\,km/h$ in a $3\,\%$ grade, and in $72.4\,km/h$ in a $6\,\%$ grade. Additionally the BEVs should be able to sustain the speed of $88.5\,km/h$ in a $3\,\%$ grade for at least $15\,min.$, when starting with a $50\,\%$ battery SOC. All of this, while loaded with two passengers with a total added weight of $150\,kg$. In contrast, according to [34], the PNGV gradability goal was set to sustain the speed of $88.5\,km/h$ at a grade of $6.5\,\%$.

When considering typical grade levels on highways, there are relatively few passages with grade levels larger than $6\,\%$, unless perhaps considering mountainous areas. There are even fewer sections with grade levels of $12\,\%$ or higher.

Based on the above, as well as the quantitative requirements in Table 4.1, it is decided that the **Highway car** should be able to sustain a speed of $130\,km/h$ at a grade 6%, and that the **Sport car** is to be able to sustain a highway speed of $130\,km/h$ even in steep grades of $12\,\%$. The **City car**, on the other hand, should have a maximum speed of at least $90\,km/h$ at the grade of $6\,\%$. Furthermore it is decided that, in coherence with the minimum goals stated in [70], all three concept vehicles should be able to **start** in a uphill gradient of at least $25\,\%$.

4.1.3 Driving range and curb weight

The NEDC driving range for 21 of the existing vehicles has been found, where the small cars have ranges between $85 - 210\,km$, with only two models above $160\,km/h$. For the medium-large cars the NEDC rage is $162 - 502\,km$ or $162 - 199\,km$ when excluding the Model S models, and for the sport cars it is $241 - 600\,km$, or $241 - 340\,km$ when excluding the Rimac Concept_One.

It is decided that the concept **City car** is to have a NEDC range of about $160\ km$, which is not as long as for the two top models in the category. As seen in Figure 3.21, this distance covers over $90\ \%$ of the average daily driven distances in many countries in the world, although real world driving will most likely lead to a different driving range. For the **Highway car** the NEDC range should be around $200\ km$, in order to match the models with the longest range, still not as long as for the Model S models. The NEDC range of the **Sport car** is to be $300\ km$, which is longer than for two of the sport models, but much shorter than than the one with the longest range.

The curb weight of all 28 BEV models was found. In general the small cars have the lowest masses and range from around $920 - 1500\ kg$. For the medium-large cars the masses range around $1500 - 2100\ kg$, or $1500 - 1800\ kg$ when excluding the Model S models, while for the sport cars it range from $1300 - 2100\ kg$.

It may be argued that a BEV's curb weight strongly depend on the vehicle's range, due to the relatively large mass of the battery in a BEV. While this is true and relevant, the weight also depend on the vehicle size as well as choice of materials. For BEVs with NEDC ranges between $150 - 200\ km$ the curb weights span between around $1200 - 1700$.

Based on the found data it is decided that the curb weight of the concept **City car** may be around $1200\ kg$ in accordance with the group of lower weight cars. The weight of the **Highway car** may be around $1700\ kg$, to reflect a value slightly above the medium for medium-large cars. Finally the concept **Sport car** is to have a curb weight of around $1900\ kg$, i.e. a rough mean value.

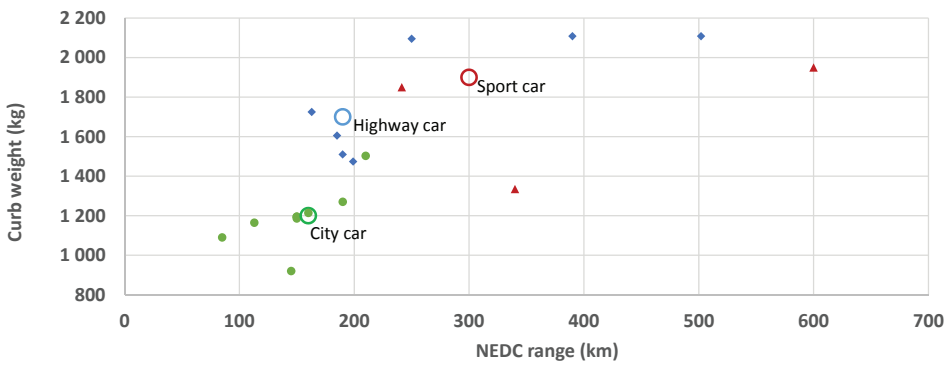

Figure 4.2 NEDC driving range vs. curb weight for the three concept BEVs as well as for the existing BEVs, where small cars are green, medium to large cars are blue and sport cars are red.

4.1.4 Cd and estimated Area

Data on vehicle front area was found for only three of the existing vehicles. For the rest of the vehicles the area has been estimated based to $84\ \%$ of the product of height and width, see Figure 4.3, since it showed to give the closest match between the methods suggested

in Chapter 2, and the found data. For simplicity it is here assumed that the same weighting factor can be used for all cars. More details regarding the estimated areas can be found in Appendix A.

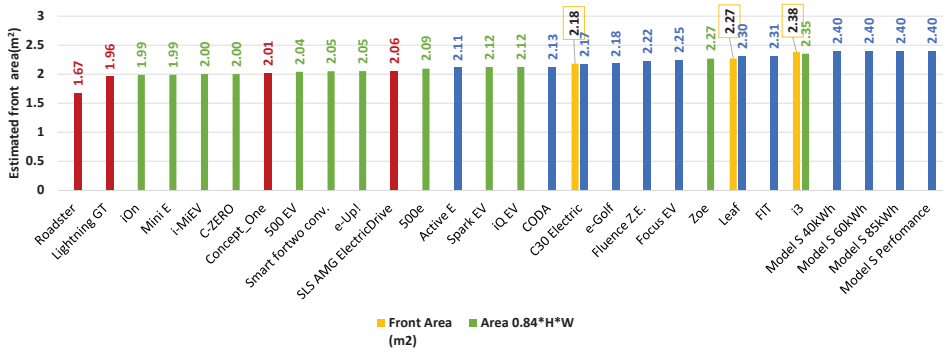

Figure 4.3 Estimated area, for existing BEVs.

In Chapter 2, typical vehicle front areas for different vehicle classes based on data from the 1990s, were presented. However since there is a lack of coherence between different categorization methods for vehicle classes based on size and utility, as well as a noted spread within each category, the practical use of such figures is rather limited. In general it can be seen that all of the estimated areas for the existing vehicles are quite large compared to those defined to be typical in the 1990s. It is thus very likely that passenger vehicles have become both wider and higher since then. It is thereby concluded that the suggested class based front areas from the 1990s will not be further considered.

The areas of the concept vehicles are mainly determined based on the estimated areas of the existing BEVs. The area of the **City car** is chosen to be $2.05\,m^2$, which resembles a small car, the **Highway car** area is chosen to be $2.3\,m^2$ which takes after the large cars, while the **Sport car** area is chosen to be $2.0\,m^2$ which is close to Lightning and Concept_One.

With the published C_d values of existing BEV's as a reference, see Figure 4.4, the C_d value of the **City car** is chosen to be 0.3, the **Highway car** 0.28, and finally the C_d value of the **Sport car** is chosen to resemble that of the Roadster, 0.35.

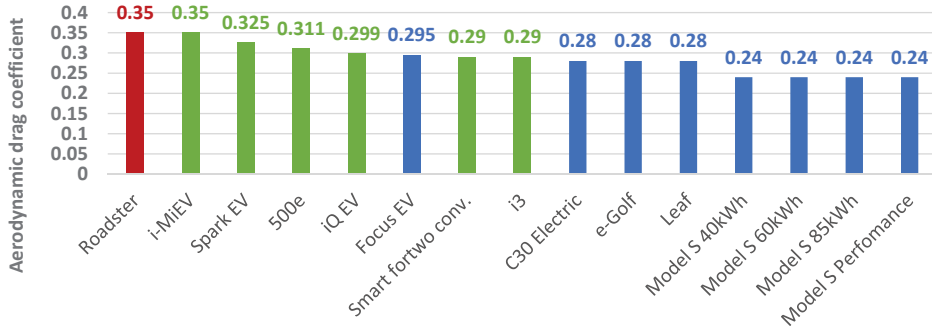

Figure 4.4 Cd-values for existing BEVs.

Data on tire radius of existing BEVs has not been found, instead it has been estimated based on tire size, see Appendix A. Estimated tire radius of the existing BEVs can be seen in Figure 4.5, and it is the base for the assumed tire radius on each of the concept vehicles which have been chosen accordingly; the **City car** $0.31\,m$, the **Highway car** $0.32\,m$, and the **Sport car** $0.34\,m$.

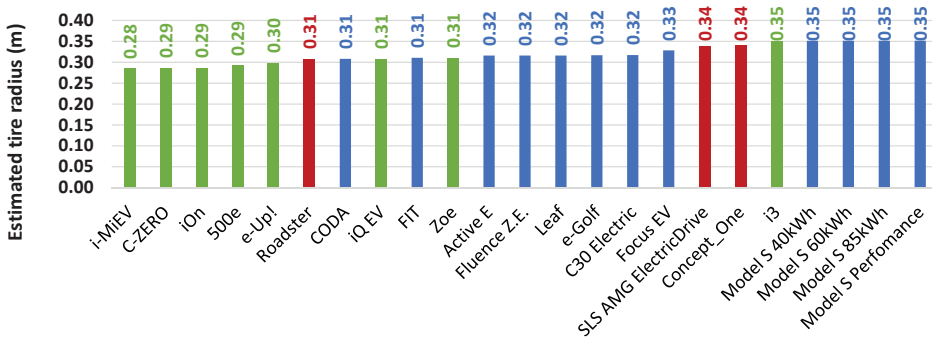

Figure 4.5 Estimated tire radius, for existing BEVs.

Finally, the tire rolling resistance coefficient should be estimated for all of the concept vehicles. Even though the rolling resistance is known to be speed dependent, there is no clear consensus on how this should be modeled unless perhaps tire specific data is available, which it is not in this case. Another aspect is that the type of study in this theses is of comparative nature, hence a possible speed dependence of the rolling resistance is expected to have a rather small impact on the final result. With these aspects as a background as well as the information presented on the topic in Chapter 2, it is assumed that the rolling resistance of the concept BEVs can be estimated by the mean values; 0.009 for both the **City car** and the **Highway car** representing low rolling resistance tires, while for the **Sport car** the tires are expected to be optimized for performance rather than energy efficiency,

leading to 0.012.

4.1.5 Summary of requirements on chosen vehicle concepts

All previously stated requirements of the three concept vehicles are summarized in Table 4.2.

Table 4.2 Prerequisites for the three chosen vehicles for this study.

	City	**HW**	**Sport**	
Seats:	4-5	5	2	kg
Mass:	1200	1700	1900	kg
Acceleration 0-100 km/h:	13	10	4	s
Top speed:	135	150	210	km/h
NEDC Range:	160	200	300	km
Aearod. drag coeff. C_d**:**	0.3	0.28	0.35	$-$
Area:	2.05	2.3	2.0	m^2
Wheel radius:	0.31	0.32	0.34	m
Rolling resist. coeff. C_r**:**	0.009	0.009	0.012	$-$
Starting gradability:	25 %	25 %	25 %	%
Gradability: (Speed at grade)	90 at 6%	130 at 6%	130 at 12%	km/h, %

4.2 Wheel load analysis of chosen concepts

In the wheel load analysis of the concept vehicles, the levels of force, speed and power at the wheels, are estimated based on the above stated quantitative vehicle requirements.

With help of the information in Chapter 2 regarding vehicle dynamics, the forces due to aerodynamic drag (2.2), rolling resistance (2.3), road grade (2.4) as well as acceleration (2.1) are calculated for all of the concept vehicles, assuming a gravitational constant, $g = 9.81\,m/s^2$ and an air density of $\rho = 1.2\,kg/m^3$. At this point no regard is taken to time duration of any of the operating points, only to the level of magnitude. The analysis is also based on finding information that is of interest for a BEV with a single speed gearbox.

4.2.1 Road load and grade

The road load wheel forces (aerodynamic drag and rolling resistance) for each of the concept BEVs have been estimated at speed levels within their specified speed ranges, as can be seen in the left part of Figure 4.6. Due to the aerodynamic drag, the wheel force shows a strong dependence on speed. The Sport car demands the largest wheel force at a certain speed level compared to the other cars, and the City car demands the lowest. The contour lines represent wheel power for a certain combination of speed and force.

As an illustrative example; if the City car is driving at its top speed, $135\,km/h$ on a level road, this demands a wheel power of about $23\,kW$, while driving at $100\,km/h$ demands roughly half of that. Furthermore, if the City car is driving at $100\,km/h$ i.e. with a wheel

power load of about $13\,kW$, while the powertrain is able to deliver up to $23\,kW$, this means that there is a potential excess wheel power of about $10\,kW$ relative to the road load demand. This excess power equals a wheel force of about $400\,N$, which could give an acceleration of about $0.3\,m/s^2$ ($\frac{400\,N}{1200\,kg}$).

In the right part of Figure 4.6, the road load force is normalized to vehicle mass. Then it can be seen that for low speed levels the Sport car has a slightly larger road load per mass, but for speed levels above around $66\,km/h$ it is the City car that has the highest road load, relative to its mass. This reflects the relatively larger aerodynamic drag compared to rolling resistance for small cars. Power level contour lines are also included in the right part of Figure 4.6, however this time each car has their own lines. The excess wheel force and power over the road load at a certain speed level, can in this diagram directly be translated into a possible acceleration. It can thus be seen that, at the same power level, the power lines for the Sport car are the lowest, while the lines for the City car are the highest, and that the deviation increases with increasing power levels. This means that, for the same speed level, a possible wheel power of $50\,kW$ in the City car would give a higher acceleration, compared to having the same power level available in the Sport car.

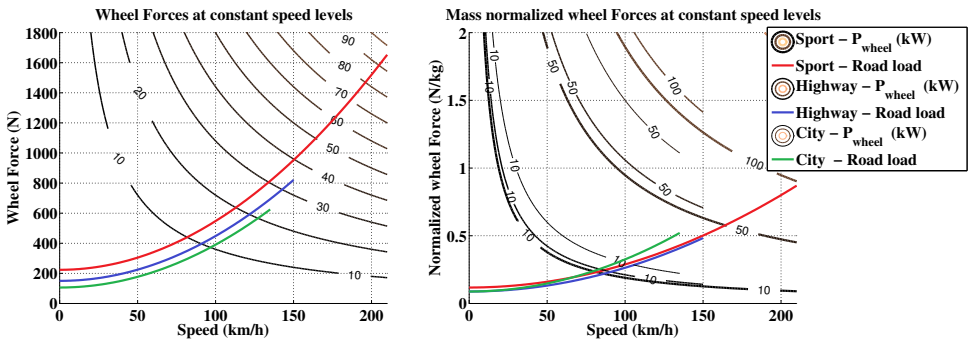

Figure 4.6 Force on wheels due to road load at different speed levels on a level road, as well as the wheel force normalized by vehicle mass, for all three concepts. The contour lines represent wheel power for a certain combination of speed and force, which is the same for all cars in the left part of the figure, however not for the right part.

Figure 4.7 shows both absolute wheel forces and mass normalized wheel forces for each concept car, for road loads at certain grade levels as well as at operating points corresponding to the specified speed and grade performance requirements.

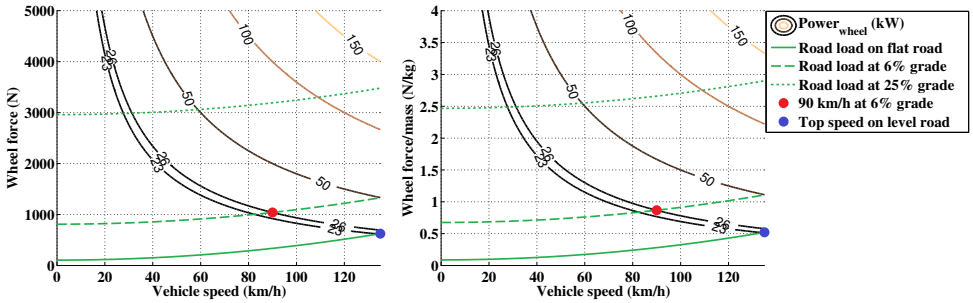

(a) City car.

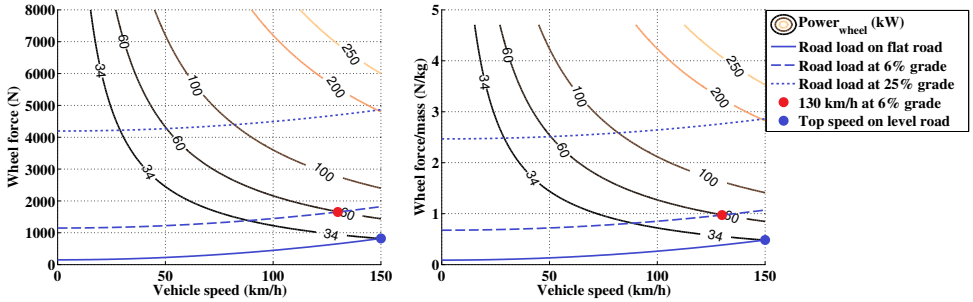

(b) Highway car.

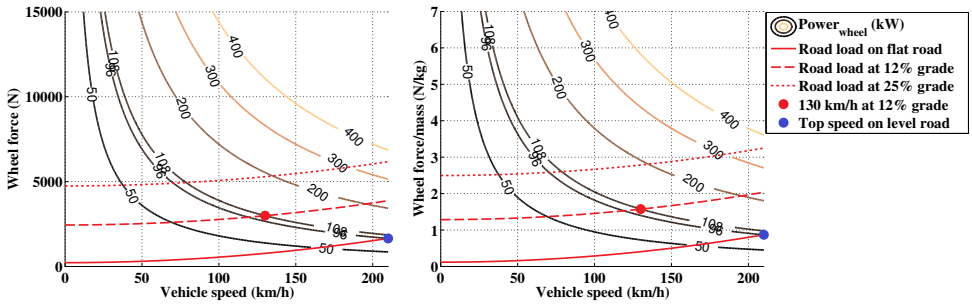

(c) Sport car.

Figure 4.7 Force on wheels due to road load per speed level, and normalized force per vehicle mass, for all three concept cars, along with contour lines representing combinations of wheel force and speed for different levels of wheel power.

Starting with the **City car**, Figure 4.7(a) shows that the top speed and the grading requirement at high speed, demand about the same levels of wheel power; $23\,kW$ and $26\,kW$ respectively, while the force level at the grading requirement is roughly twice that at the top speed (about $1\,kN$ and $0.6\,kN$ respectively). The takeoff requirement demands the largest force, almost $3\,kN$ but since the speed is low, so is the power demand. In the right part of Figure 4.7(a) it can be seen that the takeoff requirement is equal to an acceleration of almost

$2.5\,m/s^2$, as was predicted in Table 2.2, and as is also valid for the other cars. To conclude, if the wheel force is limited to $3\,kN$ at speed levels up to a power limit of $26\,kW$, above which the wheel force follows the power line, then all three specified operating points will be achievable. As mentioned, the difference between the maximum available wheel force and the road load at a certain grade, equals the vehicle's acceleration capacity. With the above limits, the initial acceleration at takeoff would be about $2.4\,m/s^2$ on a flat road, at $50\,km/h$ it would be about $1.4\,m/s^2$ and at $100\,km/h$ about $0.47\,m/s^2$.

For the **Highway car**, shown in Figure 4.7(b), the top speed demands a force of about $1\,kN$ and a power of $34\,kW$, while the high speed grading requirement demands a force of about $1.8\,kN$ and a power of $60\,kW$, i.e. a larger difference between the requirements compared to the City car (it can be seen that also for the Highway car the demanded power at $6\,\%$ grade in $90\,km/h$ is almost the same as that at the top speed). For the Highway car an initial force level of about $4.1\,kN$ is required to manage the takeoff requirement, up to about $50\,km/h$ where the power thus can be limited to $60\,kW$.

The **Sport car**, shown in Figure 4.7(c), evidently demands the highest levels of force and power compared to the other two cars. As for the City car, both the top speed and grading requirements demands roughly the same power levels $96\,kW$ and $108\,kW$ respectively. The takeoff requirement demands an initial force of about $4.8\,kN$. This force level may be sustained up to about $80\,km/h$, where the power may be limited to $108\,kW$.

4.2.2 Acceleration

Given the above stated demanded levels of force and power versus speed due to the three mentioned requirement; top speed, grade at high speed and take-off at high grade, it can be noted that the implied acceleration capacity of each car would be rather limited. Further investigations must be made to find suitable levels of force and power that will also fulfill the acceleration requirements.

By assuming a torque and speed characteristic that is typical for an electric machine, (i.e. a region of constant torque at low speeds followed by a region of constant power at higher speeds, where the torque is inversely proportional to the speed), various combinations of initial maximum levels of wheel force and wheel power limits can be found, such that they will all fulfill the acceleration requirement.

As an illustrative example in Figure 4.8, a set of increasing maximum power levels are combined with decreasing levels of maximum initial force, which all result in an acceleration time of $13\,s$, as it is the $0-100\,km/h$ acceleration requirement for the **City car**. It was found that the lowest level of power in the figure ($44\,kW$) could not be further decreased, since then regardless of the increase in magnitude of the initial force, the acceleration time was too long.

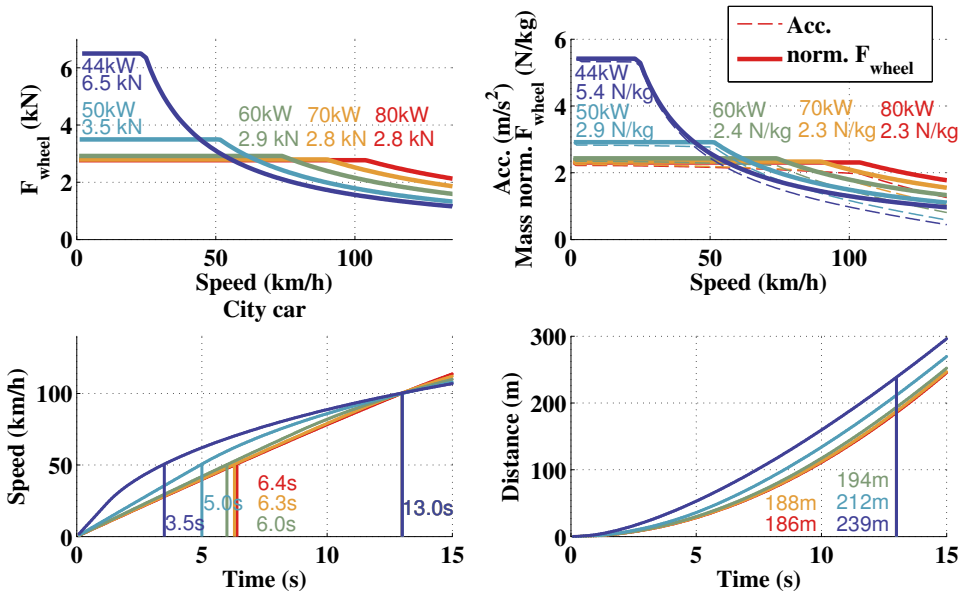

Figure 4.8 Speed and distance over time, as well as wheel force and acceleration, for various combinations of maximum wheel force and power, during $0 - 100\,km/h$ acceleration, for the concept City car.

For higher power levels the speed level at which the force becomes limited by the power, increases.

In the upper left and right part of the figure, it can be seen that for the two lowest power levels the difference in demanded initial force is much larger, compared to the difference between the two highest power levels, where the initial force levels are almost the same.

Another interesting aspect is that, even though the acceleration time from $0 - 100\,km/h$ is the same for all combinations, the acceleration time from $0 - 50\,km/h$, hence also $50 - 100\,km/h$ differs quite a lot between the two lowest power levels and the three highest. This can be seen in the lower left part of the figure, where the two lowest power levels with the highest levels of initial force, accelerate the fastest at low speed levels, while at higher speed levels their acceleration times are the longest.

Furthermore, in the lower right part of the figure, the driven distance is presented showing that the cars with the highest acceleration level at high speed (i.e. highest power levels) demand the shortest distance to reach $100\,km/h$.

It can thus be concluded that the requirement on acceleration time from $0 - 100\,km/h$ alone, is not enough when seeking to specify a vehicles acceleration performance over the operational speed range.

Few data regarding acceleration times between different speed levels have been found for existing BEVs, see Appendix A. Acceleration times for $0 - 50\,km/h$ (found for 500EV, C30 and Zoe) are $7.2\,s$, $4\,s$ and $4\,s$ and for $0 - 60\,km/h$ (found for ActiveE, i3 and Smart-

fortwo) they are $4.5\,s$, $3.7\,s$, and $4.8\,s$, while the acceleration times for $50-100\,km/h$ are $6.7\,s$, and $9.5\,s$, and for $60-100\,km/h$ they are $4.5\,s$, $3.5\,s$, and $6.7\,s$.

In Figure 4.9 electric machine power and acceleration time is presented for 22 of the existing BEVs (to connect data with car model, see Appendix chap:AppA). It can thus be seen that for an acceleration time around $13\,s$ electric machine power levels of 60 to $70\,kW$ are commonly used. For an acceleration time around $10\,s$ power levels between 90 to $125\,kW$ are typically used. Finally for acceleration times around $4\,s$ the installed power varies quite a lot, i.e. between 225 to $550\,kW$. These power levels may be used as reference values when determining suitable levels for the concept cars.

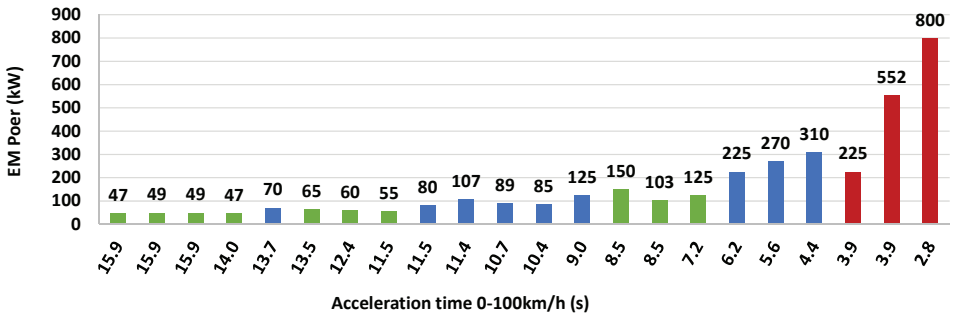

Figure 4.9 Electric machine power and time to accelerate from $0-100\,km/h$, for existing BEVs.

4.2.2.1 Acceleration performance of selected logged cars

As a reference, 7 example logged cars accelerating from $0-100\,km/h$ can be seen in Figure 4.10, covering one diesel SUV (Sport Utility Vehicle), one HEV (Hybrid Electric Vehicle), one Plug-in HEV and 4 BEVs. The logs should be considered as descriptive examples rather than hard facts, as no standardized test methods were used, yet roads with noticeable grade levels were avoided. The vehicle specifications and model year may also differ from the data specified for the BEVs in Appendix A.

In Figure 4.10 it can be seen that acceleration times of around $12\,s$ are correlated with initial acceleration levels of $3.5-4\,m/s^2$ up to a speed of about $40\,km/h$, while at a speed of $80\,km/h$ the acceleration levels are $1.9-2\,m/s^2$. For acceleration times just above $5\,s$ the initial acceleration levels are around $6.5-6.9\,m/s^2$, and sustained up to a speed of about $60\,km/h$, and at $80\,km/h$ the acceleration has dropped to just above $5\,m/s^2$.

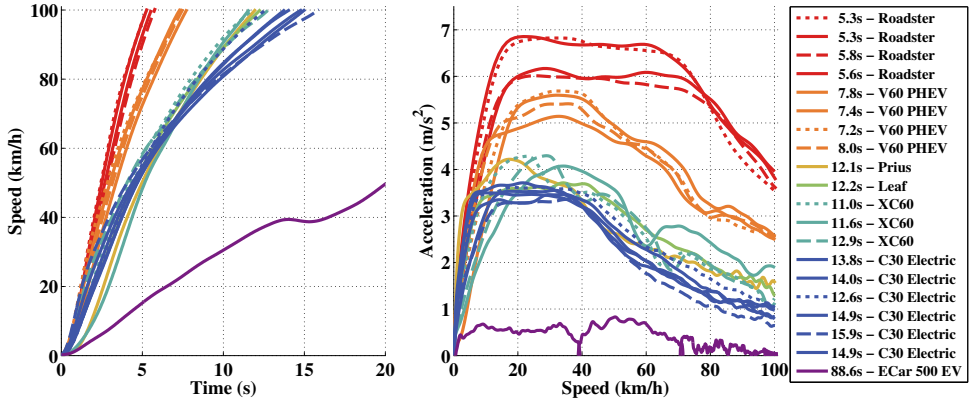

Figure 4.10 Measured speed and acceleration of Logged vehicles during $0 - 100\,km/h$ tests. The shortest time for each model is dotted, and the longest time is striped.

All logs show that the peak acceleration is not reached immediately from zero speed, but from speeds of 5 up to $15\,km/h$ for the highest levels. Evidently the fastest accelerating cars are those that reach the highest levels of acceleration, but it can also be seen that they are able to sustain the peak acceleration over a wider speed range. The base speed of the Roadster seem to be around 60 to $70\,km/h$. With a top speed of $201\,km/h$ this means a base-speed-to-top-speed ratio of around $1/3$. The same ratio for the C30 seem to be around $1/4$ to $1/3$.

Based on estimated vehicle parameters, also the wheel forces and powers have been approximately calculated, see Figure 4.11 and 4.12. For those logs with acceleration times around 12 to $15\,s$, the initial wheel force is around $6\,kN$, and the peak wheel power levels are between 50 to $90\,kW$. For the higher performing cars the initial force goes up to 8 and $11\,kN$, and the power levels to between 140 to $160\,kW$.

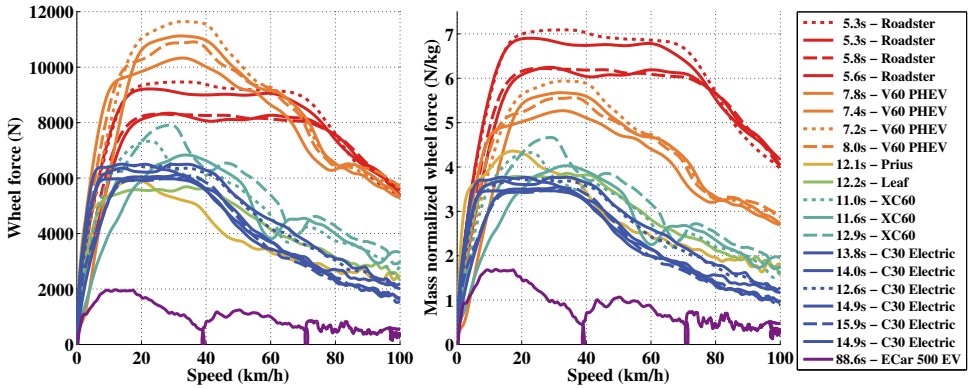

Figure 4.11 Estimated wheel force of measured speed and acceleration of Logged vehicles during $0 - 100\,km/h$ tests. The shortest time for each model is dotted, and the longest time is striped.

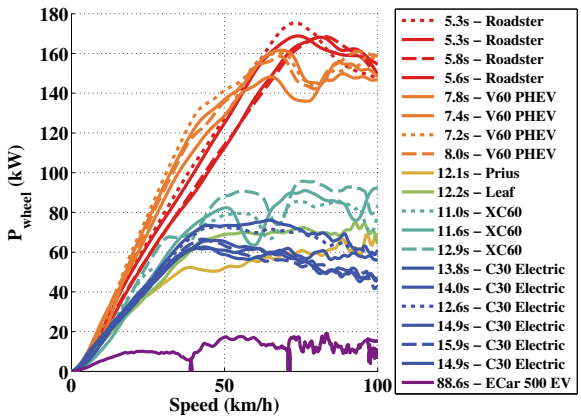

Figure 4.12 Estimated wheel power of measured speed and acceleration of Logged vehicles during $0 - 100\,km/h$ tests. The shortest time for each model is dotted, and the longest time is striped.

4.2.2.2 City car

In Figure 4.13, three other combinations of initial force and power are presented, this time with base speeds as $1/4$, $1/3$ and $1/2$ of the top speed for the City car, i.e. similar to common ratios for electric machines.

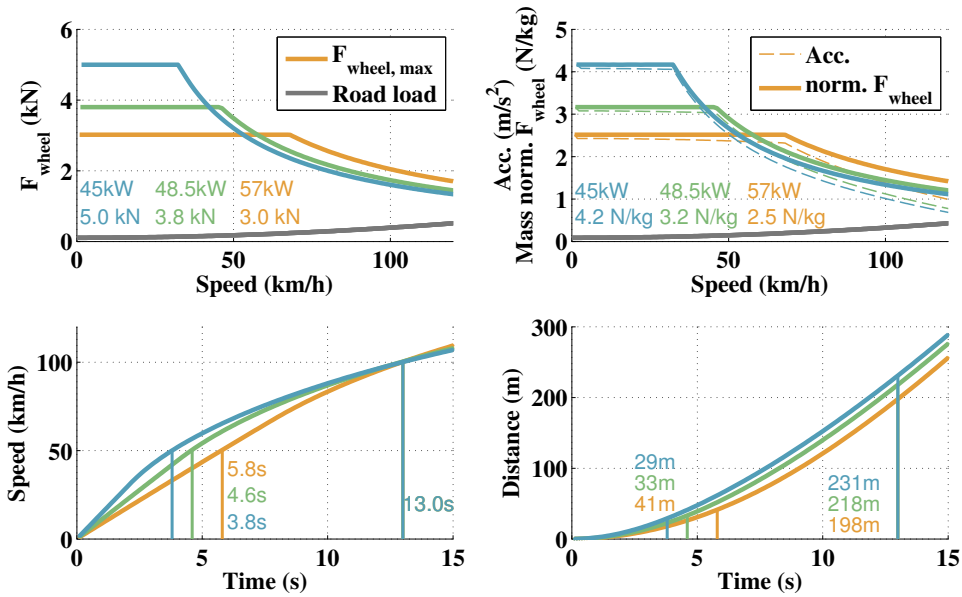

Figure 4.13 Speed and distance over time, as well as wheel force and acceleration, for base speeds that are $1/4$, $1/3$ and $1/2$ of the top speed, during $0-100\,km/h$ acceleration, for the concept City car.

As expected from previous discussion, the lowest base speed is related to the largest initial force (**5 kN**), lowest power (**45 kW**), fastest acceleration of $0-50\,km/h$ (just under $4\,s$) along with the shortest driven distance, while the acceleration time of $50-100\,km/h$ is the longest. Given that this is the City car, it can be argued that low speed acceleration performance should be preferred over high speed performance. It is thus decided that the lowest power level should be designed for. Compared to the power levels of existing BEVs with similar acceleration times, the chosen power level is smaller. However the acceleration time $0-50\,km/h$ complies rather well when comparing with some of the existing BEVs.

When comparing the results in Figure 4.13, with the ones found in Figure 4.7(a), the initial force demanded by the acceleration requirement should be around $2\,kN$ higher than that for the takeoff requirement (of $3\,kN$), while the power should be $19\,kW$ higher than that of the high speed gradient requirement (of 26 kW). It is thus the acceleration requirement that will determine the maximum force and power that has to come to the wheels (via the gear box) from the powertrain.

4.2.2.3 Highway car

Combinations of initial force and power limits have been studied in the same manner for the **Highway car** as well, see Figure 4.14.

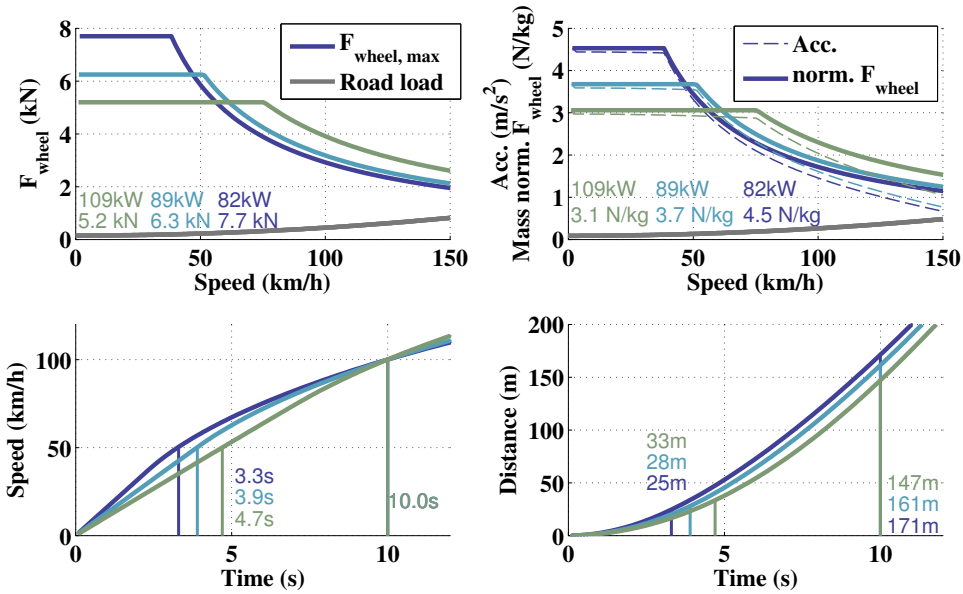

Figure 4.14 Speed and distance over time, as well as wheel force and acceleration, for base speeds that are $1/4$, $1/3$ and $1/2$ of the top speed, during $0-100\,km/h$ acceleration, for the concept Highway car.

Also here the result is that, the combination that has the highest initial force ($7.7\,kN$) and lowest power ($82\,kW$), will result in the best low speed performance ($3.3\,s$ when accelerating $0-50\,km/h$). However since the $0-50\,km/h$ and $0-60\,km/h$ acceleration times of the few existing BEVs that was found are around $4\,s$, this is here chosen as a targeted value also for the Highway car. Thus targeted initial force is **6.3 kN** and power is **89 kW**. That means that the initial force should be about $2.2\,kN$ more than what was demanded by the takeoff requirement (of $4.1\,kN$), and the power should be $29\,kW$ more than that of the high speed gradient requirement (of $60\,kW$), as seen in Figure 4.7(b). This would result in an initial acceleration level of about $3.7\,m/s^2$.

4.2.2.4 Sport car

Finally, for the **Sport car**, see Figure 4.15, an initial force of $16.6\,kN$ and a power of $251\,kW$, will result in the best low speed performance, with an initial acceleration level of $8.7m/s^2$ up to a speed of about $50\,km/h$.

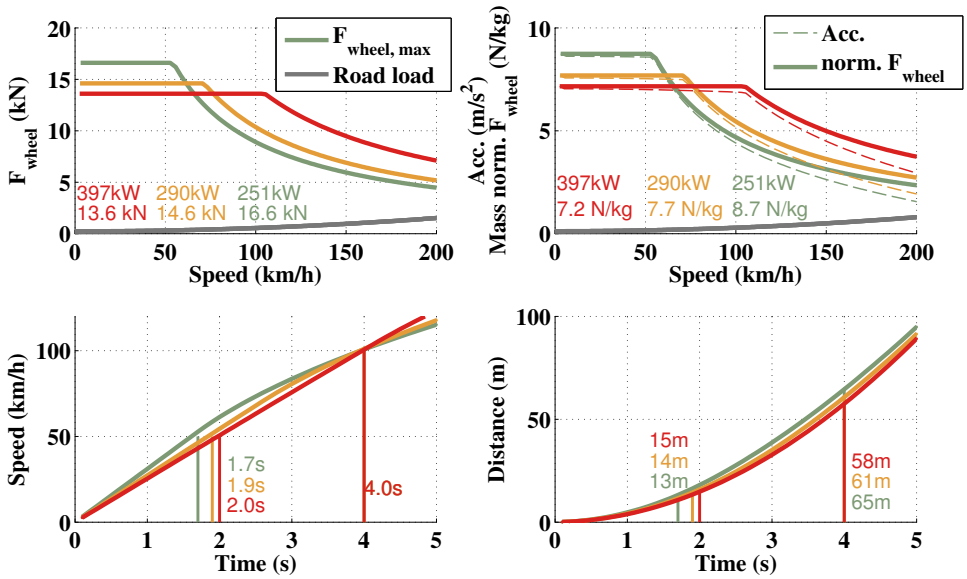

Figure 4.15 Speed and distance over time, as well as wheel force and acceleration, for base speeds that are $1/4$, $1/3$ and $1/2$ of the top speed, during $0 - 100\,km/h$ acceleration, for the concept Sport car.

According to the logged acceleration tests of the performance vehicles in Figure 4.10, the peak acceleration is kept up to around $80\,km/h$ for an acceleration time which was just above $5\,s$, hence it is decided that the Sport car should also have a similar base speed. That means that the middle curve is chosen as the desired powertrain capability, with an initial force of **14.6 kN** and a power of **290 kW**.

In this case another aspect needs to be considered; the maximum adhesive capability between the tires and the road, see Chapter 2, section Wheel force. It might not be physically feasible to sustain such a large force on two wheels without loosing the grip. By assuming the weight on the driving wheels during the acceleration is about $60\,\%$ of the vehicles weight and that the friction between the tire and the road is unity for dry asphalt and performance tires, then the maximum wheel force becomes $11.2\,kN$ ($0.6 \cdot 1900 \cdot 9.81 \cdot 1 = 11.2\,kN$). Perhaps this value could be larger if another weight distribution was assumed, or if the friction constant was a bit larger. Nevertheless, to be on the safe side, an All-Wheel-Drive (AWD) is here assumed for the Sport car, resulting in a maximum wheel force of about $18.6\,kN$.

4.3 Wheel load analysis for selected drive cycles

In this section time traces of speed profiles are used as inputs when calculating demanded wheel power and energy for the three concept cars.

4.3.1 Peak wheel power for Concept BEVs, per cycle

Figure 4.16 shows peak positive and negative wheel power per car, for the Urban, Rural and Highway test cycles. In general, the Sport car demands the largest power levels and the City car the lowest. Similarly, the Urban cycles demand the lowest levels of peak power, while the Highway cycles demand the highest. There are however a few highway cycles with similar peak power levels as some of the Urban and Rural cycles. The relation between peak positive and negative power is rather small for the Urban and most of the Rural cycles, while it is larger for many of the Highway cycles.

For the Urban cycles it is the SC03 and FTP cycles that have the highest wheel power. This can also be seen in Figure 3.7, these cycles have the highest positive peak accelerations at high speed. The same is also valid for UC LA92 and Artemis Rural for the Rural cycles and REP05 and US06 for the Highway cycles.

With a wheel power of $45\,kW$ for the City car, there may be a problem with the two rather aggressive Highway cycles; REP05 and US06, as well as full regenerative braking in UC LA92, Artemis Rural and the Artemis Motorway cycles. Naturally, the highest speed levels in Artemis150 would not be reached since it exceeds the top speed of the City car. On the contrary, if the Highway car is equipped with a maximum power of $89\,kW$, all cycles should be conceivable, except full regenerative braking in the Artemis Motorway cycles. The Sport car will have no problem following the test cycles, since the highest peak power is only $90\,kW$ compared to the powertrain's peak wheel power of $290\,kW$.

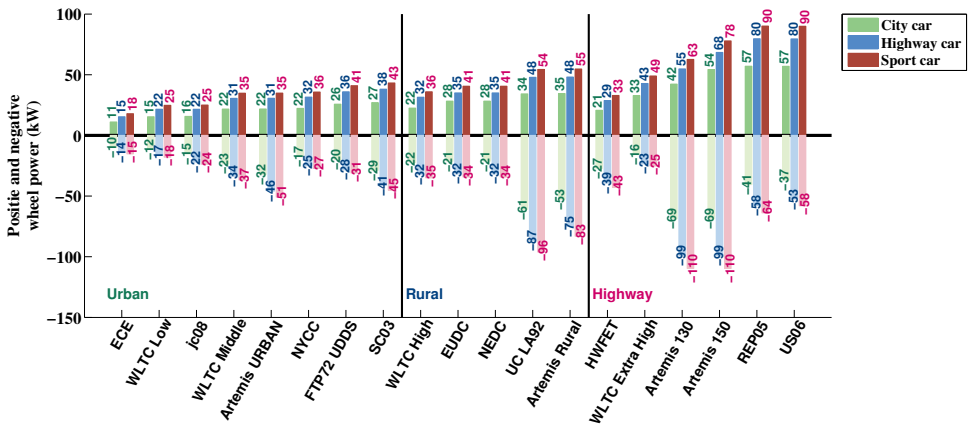

Figure 4.16 Max. positive and negative wheel power during Urban, Rural and Highway Test cycles, for all the three concept cars.

The peak power levels of the aerodynamic drag, rolling resistance and acceleration during each cycle, are visualized in Figure 4.17 to 4.19. Note that the peak power of the acceleration does not necessarily coincide in time with the peak power of the aerodynamic

drag, thus the sum of the three contributors are sometimes larger than the peak power per cycle. With two exceptions, for the City car in EUDC and NEDC, the acceleration peak power is the largest of the three, followed by the aerodynamic drag. The aerodynamic drag is naturally larger for those cycles with higher top speed levels.

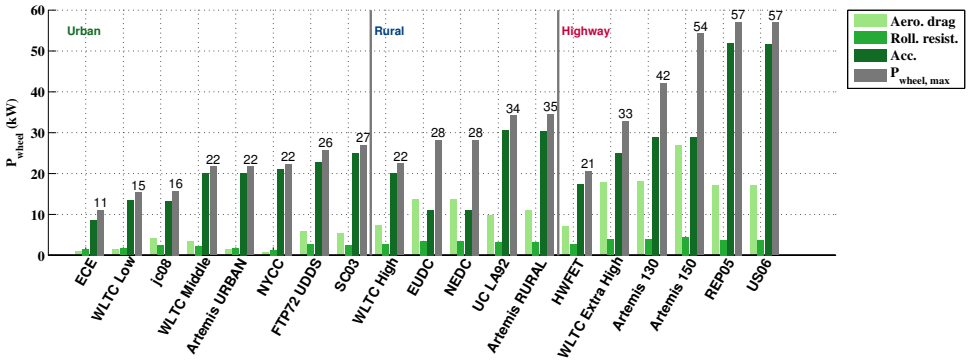

Figure 4.17 Max. Positive wheel power during Urban, Rural and Highway Test cycles, for the concept City car.

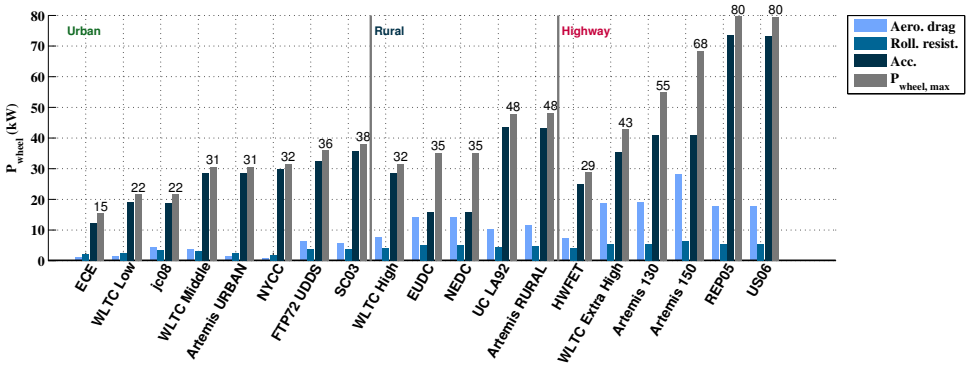

Figure 4.18 Max. Positive wheel power during Urban, Rural and Highway Test cycles, for the concept Highway car.

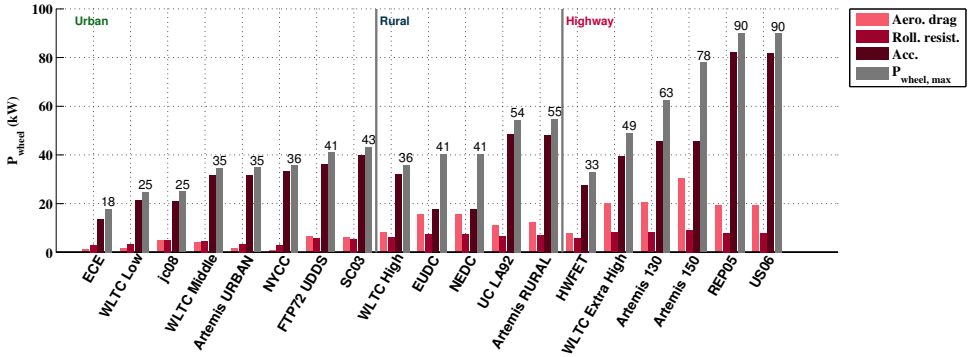

Figure 4.19 Max. Positive wheel power during Urban, Rural and Highway Test cycles, for the concept Sport car.

The maximum positive and negative wheel power for the logged cycles can be seen in Figure 4.20. It can be seen that the City car may have problem to reach some operating points in 2 of the Urban cycles, 3 of the Rural cycles and 3 of the Highway cycles, while the Highway car may have problem with only one of the Rural cycles, and the Sport car is likely to not have any problem to fulfill all power levels.

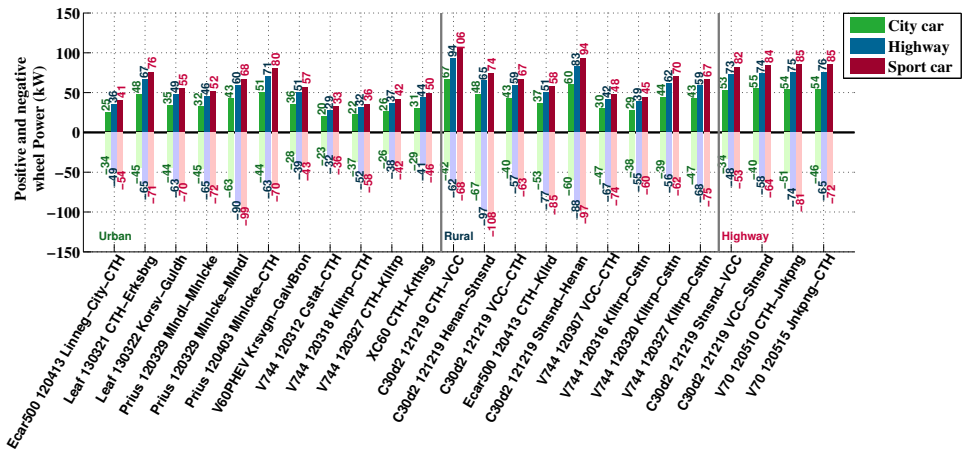

Figure 4.20 Max. positive and negative wheel power during Logged Urban, Rural and Highway cycles, for all the three concept cars.

4.3.2 Wheel energy per distance, per cycle

In this section both the total positive and negative wheel energy per cycle are calculated and divided by the cycle distance, in order to find the energy consumption for each of the

concept cars. As a frame of reference, certified energy consumptions per driven NEDC cycle for 16 commercial BEVs, are also presented.

4.3.2.1 Concept BEVs

Cycle energy per distance for the three concept cars can be seen in Figure 4.21. Over all, the consumption levels are similar for both Urban and Rural cycles, while they are somewhat higher for the Highway cycles. It is clear that the relative amount of braking energy is much larger for the Urban cycles, and rather limited for the Highway cycles. Furthermore, for the Urban cycles, acceleration and rolling resistance are the main causes of energy consumption, while the aerodynamic drag is rather small. Due to the somewhat higher speed levels in the Rural cycles, the aerodynamic drag becomes larger. Still for the Rural cycles the energy consumption seem to be relatively evenly chaired between the three sources. For the Highway cycles, the aerodynamic drag is the single largest cause of energy consumption, often followed by the rolling resistance. So, even though acceleration is the main force to consider when studying peak power levels; when it comes to energy consumption it is not always the superior cause, at least not according to the test cycles. For those cycles where acceleration is the main cause of energy consumption (Urban cycles in general, and NYCC, Artemis Urban and UC LA92 in particular), the braking energy is also larger compared to other cycles, thus there is a chance for recuperation.

Amongst the Urban cycles it is the NYCC and Artemis that have the highest levels of energy consumption, while ECE has the lowest. This can be related to Table 3.2 to 3.7, where it can be seen that NYCC, Artemis Urban and ECE have relatively low maximum and average speed values, but ECE have much lower maximum acceleration and RPA value than NYCC and Artemis Urban. For the Rural cycles, UC LA92 has the highest consumption and NEDC the lowest. Both cycles have similar levels of average speed but the UC LA92 has a large time share spent at higher speed levels. It is also the UC LA92 that has the highest maximum acceleration amongst the Urban cycles, as well as the highest RPA value, while NEDC has the lowest. Finally the Artemis motorway cycles have the highest consumption between the Highway cycles, and HWFET the lowest. In this case it is not the cycle with the highest acceleration or RPA values that consume the most energy, but it is that cycle that has the highest average speed and spend the most time at high speed levels.

An important note here is however that the energy consumption per driven distance is sensitive to the method which is used to estimate the acceleration from the reference speed trace. In Figure 4.22 energy per distance can be seen, where the Euler backward method is used instead of the previous method which is a combination of forward and backward Euler. For cycles with low levels of acceleration such as the NEDC cycle, no difference can be seen, while for cycles with high levels of acceleration like NYCC, the increase is over $15\,\%$ for the propulsion energy of the City car in the same time the decrease in braking energy is about $6\,\%$.

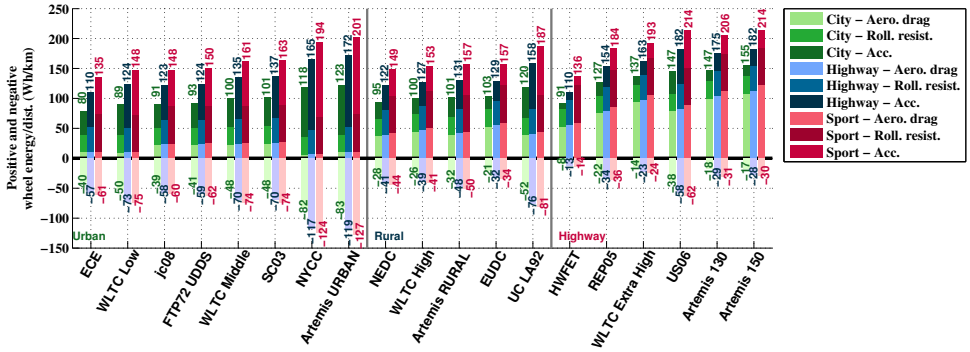

Figure 4.21 Positive and negative wheel energy per driven distance during Urban, Rural and Highway Test cycles, for all of the three concept cars, while acceleration is calculated using the described forward-backward method.

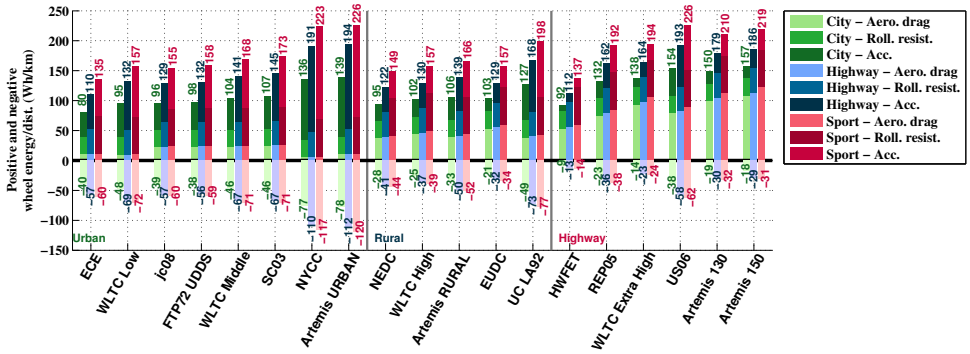

Figure 4.22 Positive and negative wheel energy per driven distance during Urban, Rural and Highway Test cycles, for all of the three concept cars, while acceleration is calculated using the Euler backward method.

In Figure 4.23, the positive and negative values of wheel energy consumption per driven distance as a function of average running speed, is plotted for all test cycles and all three of the Concept cars, along with calculated wheel energy per driven distance while driving at different constant speed levels only considering aerodynamic and rolling resistance. As can be seen, the energy per distance increases with increasing average speed. For those cycles with lower levels of average speed the acceleration relative contribution of the consumption is larger, however so is the possibility of regeneration, which reduces the influence of acceleration on the energy consumption.

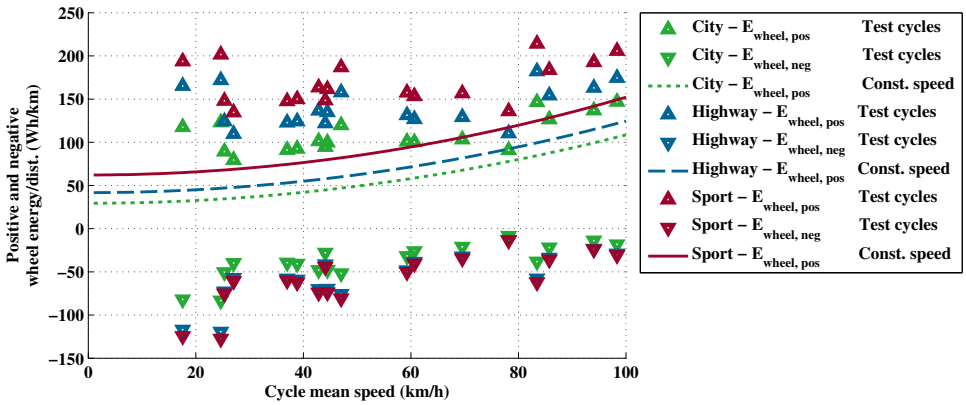

Figure 4.23 Wheel energy per driven distance during Urban, Rural and Highway Test cycles, for all the three concept cars; City-green, Highway-blue and Sport-Red.

In order to get an indication of the relative energy consumption that road grade causes for the different cycles, the potential energy increase or decrease between the end and the starting altitude level is divided by the total driven distance, and is presented in Figure 4.24. Even though there is a large altitude difference (143 and 149 m) for the two cycles V70 120510 CTH-Jnkpng and V70 120515 Jnkpng-CTH (as seen in3.20), the driven distance is also quite long. Hence it is likely that the relative energy consumption due to road grade is fairly small. In practice the energy consumption due to road grade will naturally be larger than these values, due to the looses in the powertrain.

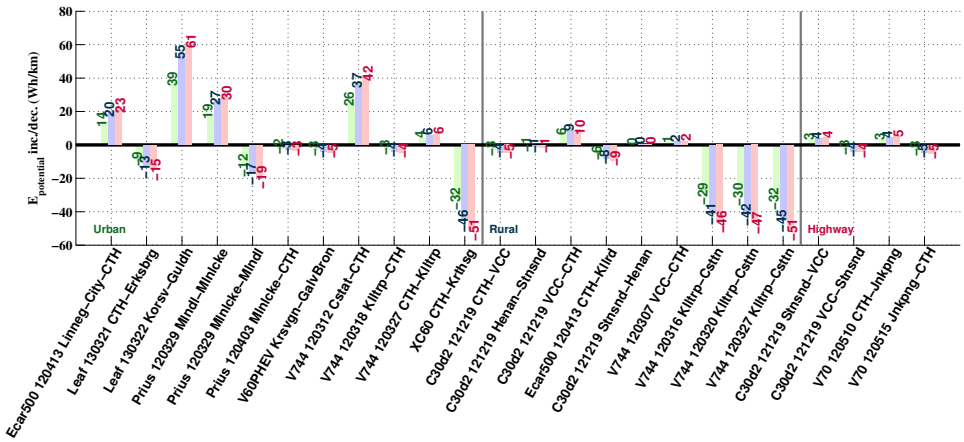

Figure 4.24 Change in potential energy between end point and starting point of the Logged cycles per driven distance, for all the three concept cars; City-green (left), Highway-blue (middle) and Sport-Red (right).

4.3.2.2 Wheel energy per distance per logged cycle, for the concept BEVs

The wheel energy consumption per driven distance for the logged cycles can be seen in Figure 4.25. In these cycles, energy consumption referred to acceleration is the major source in both Urban and Rural cycles, although the consumption due to acceleration and to grade can not be separated, thus both are included in these figures. Furthermore, no clear conclusion regarding the comparison of absolute levels between the different types of cycles can be drawn. The spread within the Urban cycles is quite large.

For comparison the energy consumption as a function of running average speed is also presented for the logged cycles in Figure 4.26, showing a rather similar result.

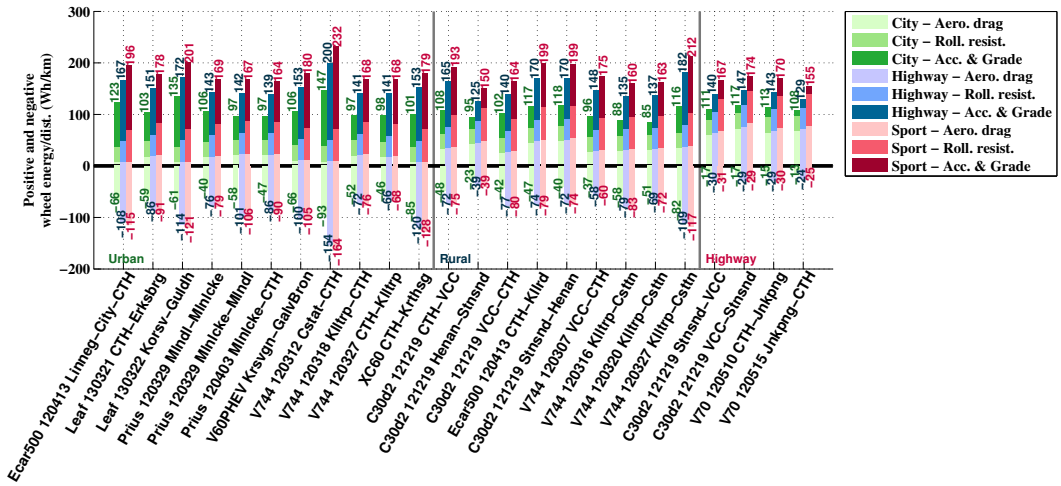

Figure 4.25 Positive and negative wheel energy per driven distance during Urban, Rural and Highway Logged cycles, for all of the three concept cars.

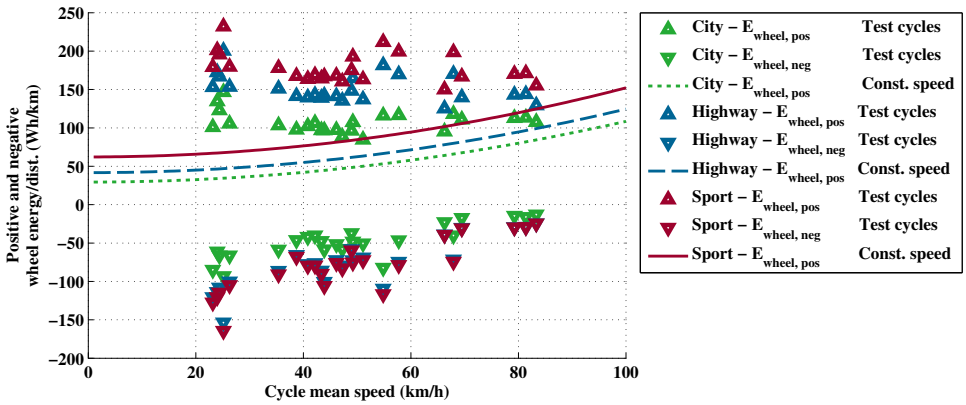

Figure 4.26 Wheel energy per driven distance during Urban, Rural and Highway Logged cycles, for all the three concept cars; City-green, Highway-blue and Sport-Red.

4.3.2.3 Existing BEVs

The certified test results of energy per driven distance while driving according to the NEDC cycle for 16 of the existing BEVs can be seen in Figure 4.27. Note that the values correspond to powertrain energy consumption, rather than wheel energy which was so far studied for the concept cars. One trend that can be noticed is a smaller energy consumption for the Small cars (marked green) compared to the Medium to Large cars (marked blue). Interestingly, the two sport cars are very far apart, with one that is quite efficient and another that is rather inefficient.

If an average powertrain efficiency of $70\,\%$ is assumed during both propulsion and braking, and all available braking energy is possible to be recuperated, then the NEDC energy consumption for each of the concept cars would be; 116, 146 and $182\,Wh/km$ for the City, Highway and Sport car respectively. These levels are similar to what can be seen for the existing BEVs.

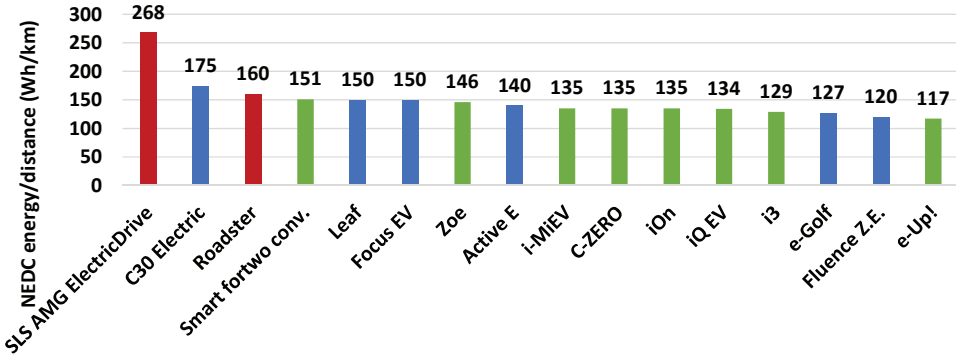

Figure 4.27 Energy per distance during NEDC for commercial BEVs.

In Figure 4.28 the energy consumption per distance is normalized per $100\,kg$ of vehicle mass. Then it seems like smaller cars and the sport cars are those that are the least efficient per mass for the NEDC cycle.

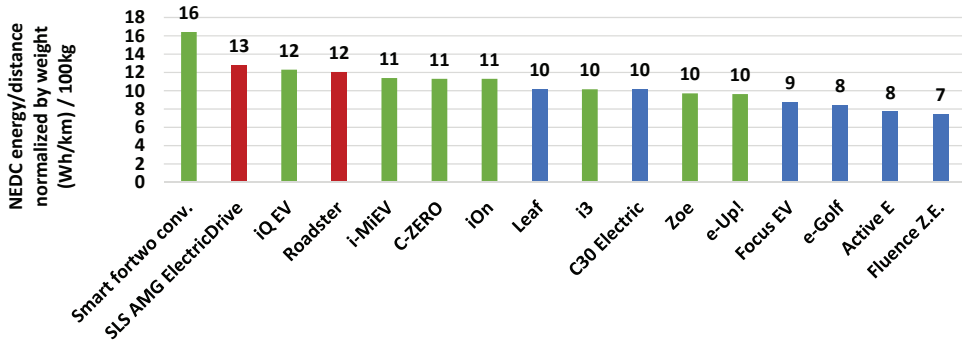

Figure 4.28 Energy per distance normalized by curb weight, during NEDC for commercial BEVs.

4.3.3 Cumulative braking energy per braking power level

In Figure 4.29 cumulative braking energy as a function of cycle speed, for all three cars and all test cycles, is depicted (there is no difference between the different cars). For the Urban cycles, $20\,\%$ of the braking energy is available at speeds up to $20\,km/h$ as lowest and $60\,km/h$ as highest. Thus, a relatively small part of the braking energy is related to low speed levels. However, for those cycles with relatively low top speed (e.g. the Urban cycles) a greater part of the braking energy is related to low speed, while it is the opposite for those cycles with long durations at high speed levels.

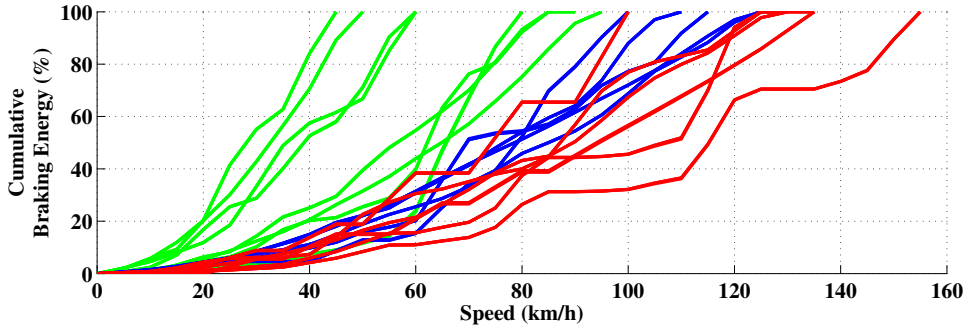

Figure 4.29 Cumulative braking energy per reach speed level, for all three concept cars, and all Test Cycles, where green, blue, red represent Urban, Rural and Highway respectively.

Similarly, in Figure 4.30 cumulative braking energy as a function of braking power, for all three cars and all test cycles, is depicted. In this case the levels of braking power differs between the cars. This type of information is interesting, when deciding how large part of the braking should be done by the electric machine respective the friction brakes in a BEV.

In order to capture all of the braking energy from the Urban cycles in the City car, $30\,kW$ of power in the generator mode is needed, while it is $41\,kW$ and $47\,kW$ for the Highway and Sport car respectively. Similarly, for the Rural cycles, $64\,kW$, $92\,kW$ and $101\,kW$ is needed for the City, Highway and Sport car respectively. Finally for the Highway cycles, the levels are $76\,kW$, $108\,kW$ and $120\,kW$. The higher the power levels the larger the spread within the same type of cycle category.

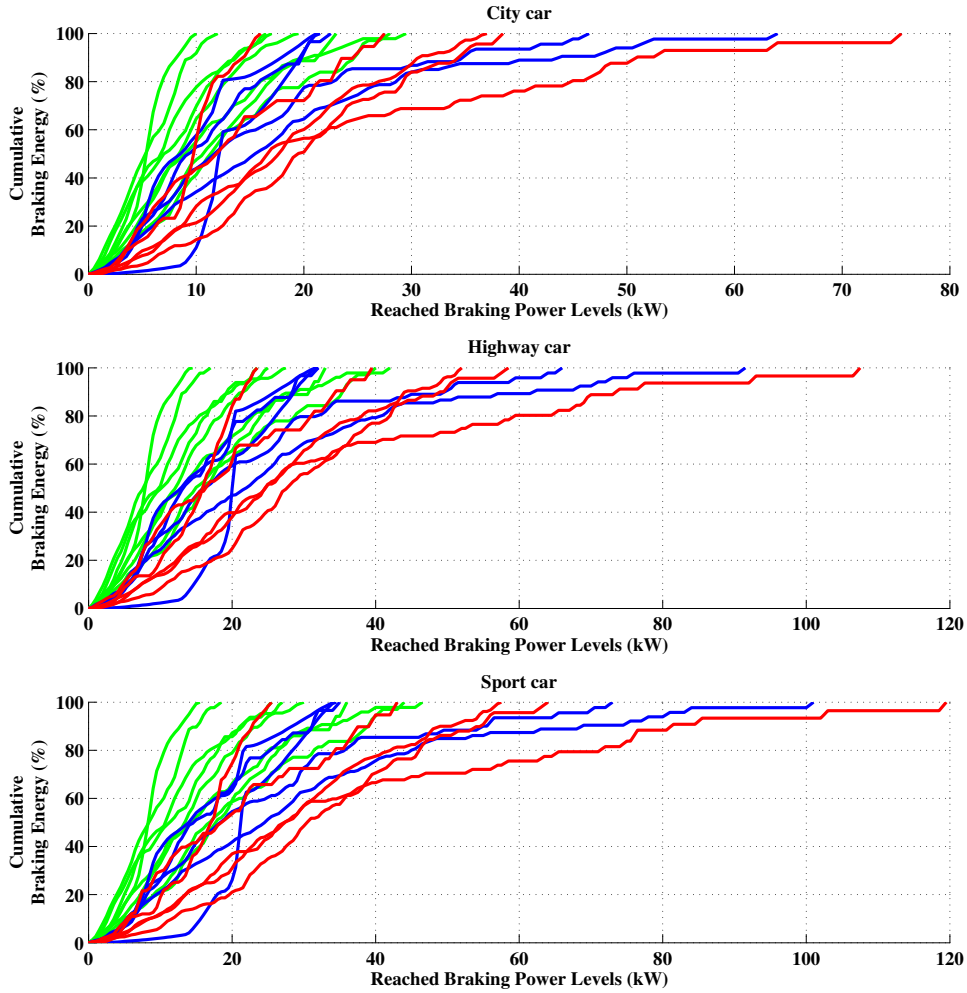

Figure 4.30 Cumulative braking energy per reached braking power level, for all three concept cars, and all Test cycles, where green, blue, red represent Urban, Rural and Highway respectively.

Chapter 5

Powertrain component sizing, modeling and vehicle simulation

As was found in Chapter 4, the demanded maximum torque and power from the powertrain can be solely determined by the acceleration requirement for all of the three concept cars. Furthermore, it was found that the acceleration requirements could be satisfied with more than one combination of maximum wheel force and power. This means that the output requirement of the powertrain has some degree of freedom to it. Therefore the final choice will to a large part depend on the characteristics of the chosen components to be used.

In this chapter each of the concept cars will be assigned a base-line powertrain set-up, including sizing of, and models for; the electric machine, converter, battery and transmission.

For simplicity auxiliary loads are excluded from the study, however they are likely to have an important impact on BEV energy consumption, especially in particulary warm and cold conditions.

Furthermore it is decided that the acceleration requirement should be achieved at a $10\,\%$ SOC level, and that the torque and power at higher SOC levels will not be functions of the available DC voltage. This means that the powertrain will be slightly oversized at higher SOC levels.

5.1 Components used for modeling

The analysis is based on the powertrain components described in this section; electric machine, battery and converters. The aim is to use components which are considered to represent typical characteristics for this type of application, rather than state-of-the-art components.

5.1.1 Converter

As can be seen in Appendix A, most commercial BEVs have DC voltage levels of around $300 - 400\,V$. The only exceptions are the sport cars where the voltage levels are higher. Hence an IGBT module with a voltage rating around $650\,V$ is well suited, since then there is a margin for increasing battery voltage during braking, but also to handle other phenomena occurring during operation such as induced voltage peaks during converter switchings caused by stray inductances. Furthermore, it is assumed that the maximum converter RMS phase current $I_{RMS,max}$ can be as high as 2/3 of the current rating in the data sheet. Converter models from Infinieon found at [71] with different current rating are used for all three cars.

5.1.2 Battery cell

The battery cell used is a Lithium-ion (cathode: $LiNiO_2$ cathode active: $LiMn_2O_4$, anode: graphite) cell of laminate type, manufactured by the Japanese company *Automotive Energy Supply Corporation* (AESC), where Nissan Motor Co. is a majority owner [72]. Their batteries have also been used in the Nissan Leaf BEV models (96 in seies and 2 in parallel). The *US Idaho National Laboratory* (INL) under the *US Department of Energy* (US DOE) have published measured data on the Nissan Leaf battery pack, including terminal voltage during a full discharge at a C/3 discharge rate, as well as the internal charge and discharge resistances as a function of energy, in [73]. Based on the published data, the cell open circuit voltage, V_{oc} has been estimated by approximating the resistive voltage drop during a C/3 discharge rate, see Figure 5.1. The figure also includes assumed maximum and minimum voltages, as well as denoted voltage levels at 10 and $90\,\%$ SOC. The average open cirquit cell voltage within the used SOC window (10 to $90\,\%$) has been estimated to $3.88\,V$, which is slightly higher than the stated nominal voltage by the manufacturer; $3.75\,V$. The mean values of the charge and discharge resistances within 10 to $90\,\%$ SOC are also presented in the figure. The average cell charge capacity is assumed to be $28.8\,Ah$, [73], which can be compared to the manufacturer value of $32.5\,Ah$.

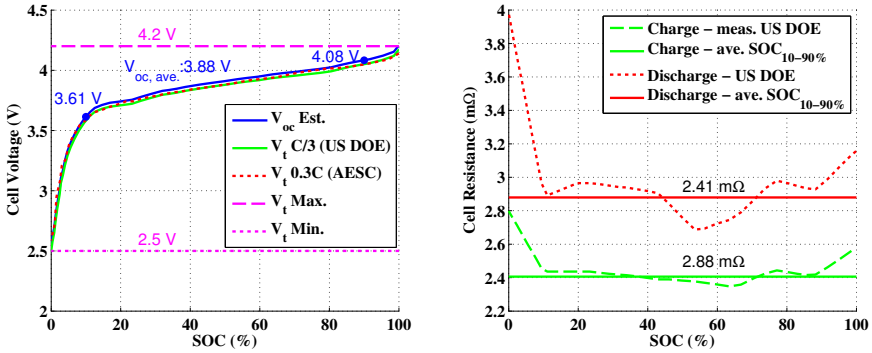

Figure 5.1 Estimated AESC battery cell no load voltage as a function of SOC, and estimated average values of cell resistances, based on data from [US DOE, AESC].

5.1.3 Electric machine

The base for the electric machine used here, is a machine that was designed and built at the division of Electric Power Engineering at Chalmers in the end of the 1990's, and is described in [74] and [75]. It is a four pole PMSM with inset magnets, designed for a series HEV application, with water cooling. Machine voltage and current ratings ([74] and [75]) along with measured machine parameters ([26]) can be seen in Table 5.1.

Table 5.1 PMSM data.

$U_{RMS,max,L-L}$:	220 V
$I_{RMS,max}$: 3 $min.$	315 A
R_s :	7.9 mΩ
L_d :	230 mH
L_q : ($i_q = 1pu$)	420 mH
Ψ_m :	104 mWb
Stator outer diameter:	189 mm
Stator inner diameter:	110 mm
Stator core length:	231 mm
Slot fill factor:	0.45
Conductors per slot:	3
Conductors in parallel:	2

Given the stated peak RMS current (which was a $3\,min.$ value) and winding structure, the maximum current density can be found to be about $12\,A/mm^2$ (with a slot fill factor of about 0.45, three turns per slot and two parallel windings the conductor area is $13.47\,mm^2$). According to [24], a liquid cooled brushless machine can have a current density between 10 to $30\,mm^2$. It is here chosen to increase the machine current density to $20\,A/mm^2$, which leads to a max RMS current of about $540\,A$.

As was done in [26] and [76], the core losses are estimated using the added core resistance R_c described in Chapter 2. The core loss resistance as a function of speed is estimated based on measured no load losses over the machine speed range, presented in [75] (paper E), as

$$R_c \approx \frac{3}{2}\frac{(w_r\,\psi)^2}{P_{fe}} \tag{5.1}$$

For each operating point, the machine core losses are then calculated as ([76])

$$P_{fe} = \frac{3}{2}\,R_c(i_{d,o} - i_d)^2 + (i_{q,o} - i_q)^2); \tag{5.2}$$

The efficiency and total losses of the originally sized electric machine (i.e. with unity scaling factors) can be seen in Figure 5.2, as well as maximum torque over speed using the MTPA control strategy as described in [76].

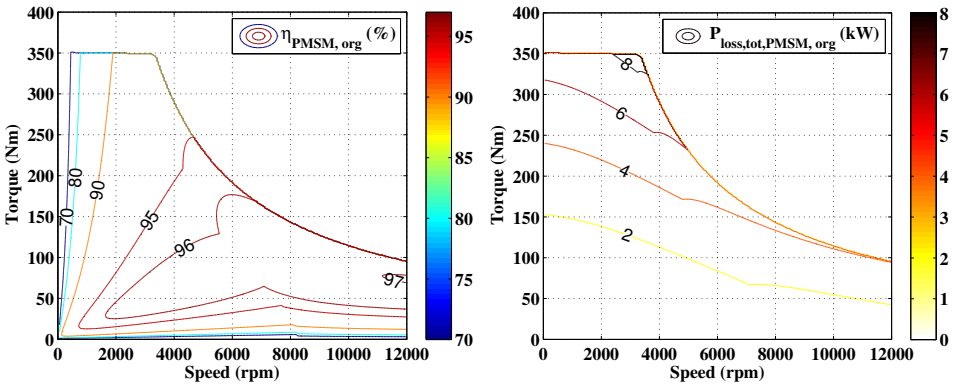

(a) Efficiency (%). (b) Losses (kW).

Figure 5.2 Efficiency and total power losses for the electric machine with the original size, i.e. unity scaling factors.

5.1.3.1 PMSM active length scaling

During production of electric machines, the iron core laminations are often stamped from core plates [24]. Since the lamination design and stamp tool is rather expensive to develop, electric machine manufacturers often offer different machine sizes that are based on the same stamped laminations, but of different stack lengths. According to [24], the stack length-to-diameter ratio is typically 1 to 3, but it can also be higher. For low length/diameter ratios, the losses in the end windings will become more dominant, and the torque production will be limited since only the stator and rotor package lenth contributes.

In order to achieve a desired output torque and power, the original machine is here scaled by changing the active length. As the flux increases with increasing length, all machine

parameters (the active parts of the stator resistance and inductance) are expected to increase linearly with the length, except the current rating. Also the no load losses used for R_c estimation are scaled accordingly.

The winding resistance thus needs to be divided into one active part and one that represents the winding overhang. According to [75] paper D p.92, the average conductor length of a half turn, l_{av} can be expressed as

$$l_{av} = l_{Fe} + 1.2\tau_p + l' \tag{5.3}$$

where l_{Fe} is the active length i.e. equal to the stack length, τ_p is the pole pitch and l' is the estimated axially directed part of the end winding. The stack length is $231\,mm$, the pole pitch is $\frac{\pi\,D}{2\,p}$, where D is the stator inner diameter ($110\,mm$) and p is the pole pair number (two pole pairs), and finally the l' is assumed to be $0.05\,m$ as in [75]. This gives a total average conductor length of $384.7\,mm$, where the active part is $231\,mm$ or $60\,\%$ and the over hang is $153.7\,mm$ or $40\,\%$, ([75] paper D p.80). The end winding inductance is assumed to be very small, hence neglected, although as mentioned in [77] it may not be a viable assumption for motors with a low length/diameter ratio.

The length scaling is implemented using the stack length scaling factor, SF_{Lstk}.

5.1.3.2 PMSM rewinding scaling

As described in [25], the machine voltage rating is assumed to be relatively freely adaptable through rewinding of the machine, such that the maximum torque, speed and power remain the same, as well as the losses and hence the efficiency. For simplicity, non-integer winding turns are here allowed.

Then the total stator resistance and both inductances are scaled using the square of the rewinding scaling factor, SF_{rw}, while the magnet flux and applied voltage is linearly scaled, and finally the current is inversely scaled with SF_{rw}.

5.2 Components sizing process

The sizing and modeling process for the City car can be seen in Figure 5.3, and for the Highway and Sport cars in Figure 5.4. As can be seen, two slightly different approaches are utilized, where some steps are independent while others build on previous steps. Each step will be further described in the following sections.

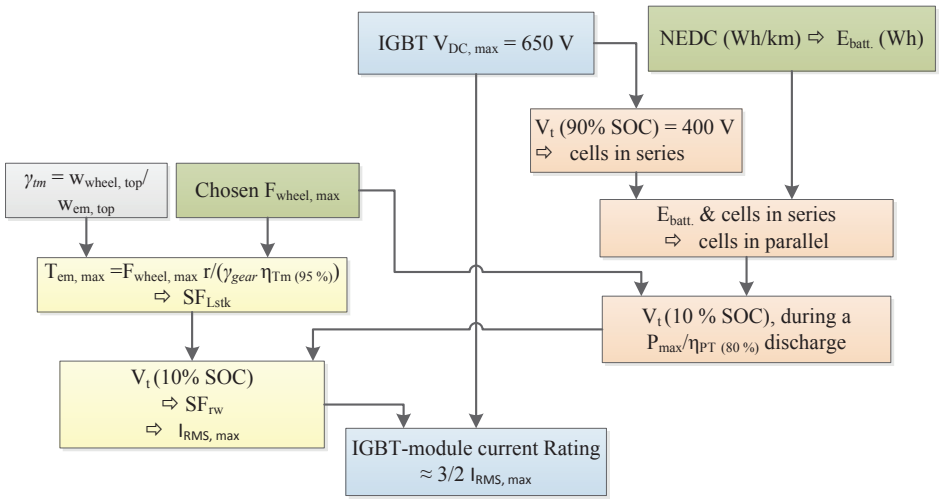

Figure 5.3 BEV powertrain sizing and modeling algorithm for the City car.

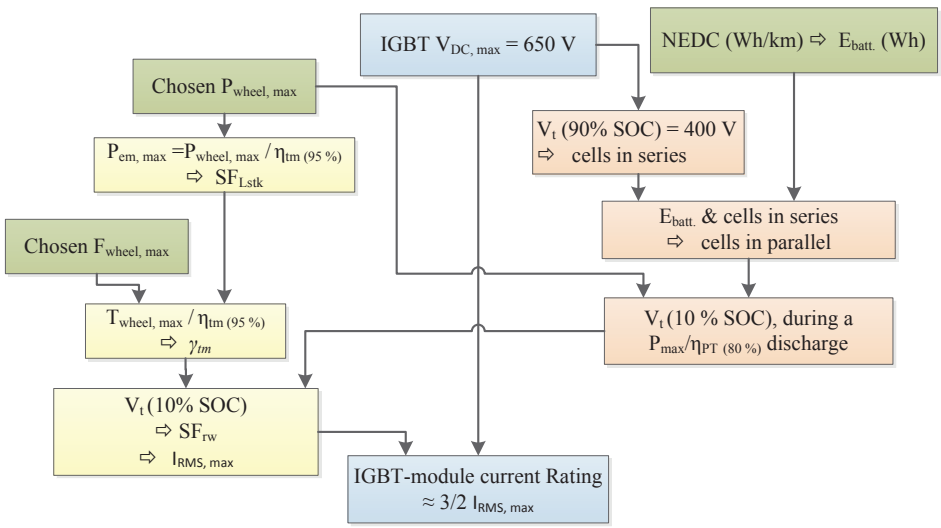

Figure 5.4 BEV powertrain sizing and modeling algorithm for the Highway and Sport cars.

5.3 Implemented battery models

The battery energy content for each car is calculated based on the respective desired NEDC driving range from Table 4.2 and the calculated wheel energy consumption for the NEDC

cycle presented in Figure 4.21. It is assumed that all of the available braking energy is recuperated. Additionally, an average powertrain efficiency of $80\,\%$ is assumed, as well as a usable SOC-window of $80\,\%$ (from 10 to $90\,\%$ SOC).

In order to have a good margin to the power electronic component breakdown voltage of $650\,V$, it is chosen that the Open Circuit voltage, V_{oc}, at $90\,\%$ SOC, should be $400\,V$. Given the assumed average AESC battery cell voltage of $4.08\,V$ at $90\,\%$ SOC, the number of needed series connected cells is 98.04, which gives a nominal voltage of $380.4\,V$. The same voltage level is used for all cars, hence the same number of series connected cells are implemented.

The number of cells in parallel can be found in two steps, where the first is to estimate the demanded pack charge capacity as the resulting ratio between the desired energy capacity relative to the pack nominal voltage. In the second step the pack charge capacity is related to the assumed cell capacity.

A summary of the parameters of the implemented batteries in all three cars can be seen in Table 5.2. The assumed pack charge resistance are taken as scaled values of the average cell charge and discharge resistances, within the chosen SOC-window.

Table 5.2 Summary of battery data for all three cars.

	City	**Highway**	**Sport**
NEDC range:	160 km	200 km	300 km
Energy:	19.3 kWh	29.9 kWh	56.6 kWh
Series cells:	98.04	98.04	98.04
Parallel cells:	1.76	2.73	5.17
V_t at $90\,\%$ SOC, $P_{EM,max}$	325 V	317 V	283 V
R_{dis}	160.4 $m\Omega$	103.4 $m\Omega$	54.6 $m\Omega$
R_{ch}	134 $m\Omega$	86.4 $m\Omega$	45.6 $m\Omega$

The calculated energy content is fairly close to official values for existing BEVs of similar driving range, as seen in Figure 5.5.

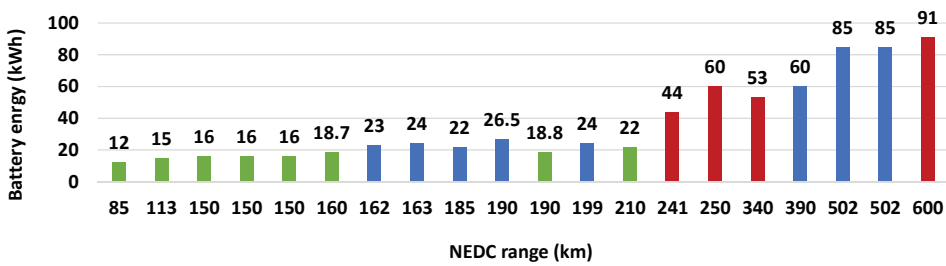

Figure 5.5 NEDC range and battery energy for existing BEVs.

The battery open circuit voltage as a function of SOC is modeled according to the left part of Figure 5.6(a), 5.6(b) and 5.6(c), which also includes the assumed maximum and

minimum voltage levels. Furthermore, the estimated voltage drops during constant current discharges at $3C$ and $5C$ are presented, as well as the voltage drop during a full constant power discharge of full electric machine power at $10\,\%$ SOC. For the City car this power is close to a $3C$ current rating

In the right part of Figure 5.6(a), maximum charge and discharge power limits, according to the three types (2.27), (2.28), (2.29) in Chapter 2 are presented for the City car. The theoretical and the voltage limited discharge power limits are rather similar, while the current limited discharge power limits are substantially lower. Also a constant discharge power of $58\,kW$ is depicted, and shows to be just a bit larger than the 3C limit. During charging, only the voltage limited charge power is presented. It shows a stronger dependence on SOC level compared to the discharge power. Similar characteristics are valid for the Highway and Sport cars as well, although not shown here.

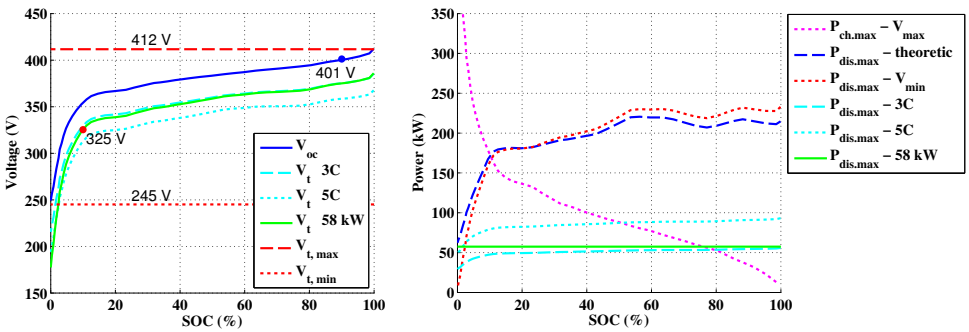

(a) City car.

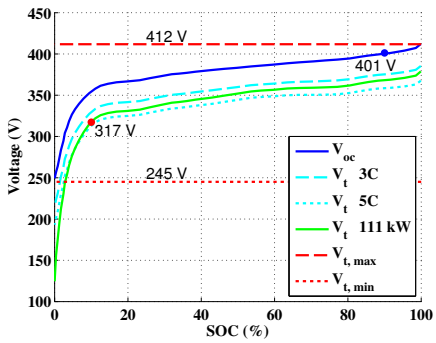

(b) Highway car.

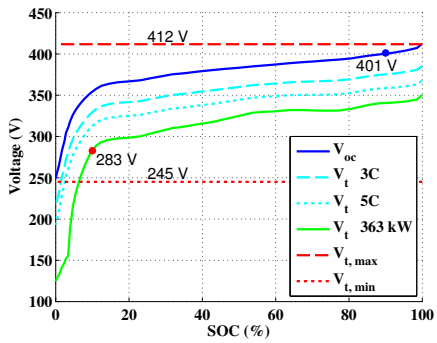

(c) Sport car.

Figure 5.6 No load voltage as a function of SOC-level, maximum and minimum terminal voltage, terminal voltage during constant current during 3 and $5C$ discharge rates, as well as terminal voltage during a constant electric machine maximum power discharge. In the right part of figure a for the City car; maximum charge and discharge power related to maximum voltage see (2.28), theoretical (2.27), current limited at 3 and $5C$ see (2.29), and finally for the electric machine maximum power.

5.4 Implemented EM models including transmissions

For the City car it is decided that the total transmission ratio should be based on the direct relationship between the vehicle and machine top speed, as the base speed then is fairly close to the desired one from Figure 4.13, as well as the power level. The wheel radius, the gear ratio γ_{tm} and the desired maximum wheel force (compensated for a transmission efficiency of $95\,\%$) are then used as inputs when finding a suitable length scaling factor. Then a value for the rewinding scaling factor is found such that the DC voltage level is matching the estimated DC voltage level during a full power discharge at SOC level of $10\,\%$. Finally, the resulting maximum RMS phase current, $I_{RMS,max}$ is noted and used as a base for choosing the converter current rating, $I_{c,nom}$. It is assumed that a reasonable current margin is achieved when $I_{c,nom} \approx 3/2\, I_{RMS,max}$.

For the Highway and Sport cars, the transmission ratio is not initially decided. Instead the stack length is scaled until the desired output wheel power is reached. In order to realize the AWD functionality in the Sport car, it is decided that two equally sized electric motors shall work in parallel; one on the rear drive axle, and one on the front. This implementation will also help keeping the length scaling down. Then the transmission ratio is decided as the ratio for which the desired wheel force is achieved (while considering the assumed transmission efficiency). Finally the rewinding scaling factor and resulting maximum RMS phase current is found in the same manner as for the City car, as well as the converter current rating.

The implemented electric machine torque and power levels as well as scaling factors and transmission ratios can be seen in Table 5.3. The transmission ratio,γ_{tm} is defined as in

$$\omega_{em} = \gamma_{tm}\, \omega_{wheel} \tag{5.4}$$

where ω_{em} is the electric machine angular speed (rad/s), ω_{wheel} is the angular speed of the wheel(rad/s).

Table 5.3 Summary of electric machine and transmission data for all three cars, along with vehicle power-to-weight ratio.

	City	**Highway**	**Sport**
γ_{tm}	10.3882	7.62	6.22
P_{max}	49 kW	97 kW	153
T_{max}	140 Nm	280 Nm	420 Nm
$F_{wheel,max}$	4750 N	6600 N	7700 N
$U_{RMS,max,L-L}$:	207 V	202 V	180 V
$I_{RMS,ph,max}$	233 A	468 A	786 A
SF_{Lstk}:	0.405	0.795	1.1925
$\frac{L_{stk}}{D_{outer}}$	0.495	0.972	1.458
SF_{rw}:	2.32	1.154	0.687
eta_{max} at 350 V:	96.2 %	96.9 %	97.0 %
Vehicle Power-to-weight ratio	41 W/kg	57 W/kg	153 W/kg

The resulting output torque and power as function of speed for all cars, can be seen in Figure 5.7, and the resulting wheel forces can be seen in Figure 5.8.

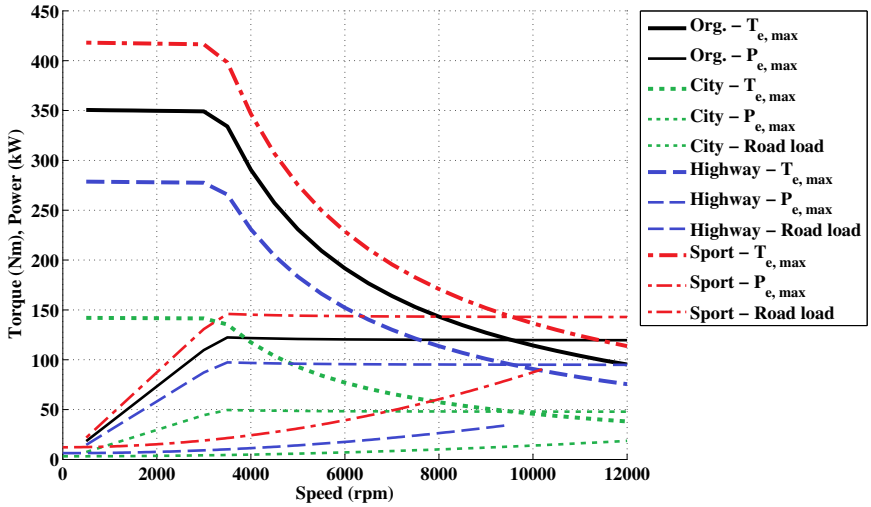

Figure 5.7 Maximum torque and power as a function of speed for the original electric machine as well as all of the concept cars's scaled machines, where the torque and power curves adhere to a DC voltage level during a full power discharge, at 10 % SOC.

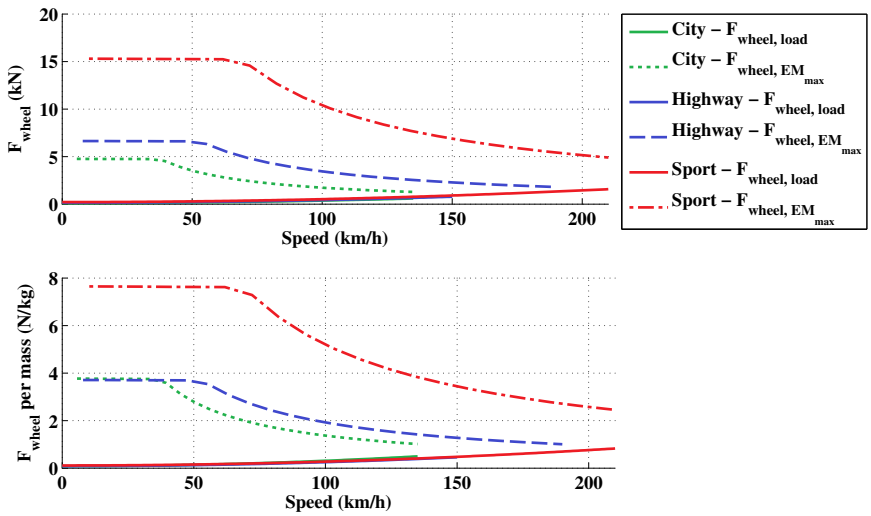

Figure 5.8 Maximum wheel force and power as a function of car speed from the electric machine at a DC voltage level during a full power discharge, at 10 % SOC.

The implemented electric machine total losses (including conduction losses as in (2.14),

and core losses as describes above), and associated energy efficiency at two different voltage levels and for all three machines, can be seen in Figure 5.9 and 5.10 for the City and Sport cars, while the characteristics of the Highway machine car lies in between. The losses increase mainly with increasing torque, and somewhat with speed. As can be seen, for each car's machine, the losses and efficiency are exactly the same up to the case of field weakening, where the losses are slightly decreased at lower voltage levels, hence the efficiency is somewhat increased. This means that the average electric machine efficiency during a drive cycle simulation will only vary depending on SOC, if any operating point is outside of the area with similar efficiency.

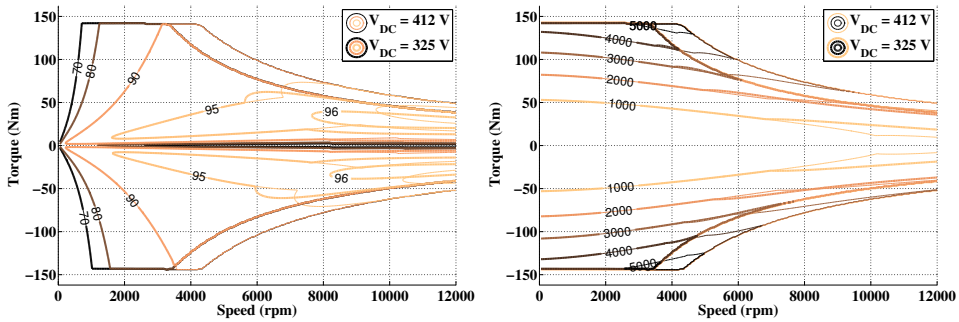

(a) Efficiency (%). (b) Losses (W).

Figure 5.9 Implemented electric machine efficiency and power loss maps, for the City car.

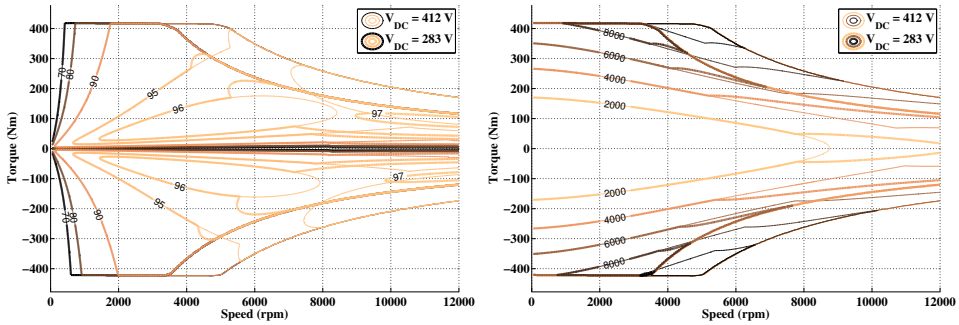

(a) Efficiency (%). (b) Losses (W).

Figure 5.10 Implemented electric machine efficiency and power loss maps, for the Sport car.

In Figure 5.11, the total powertrain efficiencies (excluding batteries) as a function of mass normalized wheel force and car speed, can be seen. For the same level of speed and acceleration, it shows that the City car powertrain is a bit more efficient compared to the Highway and sport cars's.

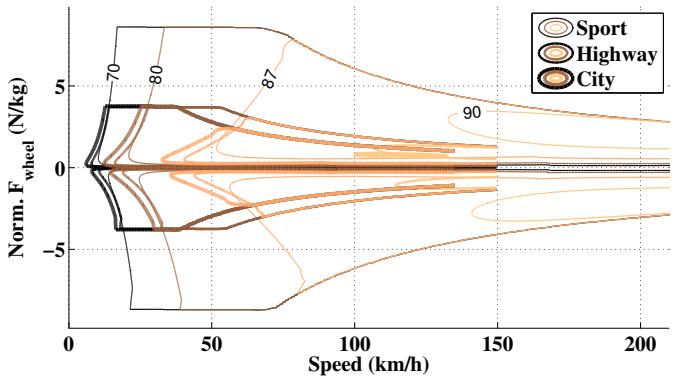

Figure 5.11 Total power train efficiency, including electric machine, converter and transmission, for the three concept cars, as a function of speed and normalized wheel force.

5.5 Implemented converter model

For the City car a converter module with current rating of $400\ A$ (Infineon FS400R07A1E3_H5) is chosen, even though the rating might be a bit too low. For the Highway car a module with current rating of $800\ A$ (Infineon FS800R07A2E3) is implemented. Finally for the Sport car; four modules are used, two in parallel for each of the two machines, where the module current rating is $600\ A$ (Infineon FS600R07A2E3). That will give a total converter current rating of $2.4\ kA$, which is assumed to be able to withstand an RMS current of $1.6\ kA$, hence it is viable for the chosen machine size.

The extracted IGBT module parameters can be seen in Table 5.4, and adhere to chip temperatures of $125\ ^{\circ}\mathrm{C}$ and a gate voltage of $15\ V$. The on-state threshold voltage and resistance parameters are estimated under consideration of expected current levels. The switching frequency is set to $10\ kHz$.

Table 5.4 IGBT module parameters, for all three cars, where the data for the Sport car represent all four modules.

	City car:		**Highway car:**		**Sport car:**	
	IGBT	**Diode**	**IGBT**	**Diode**	**IGBT**	**Diode**
$I_{c,nom}$	400 A		800 A		4*600 A	
I_{ref}:	400 A		550 A		4*400 A	
V_{ref}:	300 V		300 V		300 V	
On-state threshold voltage:	$0.709\ V$	$0.803\ V$	$0.673\ V$	$0.761\ V$	$0.66\ V$	$0.775\ V$
On-state resistance:	$2.468\ m\Omega$	$1.999\ m\Omega$	$1.336\ m\Omega$	$1.12\ m\Omega$	$0.441\ m\Omega$	$0.352\ m\Omega$
Turn-on Energy loss:	$4.2\ mJ$	-	$12\ mJ$	-	$44\ mJ$	-
Turn-off Energy loss:	$16.0\ mJ$	$7.25\ mJ$	$25\ mJ$	$9.5\ mJ$	$68\ mJ$	$28\ mJ$

The total power losses are estimated using (2.20) to (2.23), and can be seen together with energy efficiency in Figure 5.12 for the City car and in Figure 5.13 for the Sport car,

in the machine torque and speed frame of reference, while the results for the Highway converter lies in between. The converter losses mainly increase with increasing torque, while the efficiency has a strong speed dependency and increases with increasing speed. Unlike the electric machine, the converter losses vary somewhat depending on the DC voltage level in the whole operating range. The efficiency is mostly higher at lower voltage levels in the same torque and speed operating point, due to lower switching losses.

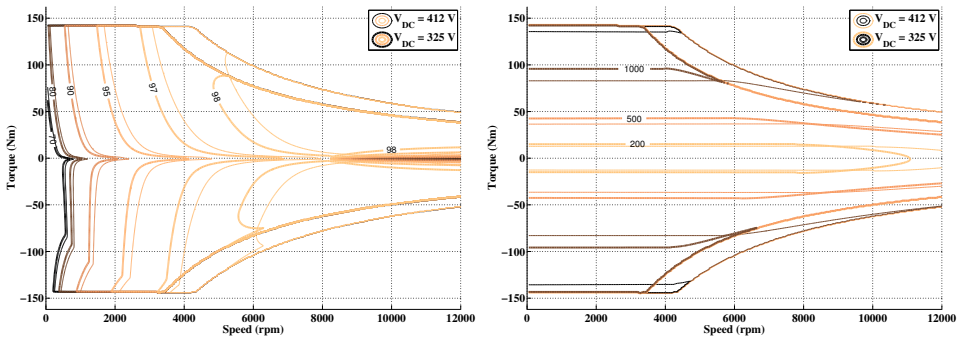

(a) Efficiency (%). (b) Losses (W).

Figure 5.12 Implemented converter efficiency and power loss maps at three DC voltage levels, for the City car.

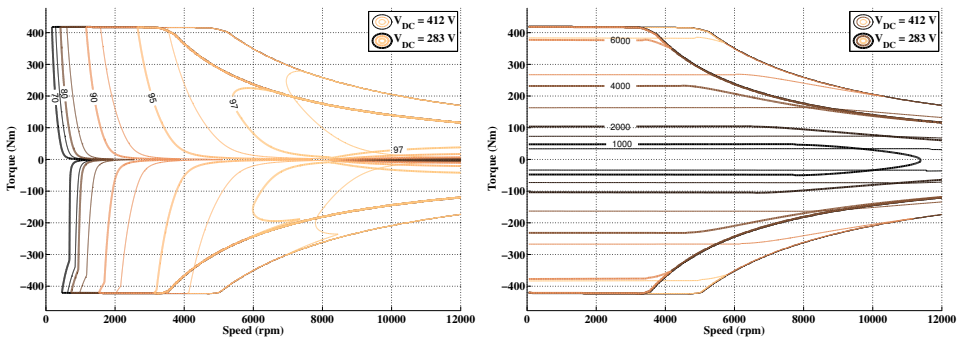

(a) Efficiency (%). (b) Losses (W).

Figure 5.13 Implemented converter efficiency and power loss maps at three DC voltage levels, for the Sport car.

5.6 Simulator structure

The input to all simulations (conducted in Matlab Simulink) are the reference speed cycles as functions of time. The time resolution of the Test cycles are all 1 Hz, while it is 20 Hz

for the Logged cycles. All simulations are executed with a fixed time step of $0.01\,s$, which proved to provide reasonable stability. For the logged cycles, also the estimated road grade levels as a function of time is an input to the simulations.

In order to allow deviation from the speed reference a PI driver model is implemented. Its input is the difference between the reference speed and the simulated speed. The proportional K_p and integral K_i gains are chosen such that the reference speed and associated acceleration are followed fairly close by the simulation output (where $K_p = K_i = 3$). The output of the driver model is a signal between -1 to 1.

The positive output from the driver model is regarded as an acceleration pedal signal and the negative part as a brake pedal signal. These signals are then scaled by the maximum torque from the electric machine in motoring and generating mode, which are implemented through look-up tables as functions of machine speed and DC-link voltage. Thus it gives the electric machine torque reference signals, via linear interpolation. It is then assumed that the electric machine can fulfill the torque reference. No wheel slip is assumed, hence the electric machine speed is simply found via the simulated vehicle speed, the wheel radius and the transmission ratio.

At each time step the sum of the resistive forces on the wheel (the vehicle's aerodynamic drag, rolling resistance and possibly also grading force) is converted to a total resistive wheel torque. Given the total resistive torque together with the wheel torque from the electric machine via the transmission, and the vehicles estimated mass inertia, (as the product of the vehicle mass and the square of the wheel radius, while ignoring additional rotating inertias), the resulting vehicle acceleration is calculated (as the rotational form of (2.1)). Furthermore, the simulated speed is then calculated as the time integral of the resulting acceleration.

Both the electric machine and converter power losses are implemented trough look-up tables that are functions of machine torque and speed, as well as DC-link voltage, where the output is found through linear interpolation. The power flow between electric machine and converter is calculated as the added or subtracted losses to the mechanical machine output, depending on mode of operation. Likewise is the DC-link power flow calculated via the additional converter losses. The DC-link power flow is then the input to the battery model, where the current is found from division of the power with the terminal voltage from the previous time step. The current is then used to estimate the SOC level, (as in (2.26)) as well as battery conduction losses together with the discharge and charge internal resistances. Finally, the terminal voltage is found as the subtracted resistive voltage drop from the SOC dependent open circuit voltage.

Next follows results from the simulations in terms of requirement and drive cycle fulfillment as well as powertrain and energy consumption for the different drive cycles.

5.7 Simulated time to accelerate $0 - 100\,km/h$

The simulation result from the $0 - 100\,km/h$ acceleration test can be seen in Figure 5.14 to 5.16, for the three cars respectively, where the ideal calculations for similar values of

the initial maximum force and power, are also presented as a reference. Note that the ideal calculations for the City car is here adjusted to comply with the implemented size of the electric machine. The tests have been conducted for both $10\,\%$ and $90\,\%$ SOC levels, which gave different results as expected.

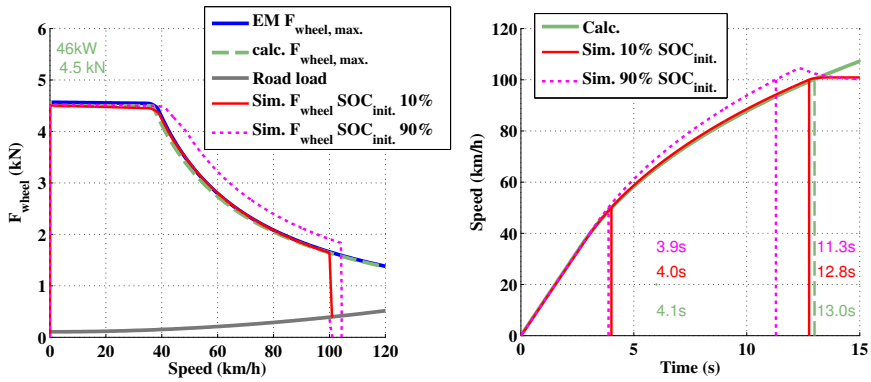

Figure 5.14 Comparison of acceleration test from $0-100\,km/h$, between calculation and simulation, as well as maximum force on wheels from the electric machine, for the City car.

For the City car, the time to accelerate from $0-100\,km/h$ by simulation was $12.8\,s$, at a battery SOC level of $10\,\%$ see Figure 5.14. This is about $1.5\,\%$ faster than the acceleration requirement for the city car, which was $13\,s$. As can be seen in the figure, above base speed the simulated wheel force is somewhat larger than the ideally calculated force, hence the acceleration will be faster. The simulated wheel force is even larger at the 90% SOC level, resulting in an acceleration time of $11.3\,s$, i.e. $7.8\,\%$ shorter then at $10\,\%$ SOC. The simulated acceleration time to $50\,km/h$ is $4\,s$ at $10\,\%$ SOC and only slightly smaller at the 90% SOC level, $3.9\,s$.

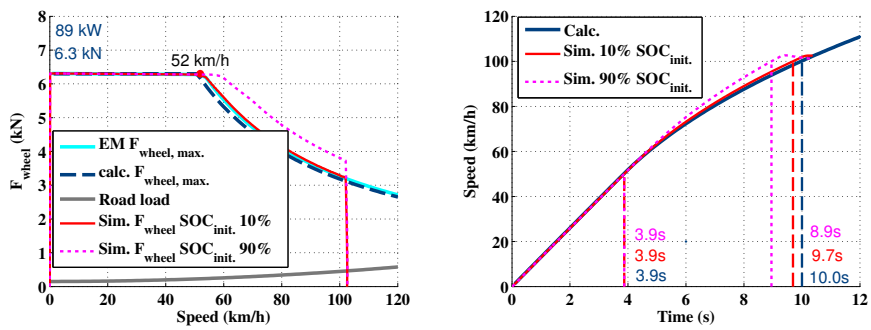

Figure 5.15 Comparison of acceleration test from $0-100\,km/h$, between calculation and simulation, as well as maximum force on wheels from the electric machine, for the Highway car.

Also the Highway car has a slightly shorter acceleration time to $100\,km/h$ compared to

the ideal calculation; $9.7\,s$, which is $3\,\%$ faster. The difference between the two SOC levels is even larger than for the City car, where the time for the 90% SOC level is $8.9\,s$ which is $8.2\,\%$ faster than at $10\,\%$ SOC. The time to $50\,km/h$ is the same for all cases.

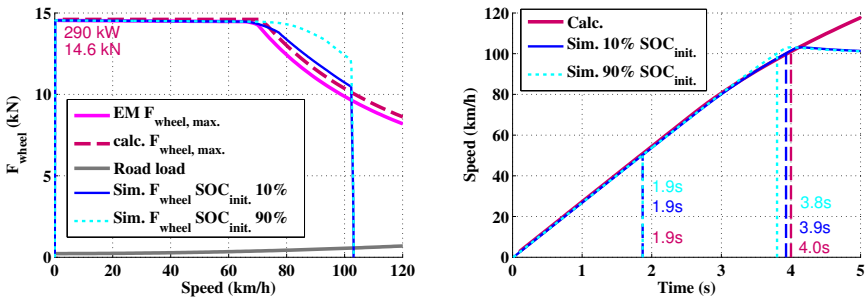

Figure 5.16 Comparison of acceleration test from $0-100\,km/h$, between calculation and simulation, as well as maximum force on wheels from the electric machine, for the Sport car.

Finally for the Sport car the time to $50\,km/h$ is the same for all cases, while the time to $100\,km/h$ is $3.9\,s$ and $3.8\,s$ for the 10 and $90\,\%$ SOC respectively, which means about 2.5 and $5\,\%$ faster then the requirement.

5.8 Simulated time to accelerate $0-100\,km/h$ with grade

Here an acceleration from $0-100\,km/h$ is again simulated, but now for the case of added road grade as a form of controlling the fulfillment of the requirement to be able to handle a grade at high speed. The results can be seen in Figure 5.17 to 5.19.

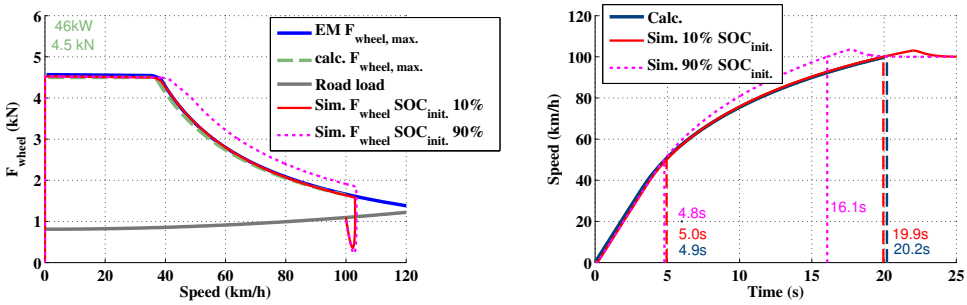

Figure 5.17 Comparison of acceleration test from $0-100\,km/h$, between calculation and simulation, as well as maximum force on wheels from the electric machine, for a road grade of $6\,\%$, for the City Car.

The City car was to be able to sustain a speed of $90\,km/h$ in a uphill grade of $6\,\%$, which it does. In this case it takes about $5\,s$ for the City car to reach $50\,km/h$ and about

$20\,s$ to reach $100\,km/h$ at $10\,\%$ SOC. The higher SOC level gives only minor effects on the time to $50\,km/h$, while it needs $3.8\,s$ less to reach $100\,km/h$ compared to the $10\,\%$ SOC.

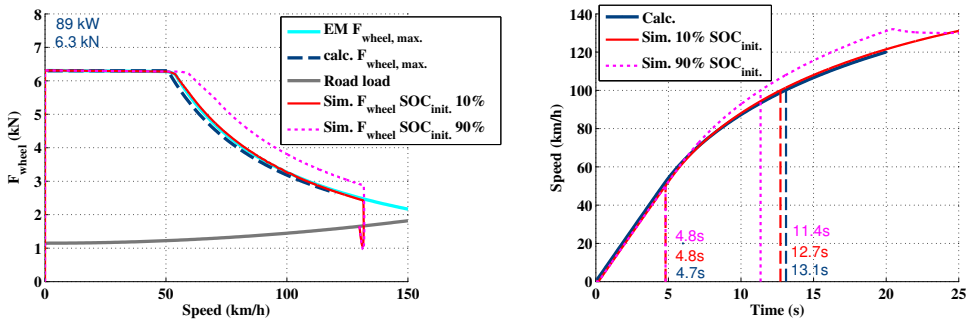

Figure 5.18 Comparison of acceleration test from $0 - 100\,km/h$, between calculation and simulation, as well as maximum force on wheels from the electric machine, for a road grade of $6\,\%$, for the Highway Car.

The Highway car is able to sustain the uphill grade of $6\,\%$ at the speed of $130\,km/h$. In this case the acceleration time difference between the no grade case is much smaller compared to the City car. Also less difference is noted between the two SOC levels, only $1.3\,s$ for $100\,km/h$, and none for $50\,km/h$.

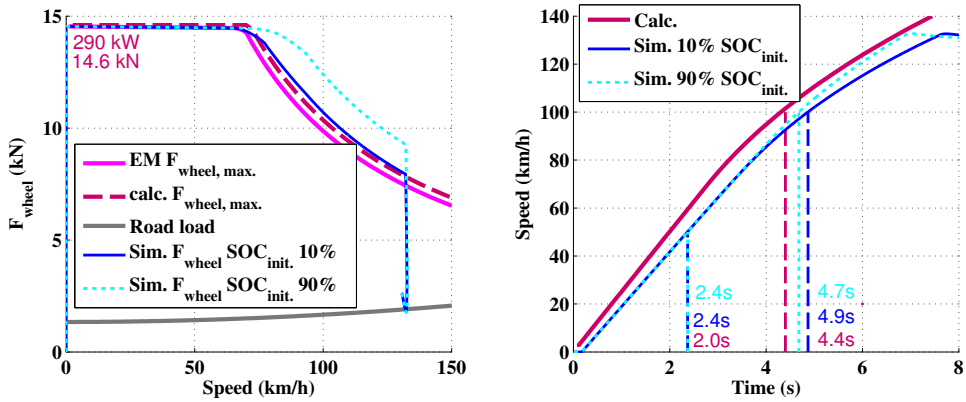

Figure 5.19 Comparison of acceleration test from $0 - 100\,km/h$, between calculation and simulation, as well as maximum force on wheels from the electric machine, for a road grade of $6\,\%$, for the Sport Car.

Finally, the Sport car can handle the $12\,\%$ uphill grade at $130\,km/h$. The time to accelerate to $100\,km/h$ only becomes $0.9\,s$ longer compared to the case with no grade, for both SOC levels.

5.9 Fulfillment of reference cycle speed in simulation

Due to the use of a driver model (i.e. a speed controller) in the simulation, naturally the simulated speed will deviate from the reference speed trace, even for operating points well within the operating area of the powertrain. Hence when analyzing energy consumption and efficiency for a certain cycle, it must be remembered that a slightly different cycle than the reference, is analyzed. As a consequence, typical values of the difference between reference speed and simulated speed have been studied. Another parameter worth studying is the difference in positive and negative average energy at the wheels per driven distance, between the simulation and the reference speed and acceleration. It might happen that there is a large speed difference at a certain time step, but that it's influence on the average energy consumption difference is rather small.

For the Test cycles the speed differences range between $0.1-0.4\,km/h$, $0.2-0.5\,km/h$ and between $0.2-0.6\,km/h$ for the City, Highway and Sport cars respectively. Typical values of the maximum difference between the simulated acceleration and the acceleration of the reference Test cycles are; $0.0-0.1\,m/s^2$, $0.0-0.2\,m/s^2$ and $0.0-0.1\,m/s^2$ for the City, Highway and Sport cars respectively. Worth noting is that the time simulation inherently is a backward calculation, hence the Euler backward method is used for the reference cycle acceleration, instead of the otherwise more accurate forward-backward method described in Chapter 3.

Moreover, during the modal European cycles (ECE, EUDC and NEDC) a minor speed overshoot is noted when the reference speed of the cycle is changing rapidly from a constant acceleration to a constant speed, which gives a relatively small difference of $0.2\,km/h$ between the reference and simulated speed. This also results in a small oscillation in the simulated acceleration of $0.7\,m/s^2$. Nevertheless, these effects are seen to have little influence on the average wheel energy consumption during the cycle, hence they are ignored.

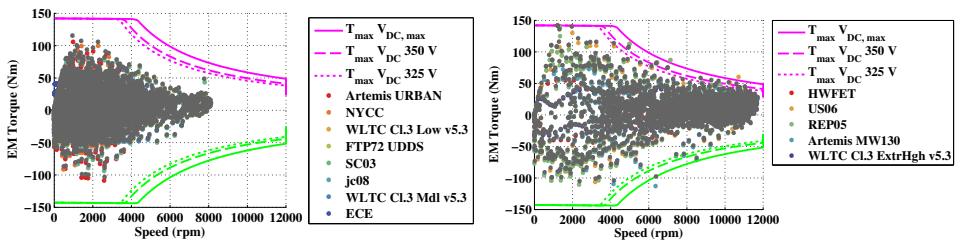

(a) Urban cycles.

(b) Highway cycles.

Figure 5.20 Electric machine operating points during the Urban and Highway cycles as gray dots, while the reference cycle dots are shown with different colors, for the City car.

For the City car, three points in each of the two cycles US06 and REP05 were outside of the powertrain's operational area, causing a maximum deviation of $1.7\,km/h$ from the reference speed, and $0.4\,m/s^2$ from the reference acceleration. These represent speed and

acceleration levels of $56\,km/h$ at $3\,m/s^2$, and $80\,km/h$ at $2.2\,m/s^2$, and finally around $120\,km/h$ at $1.3\,m/s^2$. The consequence on the average energy consumption is negligible in these cases. Also one point in the Artemis Motorway cycle during braking at high speed is outside of the operating area of the electric machine, see Figure 5.20. The operating points of the City car electric machine can be seen as gray dots in Figure 5.20 for the Urban and Highway cycles. In the same figure also ideal electric machine operating points for a lossless system is depicted for comparison, and color marked depending on the type of cycle.

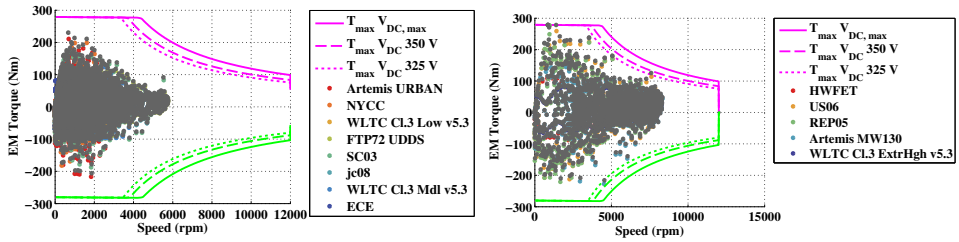

(a) Urban cycles.

(b) Highway cycles.

Figure 5.21 Electric machine operating points during the Urban and Highway cycles as gray dots, while the reference cycle dots are shown with different colors, for the Highway car.

The US06 and REP05 cycles caused some deviations also for the Highway car of maximum $1.5\,km/h$ and $0.2\,m/s^2$, however in this case the operating points that cause problem are those that demand high acceleration (almost $4\,m/s^2$) from stand still, see Figure 5.21. The problem appears twice in REP05 and once in US06. Also here there is no effect on the net average wheel energy.

For the Sport car, the operating points from all Test cycles are well within the limits of the powertrain.

Furthermore, all cars are able to follow the Logged Urban cycles, with typical maximum speed differences between the reference and simulated cycle as $0.3 - 0.8\,km/h$. One Rural cycle for the City car (C30d2 121219 Stnsnd-Henan) and all Highway cycles have single large speed deviations with a relatively large effect on the average net wheel energy. The Highway and Sport cars have no major deviations worthy to mention.

5.10 Simulated component efficiency per cycle

The average Test cycle efficiency separated into propulsion and braking mode can be seen in Figure 5.25 to 5.27, for the City, Highway and Sport cars respectively. Also the average cycle efficiency of each modeled component (electric machine, converter, battery and transmission) is depicted in the figures for comparison.

Although the differences in efficiency between the cycles and cars are quite small (a few units of percent), some trends can be seen when comparing the results between the

cycles and cars. One tendency is a slightly higher average total powertrain efficiency for the highway cycles and a somewhat lower efficiency for the Urban cycles, for all of the cars. Also the total powertrain efficiency of the City car is generally a bit higher, and a bit lower for the Sport car. Furthermore, the total powertrain cycle efficiency is normally a few units of percent higher in motoring mode compared to generating mode, which can also be seen in Figure 5.11.

The lowest total efficiency for all cars is achieved in the NYCC cycle where both the electric machine and converter efficiencies are low. The highest efficiencies are seen in the WLTC Extra high and Atermis Motorway cycles. The Sport car converter configuration proves to give a rather poor efficiency for several of the Urban cycles. Perhaps a better strategy is to implement a control system where the extra driving wheel pair is only engaged during higher power and torque demands.

The transmission efficiency is in line with the efficiency of the converter and electric machine. Perhaps a more advanced loss model of the transmission would be preferred here in order to differentiate between the various load cases.

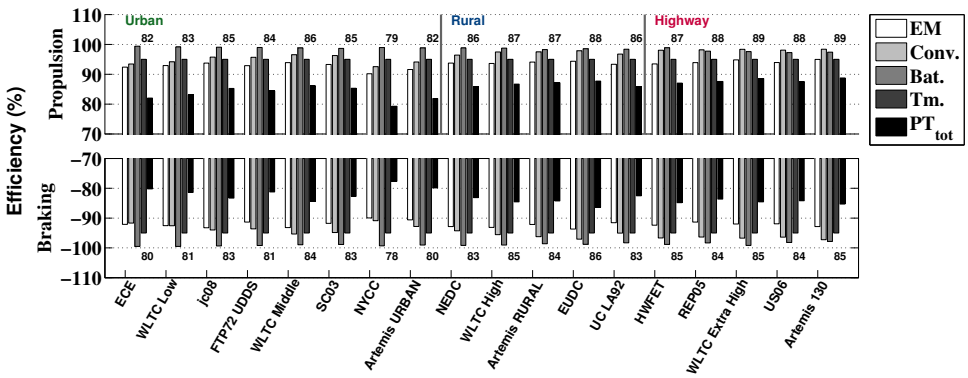

Figure 5.22 Total powertrain efficiency per cycle in propulsion vs. braking mode (negative y-axis), and efficiency broken down per component, from simulation of the City car, with 90 % initial SOC, for the Test cycles.

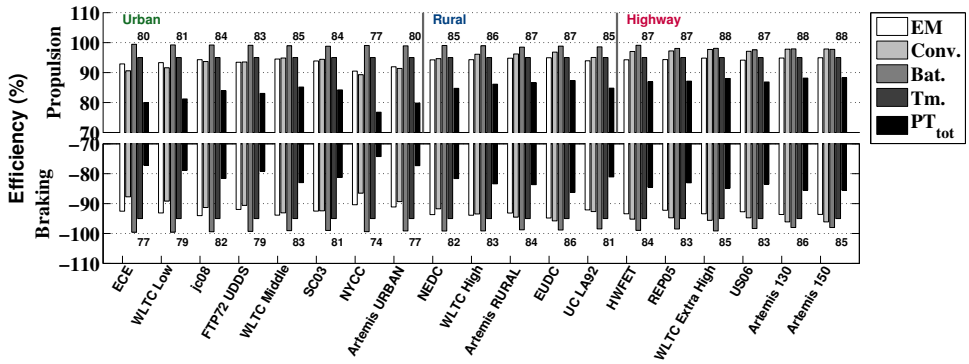

Figure 5.23 Total powertrain efficiency per cycle in propulsion vs. braking mode (negative y-axis), and efficiency broken down per component, from simulation of the Highway car, with 90 % initial SOC, for the Test cycles.

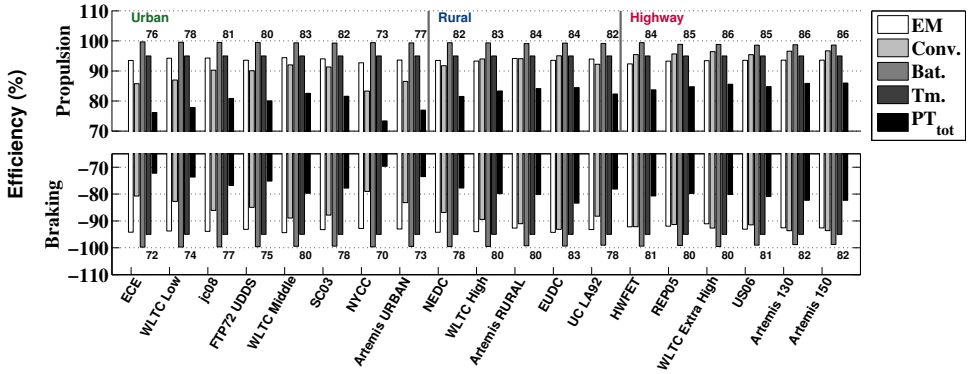

Figure 5.24 Total powertrain efficiency per cycle in propulsion vs. braking mode (negative y-axis), and efficiency broken down per component, from simulation of the Sport car, with 90 % initial SOC, for the Test cycles.

Similarly, the total powertrain efficiency for the Logged cycles can be seen in Figure 5.25 to 5.27, for the City, Highway and Sport cars respectively.

Generally the same trends can also be seen here. Nevertheless, the spread within the Urban and Rural road type categories is here a bit larger. The absolute efficiency values per car, are in line with those for the Test cycles, although a bit lower for the Logged Highway cycles compared to the Highway Test cycles.

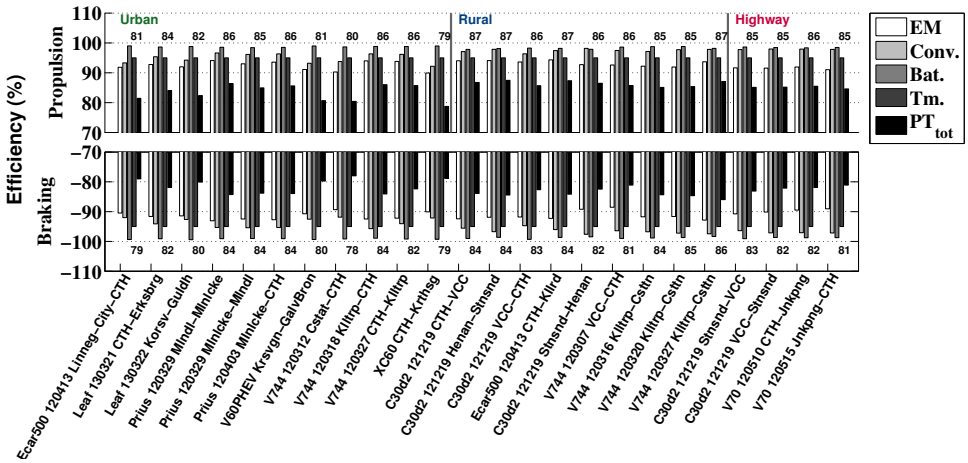

Figure 5.25 Total powertrain efficiency per cycle in propulsion vs. braking mode (negative y-axis), and efficiency broken down per component, from simulation of the City car, with 90 % initial SOC, for the Logged cycles.

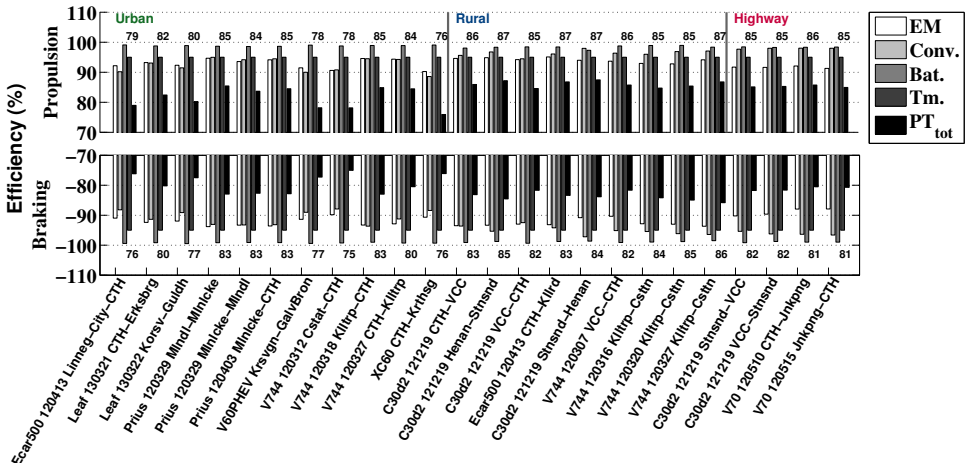

Figure 5.26 Total powertrain efficiency per cycle in propulsion vs. braking mode (negative y-axis), and efficiency broken down per component, from simulation of the Highway car, with 90 % initial SOC, for the Logged cycles.

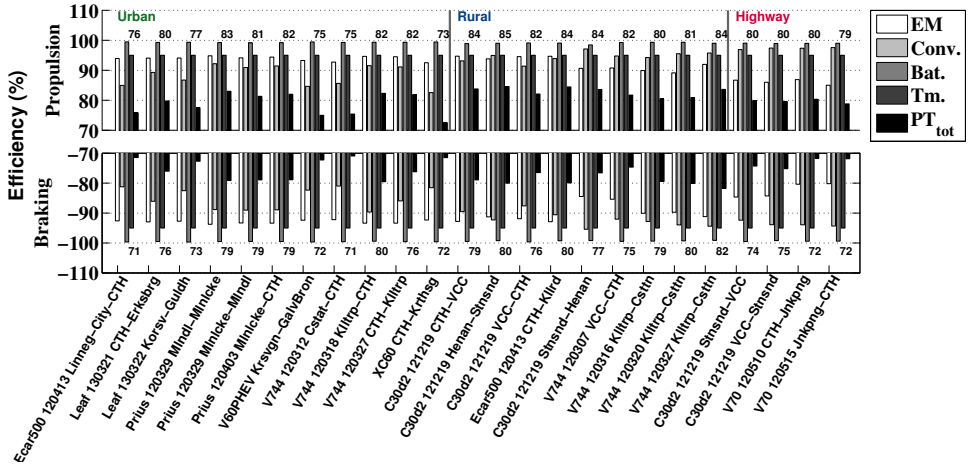

Figure 5.27 Total powertrain efficiency per cycle in propulsion vs. braking mode (negative y-axis), and efficiency broken down per component, from simulation of the Sport car, with 90 % initial SOC, for the Logged cycles.

5.11 Simulated energy per driven distance, per cycle

The resulting battery energy per driven distance of the Test cycles can be seen in Figure 5.28 to 5.30, for the City, Highway and Sport cars respectively. In the figures, data on discharge and charged energy are separated from the net battery energy flow.

Since the average powertrain efficiency is rather similar for all road types, the battery energy consumption per driven distance will to a large part depend on the drive cycle and less on the powertrain. This can also be seen when comparing the relative levels of wheel energy consumption in Figure 4.21, with the simulation results presented here.

There is a rather high coherence between the absolute values of the net energy consumption for the Urban cycles, except for the NYCC and Artemis Urban cycles whom have higher consumption, with the lowest speed levels but the highest acceleration levels. The difference between these two cycles and the rest of the cycles is the smallest for the City car and the largest for the Sport car. The lowest consumption for all cars, can be noted for the ECE cycle, which is explained by its relatively low speed levels and the lowest level of accelerations. This is also despite the relatively low powertrain efficiency for this cycle in all cars.

It can also be seen that the energy consumption of the European test cycle NEDC, is fairly close to the WLTC high and the Artemis Rural, but generally larger than for the Urban cycles and much smaller than for the Highway cycles.

The spread in absolute values is the largest for the Highway cycles, where HWFET has the lowest levels of consumption per distance due to its low speed, while the Artemis Motorway cycles have the highest consumption as well as speed levels. In general, the

simulations show a higher energy consumption per driven distance for the Highway cycles.

Those cycles with the highest discharge energy consumption are also those with high or the highest levels of acceleration and RPA value, within the same road type, and in the same time they often have low maximum and average levels of speed. This is valid for NYCC, Artemis Urban, UC LA92 and US06.

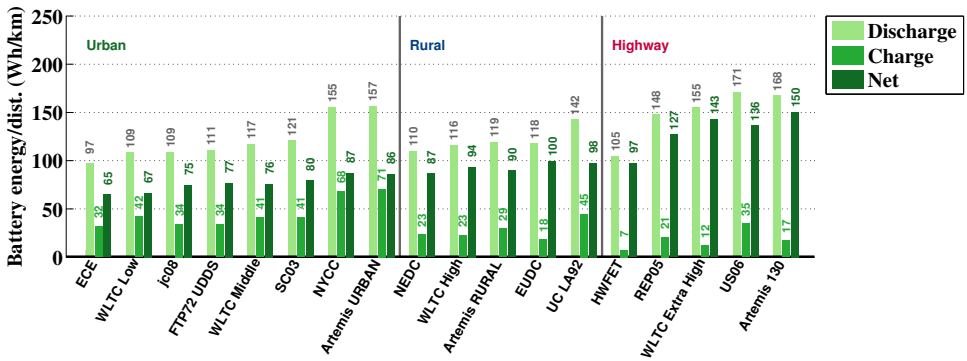

Figure 5.28 Average powertrain propulsion, braking and net energy consumption per driven distance, from simulation of the City car, with 90 % initial SOC, for the Test cycles.

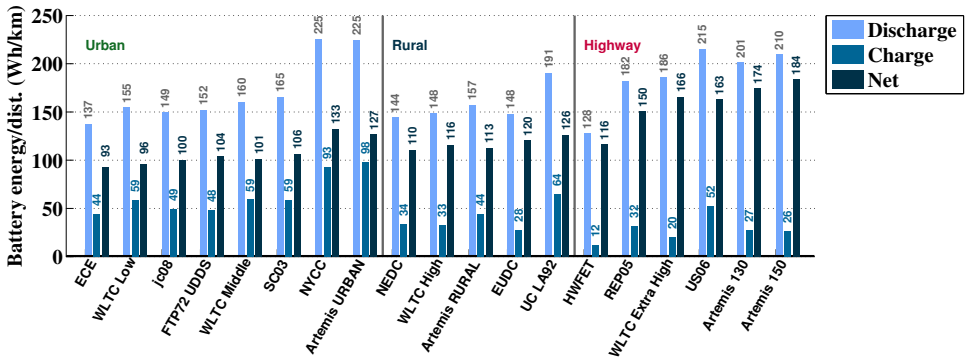

Figure 5.29 Average powertrain propulsion, braking and net energy consumption per driven distance, from simulation of the Highway car, with 90 % initial SOC.

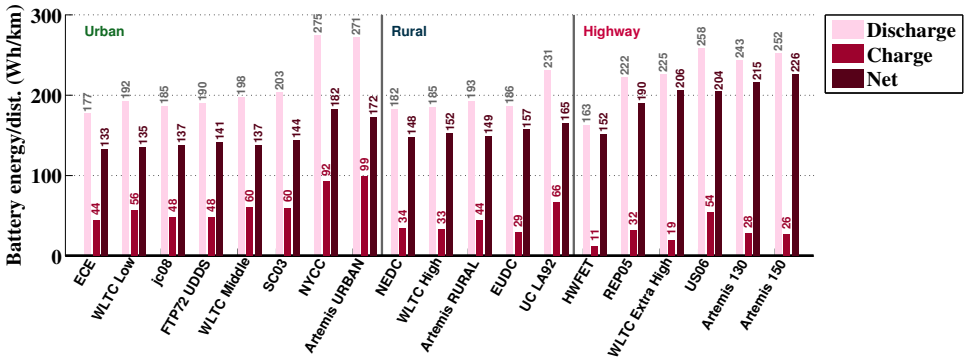

Figure 5.30 Average powertrain propulsion, braking and net energy consumption per driven distance, from simulation of the Sport car, with 90 % initial SOC.

Similarly, the discharge, charged and net battery energy flow for the Logged cycles can be seen in Figure 5.31 to 5.33, for all three cars. Perhaps more examples are needed in order to draw any general conclusions though.

The energy consumption coherence between the Logged road types, is not as high as for the Test cycles, except when it comes to the Highway cycles which are very coherent. Not to forget, for the Logged cycles, not only speed and acceleration but also road grade levels are included in the energy consumption figures shown.

The two cycles with the highest energy consumption for all three cars are the Urban classified cycles; Leaf 130322 Korsv-Guldh and V744 120312 Cstat-CTH. Also the cycle Ecar500 120413 Linneg-City-CTH has a relatively high energy consumption. From Figure 4.24, the reason is a rather long uphill climbing which in these short cycles has a major impact on the energy consumption.

It can also be seen that for the three cycles V744 Klltrp-Csttn at different days, two of them have similar results while the third (120327) have a higher consumption, even though the average powertrain efficiency is somewhat higher for the third case compared to the first two. In Table 3.3 it can be seen that the speed levels are similar, while as seen in Table 3.5 the maximum and average levels of acceleration as well as the RPA value is higher in the third case, hence the higher consumption.

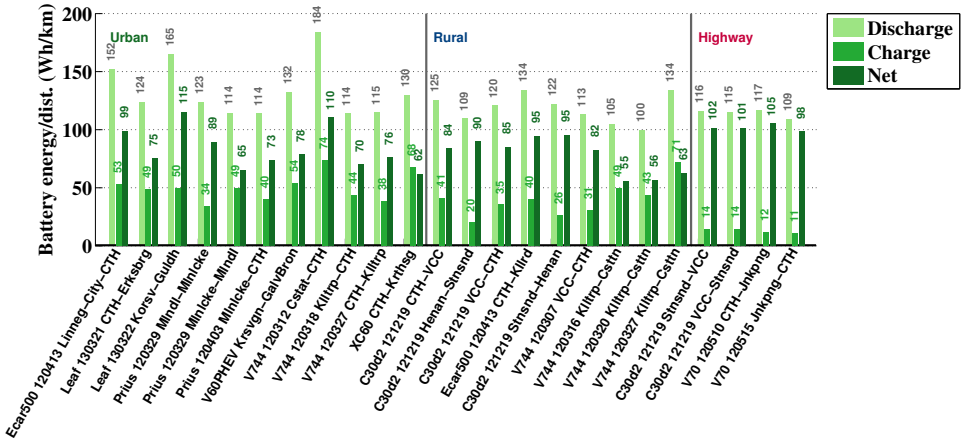

Figure 5.31 Average powertrain propulsion, braking and net energy consumption per driven distance, from simulation of the City car, with 90 % initial SOC, for the Logged cycles

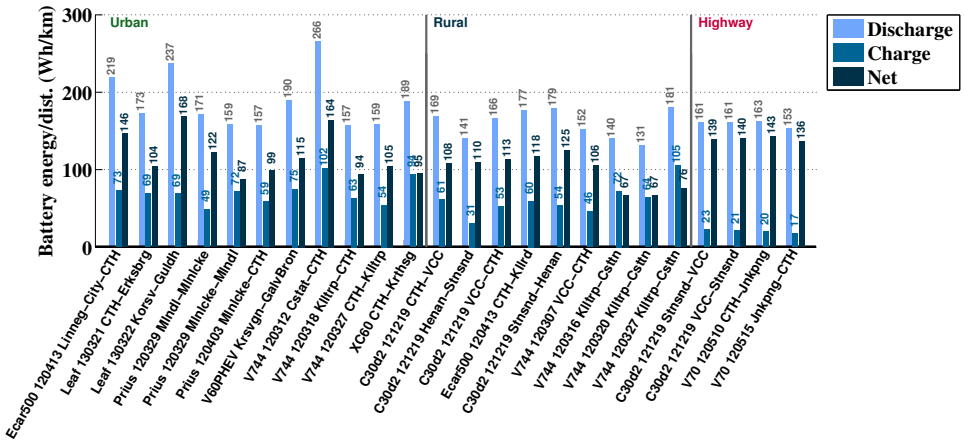

Figure 5.32 Average powertrain propulsion, braking and net energy consumption per driven distance, from simulation of the Highway car, with 90 % initial SOC, for the Logged cycles

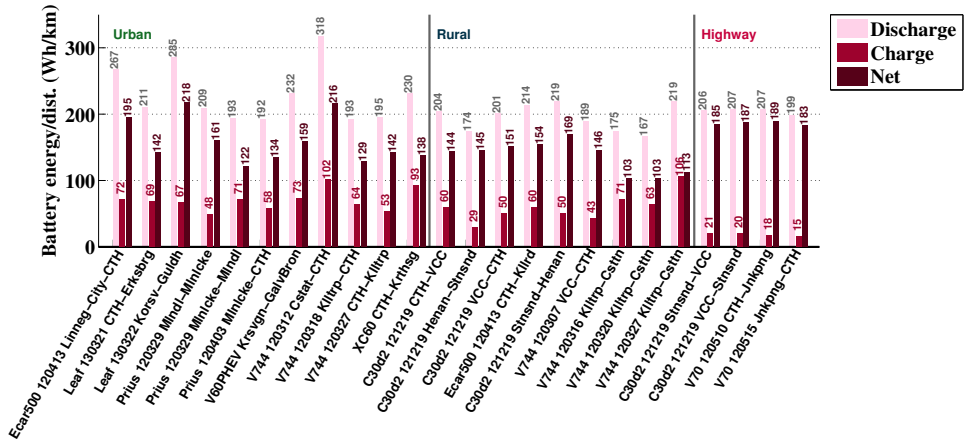

Figure 5.33 Average powertrain propulsion, braking and net energy consumption per driven distance, from simulation of the Sport car, with 90 % initial SOC, for the Logged cycles

5.12 Simulated driving range

Simulation of consecutive NEDC cycles for the City car can be seen in Figure 5.34. The resulting driven distance was $174.7\ km$, which is fairly close to the set requirement of $160\ km$. As can also be seen in the figure, the average powertrain efficiency is consistent over the discharge intervall, which can be expected as the operating points of the NEDC cycle are well within the non field weakening area of the machine even at the lowest level of SOC where the machine efficiency is the same at all voltage levels. The average cycle efficiency is $86\,\%$ in motoring mode and $83\,\%$ in generator mode, which can be compared to the efficiency estimation used ($80\,\%$) when seeking a suitable battery energy content for the range requirement.

The results from the range simulation of the Highway and Sport cars can be seen in Table 5.5. The average powertrain cycle efficiencies are higher than assumed also for the Highway and Sport cars, as can also be seen in the table. The highest average powertrain efficiency is achieved in the City car, as expected from the comparison in Figure 5.11, where the City car showed a higher efficiency for the same speed and acceleration. Given the resulting values of average efficiency, the energy capacity of the batteries could be reduced by about $3 - 10\,\%$.

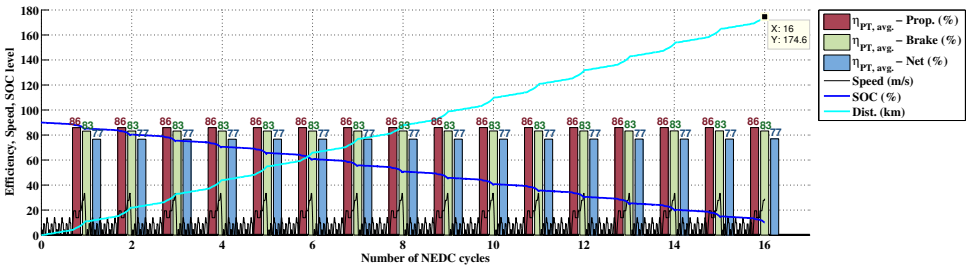

Figure 5.34 Average powertrain propulsion, braking and net efficiency from simulation of City car NEDC driving range.

Table 5.5 NEDC range simulation results compared to requirements.

	City car:	Highway car:	Sport car:
Requirement	160 km	200 km	300 km
Simulation result	174.6 km	215.7 km	307.2 km
Relative increase	+ 9.2 %	+ 7.9 %	+ 2.4
Propulsion efficiency	86 %	85 %	82 %
Braking efficiency	83 %	82 %	79 %
Net efficiency	77 %	73 %	71 %
Suggested decreased battery size	-1.9 kWh	-1.5 kWh	-1.5 kWh

Based on the simulation results of net battery energy consumption per driven distance, possible driving range has been calculated for all Test cycles with the City and Highway cars, see Figure 5.35 and 5.36. In this illustrative example, the battery energy content is estimated to $80\,\%$ of $19.3\,kWh$, which here results in a NEDC range of $178\,km$. The discrepancy with the value in Table 5.5, may be due to the assumed energy content of the battery which in the simulation varies depending on the load situation. It can be seen that the lower energy consumption for the Urban cycles generally provides $20-50\,km$ more than the NEDC cycle, while the range is shortened by about $50\,km$ for most Highway cycles.

Similarly, for the Highway car, the range increase for most Urban cycles is $10-30\,km$, and the decrease is about $20-90\,km$ for the Highway cycles, see Figure 5.36.

For comparison, the estimated driving range of the Logged cycles for the City car can be seen in Figure 5.37. The ranges are about $130-250\,km$, $160-280\,km$ and $150-160\,km$ for the Logged Urban, Rural and Highway cycles respectively, i.e. a larger variety than for the Test cycels.

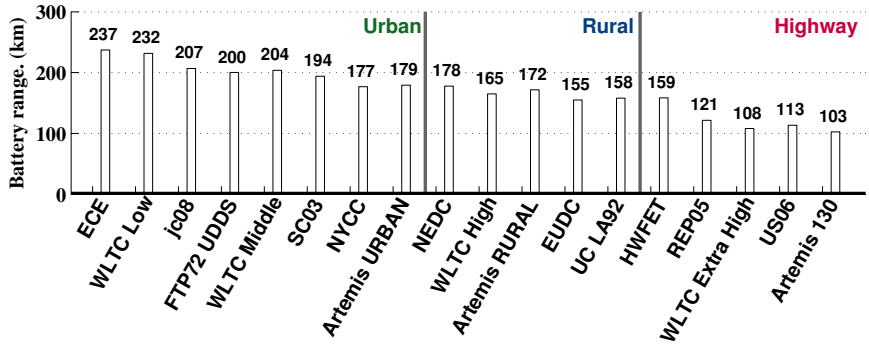

Figure 5.35 Estimated driving range for the Test Cycles with the City car.

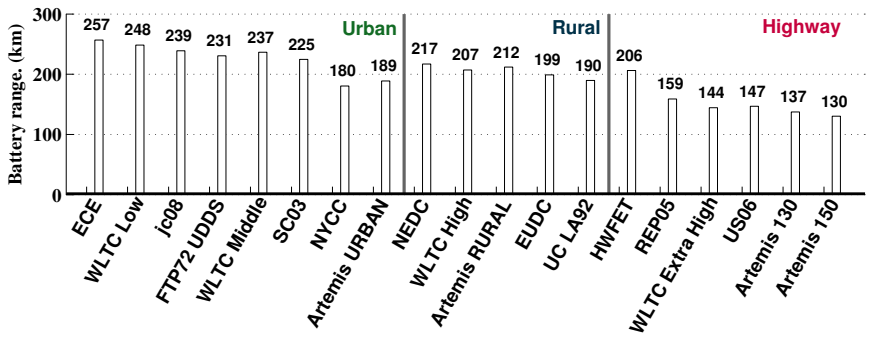

Figure 5.36 Estimated driving range for the Test Cycles with the Highway car.

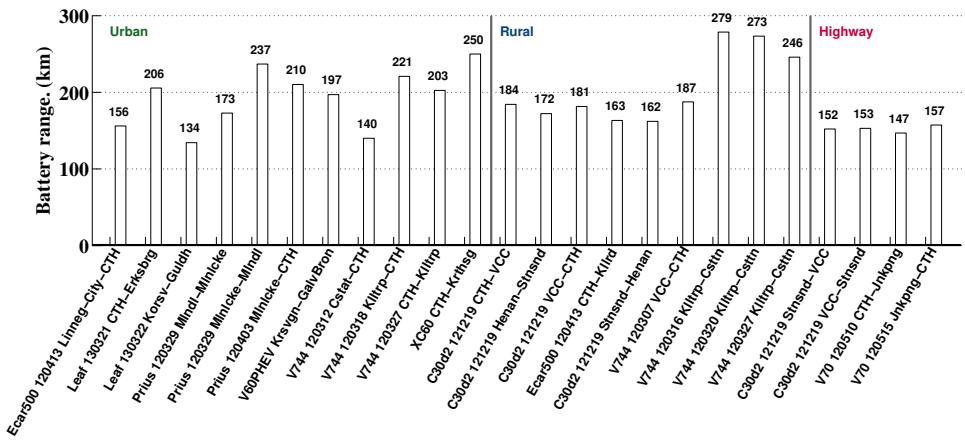

Figure 5.37 Estimated driving range for the Logged Cycles with the City car.

Chapter 6

Effects of EM resizing on performance and energy efficiency

In this chapter, the electric powertrain of the City and the Highway cars are resized in terms of torque and power capability as well as losses, and the consequence on vehicle performance and energy efficiency for the Test cycles, are studied and quantified.

The re-scaling of the electric machine is simply a linear scaling on the active length, as is described in Chapter 5. For the City car the scaling factors are here in steps of $10\,\%$, from 50 to $150\,\%$ of the baseline City electric machine studied in the previous chapter. For the Highway car, the scaling factors are in steps of $20\,\%$; from 60 to $140\,\%$. In order for the converter losses to still be reasonably representative, also the on-state resistance and switching loss parameters are scaled with the same factors, where the resistances are inversely proportional and the switching loss parameters are linearly proportional.

In this study, only the losses in motoring mode of the electric machine and converters are implemented in the models, hence it is assumed that the loss maps in the generative mode are the same as in motoring mode. The battery energy consumption per distance as well as the net powertrain efficiency, for the baseline City car during the Test cycles are identical to the results shown in 5.25 and 5.28. Hence this is an acceptable simplification.

The gear ratios, the configuration of the battery, thus it's energy content are here left unaltered, as are the vehicle masses.

6.1 City car

The resulting maximum torque and power for some of the resized electric machines can be seen in Figure 6.1, together with the vehicle's road load which remains the same in all cases.

Even the smallest machine size will be able to sustain the vehicle's top speed requirement. The initial maximum torque levels of the scaled machines, are linearly proportional to the scaling factor. As can be seen, the base speed of the machine is not affected by the scaling.

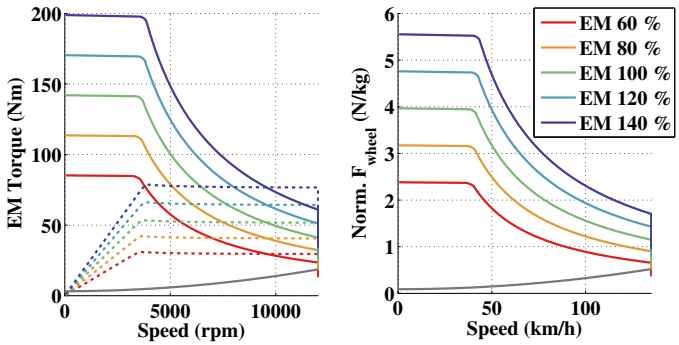

Figure 6.1 Maximum torque (solid) and power (dotted) as a function of speed, and maximum normalized wheel force as a function of vehicle speed (at 350 V DC) along with road load (gray), for the resized electric machines to the City car.

As can be seen in Figure 6.2, the time to accelerate is highly effected by a change in the size of electric powertrain. For example, the acceleration time to $100\,km/h$ of the $60\,\%$ system is $23.7\,s$ which is about $11\,s$ or $87\,\%$ slower than the for the ($100\,\%$) baseline system. Also, the acceleration time to $100\,km/h$ of the $140\,\%$ system is $8.6\,s$, i.e. about $4\,s$ or $32\,\%$ faster. The increase in acceleration time to $50\,km/h$ for the $60,\%$ system is $2.8\,s$ ($70\,\%$), and the decrease for the $140\,\%$ system is $1.2\,s$ ($30\,\%$).

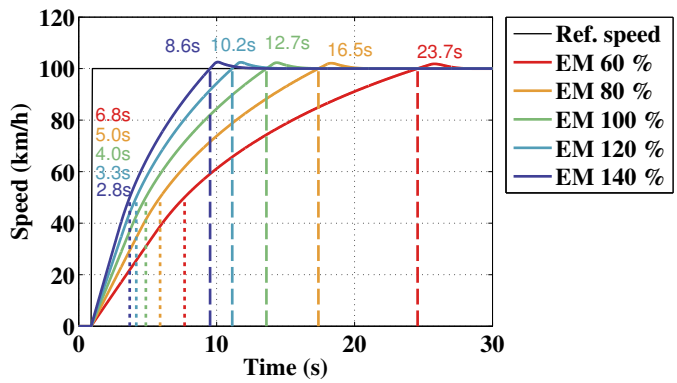

Figure 6.2 Selected times to accelerate $0-50\,km/h$ and $0-100\,km/h$ at $10\,\%$ SOC, for the resized electric machines to the City car.

As a comparison, the total powertrain energy efficiency (excluding the battery) of the $50\,\%$ scaled system together with the baseline system, as functions of vehicle speed and

mass normalized force, is presented in Figure 6.3, for a DC voltage level of $350\,V$. For the same speed and acceleration operating points, the down-scaled system has a lower efficiency, which is caused by higher copper losses.

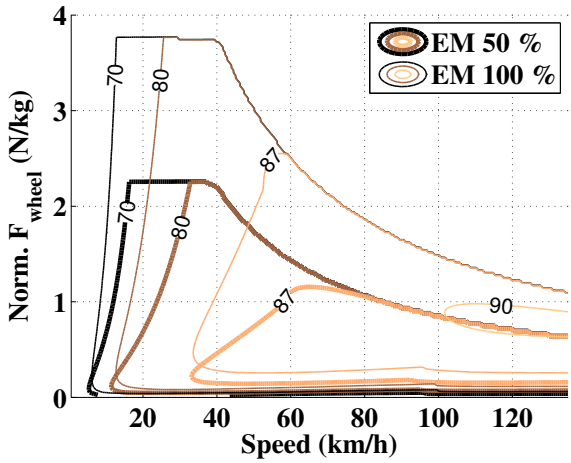

Figure 6.3 Total powertrain efficiency (excluding battery) for the $50\,\%$ down scaled machine and the base machine (100 %) at 350 V DC, for the City car.

The battery energy consumption per driven distance of all of the Test cycles has been simulated for the different City car system sizes, similarly as described in Chapter 5.

For some cycles the down-scaled systems were no longer able to sustain all of the operating points in the reference speed's time trace, due to limited acceleration capability. In these cases there may be a rather large difference between the reference speed and the simulated speed. However, as noted in the previous chapter, the effect of this deviation on the average cycle energy consumption per driven distance may be relatively small. As a measure of the change in cycle energy due to failure to follow the reference speed, the net wheel energy of the simulated cycle is compared with the net wheel energy of the reference cycle. For those cases where there is a large increase or decrease in the net wheel energy, the resulting battery energy consumption may be less relevant in the type comparative study done here, since the result is then valid for a different cycle than the reference cycle.

The results of the simulations are presented in Table 6.1 for the down-scaled systems, and in Table 6.2 for the up-scaled systems. In the tables, the following information is presented; simulation cycle increase or decrease (in %) in net wheel energy per driven distance compared to the energy per driven distance for the same vehicle according to the reference speed, as well as the maximum deviation of the simulated speed from the reference speed, and finally the increase or decrease (in %) of the net battery energy compared to the base system (i.e. the $100\,\%$ system). As the system size is stepped down, more and more cycles, particulary the high speed cycles, indicate difficulties in following the speed reference, as can be seen by the color marked values in the table. In general, there is no large difference

noted between the net wheel energy per distance of the reference cycle versus the simulation.

The battery energy consumption for the Urban cycles, increases in the order of a few percent for the $80-90\,\%$ systems, to up to around $5-10\,\%$ for $50\,\%$ system. The highest increases are seen for the ECE and WLTC Low cycles at the lowest system scalings. The NYCC and Artemis Urban cycles have $10-25\,\%$ increases in energy consumption during the lowest system scaling, however at the same time the speed deviation is also rather high and should therefore be analyzed having that in mind. Furthermore, for the $50\,\%$ down-scaled system, five of the Urban cycles, and one each of the Rural and Highway cycles can still be fulfilled, although at the price of about $6-11\,\%$ higher losses compared to the baseline system. For the Highway cycles, the energy consumption tend to decrease somewhat with decreasing system size, still only the HWFET cycle is achieved at the lowest system scaling.

For the case of the up-scaled systems in Table 6.2, the general trend is an increase in energy consumption with increased system size, however only by a few percent.

Table 6.1 Table over simulation results during down-scaling of the electric machine and converter, for the City car. For each machine size, the left column gives the increase or decrease (in %) in net wheel energy per driven distance for the simulation cycle compared to the energy per driven distance for the same vehicle according to the reference speed. The middle column gives, the maximum deviation of the simulated speed from the reference speed, and finally the right column gives the increase or decrease (in %) of the net battery energy compared to the baseline system (i.e. the $100\,\%$ system)

	50 (%)			60 (%)			70 (%)			80 (%)			90 (%)			100 (%)		
Cycle	E_{wheel} net Sim. inc. dec. (%)	Max speed diff. (km/h)	Rel. Cons. (%)	E_{wheel} net Sim. inc. dec. (%)	Max speed diff. (km/h)	Rel. Cons. (%)	E_{wheel} net Sim. inc. dec. (%)	Max speed diff. (km/h)	Rel. Cons. (%)	E_{wheel} net Sim. inc. dec. (%)	Max speed diff. (km/h)	Rel. Cons. (%)	E_{wheel} net Sim. inc. dec. (%)	Max speed diff. (km/h)	Rel. Cons. (%)	E_{wheel} net Sim. inc. dec. (%)	Max speed diff. (km/h)	Rel. Cons. (%)
ECE	0.0	0.4	9.9	0.0	0.3	5.1	0.0	0.2	2.4	0.0	0.2	0.9	0.0	0.2	0.2	0.0	0.2	0.0
WLTC Low	0.0	0.3	11.4	0.0	0.2	6.1	0.0	0.2	3.1	0.0	0.2	1.3	0.0	0.1	0.4	0.0	0.1	0.0
jpjc08	0.0	0.5	5.5	0.0	0.4	2.6	0.0	0.3	1.0	0.0	0.3	0.2	0.0	0.2	-0.1	0.0	0.2	0.0
FTP72UDDS	0.0	0.5	7.6	0.0	0.4	4.1	0.0	0.3	2.0	0.0	0.3	0.8	0.0	0.2	0.2	0.0	0.2	0.0
WLTC Mdl	0.0	0.3	6.2	0.0	0.3	3.1	0.0	0.2	1.4	0.0	0.2	0.5	0.0	0.2	0.1	0.0	0.1	0.0
SC03	0.0	4.8	7.2	0.0	1.0	4.0	0.0	0.6	2.0	0.0	0.5	0.9	0.0	0.4	0.2	0.0	0.3	0.0
NYCC	-0.2	6.8	25.6	-0.2	4.1	13.9	-0.2	1.6	7.5	-0.2	0.3	4.1	-0.2	0.3	1.6	-0.2	0.3	0.0
Artemis URBAN	0.0	5.1	22.8	-0.1	3.1	12.8	-0.1	1.9	6.7	-0.1	0.8	3.5	-0.1	0.4	1.4	-0.1	0.4	0.0
NEDC	0.0	1.0	2.3	0.0	0.3	0.9	0.0	0.2	0.0	0.0	0.2	-0.3	0.0	0.2	-0.4	0.0	0.2	0.0
WLTC Hgh	0.0	0.3	1.5	0.0	0.2	0.3	0.0	0.2	-0.2	0.0	0.2	-0.4	0.0	0.2	-0.3	0.0	0.1	0.0
Artemis RURAL	-0.2	4.7	2.6	0.0	2.0	1.1	0.0	0.4	0.4	0.0	0.4	-0.1	0.0	0.4	-0.2	0.0	0.4	0.0
EUDC	0.0	0.9	-0.5	0.0	0.3	-0.7	0.0	0.2	-0.9	0.0	0.2	-0.8	0.0	0.2	-0.6	0.0	0.2	0.0
UCLA92	-0.3	10.9	9.3	0.0	5.7	5.6	0.0	2.7	2.9	0.0	1.1	1.1	0.0	0.3	0.6	0.0	0.3	0.0
HWFET	0.0	0.3	-1.4	0.0	0.3	-1.5	0.0	0.2	-1.3	0.0	0.2	-1.0	0.0	0.2	-0.5	0.0	0.1	0.0
REP05	-0.3	21.3	0.7	-0.1	13.1	-0.4	0.0	5.9	-0.7	0.0	3.9	-0.5	0.0	3.4	-0.5	0.0	1.7	0.0
WLTC ExtrHgh	-0.4	4.7	-1.6	0.0	1.2	-0.6	0.0	0.2	-0.5	0.0	0.1	-0.5	0.0	0.1	-0.7	0.0	0.1	0.0
US06	-0.4	21.3	1.8	-0.1	13.7	0.2	0.0	7.2	-0.6	0.0	3.8	-0.5	0.0	3.4	-0.3	0.0	1.6	0.0
Artemis MW130	-0.7	8.5	-0.3	-0.1	4.0	0.0	0.0	1.3	-0.2	0.0	0.8	-0.2	0.0	0.6	-0.3	0.0	0.4	0.0

Table 6.2 Table over simulation results during up-scaling of the electric machine and converter, as is shown in 6.1.

	100 (%)			110 (%)			120 (%)			130 (%)			140 (%)			150 (%)		
Test Cycles	E_{wheel} net Sim. inc. dec. (%)	Max speed diff. (km/h)	Rel. Cons. (%)	E_{wheel} net Sim. inc. dec. (%)	Max speed diff. (km/h)	Rel. Cons. (%)	E_{wheel} net Sim. inc. dec. (%)	Max speed diff. (km/h)	Rel. Cons. (%)	E_{wheel} net Sim. inc. dec. (%)	Max speed diff. (km/h)	Rel. Cons. (%)	E_{wheel} net Sim. inc. dec. (%)	Max speed diff. (km/h)	Rel. Cons. (%)	E_{wheel} net Sim. inc. dec. (%)	Max speed diff. (km/h)	Rel. Cons. (%)
ECE	0.0	0.2	0.0	0.0	0.1	0.3	0.0	0.1	0.9	0.0	0.1	1.6	0.0	0.1	2.5	0.0	0.1	3.5
WLTC Low	0.0	0.1	0.0	0.0	0.1	0.1	0.0	0.1	0.6	0.0	0.1	1.2	0.0	0.1	2.0	0.0	0.1	2.9
jpjc08	0.0	0.2	0.0	0.0	0.2	0.4	0.0	0.2	1.0	0.0	0.1	1.6	0.0	0.1	2.4	0.0	0.1	3.3
FTP72UDDS	0.0	0.2	0.0	0.0	0.2	0.2	0.0	0.2	0.6	0.0	0.2	1.0	0.0	0.1	1.7	0.0	0.1	2.4
WLTC Mdl	0.0	0.1	0.0	0.0	0.1	0.2	0.0	0.1	0.7	0.0	0.1	1.2	0.0	0.1	1.9	0.0	0.1	2.6
SC03	0.0	0.3	0.0	0.0	0.3	0.1	0.0	0.3	0.4	0.0	0.2	0.9	0.0	0.2	1.4	0.0	0.2	2.2
NYCC	-0.2	0.3	0.0	-0.2	0.2	-0.7	-0.2	0.2	-0.8	-0.2	0.2	-0.7	-0.2	0.2	-0.2	-0.2	0.2	0.6
Artemis URBAN	-0.1	0.4	0.0	-0.1	0.3	-0.6	-0.1	0.3	-0.7	-0.1	0.3	-0.6	-0.1	0.3	-0.2	-0.1	0.3	0.4
NEDC	0.0	0.2	0.0	0.0	0.1	0.5	0.0	0.1	1.1	0.0	0.1	1.8	0.0	0.1	2.5	0.0	0.1	3.3
WLTC Hgh	0.0	0.1	0.0	0.0	0.1	0.4	0.0	0.1	1.0	0.0	0.1	1.6	0.0	0.1	2.2	0.0	0.1	2.9
Artemis RURAL	0.0	0.4	0.0	0.0	0.4	0.4	0.0	0.4	0.9	0.0	0.4	1.4	0.0	0.4	2.0	0.0	0.4	2.7
EUDC	0.0	0.2	0.0	0.0	0.1	0.6	0.0	0.1	1.2	0.0	0.1	1.8	0.0	0.1	2.5	0.0	0.1	3.2
UCLA92	0.0	0.3	0.0	0.0	0.3	0.0	0.0	0.3	0.3	0.0	0.3	0.6	0.0	0.3	1.1	0.0	0.3	1.7
HWFET	0.0	0.1	0.0	0.0	0.1	0.6	0.0	0.1	1.2	0.0	0.1	1.9	0.0	0.1	2.6	0.0	0.1	3.3
REP05	0.0	1.7	0.0	0.0	0.7	0.4	0.0	0.4	0.9	0.0	0.4	1.4	0.0	0.3	1.9	0.0	0.3	2.5
WLTC ExtrHgh	0.0	0.1	0.0	0.0	0.1	0.4	0.0	0.1	1.0	0.0	0.1	1.5	0.0	0.1	2.1	0.0	0.1	2.7
US06	0.0	1.6	0.0	0.0	0.9	0.3	0.0	0.6	0.7	0.0	0.4	1.1	0.0	0.4	1.6	0.0	0.3	2.1
Artemis MW130	0.0	0.4	0.0	0.0	0.4	0.3	0.0	0.3	0.8	0.0	0.3	1.3	0.0	0.3	1.8	0.0	0.3	2.4

As an illustrative example, the speed time trace from the NYCC reference cycle and from the simulated cycle, as well as the speed deviation, can be seen in Figure 6.4. After around 200 s there is a large speed deviation for the smaller system sizes. The bottom sub-figure shows this event in an extracted time frame, where the effect of the limited acceleration capability can be seen.

The resulting battery energy consumption per driven distance, the battery energy normalized to the base system size, and powertrain energy efficiency can be seen in Figure 6.5. The average powertrain efficiency decreases both for down-scaled and up-scaled systems. Then more energy is required for propulsion, and less energy is regenerated, hence the energy consumption per distance increases, still the energy fed to the wheels is unchanged.

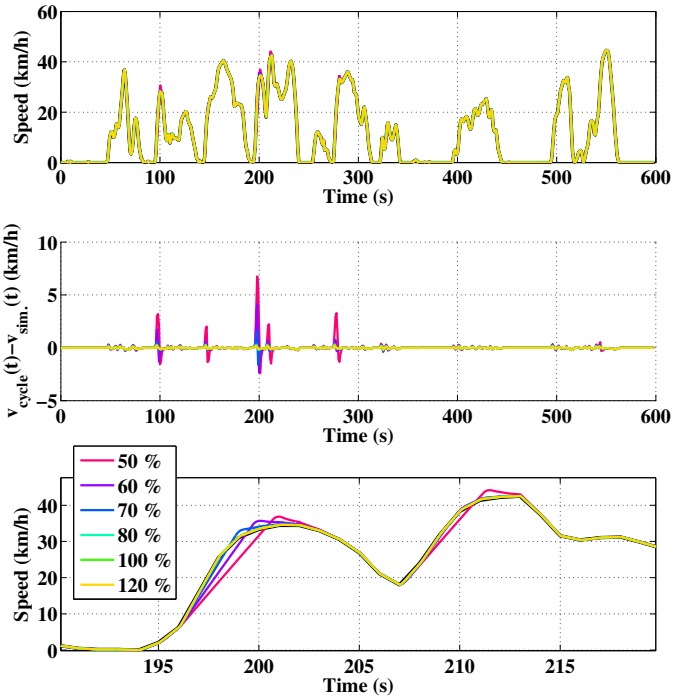

Figure 6.4 Speed and acceleration time traces as well as deviation from the NYCC reference cycle, for all resized City cars.

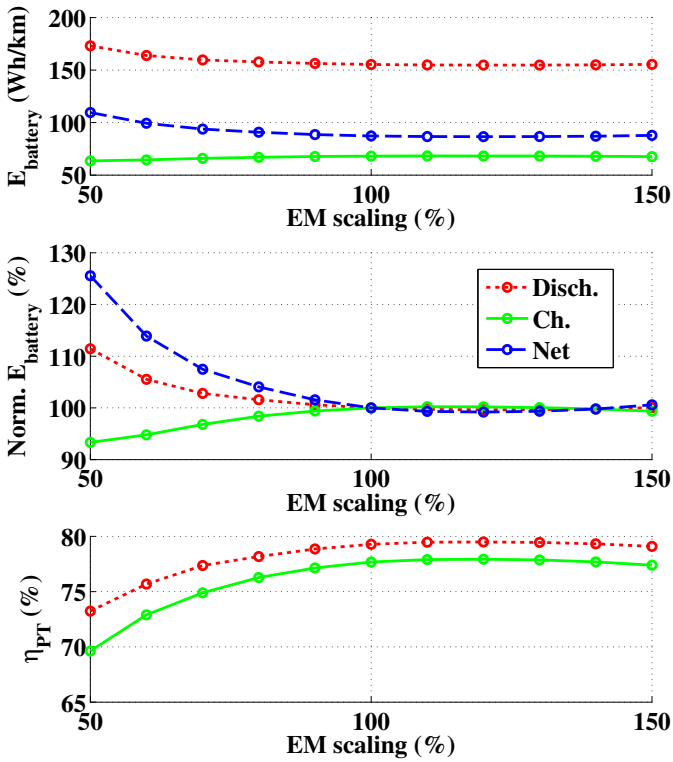

Figure 6.5 Resulting battery energy consumption per driven distance for all resized City cars, and energy consumption normalized to the 100 % base line, along with average cycle powertrain efficiency in motoring and generative mode, for the NYCC cycle.

Another example is the HWFET cycle who's speed deviation is kept small in all cases, as can be seen in Figure 6.6.

Here the average powertrain propulsion efficiency mainly decreases by an increase in system size, while the regenerative efficiency decreases for system sizes larger and smaller then the $70 - 80\,\%$ systems. The highest average powertrain efficiency is reached for the $60\,\%$ down-scaling, as seen in Figure 6.7.

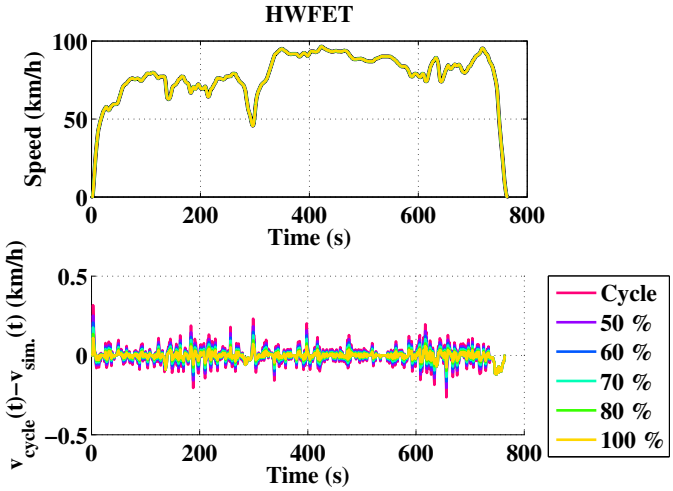

Figure 6.6 Speed and acceleration time traces as well as deviation from the HWFET reference cycle, for all resized City cars.

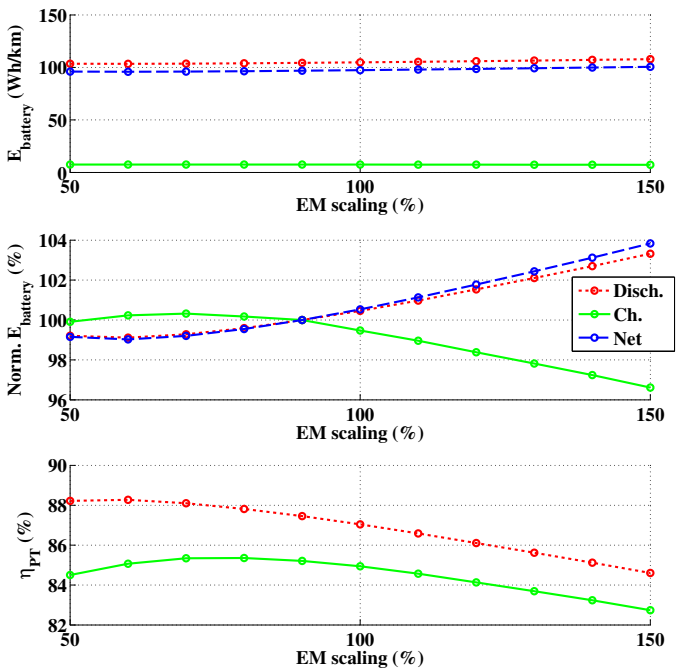

Figure 6.7 Resulting battery energy consumption per driven distance for all resized City car systems, and energy consumption normalized to the 100 % base line, along with average cycle powertrain efficiency in motoring and generative mode, for the HWFET cycle.

The total powertrain efficiency along with the efficiency of each component for the 60 % system can be seen in Figure 6.8. For some of the urban cycles, particulary for the NYCC and Artemis Urban cycles, the efficiency of the down-scaled system is somewhat lower compared to the baseline system (see Figure 5.25), while for the Rural and Highway cycles the total powertrain efficiency remain unchanged.

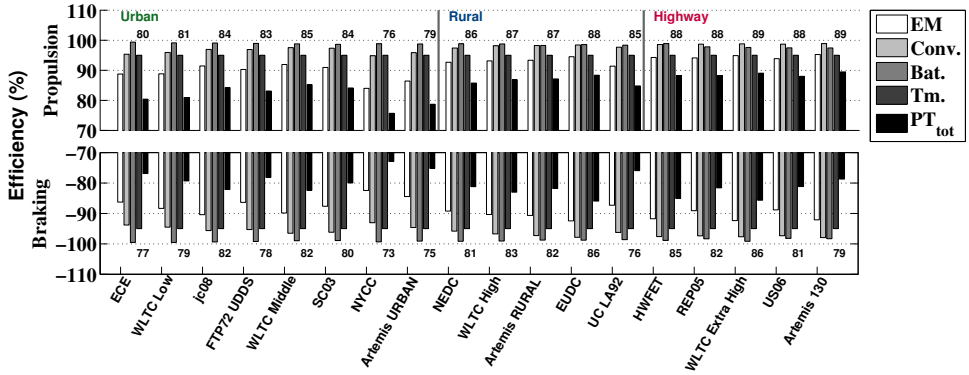

Figure 6.8 Resulting powertrain energy efficiency for the City 60 % system.

6.2 Highway car

For the Highway car, the maximum torque and power for the scaled electric machines can be seen in Figure 6.9, along with the vehicle's road load. Also in this case, the top speed is reached in all cases.

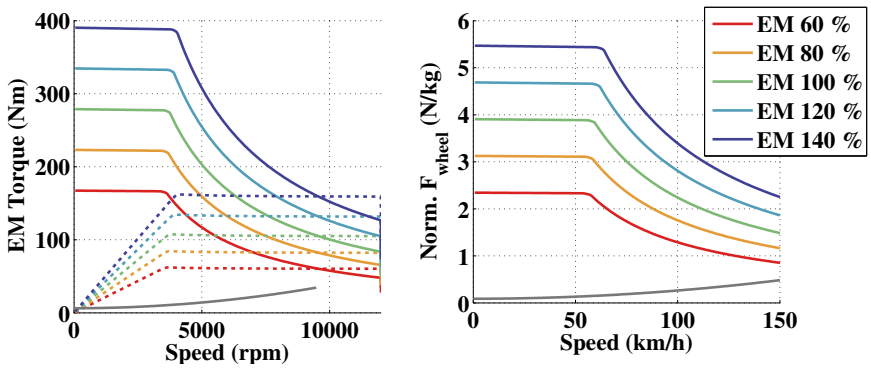

Figure 6.9 Maximum torque (solid) and power (dotted) as a function of speed, and maximum normalized wheel force as a function of vehicle speed (at 350 V DC) along with road load (gray), for the resized electric machines to the Highway car.

The time to accelerate from $0 - 100\,km/h$ for the different system sizes can be seen in

Figure 6.10. The $60\,\%$ system takes about $7\,s$ longer time to accelerate to $100\,km/h$, and $2.7\,s$ longer to $50\,km/h$, i.e. a change of around $70\,\%$. Instead, the $140\,\%$ system takes $3\,s$ shorter time to $100\,km/h$, and $1.2\,s$ shorter to $50\,km/h$; that is a change of around $30\,\%$.

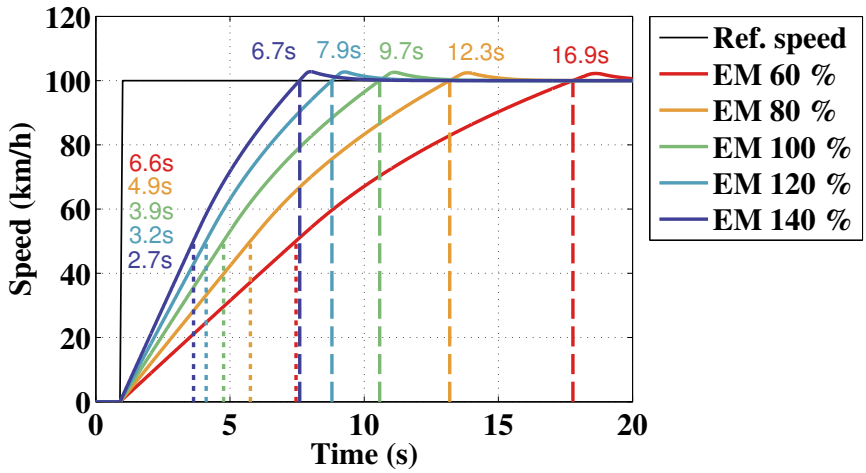

Figure 6.10 Time to accelerate $0-50\,km/h$ and $0-100\,km/h$ at $10\,\%$ SOC, for the resized electric machines to the Highway car.

The total powertrain energy efficiency of the $60\,\%$ scaled system together with the baseline system, as functions of vehicle speed and mass normalized force, is presented in Figure 6.11, for a DC voltage level of $350\,V$. As for the City car, the smaller system has a lower powertrain efficiency for the same speed and acceleration operating point.

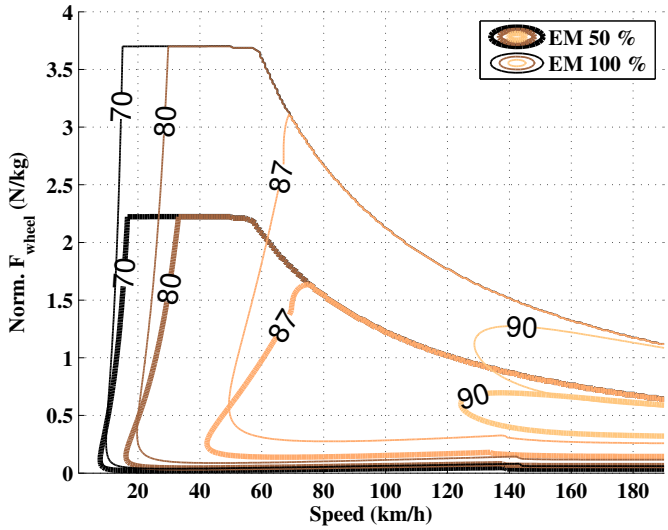

Figure 6.11 Total powertrain efficiency (excluding battery) for the 50 % down scaled machine and the base machine (100 %) at 350 V DC, for the Highway car.

The resulting battery energy consumption per driven distance along with the relative change in wheel energy per distance between the reference cycle and the simulated cycle, and the maximum speed difference, can be seen in Table 6.3. The up-scaled systems have no large speed deviations, while the down-scaled systems have speed deviations on similar cycles as the City car.

The energy consumption increases a few percent for the up-scaled systems, about $1-3\,\%$ for the $120\,\%$ system and $2-7\,\%$ for the $140\,\%$ system. The largest increases can be seen for the Urban cycles. For the down-scaled systems the change is generally smaller, $0-1\,\%$, with the largest decrease for the HWFET cycle by $2.2\,\%$ for the $60\,\%$ system.

Table 6.3 Table over simulation results during up-scaling of electric machine.

	60 (%)			80 (%)			100 (%)		120 (%)			140 (%)		
Test Cycles	E_{wheel} net Sim. inc. dec. (%)	Max speed diff. (km/h)	Rel. Cons. (%)	E_{wheel} net Sim. inc. dec. (%)	Max speed diff. (km/h)	Rel. Cons. (%)	E_{wheel} net Sim. inc. dec. (%)	Max speed diff. (km/h)	E_{wheel} net Sim. inc. dec. (%)	Max speed diff. (km/h)	Rel. Cons. (%)	E_{wheel} net Sim. inc. dec. (%)	Max speed diff. (km/h)	Rel. Cons. (%)
ECE	0.0	0.3	-0.3	0.0	0.2	-1.4	0.0	0.2	0.0	0.1	3.3	0.0	0.1	7.3
WLTC Low	0.0	0.2	0.4	0.0	0.2	-1.2	0.0	0.2	0.0	0.2	3.2	0.0	0.2	7.1
jpjc08	0.0	0.4	-0.8	0.0	0.3	-1.3	0.0	0.2	0.0	0.2	2.6	0.0	0.1	5.7
FTP72UDDS	0.0	0.4	0.4	0.0	0.3	-0.8	0.0	0.2	0.0	0.2	2.3	0.0	0.2	5.2
WLTC Mdl	0.0	0.3	0.0	0.0	0.2	-0.9	0.0	0.2	0.0	0.2	2.2	0.0	0.2	4.9
SC03	0.0	1.1	0.6	0.0	0.4	-0.7	0.0	0.3	0.0	0.3	2.1	0.0	0.3	4.7
NYCC	-0.2	4.3	3.8	-0.2	0.3	-0.1	-0.2	0.3	-0.2	0.3	3.2	-0.2	0.3	7.5
Artemis URBAN	-0.1	3.2	4.5	-0.1	0.9	0.1	-0.1	0.4	-0.1	0.4	2.6	-0.1	0.4	6.3
NEDC	0.0	0.3	-1.3	0.0	0.2	-1.3	0.0	0.2	0.0	0.2	2.2	0.0	0.2	4.7
WLTC Hgh	0.0	0.2	-1.2	0.0	0.2	-1.1	0.0	0.2	0.0	0.2	1.8	0.0	0.2	3.8
Artemis RURAL	0.0	1.3	-0.3	0.0	0.5	-0.8	0.0	0.5	0.0	0.5	1.7	0.0	0.5	3.7
EUDC	0.0	0.2	-1.9	0.0	0.2	-1.2	0.0	0.2	0.0	0.2	1.7	0.0	0.2	3.5
UCLA92	0.0	6.1	2.1	0.0	1.3	-0.3	0.0	0.5	0.0	0.5	1.8	0.0	0.5	4.1
HWFET	0.0	0.3	-2.2	0.0	0.2	-1.3	0.0	0.2	0.0	0.2	1.6	0.0	0.2	3.4
REP05	0.0	10.4	-0.9	0.0	3.9	-0.8	0.0	1.5	0.0	0.4	1.3	0.0	0.4	2.8
WLTC ExtrHgh	0.0	0.2	-1.5	0.0	0.2	-0.9	0.0	0.2	0.0	0.2	1.3	0.0	0.2	2.7
US06	0.1	13.0	-0.3	0.0	3.7	-0.7	0.0	1.4	0.0	0.4	1.2	0.0	0.4	2.7
Artemis MW130	0.0	0.5	-0.9	0.0	0.4	-0.8	0.0	0.4	0.0	0.4	1.2	0.0	0.4	2.5
Artemis MW150	0.0	1.6	-1.0	0.0	0.4	-0.8	0.0	0.4	0.0	0.4	1.2	0.0	0.4	2.4

6.3 Energy consumption sensitivity to vehicle mass

As a comparison, the consequence on energy consumption per driven distance for different vehicle masses is also studied, see Table 6.4 for the City car and Table 6.5 for the Highway car. The reason is that the change in mass was disregarded in the study of the energy consequence due to resizing of the powertrain. It is however likely that a system resizing will also have an affect on the total mass of the vehicle.

As can be seen, the energy consumption per distance is fairly linearly dependent on vehicle mass. For a change of $100\,kg$ ($8.3\,\%$) for the City car, the change is $6-8\,\%$ for the Urban cycles, $3-5\,\%$ for the Rural cycles and $2-3\,\%$ for the Highway cycles. For a change of $100\,kg$ ($5.9\,\%$) for the Highway car, the change in energy consumption per distance is $4-6\,\%$ for the Urban cycles, $3-4\,\%$ for the Rural cycles and $2-3\,\%$ for the Highway cycles.

Table 6.4 Table over simulation results of different vehicle mass for the City car.

	-300 (kg)		-200 (kg)		-100 (kg)		City base	+100 (kg)		+200 (kg)		+300 (kg)	
Test Cycles	Max speed diff. (km/h)	Rel. Cons. (%)	Max speed diff. (km/h)	Rel. Cons. (%)	Max speed diff. (km/h)	Rel. Cons. (%)	Max speed diff. (km/h)	Max speed diff.	Rel. Cons. (%)	Max speed diff. (km/h)	Rel. Cons. (%)	Max speed diff. (km/h)	Rel. Cons. (%)
ECE	0.1	-20.7	0.1	-13.9	0.1	-7.0	0.2	0.2	7.1	0.2	14.2	0.2	21.4
WLTC Low	0.1	-21.5	0.1	-14.4	0.1	-7.3	0.1	0.1	7.4	0.1	14.8	0.2	22.3
jpjc08	0.1	-16.6	0.2	-11.1	0.2	-5.6	0.2	0.2	5.6	0.2	11.3	0.3	17.1
FTP72UDDS	0.2	-17.0	0.2	-11.4	0.2	-5.7	0.2	0.2	5.8	0.3	11.6	0.3	17.5
WLTC Mdl	0.1	-16.7	0.1	-11.2	0.1	-5.6	0.1	0.2	5.7	0.2	11.4	0.2	17.2
SC03	0.2	-16.8	0.3	-11.3	0.3	-5.7	0.3	0.4	5.7	0.4	11.5	0.4	17.3
NYCC	0.2	-24.8	0.2	-16.7	0.2	-8.4	0.3	0.3	8.5	0.3	17.2	0.3	25.9
Artemis URBAN	0.3	-23.1	0.3	-15.5	0.3	-7.8	0.4	0.4	7.9	0.4	16.0	0.8	24.1
NEDC	0.2	-12.7	0.2	-8.5	0.2	-4.3	0.2	0.2	4.3	0.2	8.6	0.2	13.0
WLTC Hgh	0.1	-11.3	0.1	-7.6	0.1	-3.8	0.1	0.1	3.8	0.1	7.6	0.2	11.5
Artemis RURAL	0.3	-12.5	0.3	-8.4	0.3	-4.2	0.4	0.4	4.2	0.4	8.5	0.4	12.9
EUDC	0.1	-9.7	0.2	-6.5	0.2	-3.2	0.2	0.2	3.3	0.2	6.5	0.2	9.8
UCLA92	0.3	-14.3	0.3	-9.6	0.3	-4.8	0.3	0.4	4.9	0.5	9.9	1.1	15.0
HWFET	0.1	-9.0	0.1	-6.0	0.1	-3.0	0.1	0.1	3.0	0.2	6.1	0.2	9.1
REP05	0.4	-8.2	0.4	-5.5	0.9	-2.8	1.7	2.6	2.8	3.9	5.6	3.7	8.4
WLTC ExtrHgh	0.1	-6.5	0.1	-4.4	0.1	-2.2	0.1	0.1	2.2	0.2	4.4	0.2	6.7
US06	0.5	-8.8	0.8	-5.9	1.0	-3.0	1.6	2.4	3.0	3.4	5.9	3.9	8.7
Artemis MW130	0.3	-6.5	0.3	-4.4	0.4	-2.2	0.4	0.5	2.2	0.5	4.5	0.6	6.8

Table 6.5 Table over simulation results of different vehicle mass for the Highway car.

	-300 (kg)		-200 (kg)		-100 (kg)		Highway Base	+100 (kg)		+200 (kg)		+300 (kg)	
Test Cycles	Max speed diff. (km/h)	Rel. Cons. (%)	Max speed diff. (km/h)	Rel. Cons. (%)	Max speed diff. (km/h)	Rel. Cons. (%)	Max speed diff. (km/h)	Max speed diff. (km/h)	Rel. Cons. (%)	Max speed diff. (km/h)	Rel. Cons. (%)	Max speed diff. (km/h)	Rel. Cons. (%)
ECE	0.1	-15.5	0.1	-10.4	0.1	-5.2	0.2	0.2	5.3	0.2	10.5	0.2	15.9
WLTC Low	0.2	-16.1	0.2	-10.7	0.2	-5.4	0.2	0.2	5.4	0.2	10.9	0.2	16.4
jpjc08	0.2	-13.1	0.2	-8.8	0.2	-4.4	0.2	0.2	4.4	0.2	8.9	0.2	13.3
FTP72UDDS	0.2	-13.4	0.2	-8.9	0.2	-4.5	0.2	0.2	4.5	0.2	9.0	0.3	13.6
WLTC Mdl	0.2	-13.2	0.2	-8.8	0.2	-4.4	0.2	0.2	4.4	0.2	8.9	0.2	13.4
SC03	0.3	-13.3	0.3	-8.9	0.3	-4.4	0.3	0.4	4.5	0.4	9.0	0.4	13.5
NYCC	0.3	-17.9	0.3	-12.0	0.3	-6.0	0.3	0.4	6.1	0.4	12.2	0.4	18.4
Artemis URBAN	0.3	-17.0	0.3	-11.4	0.4	-5.7	0.4	0.4	5.8	0.4	11.6	0.5	17.4
NEDC	0.1	-10.5	0.2	-7.0	0.2	-3.5	0.2	0.2	3.5	0.2	7.1	0.2	10.7
WLTC Hgh	0.2	-9.4	0.2	-6.3	0.2	-3.2	0.2	0.2	3.2	0.2	6.4	0.2	9.6
Artemis RURAL	0.4	-10.4	0.5	-6.9	0.5	-3.5	0.5	0.6	3.5	0.6	7.0	0.6	10.6
EUDC	0.1	-8.2	0.2	-5.5	0.2	-2.8	0.2	0.2	2.8	0.2	5.5	0.2	8.3
UCLA92	0.4	-11.6	0.4	-7.8	0.5	-3.9	0.5	0.5	3.9	0.6	7.9	0.7	11.9
HWFET	0.1	-7.7	0.2	-5.1	0.2	-2.6	0.2	0.2	2.6	0.2	5.2	0.2	7.7
REP05	0.4	-7.2	0.4	-4.8	0.8	-2.4	1.5	2.1	2.4	2.7	4.9	3.3	7.3
WLTC ExtrHgh	0.2	-5.8	0.2	-3.9	0.2	-1.9	0.2	0.2	2.0	0.2	3.9	0.2	5.9
US06	0.4	-7.7	0.4	-5.2	0.7	-2.6	1.4	2.0	2.6	2.6	5.2	3.1	7.7
Artemis MW130	0.3	-5.8	0.4	-3.9	0.4	-1.9	0.4	0.4	1.9	0.5	3.9	0.5	5.8

Chapter 7

Conclusions and future work

7.1 Conclusions

In this thesis, various drive cycles, legislative, official real-world and measured within the frame of the project, have been studied and characterized in terms of speed and acceleration cycle parameters, as well as acceleration and speed distribution. The objective was to assess typical vehicle usage on different road types, but also to study the implication on vehicle energy consumption due to the drive cycle's characteristics. For this evaluation, three reference vehicles were designed after different set performance requirements, with data on existing BEVs as a frame of reference. An available traction motor, power electronic module and battery cell were utilized, where the motor was scaled by active length. Finally, the consequence of downsizing the electric drive system in terms of energy consumption and performance was also studied.

It was revealed that most of the legislative drive cycles were developed a few decades ago, when the performance of passenger cars were generally lower than today's cars, hence the drive cycles are not fully representative of today's typical driving. Through comparison with measured drive cycles, it was found that the measured cycles report higher peak levels of acceleration for a certain speed level. On the other hand, when studying the relative time spent at certain levels of acceleration and speed, the measured cycles spend only slightly more time at higher levels of acceleration compared to the official cycles, at least on average over a group of similar cycles.

From a literature study various estimation methods of vehicle frontal area were found. These were compared to a few found manufacturer data regarding three vehicle models. It was found that a suitable estimation of the area is $84\,\%$ of the product of vehicle track width and height. Furthermore, different, often referred to, estimations regarding the speed dependency of tire rolling resistance were found to deviate from each other rather much.

Through the mapping of existing BEVs it was found that there is a wide spread regarding their top speed and acceleration performance, as well as driving range, which made a

categorization ambiguous.

The reference cars consists of a City car, a Highway car and a Sport car. When comparing their road load per mass while driving at a constant speed, it was found that the City car has a stronger speed dependency than the other two, due to its relatively higher aerodynamic drag. This causes it to have a higher road load relative to its mass for speed levels greater than $66\,km/h$, compared to the Highway and Sport cars.

The needed wheel force and power, due to performance requirements regarding top speed, time to accelerate to $100\,km/h$, take off at $25\,\%$ grade, and driving at a high grade in a high speed were studied. In a comparison it turned out that the acceleration requirement was the dominating one, hence the only one considered when specifying the needed output from the powertrain.

Furthermore, it was found that the time to accelerate can be achieved with various combinations of initial maximum force and maximum power. For a higher initial maximum force, the needed maximum power to reach $100\,km/h$ at the specified time is lower. This will lead to shorter time to accelerate to $50\,km/h$, but longer time to accelerate from 50 to $100\,km/h$. The conclusion is that a requirement of time to accelerate from 0 to $100\,km/h$ is not enough to describe the desired performance of a vehicle, there must also be an expressed requirement on low and high speed performance, respectively.

Another important finding is that the time resolution of the speed time traces, that defines the official cycles, is relatively low compared to the rate of change of speed. Then the estimated correlated acceleration is highly dependent on the method used for calculation, whether it is a forward and backward looking method or a simpler just backward looking method. The consequence on cycle energy consumption per distance is then highly sensitive to the method used for estimation of acceleration, where the difference may be as large as $15\,\%$ for some cycles.

Within the same road-type category, those cycles that spend most time at high acceleration and speed levels are those who consume the most energy per distance during propulsion. At the same time, in these cycles more braking energy is also available for regenerative braking, which makes the total energy consumption a bit less sensitive to speed fluctuations and high acceleration levels, still the tendency is a higher energy consumption per driven distance.

As an example, it was noted that two cycles, Artemis Urban and WLTC Low, have similar speed parameters such as maximum and average speed and time share at low speed, although their speed time traces are very different, where the Artemis Urban has many more speed fluctuations as well as higher acceleration parameters (maximum, minimum and average, as well as more time spent at higher acceleration levels for the same speed value and time share at acceleration $1 - 2\,m/s^2$). These differences lead to $28\,\%$ higher net battery energy consumption per distance for the Artemis Urban cycle, compared to the WLTC Low, for the City car.

By down-scaling the electric drive system of the City car by $40\,\%$, the time to accelerate to $100\,km/h$ becomes $87\,\%$ longer, while an up scaling by $40\,\%$ results in a decrease of the acceleration time by $32\,\%$. For the $40\,\%$ down-scaling, the energy per driven distance

for Urban cycles increase about $3-6\,\%$, while for a $50\,\%$ down scaling the increase in energy consumption is $5-11\,\%$. In both cases, the vehicle is only able to follow 5 of the 8 Urban cycles, due to limited acceleration capability. When up scaling the system by $40\,\%$ the increase in energy consumption per distance for Urban and Highway cycles is $1-3\,\%$.

By down-scaling the electric drive system of the Highway car by $40\,\%$, the time to accelerate to $100\,km/h$ becomes $70\,\%$ longer, while an up scaling by $40\,\%$ results in a decrease of the acceleration time by $30\,\%$. For the $40\,\%$ down-scaling, the energy per driven distance decrease by less than $1\,\%$ for some of the Urban cycles and increase by about $0.5\,\%$ for others. Also, the vehicle is only able to follow 5 of the 8 Urban cycles, due to limited acceleration capability. Furthermore, for the $40\,\%$ down-scaling, the Highway car is able to follow 3 of the 6 Highway cycles, and then the energy consumption per distance is decreased by $1-2\,\%$. When up scaling the system by $40\,\%$ the increase in energy consumption per distance for Urban cycles increases by $5-8\,\%$, and for the Highway cycles it increases by around $3\,\%$.

The conclusion is that a much smaller change in energy consumption can be seen for the down-scaled Highway car's drive system compared to a down scaling of similar relation of the City car's drive system. When it comes to the up scaling the results show a larger change for the Highway car.

Finally, the consequence on energy consumption per distance for different vehicle masses, indicate a relatively important linear relation. As an example, a decrease of the City car mass by $8.3\,\%$, leads to a decrease of the energy consumption per distance by $6-8\,\%$ for the Urban cycles, $3-5\,\%$ for the Rural cycles and $2-3\,\%$ for the Highway cycles. An increase in vehicle weight by the same factor instead cause increases in energy consumption of the same levels. Similar results can also be seen for the Highway car.

7.2 Future Work

As the presented results are valid under the assumptions made and models used during the study, perhaps it would be valuable to assess the consequence on energy consumption while improving the level of detail regarding some of the assumptions and models used. For example, by modeling the rolling resistance as a function of speed, and by implementing a wheel slip model, the change in energy consumption could be assessed in order to be able to draw conclusions on the necessary level of detail in the modeling of these phenomena. In general, a sensitivity study on the influence on energy consumption due to different values of vehicle frontal areas and aerodynamic drag coefficients would be interesting.

The results show that the energy efficiencies of the different powertrain components are rather similar. In order to increase the validity of the results in the study, perhaps also the transmission losses could be modeled as depending on load level and speed, as were the case with the other components.

The results of the mass sensitivity study show that the change in energy consumption per distance due to a change in mass may sometimes be in relation to the change in energy

consumption due to a rescaling. Therefore, as the size of the drive system is changed, the effect on the vehicle mass should perhaps also be considered, in order to improve the detail level of the results.

Furthermore, the loss modeling of the electric machine was done using constant machine parameters. By modeling the machine in a FEM calculation software, load dependent machine parameters can be extracted and utilized.

Also the modeling of the battery losses and voltage trajectory could be improved by adding RC-links, although then perhaps a different battery cell should be modeled where more data is available.

Furthermore, it would be interesting to deepen the study of the relation between the cycle parameters regarding speed and acceleration on the one hand and BEV energy consumption per distance on the other.

Apart from energy consumption, aspects such as life cycle cost and environmental effects of the BEV powertrain design choices, are of vital importance and should be included in future studies.

Moreover, this study has ignored thermal aspects in the powertrain design and evaluation, while these effects are highly important. As a continuation of the work, thermal effects could be considered, in order to be able to draw conclusions on necessary cooling and transient performance of the electric machine with respect to the different drive cycles. Different cooling strategies can also be developed, e.g. one for summer and one for winter, where in the winter the losses could be used to heat the drivers compartment. Another possibility is to consider an active cooling strategy during driving.

Finally, the derived drive cycles from the measured GPS and accelerometer signals, could perhaps be improved using more advanced filtering techniques.

References

[1] E. Ericsson. (2000) Driving pattern in urban areas - descriptive analysis and initial prediction model. Lund Institue of Technology, Department of Technology and Society, Traffic Planning. Accessed 2013-12-11. [Online]. Available: http://www.lunduniversity.lu.se/o.o.i.s?id=12683&postid=627123

[2] (2006, dec) Final technical support document, fuel economy labeling of motor vehicle revisions to improve calculation of fuel economy estimates. US Environmental Protection Agency (EPA), Office of Transportation and Air Quality. Accessed 2013-12-09. [Online]. Available: http://www.epa.gov/carlabel/documents/420r06017.pdf

[3] E. Ericsson, "Independent driving pattern factors and their influence on fuel-use and exhaust emission factors," *Transportation Research Part D: Transport and Environment*, vol. 6, no. 5, pp. 325 – 345, 2001. [Online]. Available: http://www.sciencedirect.com/science/article/pii/S1361920901000037

[4] S. Samuel, L. Austin, and D. Morrey, "Automotive test drive cycles for emission measurement and real-world emission levels - a review," *Proceedings of the Institution of Mechanical Engineers, Part D: Journal of Automobile Engineering*, vol. 216, no. 7, pp. 555–564, 2002, cited By (since 1996)34. [Online]. Available: http://www.scopus.com/inward/record.url?eid=2-s2.0-0036964445&partnerID=40&md5=7dfe8159f1a6d5b00f7a8e1153ee5aa4

[5] F. L. Berr, A. Abdelli, and R. Benlamine, "Sensitivity study on the design methodology of an electric vehicle," 04 2012. [Online]. Available: http://dx.doi.org/10.4271/2012-01-0820

[6] A. Abdelli, F. L. Berr, and R. Benlamine, "Efficient design methodology of an all-electric vehicle powertrain using multi-objective genetic optimization algorithm," 04 2013. [Online]. Available: http://dx.doi.org/10.4271/2013-01-1758

[7] L. Chen, J. Wang, P. Lazari, and X. Chen, "Optimizations of a permanent magnet machine targeting different driving cycles for electric vehicles," in *Electric Machines Drives Conference (IEMDC), 2013 IEEE International*, May 2013, pp. 855–862.

[8] R. Sehab, B. Barbedette, and M. Chauvin, "Electric vehicle drivetrain: Sizing and validation using general and particular mission profiles," in *Mechatronics (ICM), 2011 IEEE International Conference on*, April 2011, pp. 77–83.

[9] M. Ehsani, K. Rahman, and H. Toliyat, "Propulsion system design of electric and hybrid vehicles," *Industrial Electronics, IEEE Transactions on*, vol. 44, no. 1, pp. 19–27, Feb 1997.

[10] M. Pourabdollah, “On optimization of plug-in hybrid electric vehicles,” Thesis for the degree of Licentiate of Engineering, Chalmers University of Technology, 2012. [Online]. Available: http://publications.lib.chalmers.se/records/fulltext/170631/170631.pdf

[11] A. Ayman, G. Singh, S. Singh, S. Fellah, and A. Rousseau. (2009) Impact of real world drive cycles on phev fuel efficiency and cost for different powertrain and battery characteristics. Argonne National Laboratory, USA. [Online]. Available: http://www.transportation.anl.gov/pdfs/HV/564.pdf

[12] J. Kwon, J. Kim, E. Fallas, S. Pagerit, and A. Rousseau, “Impact of drive cycles on phev component requirements,” 04 2008. [Online]. Available: http://dx.doi.org/10.4271/2008-01-1337

[13] J. M. Miller, *Propulsion Systems for Hybrid Vehicles*. Institution of Engineering and Technology, London, United Kingdom, 2010. [Online]. Available: http://digital-library.theiet.org/content/books/rn/pbrn007e

[14] T. D. Gillespie, *Fundamentals Of Vehicle Dynamics*, 1st ed. Society of Automotive Engineers, Inc., 1992.

[15] W.-H. Hucho, Ed., *Aerodynamics of Road Vehicles, From Fluid Mechanics to Vehicle Engineering*, 4th ed. Society of Automotive Engineers, Inc., 1998.

[16] (2014, jan) Density of air. English Wikipedia, the free encyclopedia. Accessed 2014-01-03. [Online]. Available: http://en.wikipedia.org/wiki/Density_of_air

[17] T. C. Moore and A. B. Lovins. (1995) Vehicle design strategies to meet and exceed pngv goals. SAE Technical Paper 951906. [Online]. Available: http://citeseerx.ist.psu.edu/viewdoc/download?rep=rep1&type=pdf&doi=10.1.1.199.7444

[18] J. Y. Wong, Ed., *Theory of Ground Vehicles*, 4th ed. John Wiley & Sons , Inc., 2008.

[19] R. B. GmbH, *Automotive Handbook*, 8th ed. John Wiley Sons, 2011.

[20] (2006, feb) The pneumatic tire, dot hs 810 561. NHTSA, National Highway Traffic Safety Administration, U.S. Department of Transportation. Accessed 2014-02-19. [Online]. Available: http://www.nhtsa.gov/staticfiles/safercar/pdf/PneumaticTire_HS-810-561.pdf

[21] L. Guzzella and A. Sciarretta, *Vehicle Propulsion Systems - Introduction to Modeling and Optimization*, 2nd ed. Springer, 2007.

[22] M. Ehsani, Y. Gao, and A. Emadi, *Modern Electric, Hybrid Electric, and Fuel Cell Vehicles: Fundamentals, Theory, and Design*, 2nd ed. CRC Press, Taylor & Francis Group., 2010.

[23] (2006) Tires and passenger vehicle fuel economy, informing consumers, improving performance, transportation research board special report 286. Transportation Research Board. Accessed 2014-02-19. [Online]. Available: http://onlinepubs.trb.org/onlinepubs/sr/sr286.pdf

[24] J. Hendershot and T. Miller, *Design of Brushless Permanent-Magnet Machines*. Motor Design Books LLC, 2010.

[25] A. Rabiei, "Energy efficiency of an electric vehicle propulsion inverter using various semiconductor technologies," Thesis for the degree of Licentiate of Engineering, Chalmers University of Technology, 2013. [Online]. Available: http://publications.lib.chalmers.se/records/fulltext/187097/187097.pdf

[26] O. Wallmarki, "On control of permanent-magnet synchronous motors in hybrid-electric vehicle applications," Thesis for the degree of Licentiate of Engineering, Chalmers University of Technology, 2004. [Online]. Available: http://publications.lib.chalmers.se/records/fulltext/2386.pdf

[27] A. Wintrich, U. Nicolai, W. Tursky, and T. Reimann. (2011) Application manual power semiconductors. Semikron International GmbH. [Online]. Available: http://www.semikron.com/skcompub/en/SEMIKRON_Application_Manual_Power_Semiconductors_.pdf

[28] O. Josefsson, "Energy efficiency comparison between two-level and multilevel inverters for electric vehicle applications," Thesis for the degree of Licentiate of Engineering, Chalmers University of Technology, 2013. [Online]. Available: http://publications.lib.chalmers.se/records/fulltext/174182/174182.pdf

[29] V. Johnson, "Battery performance models in {ADVISOR}," *Journal of Power Sources*, vol. 110, no. 2, pp. 321 – 329, 2002. [Online]. Available: http://www.sciencedirect.com/science/article/pii/S0378775302001945

[30] T. Reddy and D. Linden, *Handbook of batteries*, 4th ed. Mcgraw-Hill's, 2011.

[31] J. Croes and S. Iqbal. D2.1 document 1: Literature survey: Gearlosses. ESToMaD, Energy Software Tools for Sustainable Machine Design. Accessed 2014-04-25. [Online]. Available: http://www.estomad.org/documenten/D2_1/D2_1%20Document%201%20%20Literature%20survey%20gears.pdf

[32] E. Nam. (2004) Advanced technology vehicle modeling in pere. EPA, United States Environmental Protection Agency, Office of Transportation and Air Quality. Accessed 2014-04-15. [Online]. Available: http://www.epa.gov/otaq/models/ngm/420d04002.pdf

[33] T. Hofman and C. H. Dai, "Energy efficiency analysis and comparison of transmission technologies for an electric vehicle," in *Vehicle Power and Propulsion Conference (VPPC), 2010 IEEE*, Sept 2010, pp. 1–6.

[34] M. A. M. Chris Mi and D. W. Gao, *Hybrid Electric Vehicles: Principles and Applications with Practical Perspectives*, 1st ed. John Wiley & Sons , Inc., 2011.

[35] F. Sprei, S. Karlsson, and J. Holmberg, "Better performance or lower fuel consumption. technological development in the swedish new-car fleet..." *Transportation Research Part D: Transport and Environment*, vol. 13:2, s. 75-85, 2008.

[36] S. Karlsson. (2013) The swedish car movement data project final report. Division of Physical resource Theory, Chalmers University of Technology. [Online]. Available: http://publications.lib.chalmers.se/records/fulltext/187380/local_187380.pdf

[37] H. Watson. (1978) Vehicle driving patterns and measurement methods for energy and emission assessment. Bureau of Transport Economics, Canberra. Accessed 2014-01-15. [Online]. Available: http://www.bitre.gov.au/publications/1978/files/op_030.pdf

[38] I. M. Berry, "The effects of driving style and vehicle performance on the real-world fuel consumption of u.s. light-duty vehicles," Master of Science in Mechanical Engineering and Master of Science in Technology and Policy, Massachusetts Institute of Technology, feb 2010, accessed 2011-12-20. [Online]. Available: http://web.mit.edu/sloan-auto-lab/research/beforeh2/files/IreneBerry_Thesis_February2010.pdf

[39] (1995, jan) Final technical report on aggressive driving behavior for the revised federal test procedure notice of proposed rulemaking. US Environmental Protection Agency (EPA), Office of Transportation and Air Quality and U.S. Department of Transportation, National Highway Traffic Safety Administration (NHTSA). Accessed 2014-01-21. [Online]. Available: http://www.epa.gov/OMS/regs/ld-hwy/ftp-rev/ftp-us06.pdf

[40] (2011) Final rule, federal register, vol. 76, no. 129, part ii, 40 cfr parts 85, 86 and 600. EPA, United States Environmental Protection Agency, Office of Transportation and Air Quality. Accessed 2013-12-10. [Online]. Available: www.gpo.gov/fdsys/pkg/FR-2011-07-06/pdf/2011-14291.pdf

[41] Council. (1970, march) Council directive 70/220/eec of 20 march 1970 on the approximation of the laws of the member states relating to measures to be taken against air pollution by gases from positive-ignition engines of motor vehicles. Official Journal of the European Communities. Accessed 2014-01-15. [Online]. Available: http://ec.europa.eu/enterprise/sectors/automotive/documents/directives/motor-vehicles/

[42] (2014, january) Emission standards, summary of wolrdwide engine emission standards. DieselNet, Ecopint Inc., Canada. Accessed 2014-01-16. [Online]. Available: http://www.dieselnet.com/standards/

[43] A. Faiz, C. S. Weaver, and M. P. Walsh. (1996) Air pollition from motor vehicles - standards and technolgies fro controlling emissions. The International Bank for Reconstruction and Development, The World Bank, Washington, D.C. Accessed 2014-01-15. [Online]. Available: http://www.un.org/esa/gite/iandm/faizpaper.pdf

[44] M. Andre. (2004, jun) Real-world driving cycles for measuring cars pollutant emissions, part a: The artemis european driving cycles. ARTEMIS - Assessment and reliability of transport emission models and inventory systems. Accessed 2014-01-10. [Online]. Available: http://inrets.fr/ur/lte/publi-autresactions/fichesresultats/ficheartemis/road3/method31/Artemis_cycles_report_LTE0411.pdf

[45] (2013, nov) Development of a world-wide worldwide harmonized light duty driving test cycle (wltc), draft technical report. United Nations Economic Commission for Europe, Working Party on Pollution and Energy (GRPE), Worldwide harmonized Light vehicles Test Procedure (WLTP), WLTP Sub-group on the Development of the Harmonized driving Cycle (DHC). Accessed 2013-11-14. [Online]. Available: https://www2.unece.org/wiki/download/attachments/15237269/WLTP-DHC-draft_technical_report_ver131101-4.doc?api=v2

[46] (2013, september) Speed limits by country. English Wikipedia, the free encyclopedia. Accessed 2013-09-13. [Online]. Available: http://en.wikipedia.org/wiki/Speed_limits_by_country

[47] (2012) Eu transport in figures - statistical pocketbook 2012. European Commission Transport. Accessed 2013-09-13. [Online]. Available: http://ec.europa.eu/transport/facts-fundings/statistics/doc/2012/pocketbook2012.pdf

[48] (2014, january) Speed. The Insurance Institute for Highway Safety (IIHS). Accessed 2014-01-10. [Online]. Available: http://www.iihs.org/iihs/topics/laws/speedlimits?topicName=speed#tableData

[49] (2009, aug) Proposal for wltc methodology and guidelines for in-use data collection, proposed by uk and japan dhc group under grpe/wltp informal group. United Nations Economic Commission for Europe, Working Party on Pollution and Energy (GRPE), Worldwide harmonized Light vehicles Test Procedure (WLTP), WLTP Sub-group on the Development of the Harmonized driving Cycle (DHC). Accessed 2014-01-10. [Online]. Available: http://www.unece.org/fileadmin/DAM/trans/doc/2009/wp29grpe/WLTP-DHC-01-04e.pdf

[50] (2011, may) Proposal for the threshold vehicle speed of low/middle/high(/extra-high) phase. United Nations Economic Commission for Europe, Working Party on Pollution and Energy (GRPE), Worldwide harmonized Light vehicles Test Procedure (WLTP), WLTP Sub-group on the Development of the Harmonized driving Cycle (DHC). Accessed 2014-01-10. [Online]. Available: http://www.unece.org/fileadmin/DAM/trans/doc/2011/wp29grpe/WLTP-DHC-07-02e.pdf

[51] (2013, feb) Dynamometer drive schedules. EPA, United States Environmental Protection Agency, Transportation and Air Quality. Accessed 2011-12-19. [Online]. Available: http://www.epa.gov/nvfel/testing/dynamometer.htm#vehcycles/

[52] (2012, may) Regulation no 101, official journal of european union. Economic Commission for Europe of the United Nations. Accessed 2012-10-31. [Online]. Available: http://eur-lex.europa.eu/LexUriServ/LexUriServ.do?uri=OJ:L:2012:138:0001:0077:en:PDF

[53] (2013, jan) Finalized test cycle, wltc. UNECE, United Nations Economic Commission for Europe, Worldwide harmonized Light vehicles Test Procedure (WLTP). Accessed 2013-11-14. [Online]. Available: https://www2.unece.org/wiki/download/attachments/5801079/WLTP-DHC-16-06e_rev.xlsx?api=v2

[54] (2012) Krav för vägars och gators utformning. Trafikverket. Accessed 2013-10-01. [Online]. Available: http://www.dot.state.fl.us/rddesign/qa/Data/AASHTO-InterstateDesignStandards.pdf

[55] (2005) A policy on design standards interstate system. American Association of State Highway and Transport Officials. Accessed 2013-10-01. [Online]. Available: http://publikationswebbutik.vv.se/shopping/ShowItem.aspx?id=5848

[56] (2013) San fransisco, ca, usa, streets colored by slope. Trafikverket. Accessed 2013-10-01. [Online]. Available: https://pmsv3.trafikverket.se/Pages/EnkelSok/EnkelSokView.aspx

[57] (2009, nov) San fransisco, ca, usa, streets colored by slope. Data Pointed. Accessed 2013-10-01. [Online]. Available: http://www.datapointed.net/visualizations/maps/san-francisco/streets-slope/

[58] N. S. Pearre, W. Kempton, R. L. Guensler, and V. V. Elango, "Electric vehicles: How much range is required for a day's driving?" *Transportation Research Part C: Emerging Technologies*, vol. 19, no. 6, pp. 1171 – 1184, 2011. [Online]. Available: http://www.sciencedirect.com/science/article/pii/S0968090X1100012X

[59] (2011) Summary of travel trends: 2009 national household travel survey. US Department of Transportation, Federal Highway Administration. Accessed 2013-10-09. [Online]. Available: http://nhts.ornl.gov/2009/pub/stt.pdf

[60] (2007) Res 2005-2006, den nationella resvaneundersökningen. SIKA Statistik, Statens institut för kommunikationsanalys. Accessed 2010-12-21. [Online]. Available: http://trafa.se/PageDocuments/ss_2007_19_1.pdf

[61] (2007) Körsträckor øor 2006. SIKA Statistik, Statens institut för kommunikationsanalys. Accessed 2010-12-21. [Online]. Available: http://www.scb.se/Statistik/TK/_dokument/Korstr_2006.pdf

[62] (2012) Driving and parking patterns of european car drivers, a mobility survey. European Commission. Accessed 2013-10-10. [Online]. Available: http://publications.jrc.ec.europa.eu/repository/handle/111111111/26994/1/

[63] (2010) Ample driving range for everyday deeds. Nissan Motor Corporation. Accessed 2013-04-02. [Online]. Available: http://www.newsroom.nissan-europe.com/download/media/specialfile/41486_3_6.aspx

[64] S. Karlsson and E. Jonson, "The importance of car movement data for determining design, viability and potential of phevs," *Proceedings of International Advanced Mobility Forum (IAMF) 2011, Geneva Switzerland*, 2011.

[65] L.-H. Kullingsjö and S. Karlsson. (2012) The swedish car movement data project. Division of Physical resource Theory, Chalmers University of Technology. [Online]. Available: http://publications.lib.chalmers.se/records/fulltext/local_165497.pdf

[66] (2007) Resvanor i göteborgsregionen 2005. Göteborgs Stad, Vägverket and Västtrafik. Accessed 2011-10-11. [Online]. Available: http://www2.trafikkontoret.goteborg.se/resourcelibrary/Resvanor.pdf

[67] J. Krumm, "How people use their vehicles: Statistics from the 2009 national household travel survey," 04 2012. [Online]. Available: http://dx.doi.org/10.4271/2012-01-0489

[68] (2007) Axp course design - baseline driving statistics. Automotive Xprice. Accessed 2011-10-08. [Online]. Available: http://www.progressiveautoxprize.org/files/downloads/auto/AXP_FHWA_driving_stats.pdf

[69] R. van Haaren. (2012) Assessment of electric car's range requirements and usage pattern based on driving behavior recorded in the national household travel survey of 2009. Automotive Xprice. Accessed 2011-10-07. [Online]. Available: http://www.solarjourneyusa.com/HowFarWeDrive_v1.3.pdf

[70] (1999, oct) 1999 ev america technical specifications. Electric Transportation Applications. Accessed 2014-02-04. [Online]. Available: http://avt.inl.gov/fsev.shtml

[71] (2014) Igbt modules up to 600v, 650v. Infineon. Accessed 2014-03-20. [Online]. Available: http://www.infineon.com/cms/en/product/power/igbt/igbt-module/igbt-module-600v-650v/channel.html?channel=ff80808112ab681d0112ab69e70c0364

[72] (2014, jan) Aesc home page. AESC, Automotive Energy Supply Corporation. Accessed 2014-03-14. [Online]. Available: http://www.eco-aesc-lb.com/en/aboutus/company/

[73] (2011) 2011 nissan leaf - vin 0356. Idaho National Laboratory (INL), Advanced Vehicle Testing Activity (AVTA). Accessed 2014-02-04. [Online]. Available: http://avt.inel.gov/pdf/fsev/batteryleaf0356.pdf

[74] J. Hellsing, "Design and otimization of a permanent magnet motor for a hybrid electric vehicle," Licentiate of Engineering, Technical Report No. 282L, Chalmers University of Technology, mar 1998.

[75] J. Lindström, "Development of an experimental permanent-magnet motor drive," Licentiate of Engineering, Technical Report No. 312L, Chalmers University of Technology, apr 1999.

[76] A. Rabiei, T. Thiringer, and J. Lindberg, "Maximizing the energy efficiency of a pmsm for vehicular applications using an iron loss accounting optimization based on nonlinear programming," in *Electrical Machines (ICEM), 2012 XXth International Conference on*, Sept 2012, pp. 1001–1007.

[77] M.-F. Hsieh, Y.-C. Hsu, D. Dorrell, and K.-H. Hu, "Investigation on end winding inductance in motor stator windings," *Magnetics, IEEE Transactions on*, vol. 43, no. 6, pp. 2513–2515, June 2007.

[78] (2014, feb) Electric car use by country. English Wikipedia, the free encyclopedia. Accessed 2014-02-11. [Online]. Available: http://en.wikipedia.org/wiki/Electric_car_use_by_country

[79] (2014, jan) The 100,000th nissan leaf owner. Nissan Motor Corporation. Accessed 2014-01-21. [Online]. Available: http://reports.nissan-global.com/EN/?p=14296

Appendix A

Vehicle data

According to [78], some of the top selling BEV models around the world so far, are the Nissan Leaf (with over one hundred thousand cars sold up until January 2014, according to [79]), Tesla Model S, Mitsubishi i-Miev, Peugeot iOn, Citröen C-Zero, Smart-for-two and the Renault Zoe. As a frame of reference in this study, data on these vehicles and a number of additional vehicle models (totally 28 models) have been gathered from different sources, and is presented in the following sections.

A.1 Data on existing BEVs

Data on found existing BEVs are presented in Table A.1, A.3 and A.5, with associated references in A.2, A.4 and A.6 for the three data tables respectively.

Table A.1 Table over collected size related data on selected BEVs.

Brand	Model	Model year	Seats	Class	Curb weight (kg)	Max cargo (kg)	Track width (cm)	Width (cm)	Height (cm)	Front Area (m^2)	Air drag coeff. Cd	A*Cd (m^2)
Lightning	Lightning GT	2013	2	Sport	1 850[a]		167[b]	194[b]	120[b]			
Tesla	Roadster	2012	2	Sport	1 335[c]		143[d]	173[d]	115[d]		0.35[e]	
Rimac	Concept_One	2014	2	Sport	1 950[f]			200[f]	120[f]			
Mercedes-Benz	SLS AMG ElectricDrive	2014	2	Sport	2 095[g]			194[h]	126[h]			
Volkswagen	e-Up!	2013	5	Small	1 214[i]		146[i]	164[i]	149[i]			
BMW	i3	2013	5	Small	1 270[j]	425[j]	157[j]	178[j]	158[j]	2.38[j]	0.29[j]	
Renault	Zoe	2013	5	Small	1 503[k]	440[k]	151[k]	173[l]	156[k]			
Fiat	500e	2013	4	Small	1 355[m]		141[m]	163[m]	153[m]		0.311[m]	
Ecar	500 EV	2013	4	Small	1 165[n]	300[n]	156[n]	163[n]	149[n]			
Citroën	C-ZERO	2013	4	Small	1 195[o]	255[o]	129[p]	148[o]	161[o]			
Mitsubishi	i-MiEV	2013	4	Small	1 186[q]	264[q]	129[r]	148[r]	161[r]		0.35[s]	
Peugeot	iOn	2013	4	Small	1 195[t]	255[t]	129[t]	147[t]	161[t]			0.706[u]
Scion	iQ EV	2013	4	Small	1 090[v]		147[w]	168[w]	150[w]		0.299[x]	
Chevrolet	Spark EV	2014	4	Small	1 355[y]		140[y]	163[y]	155[aab]		0.325[z]	
Smart	Smart fortwo conv.	2013	2	Small	920[aa]	230[aa]	133[aa]	156[aa]	157[aa]		0.29[ab]	
Mini	Mini E	2013	2	Small	1 465[ac]	195[ac]	146[ac]	168[ac]	141[ac]			
BMW	Active E	2013	5	Medium-Large	1814[ad]	335[ad]	151[ad]	175[ad]	144[ad]			
Volvo	C30 Electric	2013	5	Medium-Large	1 725[ae]		155[af]	178[ag]	145[ag]	2.18[ah]	0.28[ag]	
Coda	CODA	2013	5	Medium-Large	1 664[ai]		148[ai]	171[ai]	148[ai]			
Volkswagen	e-Golf	2013	5	Medium-Large	1 510[aj]		154[ak]	179[al]	145[al]		0.28[am]	
Honda	FIT	2013	5	Medium-Large	1 475[an]		148[an]	172[an]	160[an]		0.301[ao]	
Renault	Fluence Z.E.	2013	5	Medium-Large	1 605[ap]	418[ap]	155[ap]	181[aq]	146[aq]			0.67[ap]
Ford	Focus EV	2013	5	Medium-Large	1 720[ar]	365[ar]	153[as]	182[as]	147[as]		0.295[at]	
Nissan	Leaf	2013	5	Medium-Large	1 474[au]	471[au]	154[av]	177[av]	155[av]	2.27[aw]	0.28[ax]	
Tesla	Model S 40kWh	2012	5	Medium-Large	2 108[ay]		168[az]	196[az]	146[az]		0.24[aaa]	
Tesla	Model S 60kWh	2013	5	Medium-Large	2 108[ay]		168[az]	196[az]	146[az]		0.24[aaa]	
Tesla	Model S 85kWh	2013	5	Medium-Large	2 108[ay]		168[az]	196[az]	146[az]		0.24[aaa]	
Tesla	Model S Perfomance	2013	5	Medium-Large	2 108[ay]		168[az]	196[az]	146[az]		0.24[aaa]	

Table A.2 References to Table A.1.

Ref.	Organization	Webpage	Date accessed
a	Wikipedia English	http://en.wikipedia.org/wiki/Lightning_GT	2013-09-17
b	Autodelicious.com	http://www.autodelicious.com/autonews/LightningGT_700hp0-60in4seconds.asp	2013-09-17
c	Miljöfordon.se	http://www.miljofordon.se	2013-09-05
d	Tesla Motors USA	http://www.teslamotors.com/roadster/specs	2012-04-17
e	Autoblog green	http://green.autoblog.com/2009/03/26/tesla-model-s-50-000-ev-sedan-seats-seven-300-mile-range-0-6/	2013-09-05
f	Rimac Automobili	http://www.rimac-automobili.com/concept_one/specifications-10	2014-02-11
g	Green Highway	http://media.greenhighway.nu/2012/05/Elbils-och-laddhybridguide-2013_svenska.pdf	2014-02-11
h	Mercedes AMG	http://www.mercedes-amg.com/slsgtcfinal.php?lang=eng	2014-02-11
i	Volkswagen Sweden	http://personbilar.volkswagen.se/sv/models/up/utrustning.s9_trimlevel_detail.suffix.html/e-up-~2Fe-up-.html#/tab=dcfa95c9f7799ed6388db420cceae8554	2013-09-10
j	BMW Press	https://www.press.bmwgroup.com/united-kingdom/download.html?textId=1909858&textAttachmentId=234889	2014-02-26
k	Renault Denmark	http://www.renault.dk/e-brochure/ZOEB10/pdf/fullPDF.pdf	2013-09-10
l	Gröna Bilister Test	http://www.gronabilister.se/biltest_renault-zoe-062013.pdf?cms_fileid=c1913438326f5fa4a55120b027fbb18b	2013-09-09
m	Chrysler Media	http://chryslermedia.iconicweb.com/mediasite/specs/09_2013_Fiat_500e_SP.pdf	2014-02-10
n	E Car Norway	http://www.ecar.as/ecar-500-ev.html	2013-09-10
o	Citröen Sweden	http://www.citroen.se/Resources/Content/SE/Brochures/Produktfakta/Produktfakta_C_Zero.pdf	2013-09-09
p	Citröen Sweden	http://www.e-pages.dk/citroen_se/47/	2013-09-09
q	Mitsubishi Sweden	http://www.mitsubishimotors.se/TechnicalSpecification.aspx?PMID=988&BTID=26678&VID1=50488&VID2=0&LangType=1053	2013-09-05
r	Mitsubishi Sweden	http://www.mitsubishimotors.se/uploadedFiles/Parent_Site/Digital_Brochure/Broschyr_i-MiEV_MY12.pdf	2013-09-05
s	NREL	http://www.nrel.gov/docs/fy12osti/48528.pdf	2013-09-05
t	Peugeot Sweden	http://www.peugeot.se/media/deliacms/media/65/6544-a47435.pdf	2013-09-09
u	AutoViva	http://www.autoviva.com/peugeot_ion-specs/version/28525?chg_unit=1&spec_unit=european	2014-02-13
v	Auto blog Toyota Press	http://www.autoblog.com/2012/09/24/toyota-kills-plans-for-widespread-iq-ev-sales-after-misreading-d/	2013-09-17
w	Scion	http://www.scion.com/cars/iQ/specs/	2013-09-17
x	Ecomodder.com	http://ecomodder.com/wiki/index.php/Vehicle_Coefficient_of_Drag_List	2013-09-09
y	Chevrolet	http://www.chevrolet.com/spark-ev-electric-vehicle/specs/trims.html	2014-02-12
z	Automobile	http://rumors.automobilemag.com/los-angeles-2012-chevrolet-shows-full-2014-spark-ev-photos-hints-at-32500-base-price-187789.html#axzz2e7pGOSow	2013-09-09
aa	Smart UK	http://tools.mercedes-benz.co.uk/current/smart/brochures/smart-electric-drive.pdf	2013-09-09
ab	Cars.com	http://www.cars.com/smart/fortwo/2012/specifications/	2013-09-09
ac	Mini USA	http://www.miniusa.com/minie-usa/pdf/MINI-E-spec-sheet.pdf	2013-09-10
ad	BMW USA	http://content.bmwusa.com/bmw_xp2/content/pdf/TechSpecs.pdf	2013-09-15
ae	Volvo Cars	https://www.media.volvocars.com/global/en-gb/download/48779	2013-09-05
af	Volvo Cars	https://www.media.volvocars.com/global/en-gb/download/31361	2013-09-10
ag	Volvo Cars	https://www.media.volvocars.com/global/en-gb/download/18937	2013-09-10
ah	Volvo Cars	https://www.media.volvocars.com/global/en-gb/download/31361	2013-09-05
ai	Coda Automotive	http://app.codaautomotive.com/CarConfigurator/View/Specifications	2013-09-05
aj	InsideEVs	http://insideevs.com/volkswagen-e-golf-test-drive-review/	2014-02-14
ak	Volkswagen Sweden	http://personbilar.volkswagen.se/content/medialib/vwd4/se/pdf/modeller/golf/golf-vii-2013-.	2013-09-17
al	Teknikens Värld Sweden	http://www.teknikensvarld.se/2013/02/21/38225/volkswagen-e-golf-hojer-spanningen-i-geneve/	2013-09-10
am	InsideEVs	http://insideevs.com/2015-volkswagen-e-golf-makes-us-debut-at-2013-la-auto-show/	2014-02-14
an	Honda USA	http://automobiles.honda.com/fit-ev/specifications.aspx	2013-09-05
ao	Automobile	http://www.automobilemag.com/reviews/driven/1207_2013_honda_fit_ev/	2013-09-05
ap	Renault UK	http://www.renault.co.uk/Resources/PDF/Brochures/fluenceze.pdf	2013-09-09
aq	Renault UK	http://www.renault.co.uk/cars/model/fluence-ze/trim/dynamique/PricesAndSpecs.aspx	2013-09-09
ar	miljöfordon.se	http://www.miljofordon.se/fordon?view=detalj&id=43532	2014-02-13
as	Ford USA	http://www.ford.com/cars/focus/trim/electric/	2014-02-13
at	Ford media	https://media.ford.com/content/fordmedia/fna/us/en/news/2011/01/24/streamlined-all-new-ford-focus-significantly-reduces-aerodynamic.html	2014-02-13
au	miljöfordon.se (Autonet)	http://www.miljofordon.se/fordon?view=detalj&id=44063	2014-02-14
av	Nissan.se	http://www.nissan.se/SE/sv/vehicle/electric-vehicles/leaf/charging-and-battery/charging-nissan-leaf-and-battery.html	2014-02-14
aw	carfolio.com	http://www.carfolio.com/specifications/models/car/?car=220715	2014-02-07
ax	Nissan USA	http://www.nissanusa.com/electric-cars/leaf/versions-specs/	2014-02-07
ay	Miljöfordon	http://www.miljofordon.se/detaljamforelse?compare[]=44654&compare[]=44650&compare[]=44652&compare[]=44651	2014-02-13
az	Tesla Motors Sweden	http://www.teslamotors.com/en_SE/models/specs	2013-09-09
aaa	Elon Musk and JB Straubel	http://www.teslamotors.com/blog/model-s-efficiency-and-range	2013-09-09
aab	Wikipedia English	http://en.wikipedia.org/wiki/Chevrolet_Spark#Spark_EV	2014-02-12

Table A.3 Table over collected test related data on selected BEVs.

Brand	Model	Range NEDC (km)	Range EPA City eq. (km)	Range EPA Highw. eq. (km)	Range EPA Comb. eq. (km)	Top speed (km/h)	0-100 km/h (s)	0-60 mph (s)	(XX-YY) km/h (s)	Energy/dist NEDC (Wh/km)	Energy/dist EPA City eq. (Wh/km)	Energy/dist EPA Highw. eq. (Wh/km)	Energy/dist EPA Comb. eq. (Wh/km)
Lightning	Lightning GT	241.4[a]				209[a]		4[b]					
Tesla	Roadster	340[c]			394[d]	201[c]	3.9[c]			160[c]			
Rimac	Concept_One	600[e]				300[e]	2.8[e]						
Mercedes-Benz	SLS AMG ElectricDrive	250[f]				250[g]	3.9[g]			268[g]			
Fiat	500e		148[h]	131[h]	140[h]	137[i]		8.9[j]			174[h]	193[h]	180[h]
Ecar	500 EV	113[k]				130[l]			7.2 (0-50)[aaa]				
Citroën	C-ZERO	150[m]				130[m]	15.9[n]			135[m]			
Volkswagen	e-Up!	160[o]				130[p]	12.4[p]			117[p]			
Smart	Smart fortwo conv.	145[q]	122[r]	95[r]	109[r]	126[q]	11.5[q]		4.8 (0-60)[q]	151[q]	174[r]	224[r]	199[r]
BMW	i3	190[s]				150[s]	7.2[s]	7[t]	3.5 (0-60) [u]	129[s]			
Mitsubishi	i-MiEV	150[v]	110[w]	88[w]	100[w]	130[v]	15.9[v]			135[v]	168[w]	211[w]	186[w]
Peugeot	iOn	150[x]				130[x]	15.9[x]			135[x]			
Scion	iQ EV	85[y]	68[w]	51[w]	61[w]	125.5[y]	14[y]	13.4[z]		134[y]	149[w]	199[w]	174[w]
Mini	Mini E		250[aa]	220[aa]	239[aa]	152[aa]	8.5[aa]				136.7[aa]		
Chevrolet	Spark EV		141[w]	120[w]	132[w]	145[ab]	8.5[ac]	8[ab]			162[w]	193[w]	174[w]
Renault	Zoe	210[ad]				135[ad]	13.5[ad]		4 (0-5)[ad]	146[ae]			
BMW	Active E		241.4[af]		152[ag]	145[af]	9[af]	8.5[ag]	4.5 (0-60)[aab]	140[ah]	118[af]		
Volvo	C30 Electric	163[ai]				125[ai]	10.7[ai]		4 (0-50)[aj]	175[ai]			
Coda	CODA		150.6[w]	130.8[w]	142[w]	137[ak]		9.5[al]			273[w]	311[w]	286[w]
Volkswagen	e-Golf	190[am]				135[an]	10.4[am]			127[ao]			
Honda	FIT		145[w]	118[w]	132[w]	145[ap]		9.5[aq]			162[w]	199[w]	180[w]
Renault	Fluence Z.E.	185[ar]				135[ar]	13.7[ar]			120[as]			
Ford	Focus EV	162[at]	128[w]	115[w]	122[w]	135[au]	11.4[at]	10[av]		150[at]	193[w]	211[w]	199[w]
Nissan	Leaf	199[aw]	132(w)	106[w]	121[w]	144[aw]	11.5[aw]			150[aw]	162[w]	205[w]	180[w]
Tesla	Model S 40kWh		223[w]	226[w]	224[w]	177[w]		6.5[ax]			224[w]	217[w]	224[w]
Tesla	Model S 60kWh	390[ay]	331[w]	339[w]	335[w]	190[ay]	6.2[ay]	5.9[az]			224[w]	217[w]	217[w]
Tesla	Model S 85kWh	502[ay]	423[w]	429[w]	427[w]	200[ay]	5.6[ay]	5.4[az]			236[w]	230[w]	236[w]
Tesla	Model S Perfomance	502[ay]			427[w]	210[ay]	4.4[ay]	4.2[az]					

Table A.4 References to Table A.3.

Ref.	Organization	Webpage	Date accessed
a	Lightning	http://www.lightningcarcompany.co.uk/Lightning/_PERFORMANCE.html	2013-09-17
b	CNET News	http://news.cnet.com/8301-17912_3-9997197-72.html	2013-09-17
c	miljöfordon.se (Autonet)	http://www.miljofordon.se	2013-09-05
d	Tesla Motors USA	http://www.teslamotors.com/roadster/specs	2012-04-17
e	Rimac Automobili	http://www.rimac-automobili.com/concept_one/specifications-10	2014-02-11
f	Deimler Media	http://media.daimler.com/dcmedia/0-921-614307-1-1535313-1-0-0-0-0-1-11702-0-0-1-0-0-0-0-0.html?TS=1348753762840	2014-02-12
g	Mercedes-Benz Sweden	http://www2.mercedes-benz.se/content/sweden/mpc/mpc_sweden_website/sv/home_mpc/passengercars/home/new_cars/models/sls_amg/_c197/facts_/drivetrain/alternativetransmission.html	2014-02-12
h	US Dept. Of Energy	http://www.fueleconomy.gov/feg/download.shtml	2013-09-05
i	Chrysler Media	http://chryslermedia.iconicweb.com/mediasite/specs/09_2013_Fiat_500e_SP.pdf	2014-02-10
j	Car and Driver	http://www.caranddriver.com/reviews/2013-fiat-500e-ev-first-drive-review	2013-09-11
k	E Car Norway	http://www.ecar.as/ecar-500-ev.html	2013-09-10
l	E Car	http://ecarsweden.com/?page_id=189	2013-09-10
m	Citröen Sweden	http://www.citroen.se/Resources/Content/SE/Brochures/Produktfakta/Produktfakta_C_Zero.pdf	2013-09-09
n	Citröen Sweden	http://www.e-pages.dk/citroen_se/47/	2013-09-09
o	Volkswagen Sweden	http://personbilar.volkswagen.se/content/medialib/vwd4/se/pdf/modeller/up-/up-2013-06/_jcr_content/renditions/rendition_1.download_attachment.file/vw-1035-up_modellbroschyr_100dpi.pdf	2013-09-17
p	Volkswagen Sweden	http://personbilar.volkswagen.se/sv/models/up/utrustning.s9_trimlevel_detail.suffix.html/e-up-~2Fe-up-	2013-09-17
q	Smart UK	http://tools.mercedes-benz.co.uk/current/smart/brochures/smart-electric-drive.pdf	2013-09-09
r	US Dept. Of Energy	http://www.fueleconomy.gov/feg/download.shtml	2013-09-05
s	BMW	http://www.bmw.com/com/en/newvehicles/i/i3/2013/showroom/technical_data.html	2013-09-10
t	BMW USA	http://www.bmwusa.com/standard/content/vehicles/2014/bmwi/bmwi.aspx#i3	2013-09-10
u	BMW Sweden	http://www.bmw.se/se/sv/newvehicles/i/i3/2013/showroom/drive.html	2013-09-05
v	Mitsubishi Sweden	http://www.mitsubishimotors.se/uploadedFiles/Parent_Site/Digital_Brochure/Broschyr_i-MiEV_MY12.pdf	2013-09-09
w	US Dept. Of Energy	http://www.fueleconomy.gov/feg/download.shtml	2013-09-05
x	Peugeot Sweden	http://www.peugeot.se/media/deliacms/media/65/6544-a47435.pdf	2013-09-09
y	Auto blog Toyota Press	http://www.autoblog.com/2012/09/24/toyota-kills-plans-for-widespread-iq-ev-sales-after-misreading-d/	2013-09-17
z	Toyota USA	http://pressroom.toyota.com/releases/scion+iq+electric+vehicle+denver+oct17.htm	2013-09-09
aa	Mini USA	http://www.miniusa.com/minie-usa/pdf/MINI-E-spec-sheet.pdf	2013-09-10
ab	Consumer Reports.org	http://www.consumerreports.org/cro/news/2013/06/first-drive-the-chevrolet-spark-ev-shocks-us/index.htm	2013-09-09
ac	Chevrolet.se	http://www.chevrolet.se/upplev/framtida-bilar/spark-ev.html	2013-09-09
ad	Renault Denmark	http://www.renault.dk/e-brochure/ZOEB10/pdf/fullPDF.pdf	2013-09-10
ae	Renault Germany	http://www.renault.de/renault-modellpalette/ze-elektrofahrzeuge/zoe/zoe/konfigurator/#/configurator	2013-09-10
af	BMW USA	http://content.bmwusa.com/bmw_xp2/content/pdf/TechSpecs.pdf	2013-09-10
ag	eVgo	http://www.evgonetwork.com/electric-car-reviews-bmw-active-e/	2013-09-10
ah	BMW Germany	http://www.bmw.com/com/de/newvehicles/1series/activee/2011/showroom/index.html	2013-09-10
ai	Volvo Cars	https://www.media.volvocars.com/global/en-gb/download/48779	2013-09-05
aj	Volvo Cars	https://www.media.volvocars.com/global/en-gb/download/31447	2013-09-05
ak	Coda Automotive	http://app.codaautomotive.com/CarConfigurator/View/Specifications	2013-09-06
al	MotorWeek.org	http://www.motorweek.org/reviews/road_tests/coda	2013-09-06
am	InsideEVs	http://insideevs.com/2015-volkswagen-e-golf-makes-us-debut-at-2013-la-auto-show/	2014-02-14
an	Teknikens Värld Sweden	http://www.teknikensvarld.se/2013/02/21/38225/volkswagen-e-golf-hojer-spanningen-i-geneve/	2013-09-10
ao	Business Standard	http://www.business-standard.com/article/news-cd/new-battery-powered-vw-e-up-and-e-golf-to-debut-at-frankfurt-2013-113082701179_1.html	2013-09-10
ap	eVgo	http://www.evgonetwork.com/electric-car-reviews-honda-fit-ev/	2013-09-13
aq	AutoWeek	http://www.autoweek.com/article/20120628/carnews/120629830	2013-09-13
ar	Renault UK	http://www.renault.co.uk/Resources/PDF/Brochures/fluenceze.pdf	2013-09-09
as	New Electric Cars	http://newelectriccars.wordpress.com/electric-concept-cars-2/renault-fluence-ze/	2013-09-09
at	miljöfordon.se	http://www.miljofordon.se/fordon?view=detalj&id=43532	2014-02-13
au	Ford.se	http://www.ford.se/Personbilar/Focus-Electric	2014-02-13
av	AutoWeek	http://www.autoweek.com/article/20120417/CARREVIEWS/120419856	2014-02-13
aw	miljöfordon.se (Autonet)	http://www.miljofordon.se/fordon?view=detalj&id=44063	2014-02-14
ax	Tesla USA	http://teslamotors.com/models/options	2012-04-17
ay	Tesla Sverige	http://www.teslamotors.com/sv_SE/models/features#/battery	2014-02-13
az	Tesla USA	http://www.teslamotors.com/models/features#/performance	2012-04-17
aaa	E Car	Product Broshure	2013
aab	BMW	http://www.bmw.com/com/en/newvehicles/1series/activee/2011/_shared/pdf/active_e_flyer.pdf	2013-09-15

Table A.5 Table over collected powertrain related data on selected BEVs.

Brand	Model	EM power (kW)	Speed at Max power (rpm)	Max EM torque (Nm)	Speed at max Torque (rpm)	Motor type	Battery Energy (kWh)	Used Energy (%)	Battery Capacity (Ah)	Battery weight (kg)	Battery Specific Energy (Wh/kg)	Battery total voltage (V)	Battery Type	Transm. ratio	Drive	Tire
Lightning	Lightning GT	300[a]		4000[a]		2*EM[a]	44[a]					450[a]	Li-Ti[a]	5.5:1[b]	Rear[a]	
Tesla	Roadster	225[c]	5000[c]	370[c]	5400[c]	IM[c]	53[d]			450[d]		375[d]		8.28:1[c] 3.12:1		175/55 R16[c] 225/45 R17
Rimac	Concept_One	800[e]		1600[e]	6500[e]	4*PMSM[e]	91[e]					650[e]	LiFePO4[e]	3.5[e]		245/35R20[ae] 295/30R20
Mercedes-Benz	SLS AMG ElectricDrive	552[f]		1000[f]		4*PMSM[f]	60[f]			548[f]		400[f]	Li-ion[f]			265/35R19[f] 295/30R20
Fiat	500e	83[g]				IPM[h]	24[g]		63[h]		88[h]	364[g]	Li-ion[g]	9.59[g]	Front[g]	185/55R15[g]
Ecar	500 EV	30[i]					15[i]									
Citroën	C-ZERO	47[j]	2500[j]	180[j]	2500[j]	PMSM[j]	16[j]			238.5[k]		330[j]				145/65R15[j] 175/55R15
Volkswagen	e-Up!	60[l]		210[l]			18.7[m]									
Smart	Smart fortwo conv.	55[n]		130[n]		PM[h]	17.6[n]		52[h]		99[h]	339[h]	Li-ion[h]		Rear[h]	
BMW	i3	125[o]		250[o]			18.8[o]									155/70R19[o]
Mitsubishi	i-MIEV	49[p]	2500[p]	180[p]	2000[p]	PMSM[p]	16[p]		50[h]		67[h]	330[p]	Li-ion[p]	6.066[p]	Rear[p]	145/65R15[p] 175/55R15
Peugeot	iOn	49[q]	2500[q]	180[q]	2000[q]		16[q]			230[r]		330[r]				145/65R15[q] 175/55R15
Scion	iQ EV	47[s]		162.7[s]			12[s]		43[h]		55[h]	278[h]	Li-ion(h)		Front[h]	
Mini	Mini E	150[t]		220[t]		IM[t]	35[t]	86[t]		260[t]						
Chevrolet	Spark EV	103[u]		542[u]		PMSM[h]	20[u]	85[v]	60[h]	250[v]	83[h]	370[h]	Li-ion(h)		Front(h)	
Renault	Zoe	65[w]	3000[w]	220[w]	2500[w]		22[w]			290[w]		400[w]				185/65R15[x]
BMW	Active E	125[y]	4775[y]	250[y]	4775[y]	SM[z]	32[z]		40[z]	450[z]					Rear[y]	205/55R16[z]
Volvo	C30 Electric	89[aa]		250[aa]			24[aa]	95[aa]		330[aa]						
Coda	CODA	100[ab]		300[ab]		PM[h]	31[ab]		96[h]		79[h]	333[ab]	Li-ion[h]	6.54:1[ab]	Front[h]	
Volkswagen	e-Golf	85[ac]		270[ac]			26.5[ac]	91.3[ad]								
Honda	FIT	92[ae]		256[ae]		PM[h]	20[ae]		20[h]		89[h]	330[h]	Li-ion[h]		Front[h]	
Renault	Fluence Z.E.	70[af]	3000[af]	226[af]	2500[af]	SM[ah]	22[af]			280[af]						205/55R16[ae]
Ford	Focus EV	107[ai]		250[ai]		PMSM[h]	23[ai]		75[h]		80[h]	350[h]	Li-ion[h]		Front[h]	
Nissan	Leaf	80[aj]	3008[aj]	254[aj]	3008[aj]	PM[h]	24[ak]		66[h]	218[al]	88[h]	360[h]	Li-ion[h]		Front[h]	
Tesla	Model S 40kWh	225[h]				IM[h]	40[h]					400[h]	Li-ion[h]		Rear[h]	
Tesla	Model S 60kWh	225(h)		440[am]	5900[am]	IM[h]	60[h]					400[h]	Li-ion[h]		Rear[h]	245/45R19[am]
Tesla	Model S 85kWh	270[h]		440[am]	5900[am]	IM[h]	85[h]		245[h]		170[h]	400[h]	Li-ion[h]	9.73:1[an]	Rear[h]	
Tesla	Model S Perfomance	310[h]		600[am]	5300[an]	IM[h]	85[am]					400[h]	Li-ion[h]			

Table A.6 References to Table A.5.

Ref.	Organization	Webpage	Date accessed
a	Lightning	http://www.lightningcarcompany.co.uk/Lightning/_PERFORMANCE.html	2013-09-17
b	Wikipedia English	http://en.wikipedia.org/wiki/Lightning_GT	2013-09-17
c	Tesla Motors USA	http://www.teslamotors.com/roadster/specs	2012-04-17
d	Autoblog green	http://green.autoblog.com/2009/03/26/tesla-model-s-50-000-ev-sedan-seats-seven-300-mile-range-0-6/	2014-02-13
e	Rimac Automobili	http://www.rimac-automobili.com/concept_one/specifications-10	2014-02-11
f	Deimler Media	http://media.daimler.com/dcmedia/0-921-614307-1-1535313-1-0-0-0-0-1-11702-0-0-1-0-0-0-0-0.html?TS=1348753762840	2014-02-12
g	Chrysler Media	http://chryslermedia.iconicweb.com/mediasite/specs/09_2013_Fiat_500e_SP.pdf	2014-02-10
h	US Dept. Of Energy	http://www.fueleconomy.gov/feg/download.shtml	2013-09-05
i	E Car	Product Broshure	2013
j	Citröen Sweden	http://www.citroen.se/Resources/Content/SE/Brochures/Produktfakta/Produktfakta_C_Zero.pdf	2013-09-09
k	Citröen Sweden	http://www.e-pages.dk/citroen_se/47/	2013-09-09
l	Volkswagen Sweden	http://personbilar.volkswagen.se/sv/models/up/utrustning.s9_trimlevel_detail.suffix.html/e-up-~2Fe-up-.html#/tab=dcfa95c9f7799ed638db420cceae8554	2013-09-17
m	Volkswagen UK	http://www.volkswagen.co.uk/about-us/news/490	2013-09-10
n	Smart UK	http://tools.mercedes-benz.co.uk/current/smart/brochures/smart-electric-drive.pdf	2013-09-09
o	BMW	http://www.bmw.com/com/en/newvehicles/i/i3/2013/showroom/technical_data.html	2013-09-10
p	Mitsubishi Sweden	http://www.mitsubishimotors.se/uploadedFiles/Parent_Site/Digital_Brochure/Broschyr_i-MiEV_MY12.pdf	2013-09-09
q	Peugeot Sweden	http://www.peugeot.se/media/dellacms/media/65/6544-a47435.pdf	2013-09-09
r	Teknikens Värld	http://www.teknikensvarld.se/2010/10/14/17142/provkorning-av-peugeot-ion/	2013-09-09
s	Toyota USA	http://pressroom.toyota.com/releases/scion+iq+electric+vehicle+denver+oct17.htm	2013-09-09
t	Mini USA	http://www.miniusa.com/minie-usa/pdf/MINI-E-spec-sheet.pdf	2013-09-10
u	Chevrolet	http://www.chevrolet.com/spark-ev-electric-vehicle/specs/trims.html	2014-03-12
v	Green Car Reports	http://www.greencarreports.com/news/1080487_2014-chevy-spark-ev-prototype-electric-car-first-drive	2014-03-12
w	Renault Denmark	http://www.renault.dk/e-brochure/ZOEB10/pdf/fullPDF.pdf	2013-09-10
x	Renault Germany	http://www.renault.de/renault-modellpalette/ze-elektrofahrzeuge/zoe/zoe/konfigurator/#/configurator	2013-09-10
y	BMW	http://www.bmw.com/com/en/newvehicles/1series/activee/2011/_shared/pdf/active_e_flyer.pdf	2013-09-15
z	BMW USA	http://content.bmwusa.com/bmw_xp2/content/pdf/TechSpecs.pdf	2013-09-10
aa	Volvo Cars	https://www.media.volvocars.com/global/en-gb/download/48779	2013-09-05
ab	Coda Automotive	http://app.codaautomotive.com/CarConfigurator/View/Specifications	2013-09-06
ac	Teknikens Värld Sweden	http://www.teknikensvarld.se/2013/02/21/38225/volkswagen-e-golf-hojer-spanningen-i-geneve/	2013-09-10
ad	Business Standard	http://www.business-standard.com/article/news-cd/new-battery-powered-vw-e-up-and-e-golf-to-debut-at-frankfurt-2013-113082701179_1.html	2013-09-10
ae	Honda USA	http://automobiles.honda.com/fit-ev/specifications.aspx	2014-02-13
af	Renault UK	http://www.renault.co.uk/Resources/PDF/Brochures/fluenceze.pdf	2013-09-09
ag	Renault UK	http://www.renault.co.uk/cars/model/fluence-ze/trim/dynamique/PricesAndSpecs.aspx	2014-02-07
ah	Wikipedia English	http://sv.wikipedia.org/wiki/Renault_Fluence#Renault_Fluence_Z.E.	2014-02-07
ai	miljöfordon.se	http://www.miljofordon.se/fordon?view=detalj&id=43532	2014-02-13
aj	Nissan.se	http://www.nissan.se/SE/sv/vehicle/electric-vehicles/leaf/prices-and-equipment/prices-and-specifications/model-details.501255_500744_501205.html	2014-02-14
ak	miljöfordon.se (Autonet)	http://www.miljofordon.se/fordon?view=detalj&id=44063	2014-02-14
al	Nissan USA	http://www.nissanusa.com/electric-cars/leaf/versions-specs/	2014-02-12
am	Tesla Sverige	http://www.teslamotors.com/sv_SE/models/features#/battery	2014-02-13
an	Tesla Motors Sweden	http://www.teslamotors.com/en_SE/models/specs	2013-09-09
ao	Supercarsempire	http://www.supercarsempire.com/2012/07/2013-rimac-one-new-supercar-from.html	2014-02-18

Found data regarding top speed and time to accelerate from $0 - 100\,km/h$ and $0 - 60\,mph$ can be seen in Figure A.1 and A.2.

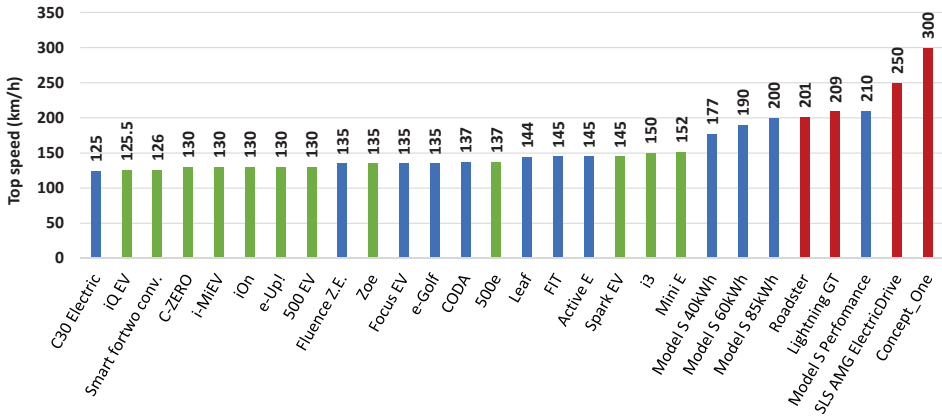

Figure A.1 Top speed for existing BEVs, where the small, medium, sport and Model S models are colored green, blue, red and orange respectively.

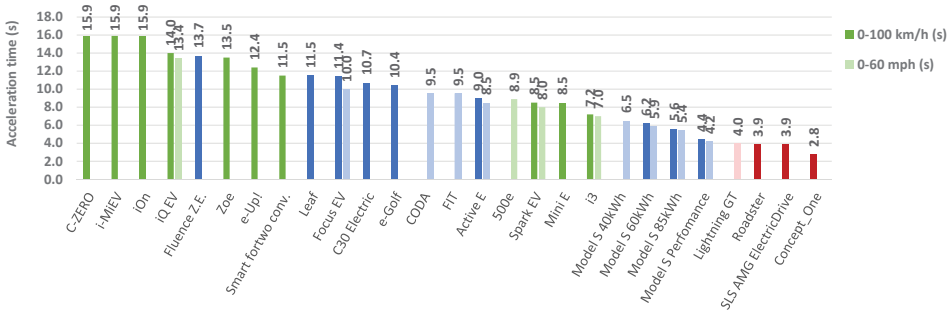

Figure A.2 Time to accelerate $0 - 100\,km/h$ and $0 - 60\,mph$ for existing BEVs, where the small, medium, sport and Model S models are colored green, blue, red and orange respectively.

Time to accelerate from $0 - 50\,km/h$ and $50 - 100\,km/h$ as well as $0 - 60\,km/h$ and $60 - 100\,km/h$ for six of the existing BEVs can be seen in Table A.7

Table A.7 Time to accelerate between different speed levels, for a six existing BEV models.

	0-50 km/h	50-100 km/h	0-60 km/h	60-100 km/h
ECar, 500 EV:	7.2 s			
Volvo, C30 Electric:	4 s	6.7 s		
Renault, Zoe:	4 s	9.5 s		
BWM, Active E:			4.5 s	4.5 s
BMW, i3:			3.7 s	3.5 s
Smart, Smart-for-two:			4.8 s	6.7 s

Found data regarding curb weight and driving range can be seen in Figure A.3 and A.4.

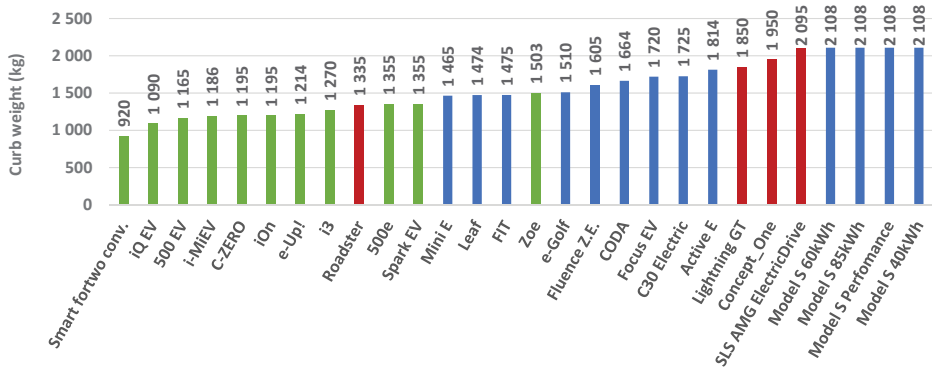

Figure A.3 Curb weight of commercial BEVs, sorted after number of seats. Low speed vehicles are marked green, medium speed vehicles are marked orange and high speed vehicles are marked red. Also one vehicle is marked blue, since it has a top speed much lower than the desired 130 km/h.

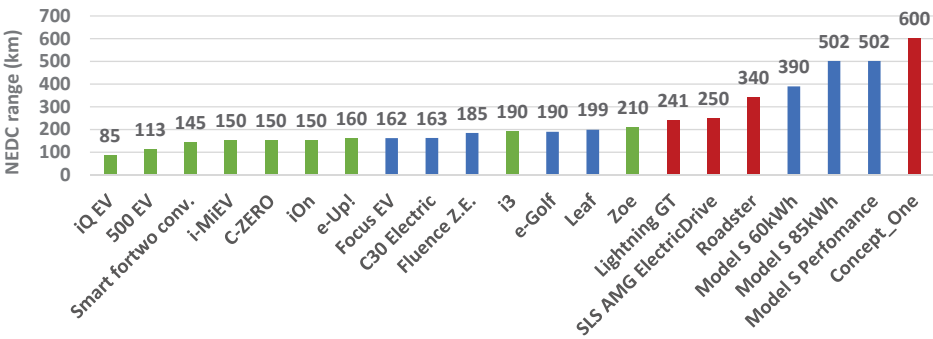

Figure A.4 Driving range on NEDC for existing BEVs, where the small, medium, sport and Model S models are colored green, blue, red and orange respectively.

A.2 Area estimation

Figure A.5 shows the resulting estimated areas using three different calculations based on the methods mentioned in Chapter 2; $79\,\%$ and $84\,\%$ of the product of height and width, and $90\,\%$ of the product of height and track width. For those BEVs where the width is stated excluding the side mirrors, this value has been used. The figure also includes area values for three cars, where one (C30) was found via the manufacturers web site, while the other two (Leaf and i3) were found at a car enthusiast's web site.

Generally the estimation based on $90\,\%$ of height and track width is the smallest of the three (with one exception), while the one using $84\,\%$ of height and width is the largest. For most vehicles the estimation based on $90\,\%$ of height and track width and the one based on $79\,\%$ of the height and width, are fairly close. The largest difference between the highest and lowest estimated values is $0.23\,m^2$ for Focus EV, and the smallest difference is $0.12\,m^2$ for both e-Up and iOn, while the mean value of the differences is $0.16\,m^2$.

When comparing the estimation methods with the data found for the three models, it is clear that the estimation based on $84\,\%$ of the product of height and width is the one that is closest in all three cases, with a difference of only $0.01 - 0.03\,m^2$. For the C30, the error is about $0.6\,\%$.

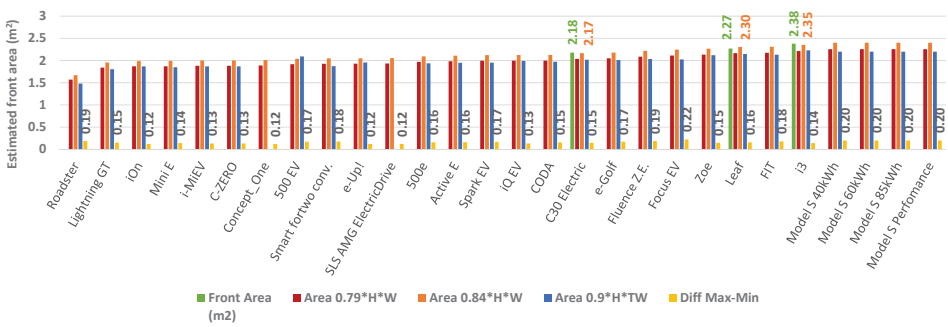

Figure A.5 Estimated area, for existing BEVs, included two found data for Leaf and i3.

A.3 Tire radius estimation

Tire dimension specifications are normally given in the format "*width*"/ "*aspect ratio*" R "*rim*". As an example, the specification 205/55R16, means that the width is $205\,mm$. The aspect ratio or profile is the tire height from the inner (rim) diameter to the outer, as a percentage of the width, in this case $55\,\%$. Finally the tire rim diameter is 16 inch. Based on this type of data, the tire radius (in meter) r_{wheel} can be estimated as

$$r_{wheel} = 0.001\,\frac{(25.4\,rim(inch)) + (\frac{2\,asp.ratio(\%)}{100}\,width)}{2} \tag{A.1}$$

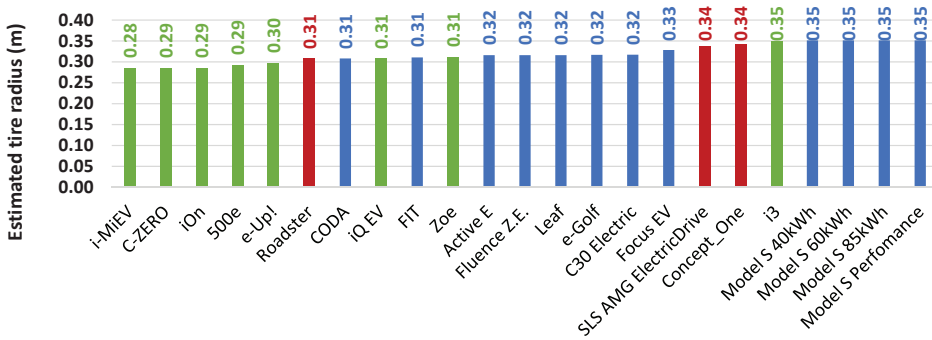

Figure A.6 Estimated tire radius, for existing BEVs.

Appendix B

GPS-accelerometer measurement system

B.1 Description of the measurement system

The measurement system is called MX3 and was delivered by HostMobility in Gothenburg. Two units were purchased. Each unit includes a GPS along with a roof top mountable antenna, a 3D accelerometer and 2 temperature sensors attached to the end of extension cables of 1m and 3 m respectively. The GPS module is an IT500, by FasTrax. The accelerometer is a MMA7455L, by Freescale[1], with a range of $\pm 2g$, and a resolution of $g/64 = 0.15328(m/s^2)$. The temperature sensors are SMT16030 by Smartec.

The unit is strapped on a flat surface in the test vehicle, with the accelerometer coordinate frame aligned with the vehicle's coordinate frame. An external voltage source is needed to power the unit, e.g. the vehicles $12V$ outlet or an external battery, see Figure B.1.

Data is then logged on a PC via a RS232/USB connection and a terminal software. The sampling frequency of the GPS signal is $5\,Hz$, that of the accelerometer signal is $20\,Hz$ and that of the temperature signal is $1\,Hz$.

GPS data regarding GPS time, position (latitude, longitude and altitude), speed, dilution of precision (hdop, vdop and pdop), nuber of satelites in fix etc. is received according to the NMEA format, from the GGA, GSA, GSV, and RMC packages. That is, no raw data from the satellite communication (e.g distance to satellite) are available. According to FasTrax, the GPS position accuracy is $1.8\,m$, and the velocity accuracy is $0.1\,m/s$. DGPS has not been utilized.

[1]The data sheet can be found at http://www.freescale.com/files/sensors/doc/data_sheet/MMA7455L.pdf

(a) One of the measurement units. (b) The measurement unit strapped in a car.

Figure B.1 The measurement unit and an example of usage.

B.2 Filtering of measurement Data

The speed and altitude signals are low pass filtered with a cut off frequency of $0.5\ Hz$, and the acceleration signal with a frequency of $2\ Hz$. Then both speed and altitude are resampled to $20\ Hz$. Traveled distance was calculated as the time integral of the speed signal.

Road slope was estimated as the inverse sine of the ratio between a change in altitude (dh) and a change in traveled distance dS, for each sample ($\alpha = \arcsin(\frac{dh}{dS})$). It proved to be rather difficult to attain a fair estimate of the road slope, especially at low speed levels close to stand still where with very small values of dh and dS, causing an unstable grade value. In order to deal with this, a few different limiting strategies were applied, e.g. to smooth the grade within a time frame of $2\ s$ during the mentioned situations.

Finally the estimated grade was utilized to compensate that part of the accelerometer signal that is caused by road grade, see Figure B.2.

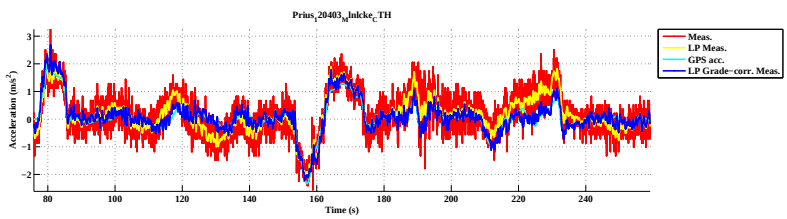

Figure B.2 Example of correction for road grade of acceleration.

B.3 Ambiguity of measurements

Even though the same driver was using the same car, drove the same route, at similar times of the day, the logs are different, as can be seen in Table B.1, and Figure B.3 to B.5.

Table B.1 Cycle data for all CTH - Kålltorp logs.

V744 CTH-Klltrp Cycles	Cycle duration (s)	Driven distance (m)	Max. speed (km/h)	Average speed (km/h)	Average running speed (km/h)	Std. speed (km/h)	Max. pos. acc. (m/s^2)	Max. neg. acc (m/s^2)	Average pos. acc. (m/s^2)	Average neg. acc. (m/s^2)	Std. pos. acc. (m/s^2)	Std. neg. acc. (m/s^2)	RPA (m/s^2)	Time share pos. acc. (%)	Time share neg. acc. (%)	Time share standing (%)
120306	897	8 023	57	32	32	17	2.98	-3.10	0.42	-0.37	0.49	0.48	0.18	46	54	0.7
120307	769	7 937	63	37	37	15	2.17	-3.96	0.39	-0.40	0.36	0.47	0.18	51	49	0.2
120320	844	7 930	53	34	34	15	3.48	-3.60	0.38	-0.35	0.44	0.44	0.15	47	53	1.3
120325	737	7 854	60	38	38	16	3.28	-3.33	0.42	-0.41	0.51	0.49	0.16	45	55	0.1
120327	806	7 932	64	35	36	18	2.99	-2.70	0.43	-0.45	0.43	0.48	0.21	54	46	1.5
MEAN	811	7 935	59	35	36	16	2.98	-3.34	0.41	-0.40	0.45	0.47	0.18	49	51	0.8

As can be seen in Figure B.3, the exact same route was driven.

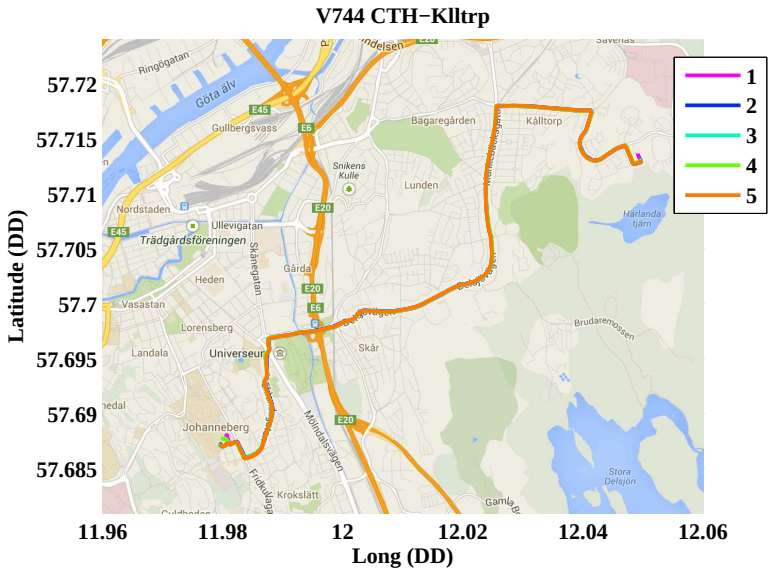

Figure B.3 Logs on map.

As can be seen in the upper right subplot in Figure B.4, the speed varies from log to log. The difference may be about $20\,km/h$.

As can be seen in the lower right subplot in Figure B.4, the estimated road grade may also vary from log to log. But there is a fair level of consistency.

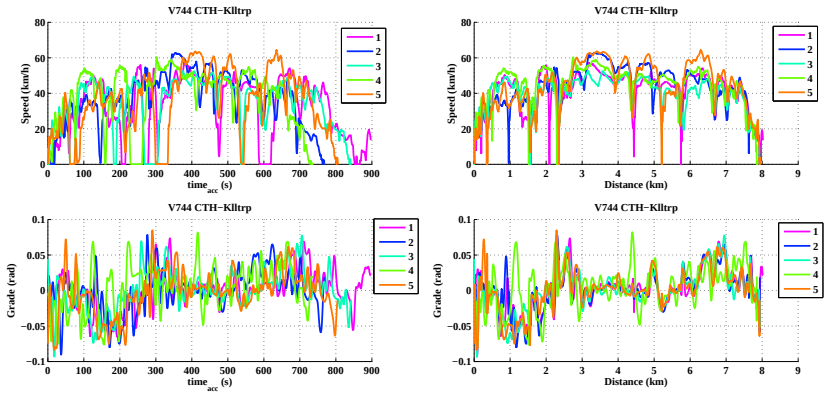

Figure B.4 Logged Speed and road grade.

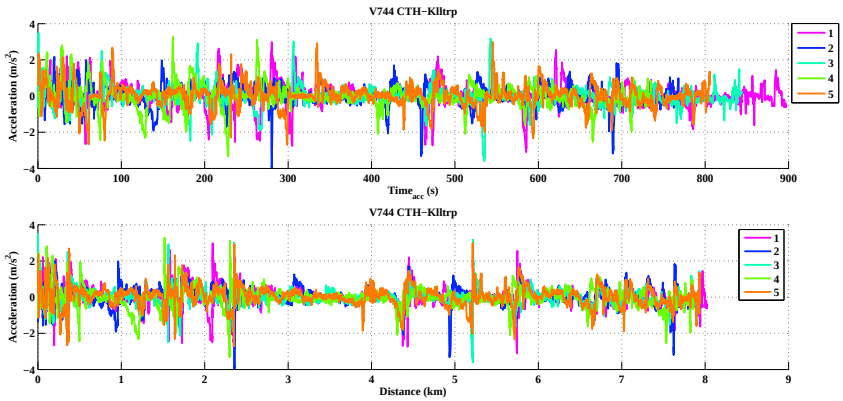

Figure B.5 Logged Acceleration.

B.4 Logged vehicles

Curb weight, powertrain power and the resulting power-to-weight-ratio for the vehicles used during logging can be seen in Table B.2.

Table B.2 Selected data on logged vehicles.

Brand	**Model**	**Fuel type**	**Curb weight** ***(kg)***	**Max. Power** ***(kW)***	**Power-to-weight ratio** ***(kW/kg)***
E CAR	500 EV	El.	1165	30	26
Nissan	Leaf	El.	1613	80	50
Tesla	Roadster	El.	1235	225	182
Toyota	Prius	Gasoline	1365-1425	73	53
Volvo	C30 D2	Diesel	1428	84	59
Volvo	C30 Electric	El.	1660	82	49
Volvo	V744	Gasoline	1370	86	63
Volvo	V70	Gasoline	1640	125	76
Volvo	XC60	Diesel	1920	120	63
Volvo	V60 PHEV	Diesel & El.	2000	160+50	80 or 105

Appendix C

Speed and acceleration dither

In order to get an idea of the total and relative time spent at different speed and acceleration operating points for the Urban, Rural and Highway cycles, each cycle value is attributed to a certain acceleration and speed bin, of $0.5\,m/s^2$ and $5\,km/h$, see Figure C.1(a) for the Urban Test cycles. The result can also be visualized in a contour plot, see Figure C.2(a) for total time in each bin and Figure C.2(b) for the share of total time in each bin.

In order to get a more smooth looking contour plot, a random gaussian noise (with zero mean, and $0.5\,m/s^2$ respectively $1\,m/s$ standard deviation) was added to each operating point, so called dithering. Furthermore, each drive cycle with the added noise is looped 100 times, after which the total and relative time spent in each bin is divided by the number of loops. The results can be seen in Figure C.1(b) and C.3(b), for the Urban cycles, and in Figure C.4 and C.5 for the Rural and Highway cycles respectively.

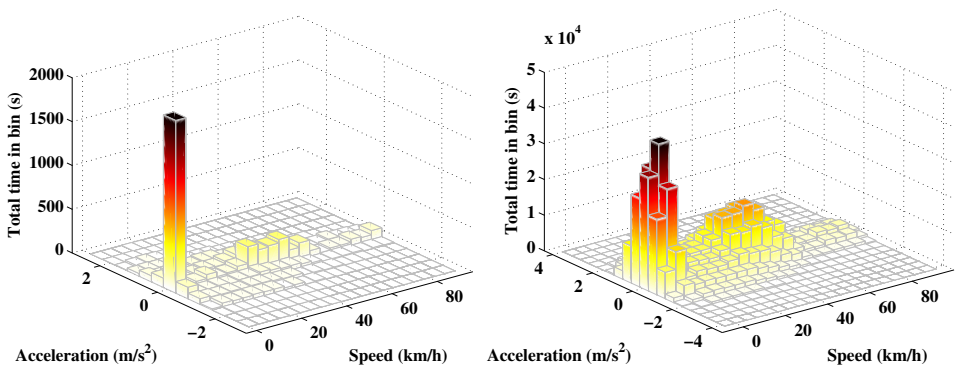

(a) No added noise.

(b) With added noise during 100 loops.

Figure C.1 Share of total time $(\%)$ of operation in acceleration bins of $0.5\ m/s^2$ and speed bins of $5\ km/h$, for all Urban test cycles.

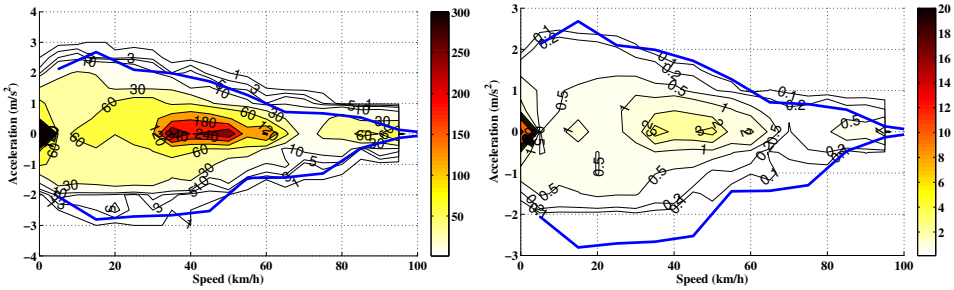

(a) Total time. (b) Share of total time.

Figure C.2 Total time (s) vs. Share of total time $(\%)$ of operation in acceleration bins of $0.5\ m/s^2$ and speed bins of $5\ km/h$, for all Urban test cycles, no added noise.

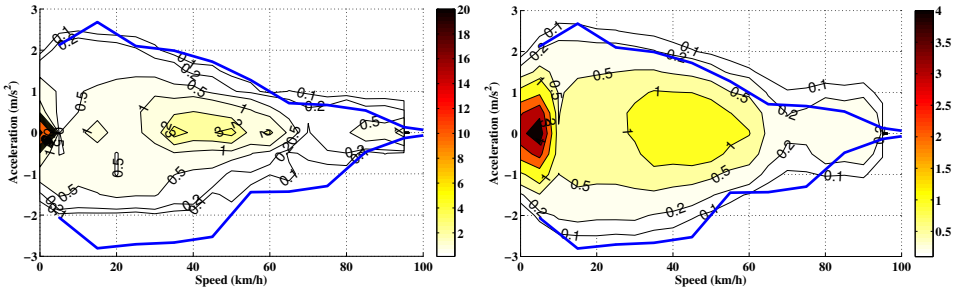

(a) No added noise. (b) With added noise during 100 loops.

Figure C.3 Share of total time $(\%)$ of operation in acceleration bins of $0.5\ m/s^2$ and speed bins of $5\ km/h$, for all Urban test cycles.

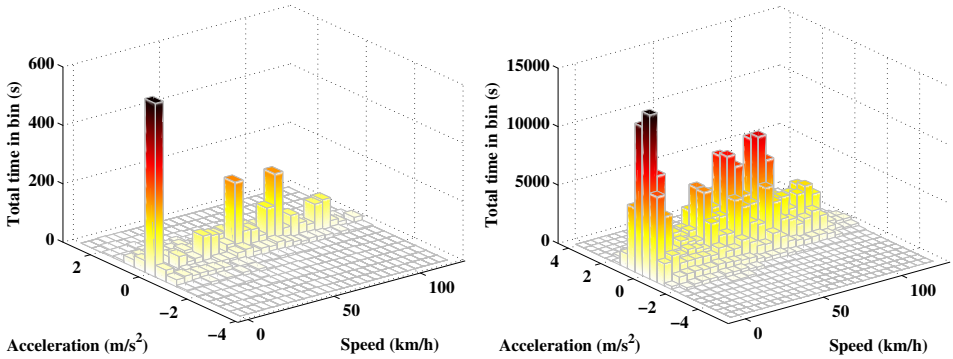

(a) No added noise.

(b) With added noise during 100 loops.

Figure C.4 Share of total time $(\%)$ of operation in acceleration bins of $0.5\ m/s^2$ and speed bins of $5\ km/h$, for all Rural test cycles.

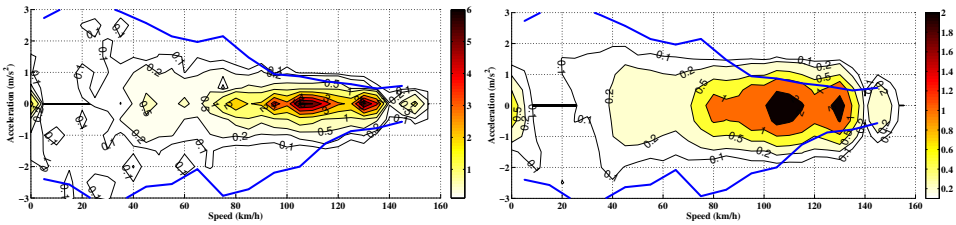

(a) No added noise.

(b) With added noise during 100 loops.

Figure C.5 Share of total time $(\%)$ of operation in acceleration bins of $0.5\ m/s^2$ and speed bins of $5\ km/h$, for all Highway test cycles.